ANALYSIS OF ZIRCONIUM-CONTAINING MATERIALS USING MULTIPLE DIGESTION AND SPECTROMETRIC TECHNIQUES

by

Steven James Lötter

A thesis submitted in fulfilment of the requirements for the degree of

Philosophiae Doctor

Department of Chemistry, University of the Free State

October 2014

Supervisor: Prof. W. Purcell

Co-supervisor: Dr J.T. Nel

DECLARATION

I declare that the thesis hereby submitted by me for the Philosophiae Doctor (Analytical Chemistry) degree at the University of the Free State is my own independent work and has not previously been submitted by me at another university/faculty. I furthermore cede copyright of the thesis in favour of the University of the Free State.

_____ _____

Steven James Lötter Date

ACKNOWLEDGMENTS

I would hereby like to thank all those people and entities involved in the research presented herein, these being:

Prof. W. Purcell, my supervisor, for his guidance and assistance.

Dr J.T. Nel, my co-supervisor, for his valuable insight and knowledge of the field.

Prof. H.G. Visser and Dr B. van Brecht for their assistance with X-ray crystallography.

The personnel of the Department of Chemistry at the University of the Free State for their support and help.

Cliff Thompson for assistance with and insight into the pressing of powders.

Ryno van der Merwe for assistance with SEM/EDS analyses and density determinations.

My mother, Mrs N.J. Lötter, for her excellent grammatical and language editing.

My wife, Antoinette, for her love and support.

The South African Nuclear Energy Corporation Limited (Necsa) for their funding and assistance throughout the course of the project.

The Department of Science and Technology (DST) for funding through the Advanced Metals Initiative (AMI) and the Nuclear Materials Development Network (NMDN).

Key Words

Zircon

Mineral

Digestion

Zirconium

Hafnium

Analysis

Determination

Quantification

Trace

Impurities

Fusion

Microwave

Inductively coupled plasma optical emission spectroscopy (ICP-OES)

Inductively coupled plasma mass spectrometry (ICP-MS)

Glow discharge optical emission spectroscopy (GD-OES)

SUMMARY

The preparation of pure zirconium metal for nuclear applications is difficult due to the non-reactivity of zirconium minerals, such as zircon. The ability to accurately analyse zirconium-containing materials across the whole beneficiation chain is of crucial importance to the zirconium industry as a whole. The development of such an analytical technique is problematic, however, as the very properties which make these materials desirable also make quantification of their components extremely difficult.

Certified reference materials for the fluoride-containing Necsa zirconium process products were not available. Therefore in-house reference materials were created by crystallisation of several $(cation)_xZrF_{4+x}$ compounds. Potassium catena di-μ-fluorido-tetrafluoridozirconate(IV), cesium hexafluoridozirconate(IV) and tetraethyl ammonium catena di-μ-fluorido-bis-(trifluoridozirconate(IV)) monohydrate were prepared and characterised by X-ray crystallography and qualitative XRD. Coordination numbers for the zirconium atoms in each of these crystals were found to be 8, 6 and 7 respectively. Bridging fluorine bond lengths were determined to be approximately 2.06 and 1.97 Å for the potassium and tetraethyl ammonium complexes while terminal bond lengths were found to be 2.17 (potassium), 2.007 (cesium) and 2.15 (tetraethyl ammonium) Å. ICP-OES lower limits of detection for zirconium in the 3.25% nitric acid matrix were found to be 1.6 ppb with lower limits of quantification being ten times this value. ICP-OES zirconium recoveries for these crystals were 101(1) and 100(2)% for the potassium and cesium crystals respectively.

Dissolution of various commercial and Necsa process samples was problematic and thus several digestion methods were investigated. Sulphuric acid, ammonium bifluoride and hydrofluoric acid were all investigated along with microwave assistance. A microwave-assisted acid digestion method was developed capable of complete dissolution of all zirconium compounds with ICP-OES analytical recoveries of 102.0(9), 100(2) and 101(3)% for 99.98% zirconium metal foil, ZrC and ZrH_2 respectively.

In order to circumvent the dissolution step a solid state GD-OES method was developed wherein sample powders were pressed into disks with a binder material, either copper or graphite. Initially instrument response across different samples was

inconsistent but after optimisation of several instrument parameters, such as applied voltage and pre-burn time, a calibration curve with a R^2 value of 0.9805 was achieved using multiple sample materials. This was achieved using the radio frequency glow discharge source operating at 900 V applied voltage and 14 W applied power with a 5-minute pre-burn period. Results for Necsa process products were largely in line with those achieved by the ICP-OES method.

OPSOMMING

Die voorbereiding van suiwer sirkoniummetaal vir aanwending in die kernindustrie is problematies as gevolg van die onreaktiwiteit van sirkoniumminerale, soos sirkoon. Die vermoë om sirkonium-bevattende materiale akkuraat tydens die hele veredelingsproses te ontleed, is van kardinale belang vir die totale sirkonium-industrie. Die ontwikkeling van sulke analitiese tegnieke is moeilik, aangesien die eienskappe wat hierdie verskillende sirkoonverbindings materiaal aantreklik vir die industrie maak, ook die kwantifisering van hul komponente baie bemoeilik.

Gesertifiseerde verwysingsmateriaal (GVM) vir die fluoried-bevattende Necsa sirkonium proses produkte was nie beskikbaar nie. Daarom is GVM's in die vorm van verskeie (katioon)$_x$ZrF$_{4+x}$ verbindings in die laboratorium berei. Kalium catena di-μ-fluorido-tetrafluoridosirkonaat(IV), sesium heksafluoridosirkonaat(IV) en tetraetiel ammonium catena di-μ-fluorido-bis-(trifluoridosirkonaat(IV)) monohidraat is voorberei en met behulp van X-straal kristallografie en kwalitatiewe XRD gekarakteriseer. Koördinasie getalle vir die sirkonium-atome is onderskeidelik as 8, 6 en 7 bepaal. Gebrugde Zr-F bindingslengtes van 2.06 en 1.97 Å is vir die kalium- en tetraetiel ammonium komplekse bepaal terwyl die terminale bindinglengtes as 2.17 (kalium), 2.007 (sesium) en 2.15 (tetraetiel ammonium) Å bepaal is. Die IGP se laagste vlakke van deteksie van sirkonium is in 3.25% salpetersuur matriks as 1.6 dpb bepaal terwyl laagste vlakke van kwantifisering as 16 dpb bereken is. Die sirkoniumherwinning in die kalium- en sesiumkristalle is met behulp van die IGP as 101(1) en 100(2)% bepaal.

Ontbinding van verskeie kommersiële en Necsa prosesmonsters was problematies en is met behulp van verskeie verteringsmetodes ondersoek. Mikrogolfvertering met behulp van swawelsuur, ammoniumbifluoried en fluoorsuur is in hierdie deel van die studie ondersoek. 'n Mikrogolf-ondersteunde suurverteringsproses is ontwikkel. Hierdie nuwe metode was in staat om volledig alle sirkoniumverbindings te ontbind en te bewerkstellig met IGP analitiese resultate van 102.0(9), 100(2) en 101(3)% vir die 99.98% sirkonium metaalfoelie, ZrC en ZrH_2 is onderskeidelik verkry.

Om die verteringsstap van die verskillende verbindings te omseil, is 'n vaste toestand GD-OES metode ontwikkel waartydens monsterpoeiers in skywe, in die

teenwoordigheid van 'n bindingsmateriaal soos koper of grafiet, gedruk is. Aanvanklike kalibrasieresultate wat met verskillende monsters uitgevoer was, was teenstrydig. Tydens die optimalisering van verskeie instrumentparameters, soos byvoorbeeld die spanning en aanvanklike voorbrandingstye, is 'n kalibrasie met 'n R^2 waarde van 0.9805 met behulp van verskeie sikoonbevattendeverbindings verkry. Hierdie resultate is verkry deur van die radiofrekwensie gloeiontladingsbron by toegepaste spanning van 900 V, 'n toegepaste drywing van 14 W en 'n aanvanklike voorbrandingstyd van 5 minute gebruik te maak. Analitiese resultate vir die sirkooninhoud van verskeie Necsa-proses produkte was grootliks in lyn met dié wat deur die IGP metode verkry is.

Contents

LIST OF FIGURES

LIST OF TABLES

Chapter 1: Overview and Objectives of this Study

1.1. INTRODUCTION

Historically, crystals of zirconium dioxide (zirconia) were known as the gemstones hyacinths, jargons and matara diamonds, amongst other names, due to their striking optical properties and colours [1]. Although these materials were known throughout history it was not until the 19th century that the element zirconium was isolated and characterisation begun.

Today zirconium chemicals are used in a wide variety of industrial applications. These include, amongst others, the making of high-transparency glasses [1], antiperspirants, cathode ray tubes, catalysts, fire resistant fabrics, ceramics, foundry sands and jewellery [2]. Only a small percentage of the zirconium produced every year is refined into the pure metal, most of which is used in the nuclear industry [2]. China is currently the world's largest consumer of zircon and zirconium chemicals, primarily due to its large ceramics industry and the modernisation of its foundry casting techniques. Following China are India, the USA and Europe, with the biggest producers of zircon being centred in Australia and South Africa. World production of zirconium mineral concentrates increased from a low in 2005 of 1.15 million tons per year to 1.3 million tons per year in 2010. The biggest producers were Iluka Resources in Australia and the USA, Richards Bay Minerals in South Africa and Exxaro Resources, also in South Africa. Combined, these three firms were responsible for the production of 794 thousand tons of zirconium minerals in 2010, over 61% of total production.

In 2010 the average export price of zircon ore was between $650 and $850 USD per metric ton, rising to nearly $1400 in 2011 for prime grade zircon concentrate. By contrast as of May 2013 99% zirconium metal sells for an average price of approximately $35 000 per ton [3]. The Advanced Metals Initiative was begun by the South African Department of Science and Technology to develop local knowledge and expertise to beneficiate, amongst other materials, this zircon ore.

Zirconium metal is primarily refined by means of various techniques, usually using zircon ore as starting material. Zircon ore is generally found and mined in conjunction with titanium ores such as rutile and ilmenite [4]. Zircon ore is almost completely

chemically inert due to its crystal structure of interlocking zirconium dioxide dodecahedra and silica tetrahedral, as can be seen in **Figure 1-1**.

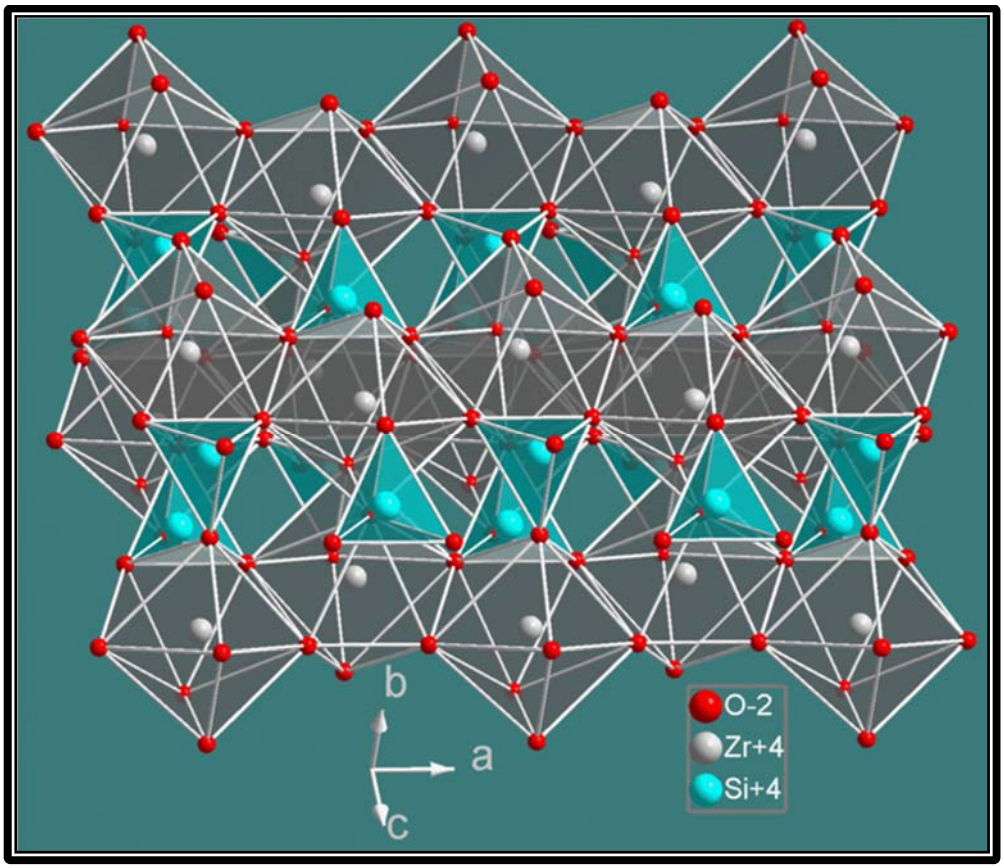

Figure 1-1: Representation of zircon crystal structure [5]

Zirconium metal is used primarily in the nuclear industry as a cladding material to protect the nuclear fuel, e.g. uranium dioxide, from the conditions within the reactor. It is useful in this role due to its good mechanical properties, resistance to corrosion and low thermal neutron capture cross-section [6]. The preparation of pure zirconium metal for nuclear application is difficult due to the non-reactivity of zirconium minerals, such as zircon and baddeleyite [2], and is further complicated by the contamination of all naturally occurring zirconium minerals with between 1 and 4% hafnium, an element with almost identical chemical behaviour to zirconium. Due to its high thermal neutron capture cross-section, hafnium (104 barns) must be almost completely removed (< 0.01%) before zirconium metal can be used for nuclear application. In the production of nuclear grade zirconium metal the hafnium is removed from the zirconium halide using a liquid-liquid extraction process which often requires multiple steps for a complete separation. The fluorides can then be converted using a variation of the Kroll process. This process was originally designed for the production of ductile titanium,

but can be used for converting the zirconium fluorides into into metallic zirconium [7]. When used in nuclear applications, the zirconium metal is alloyed with other metals such as tin, niobium and chromium. These alloys are usually referred to by their trade names, such as Zircaloy amongst others, and are also often used in the storage of nuclear waste materials.

Zircon ore is often converted to a more amenable form by rapidly heating the mineral to high temperatures (above its melting point) before rapidly cooling it to ambient temperatures. This heating process destroys the natural crystal structure of the ore and, upon cooling, results in amorphous silica embedded with small zirconia crystallites. This dissociated zirconia can then be treated with acid (or high temperature alkali), separated from the silica and converted to more useful zirconium chemicals, such as the fluorides, phosphates and oxychlorides [8].

1.2. PROBLEM DEFINITION

The ability to accurately analyse zirconium, its alloys, zircon as feed material, all intermediate and final products across the whole beneficiation chain is of crucial importance to the zirconium industry as a whole. Without this capacity it is impossible to gauge the relative success or failure of iterative steps in the purification of the zirconium compounds. It would likewise make the development of new processes for the processing of these materials extremely difficult. An accurate, precise and robust method for the quantification of various zirconium compounds is thus highly desirable. The development of such a technique is problematic, however, as the very properties which make these materials desirable also make quantification of their components extremely difficult. Many analytical procedures and techniques require that the sample be dissolved completely, a process that these materials are particularly resistant to. If they were not they would likewise not be suitable for their intended purpose.

1.3. AIMS AND OBJECTIVES

As stated previously zirconium metal used in the nuclear industry must conform to very strict specifications in terms of purity. It is crucial to the production of this material, as well as to the development of new production methods, to be able to analyse accurately for zirconium in the complete range of materials found in the production process. This range includes, but is not limited to, the chemically unreactive zircon mineral, the fluorozirconates, zirconium alloys and zirconium metal. Each of these presents different concerns with regard to sample preparation and analysis, with different obstacles and risks associated with each.

In this study the aim was to attack the problem from two directions. The first was to identify and develop a general dissolution method which would allow the analysis of these materials by such methods as require an aqueous sample matrix such as Inductively Coupled Plasma Optical Emission Spectroscopy (ICP-OES). The second was to develop a method capable of bypassing this dissolution requirement and analyse the solid sample as directly as possible by novel methods, such as Glow Discharge Optical Emission Spectroscopy (GD-OES), which to this point was not used for the analysis of zirconium-containing powders. Factors like time, safety and environmental friendliness were also considered as ideally these methods would eventually be applied to an industrial process.

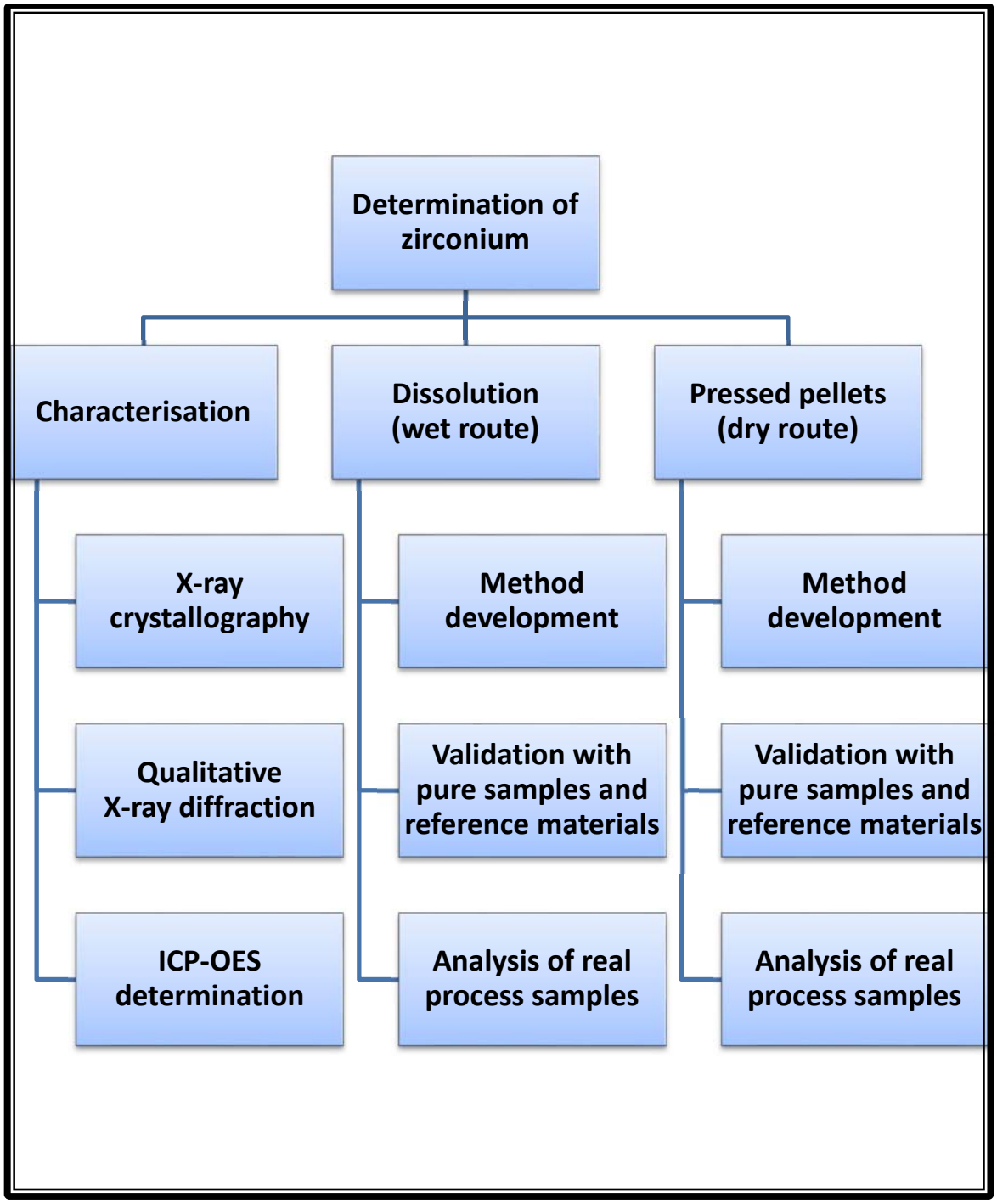

Figure 1-2: Research plan

The main objective of this study was to develop a robust, rapid and accurate method for the analysis of zirconium materials. A schematic layout of the intended research is given in **Figure 1-2**. The specific aims were:

1. Preparation of reference materials for specific compounds that were not commercially available. Crystallisation of complexes such as K_2ZrF_6, Cs_2ZrF_6, Li_2ZrF_6, Na_2ZrF_6, $CaZrF_6$, tetraethylammonium hexafluorozirconate,

tetramethylammonium hexafluorozirconate, tetrabutylammonium hexafluorozirconate, tetraphenylarsonium hexafluorozirconate and tetraphenylphosphonium hexafluorozirconate was attempted as crystals are by definition pure compounds.

2. Thorough characterisation of the newly synthesized crystalline materials mentioned in **Point 1** by such methods as X-ray crystallography and X-ray diffraction (XRD).
3. Evaluation of literature methods previously found to be successful in the analysis of various zirconium compounds and materials. Digestion methods such as acid dissolution, flux fusion and microwave-assisted acid digestion as well as quantification methods like atomic absorption spectrometry (AAS), graphite furnace atomic absorption spectrometry (GF-AAS), UV/VIS spectrophotometry, X-ray fluorescence (XRF), inductively coupled plasma mass spectrometry (ICP-MS) and ICP-OES were to be researched.
4. Identification of new analytical methods and techniques in sample preparation and determination such as powder pressing using various matrices and GD-OES with both direct current (DC) and radio frequency (RF) glow discharge lamps. Scanning electron microscopy (SEM) and energy dispersive X-ray spectroscopy (EDS) would be used for the characterisation of the surface of and glow discharge crater on solid pellets.
5. Method development using the most promising techniques identified in **Points 3** and **4**. Methods would be assessed using certified reference materials, new reference materials characterised and produced in-house as well as commercially available compounds.
6. Statistical evaluation of results for reference materials by evaluation of R^2 values, t-statistics, standard deviations, detection and quantification limits and instrument sensitivity and selectivity.
7. Comparison of these methods and techniques and application to real process samples, with focus on speed, precision, accuracy, robustness and safety.

Chapter 2: Introduction to Zirconium

2.1. INTRODUCTION

Zircon can be found in the production of many ceramic glazes and enamels and is a primary component in several colourful pigments including Vanadium Yellow (ZrO_2-V_2O_5), Turkey Blue (ZrO_2-V_2O_5-SiO_2-Na_2O) and Praseodymium Yellow (ZrO_2-Pr_6O_{11}-SiO_2), seen in **Figure 2-1**.

Figure 2-1: Samples of: (a) $Ce_{0.43}Zr_{0.37}La_{0.20}O_{1.90}$, (b) $Ce_{0.43}Zr_{0.37}Bi_{0.20}O_{1.90}$, and (c) commercial praseodymium yellow [9]

Zirconium chemicals like zirconium orthosulphate, zirconium oxychloride, zirconium basic carbonate and zirconium acid carbonate are used in paints, pigment coatings, leather tanning and inks. Aluminium zirconium chlorohydrates are used in antiperspirants and zirconium halides are used in textile production. Zirconium compounds are also used in the automotive industry in the production of catalytic converters as a substrate for the active catalyst. The zirconium chemical industry is concentrated primarily in China (approximately 90%) [10] and the remainder is situated largely in India, the USA and Europe [2].

Although most of the zirconium produced finds use in the form of its chemical compounds such as the oxide and chlorohydrates, a small amount is processed into zirconium metal where it finds use primarily in the nuclear industry. Here its low thermal neutron capture cross-section, very high resistance to corrosive attack and mechanical strength when alloyed make it an excellent fuel cladding material.

2.2. THE MINERAL ZIRCON

Zircon is commonly found in a variety of colours ranging between green, yellow, red, brown and blue. It has a Mohs' hardness of 7.5 and a variable specific gravity of between 4.2 and 4.8. [8] Due to its extraordinarily high index of refraction and birefringence, zircon was primarily used as a gemstone in ancient and medieval times [1]. Depending on their colour and transparency these gems have been known as *hyacinths*, *jacinths*, *jargons*, *Matara diamonds*, and simply *white zircons,* see **Figure 2-2**.

Figure 2-2: A gem quality zircon [11]

Zircon ore is one of several products obtained from the mining of what are called heavy minerals. The main constituent element of these heavy minerals is usually titanium in the form of ilmenite, rutile and leuxocene with zircon being a relatively minor side-product extraction of titanium from these ores. These minerals are usually found in the form of beach sand with early phases of beneficiation making use of spiral concentrators (silica removal), see **Figure 2-3**, and magnetic and electrostatic separators (ilmenite and rutile removal) [8]. Depending on the quality of the raw zircon further processing may be required. This can include processes such as attrition to remove organic or clay coatings and acid leaching to remove iron coatings on the surface of the grains. Zircon flour and opacifier products are produced by milling (micronising). Zircon output is concentrated primarily in three countries, namely Australia, South Africa and the USA, see **Table 2-1**. In these areas the actual mining

is done by a few companies with only Richard's Bay Minerals and Exxaro Resources being active in South Africa [2].

Table 2-1: World reported production of zirconium mineral concentrates by company, 2004-2010 (000t) [2]

Company	Country	2004	2005	2006	2007	2008	2009	2010
Iluka Resources	Australia	327	322	363	447	356	231	355
	USA	76	99	83	81	85	48	58
	Subtotal	*403*	*421*	*446*	*528*	*441*	*279*	*413*
Richards Bay Minerals[1]	South Africa	211	138	236	240	240	240	220
Exxaro Resources	South Africa	168	176	178	149	164	152	161
Bemax Resources	Australia	21	20	38	…	…	62	…
	Brazil	20	20	22	23	24	25	22
	Subtotal	*41*	*40*	*60*	*23*	*24*	*87*	*22*
Tiwest	Australia	76	70	72	72	58	66	70
DuPont	USA	70	65	60	40	38	32	42
Kenmare Resources	Mozambique	-	-	-	…	…	…	37
Consolidated Rutile	Australia	43	27	53	61	53	130	…
India Rare Earths[2]	India	24	23	25	19	26	19	…
Matilda Zircon	Australia	-	-	-	-	-	-	120
Kovdorsky	Russia	7	7	8	8	7	5	8
V. V. Mineral	India	-	-	-	-	8	7	…
Kerala Minerals & Metals	India	2	2	2	2	2	2	…
Lanka Mineral Sands	Sri Lanka	13	24	8	0	1	10	10
Total listed		1,058	993	1,148	1,142	1,062	929	1,003
World production		1,190	1,152	1,324	1,447	1,349	1,174	1,298
% accounted for		88.9	86.2	86.7	78.9	78.7	79.1	77.3

Notes: 1 - Estimated

2 - Years ending April 30th of that stated

Currently, of the many zirconium-containing minerals, only zircon and baddeleyite are of any commercial value due to the size and accessibility of the deposits. Eudialyte is also a potential commercial source of zirconium but to date only small quantities have been mined, mostly in Russia's Kola Peninsula.

Zircon always contains a small quantity of hafnium in the crystal structure, generally reported as hafnia (HfO_2) in quantities of between 1 and 4%. Zircon is inert to chemical

and highly resistant to mechanical weathering but does undergo metamictisation (break down of crystal structure because of radioactive decay) due to its thorium and uranium content, these radioactive elements usually occurring in concentrations of less than 500 ppm in zircon ore [2]. In conjunction with the said breakdown in crystal structure through irradiation, small impurities of other elements are chiefly responsible for the colouration of zircon crystals which are of gemstone quality. Some varieties however, such as the blue *starlites*, gain their colouration after heat treatment.

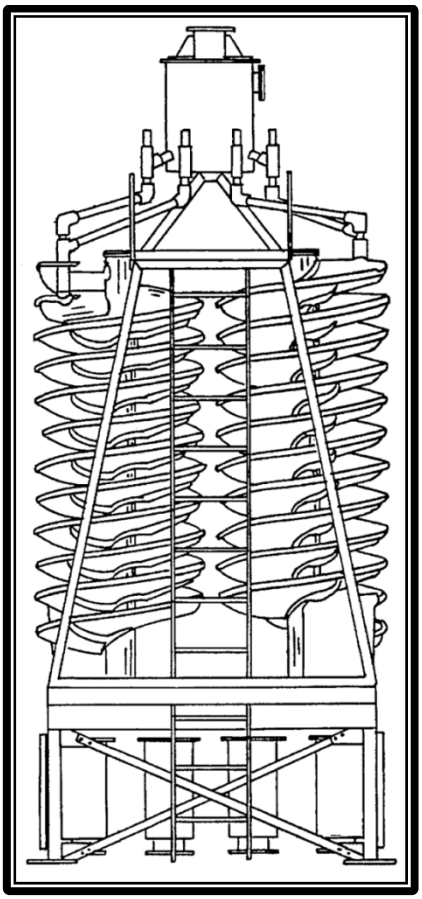

Figure 2-3: Diagram of a spiral concentrator [12]

As stated previously, China is the world's largest consumer of zircon, using the mineral largely as an opacifier in the manufacturing of ceramics with an estimated consumption of 400,000 tons in 2010. Although the worldwide demand for zircon decreased slightly in 2009 China's increase in production of ceramics has been the primary influence in its recovery and rise since 2010. Compared to this the worldwide zirconium chemical industry, which is also predominantly situated in China, only produces approximately 300,000 tons per year of other zirconium materials, of which the majority is the oxychloride compound. In the early years of zircon production grades were primarily distinguished by iron content. Zircon with an iron content of less than 0.06% Fe_2O_3 was

considered to be “premium” grade while all other zircon was labelled “standard” grade. Today commercially available zircon is marketed in several different grades, namely premium, standard, foundry, intermediate, ceramic and refractory grade, depending on purity, zirconium and hafnium content, titanium content, iron content and particle size [2, pp. 13-14].

Zircon is also used extensively in the casting industry as foundry sand with the automotive sector being the largest consumer of these casting sands. However, due to zircon being an expensive niche commodity, it is extensively recycled whenever possible and thus this industry has little effect on worldwide demand and consumption. Lately the increasing use of more advanced casting methods in China has stimulated the increased use of zircon as foundry sand, causing a small increase in demand in the market. The zircon-sand moulds are preferred over quartz-sand ones as their thermal shock resistance and dimensional stability are higher with the added benefit that they are less easily wetted by molten metal consequently producing smoother surfaces in castings [13].

The global consumption of zircon in ceramics is expected to increase significantly with projections indicating a 5.4% increase per year, driven primarily by demand from China. This will result in the total consumption of 1.33 Mt in 2010 rising to approximately 1.7 Mt by 2015. **Table 2-1** shows the total production of zirconium mineral concentrates worldwide by the largest relevant companies. As of 2013 the global production of zircon was reported as 1.44 Mt with the bulk (600 000 tons) being produced in Australia and South Africa (360 000 tons) [14].

2.3. THE CHEMISTRY OF ZIRCON

Zircon, as a mineral, is almost completely chemically inert. This is due to the resistance of the metal oxides to reduction, making the mineral almost completely unreactive to most reagents. This has resulted in it being found in certain beach sands derived from pegmatitic and granitic rocks which have been weathered down and eroded, a predominantly mechanical process.

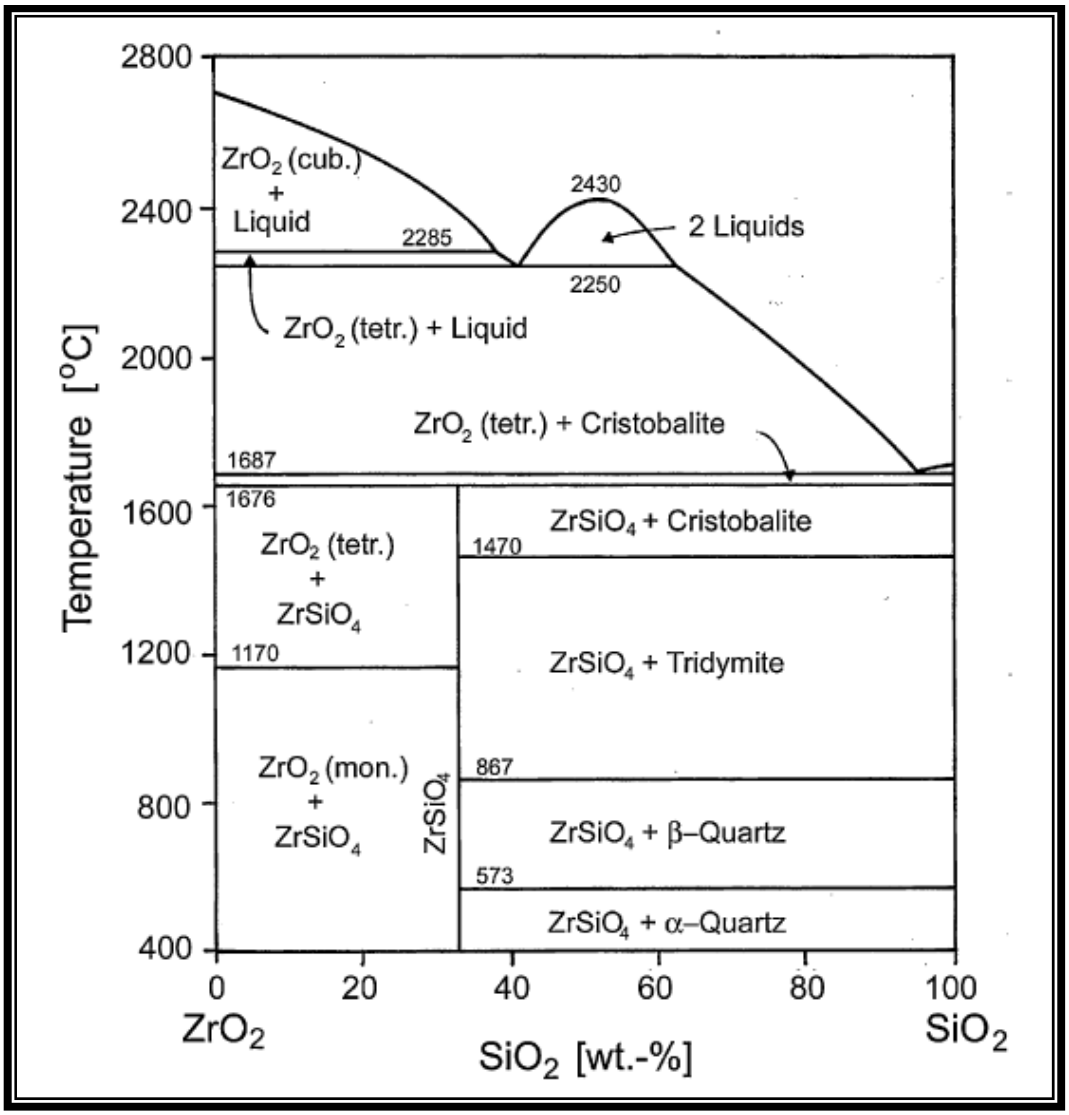

Figure 2-4: Phase diagram of zircon [15]

The chemical composition of zircon can be described by the general formula $ZrO_2 \cdot SiO_2$ and it forms a tetragonal crystal structure, see **Figure 1-1**. This gives rise to a chain of alternating silica tetrahedra and zirconia dodecahedra with each successive pair of oxygen atoms arranged transversely to the previous pair. The entire structure is bonded by coordination covalencies acting between the oxygen and zirconium atoms of neighbouring chains. This crystalline structure only begins to break down when subjected to temperatures above 1550°C or radiation. Dissolution can take place at lower temperatures, however, with appropriate reagents.

A phase diagram of zircon can be seen in **Figure 2-4**. The processing of raw zircon, which is made up of approximately two-thirds ZrO_2, requires the heating of the mineral to extremely high temperatures with rapid subsequent cooling, in order to separate the $ZrSiO_4$ into separate ZrO_2 (zirconia) and SiO_2 (silica) phases [2]. The rapid cooling

yields fine, dendritic zirconia crystals trapped in an amorphous silica matrix. This can be achieved using an arc furnace (2000°C), inductively coupled plasmas and similar techniques [16]. From the phase diagram seen in **Figure 2-4** it can be seen that this process converts the silica into a liquid phase containing the still-crystalline zirconia. The rapid cooling does not allow the original crystal structure to reform. Thus after such a heating process the stock material can be treated as a simple mixture of zirconia and silica [6], each of which alone is far more amenable to chemical treatment than the original zircon especially toward fluorine-containing chemicals. Other conventional chemical processes include carbochlorination, alkali fusion, chemical precipitation or hydrofluoric acid digestion. The heat conversion, however, is never 100% complete which results in a small quantity of inert zircon remaining behind after chemical dissolution. This remaining zircon will thus not take part in subsequent chemical reactions and this must be accounted for in beneficiation procedures.

Figure 2-5: Dendritic zirconia [17]

The carbochlorination of zircon, **Equation 2-1**, is the most common first step in the preparation of nuclear grade zirconium metal from zircon ore [18]. This process is applicable to both zircon and baddeleyite (ZrO_2) and converts the metal oxide to the tetrachloride.

$$ZrSiO_4(s) + 4C(s) + 8Cl_2(g) \xrightarrow[\Delta(900°C)]{} ZrCl_4(g) + SiCl_4(g) + 4CO(g) \qquad \textbf{2-1}$$

The zirconium tetrachloride can then be reduced to the zirconium metal by a variation on the Kroll process, **Equation 2-2** [7].

$$ZrCl_4 + 2Mg \xrightarrow[\Delta(1100^oC)]{} 2MgCl_2 + Zr \qquad \textbf{2-2}$$

Another route for the production of zirconium metal begins with dissociated zircon being converted to the acid halide using hydrofluoric acid in the following reaction, **Equation 2-3** [19].

$$ZrO_2{\cdot}SiO_2(s) + 12HF \rightarrow H_2ZrF_6 + H_2SiF_6 + 4H_2O \qquad \textbf{2-3}$$

Commonly the H_2SiF_6 is removed from the slurry by evaporation and the remaining H_2ZrF_6 is then decomposed to ZrO_2, through heating in an oxidising atmosphere, for further processing or reduced to the metal as in **Equation 2-2**.

Chemical precipitation of zircon in the production of zirconia (ZrO_2) involves the reaction of the mineral with either sodium hydroxide at 600°C or sodium carbonate at 1000°C (e.g. **Equation 2-4** [20]). This process is sometimes referred to as the "wet chemical" production method.

$$ZrSiO_4(s) + 4NaOH(s) \xrightarrow[\Delta(600°C)]{} Na_2SiO_3(s) + Na_2ZrO_3(s) + 2H_2O(g) \qquad \textbf{2-4}$$

The alkaline process, seen in **Equation 2-5** [20], is another commonly used procedure in which zircon sand is fused with calcium carbonate or dolomite at 1600°C in an electric furnace or gas-fired rotary kiln to form zirconia and calcium silicate. The calcium silicate is removed by leaching with hydrochloric acid and the zirconia is then washed and dried. This process is most commonly used when calcium- or magnesium-stabilised zirconia is required as a refractory.

$$2ZrSiO_4(s) + 5CaCO_3(s) \xrightarrow[\Delta(1600°C)]{} 2CaZrO_3(s) + (CaO)_3(SiO_2)_2(s) + CO_2(g) \qquad \textbf{2-5}$$

Zircon, in both its natural and its dissociated form, is also susceptible to attack by molten lithium tetraborate at 1100°C [21]. This has little application in the production of zirconium materials but is extremely useful in the analysis of said minerals and zirconium oxides. A fusion using lithium tetraborate allows for the production of homogenous glass discs for X-ray fluorescence (XRF) analysis and the subsequent dissolution in dilute acid allows for the use of techniques such as inductively coupled plasma optical emission spectrometry (ICP-OES). A major advantage of a borate fusion over alkali fusions is that silica content does not precipitate out upon acid dissolution. The use of dangerous hydrofluoric acid is also avoided in analytical

methods using this as a sample preparation procedure which, in turn, avoids damage to the glass components of ICP-OES/MS systems from fluoride ions.

2.4. Purification and Uses of Zirconium Materials

The primary use of zirconium metal is in the nuclear industry as a cladding material for fuel rods [16]. It is useful in this application due to its low thermal neutron capture cross-section (0.184 barns) as well as its high resistance to corrosive attack from most acids and alkalis as well as saline solutions and certain molten salts. This resistance is a result of a protective, self-healing oxide layer that forms on the surface of the metal which can also withstand temperatures of up to 300°C. Zirconium metal also exhibits adequate mechanical strength to withstand the harsh conditions prevalent inside nuclear reactors. **Figure 2-6** shows an example of nuclear fuel in a Zircaloy casing.

Figure 2-6: Uranium dioxide fuel in Zircaloy cladding [22]

However, due to the inevitable hafnium contamination found in all zircon, the metal must first be purified before it can be used for nuclear application. Hafnium (104 barns) has a thermal neutron capture cross-section nearly six hundred times greater than zirconium with the result that even a small amount of hafnium as impurity in zirconium metal renders it useless for nuclear application. In order to remove this hafnium a mixture of zirconium chloride and hafnium chloride is commonly subjected to a solvent extraction process [23]. The metal chloride is contacted with ammonium thiocyanate and then fed into an extraction solution containing hydrochloric acid and methyl

isobutyl ketone (MIBK). This is generally a multi-step sequential process wherein each successive step yields a more purified zirconium-containing mixture as the hafnium is gradually removed from the solution. This arduous process is necessitated by the chemical similarity of zirconium and hafnium, their chemistry being the two most similar elements of any on the periodic table.

An alternative purification process was developed at Iowa State University. In this process a feed liquor containing zirconium in nitric acid is contacted with a 50% solution of tributyl phosphate in *n*-heptane [24]. Hafnium and other impurities are then back-scrubbed with nitric acid after which the zirconium is recovered by scrubbing the organic phase with deionised water. This process, while capable of producing high-purity zirconium metal, is reportedly less efficient in the simultaneous production of a high-purity hafnium metal side-product as too much zirconium remains behind in the hafnium fraction.

Table 2-2: Standard specification for zirconium and zirconium alloy ingots for nuclear application [25]

	Maximum impurities (mass percentage)				
Element	UNS R60001	UNS R60802	UNS R60804	UNS R60901	UNS60904
Al	0.0075	0.0075	0.0075	0.0075	0.0075
B	0.00005	0.00005	0.00005	0.00005	0.00005
Cd	0.00005	0.00005	0.00005	0.00005	0.00005
Ca	---	0.003	0.003	---	---
C	0.027	0.027	0.027	0.027	0.027
Cr	0.02	---	---	0.02	0.02
Co	0.002	0.002	0.002	0.002	0.002
Cu	0.005	0.005	0.005	0.005	0.005
Hf	0.01	0.01	0.01	0.01	0.01
H	0.0025	0.0025	0.0025	0.0025	0.0025
Fe	0.15	---	---	0.15	0.15
Mg	0.002	0.002	0.002	0.002	0.002
Mn	0.005	0.005	0.005	0.005	0.005
Mo	0.005	0.005	0.005	0.005	0.005
Ni	0.007	---	0.007	0.007	0.007
Nb	---	0.01	0.01	---	*
N	0.008	0.008	0.008	0.008	0.008
P	---	---	---	0.002	0.002
Si	0.012	0.12	0.12	0.012	0.012
Sn	0.005	---	---	0.01	0.01
W	0.01	0.01	0.01	0.01	0.01
Ti	0.005	0.005	0.005	0.005	0.005
U	0.00035	0.00035	0.00035	0.00035	0.00035

* R60904 is an alloy containing 2.5% niobium as an alloying metal and is thus not reported as an impurity.

In order for it to be useful in a nuclear reactor, zirconium metal is almost always alloyed with various other metals, most commonly tin and chromium. These alloys, notably Zircaloy-2 (R60802), Zircaloy-4 (R60804) and Zr-2.5Nb (R60904), conform to the composition values given in **Table 2-2**. In recent years newer zirconium alloys, for instance Zircadyne, have been brought to market containing small quantities of niobium as alloying agent. For the same reason that these alloys are useful in the cladding of active fuel, they are also often used in the storage and containment of nuclear waste [26].

Zirconium as an alloying agent has also been used in the production of zirconium-niobium superconductors, high strength copper alloys and titanium aircraft alloys. The analysis of impurities and alloying agents in the pure metal is of prime importance in the production of these alloys. Determination of impurity levels in a zirconium-rich matrix as low as one tenth the quantities seen in **Table 2-2** is possible using ICP-OES techniques for all metallic elements with the exception of boron, cadmium and uranium [27]. These three elements yielded poor recovery values due to their being analysed at close to their lower limits of quantification (LLOQ) with the method employed.

Zirconium metal has also been found to be extremely useful as a minor alloying agent in the production of magnesium-based components in the automotive industry [28]. In quantities as low as 0.56% it has been shown that the addition of zirconium exhibits an exceptional grain-refinement effect as compared to pure magnesium, see **Figure 2-7**. This is achieved by the zirconium acting as a nucleant, creating a much finer microstructure than is achievable solely with magnesium. This demonstrates great potential for the strengthening of these alloys.

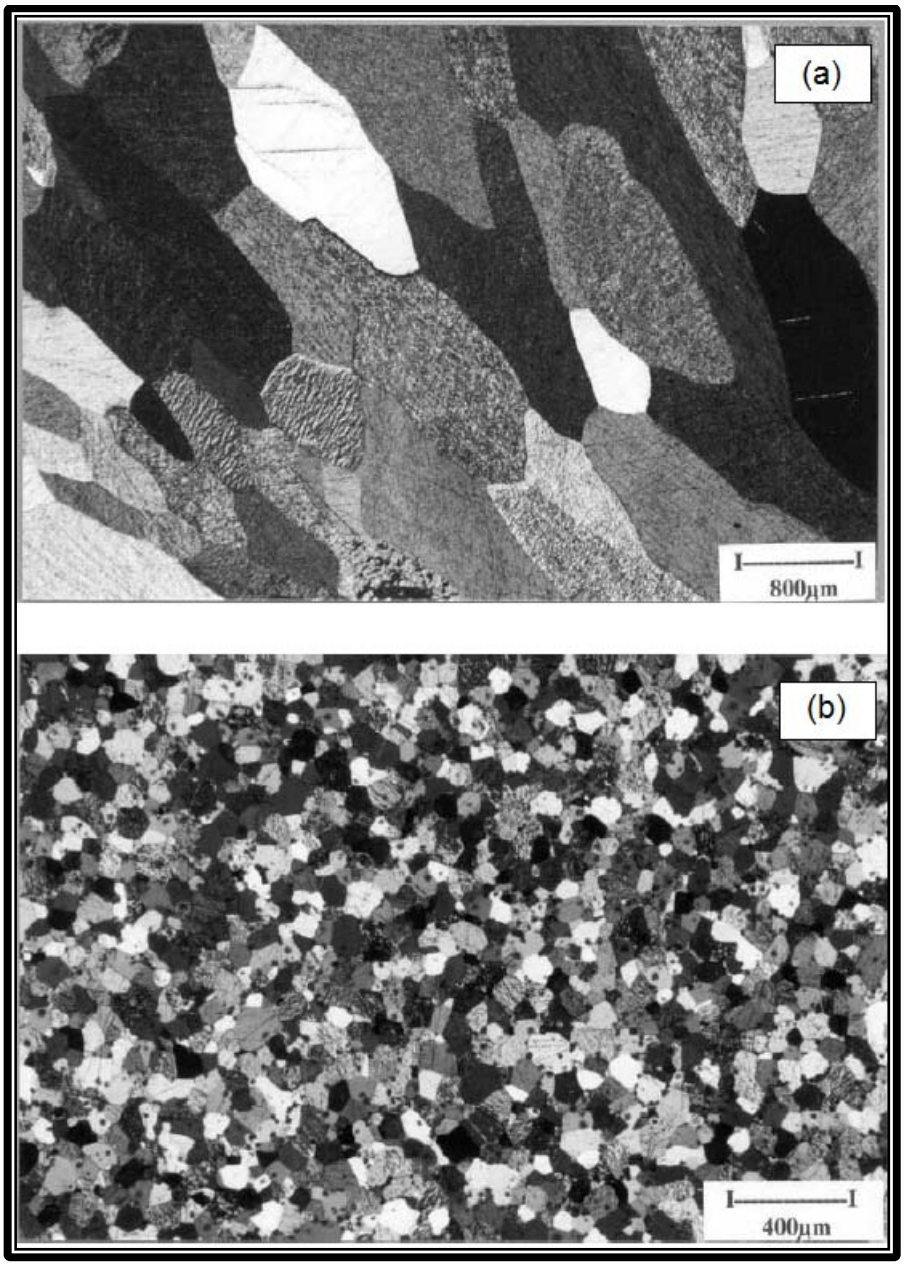

Figure 2-7: Optical micrographs showing grain size of (a) pure magnesium metal and (b) magnesium metal with 0.56% zirconium.

Zirconium oxide and tetrafluoride are used in the manufacture of certain glasses, with the tetrafluoride specifically being used in the first glasses developed to exhibit continuous high transparency from the ultraviolet to the mid-infrared range. In applications where the extreme corrosion resistance of the zirconium oxide is the primary quality of interest, yttrium oxide is sometimes added as a stabilising agent [29]. This results in a compound which is even more chemically resistant than basic zirconium oxide and which has the added mechanical benefit of decreasing the level of brittleness of the material. Yttria stabilised zirconia also exhibits piezoelectric properties which are dependent on the partial pressure of oxygen in surrounding

gases. As such yttria-stabilised cubic zirconia has been used in oxygen sensors in automotive exhausts as well as oxygen probes in molten copper and iron smelters. Stabilised zirconia has also found use in high temperature fuel cells, ceramic tubing, high-temperature heating elements, thermal barrier coatings and non-lubricated ball bearing assemblies used in space vehicles [13].

The use of zirconium oxide in the production of biomorphic ceramics has also been investigated in recent years [30]. These materials combine the physical and structural properties of biological materials, such as wood, with the chemical and thermal properties of ceramics. In one study vacuum infiltration and successive drying and annealing processes were used in order to impregnate the starting material (Oak) with a zirconyl chloride solution and subsequently to oxidise this to zirconium dioxide along with the removal of biological material such as cellulose and lignin. This process is detailed in **Figure 2-8**. Among the uses for materials such as these are catalyst supports, tooling and wear components, armour, automotive components and lightweight, porous ceramics for aerospace systems.

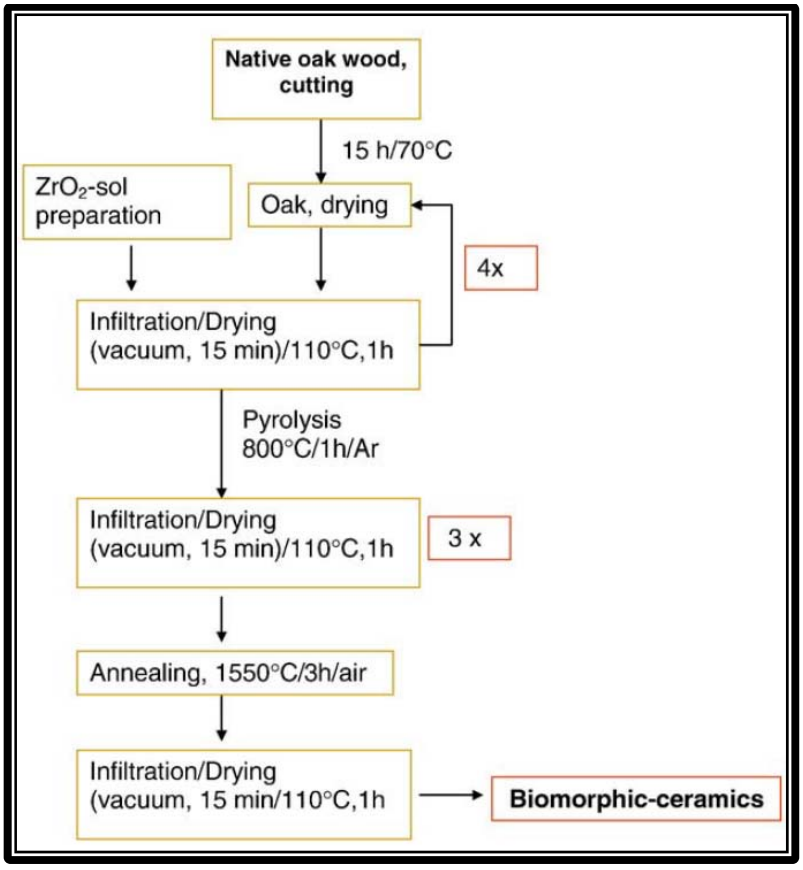

Figure 2-8: Flow chart for the manufacturing of a biomorphic zirconia ceramic [30]

The insoluble organometallic zirconium compound ammonium zirconium carbonate (NH_4ZrCO_3) has been used to enhance the fungicidal effect of copper salts in the textile industry and both this compound and zirconium acetate have been used in the manufacture of waterproof fabrics [13]. Potassium hexafluorozirconate, on the other hand, has been used in the manufacture of fire-resistant wool fabric. Zirconium sulphate is preferred over chromium salts in the tanning of leather in the production of white leathers. Zirconium carbonate has also been used in the production of acrylic-emulsion floor polishes as it is easily stripped by aqueous ammonia. Zirconium sulphate has further been used in the preparation of catalysts for the hydrogenation of vegetable oil.

Another interesting application is the use of sodium hydrogen zirconium phosphate in portable kidney dialysis machines as an ion-exchange material [13]. The urea picked up during dialysis reacts with urease to form ammonia which is absorbed by the sodium hydrogen zirconium phosphate. Zirconium phosphate also has a nuclear application in that it has been proposed to form part of permanent disposal systems of nuclear fuel waste as it absorbs caesium and other radioactive-decay products.

Due to its flammable nature, pure zirconium has been used in military ordnance including delay fuses, pyrophoric shrapnel, percussion-primer compositions and tracer rounds [13]. This attribute has also found civilian use in getters for vacuum tubes, inert-gas glove boxes and in the production of flashbulbs for photography although newer technology has made some of these uses nearly obsolete.

Thin films of lead zirconate-titanate, chemical structure $PbZr_{1-x}Ti_xO_3$, have been investigated for their interesting electrical properties [31]. These films belong to a class of materials known as perovskites and are characterised by their specific crystal structure. Their electronic properties make them useful in the development of dynamic and ferroelectric random access memory (DRAM and FERAM) components, micro-electromechanical systems (MEMS) and in the field of smart textiles and wearable computing [32]. These films are produced on relevant substrates by both physical (sputtering and pulsed laser deposition) and chemical (chemical vapour and solution deposition) methods, see **Figure 2-9**. The piezoelectric properties of perovskite materials are highly dependent on the thin film layer being chemically homogenous throughout the entire film depth and the crystal structure being well developed.

Figure 2-9: Lead zirconate-titanate thin films on 6 and 8 inch silicon substrates by Fujifilm [33]

Zirconium and titanium, amongst other elements, have been investigated for possible use in conversion coatings for aluminium alloys to replace chromate treatments due to the toxicity and carcinogenic nature of Cr(VI) [34]. Aluminium is susceptible to localised corrosion due to the formation of intermetallic compounds, thus necessitating the application of a protective layer. The excellent corrosion resistance of zirconium compounds makes them ideal for this type of application.

Zirconium oxide is also useful in the field of catalysis where it is used both as a catalyst support and as a catalyst itself [35]. It is active in catalytic reactions including the catalytic reduction of ketones and aldehydes with 2-propanol and the hydrogenation reactions of aromatic carboxylic acids. As a support it is used in the Fischer-Tropsch synthesis of alkenes using a nickel catalyst as well as in the isomerization of light alkanes by the strong solid acid tungsten oxide. Cerium-zirconium mixed oxides have been used in three-way catalysts in the automotive industry owing to their ability to store oxygen and the ability of the zirconium oxide to inhibit sintering, thus providing greater thermal stability of the catalyst.

2.5. THE CHEMISTRY OF ZIRCONIUM AND ITS COMPOUNDS

Zirconium is a group IV transition element, along with titanium and hafnium, both of which have similar chemical and mechanical characteristics. The existence of zirconium as a novel element was first proposed by M.H. Klaproth in 1789 [1]. After fusing zircon specimens from Ceylon with sodium hydroxide, he extracted a product with hydrochloric acid which exhibited a novel behaviour. It was not until 1824 though that J.J. Berzelius succeeded in isolating elementary zirconium, albeit impure, by heating a mixture of potassium hexafluorozirconate and potassium metal in a closed iron tube inside a platinum crucible. It was later found, by Weiss and Neumann, that a modification of this procedure by using absolute alcohol as washing agent instead of water could raise the purity of the resultant metal from 93.7% to 98%. Later improvements to this method would yield products reaching 99.3% purity.

It was not until 1922 that it was discovered that all zirconium recovered from the lithosphere contains a small quantity of hafnium, which was until then an unknown element [1]. Up until this point there had been several unconfirmed indications of another element possibly present in zircon with chemical behaviour so similar to zirconium as to make them almost indistinguishable. Various names were given to this novel element including *ostranium*, *noria*, *jargonia*, and *euxenia*. The existence of hafnium was finally confirmed after a careful X-ray study of zircon as this was the most likely mineral to contain the element based on general statistics of abundance of elements and the demands of quantum theory.

Figure 2-10: Zirconium metal ingots [36]

As a metal, see **Figure 2-10**, zirconium is grey/white, soft, ductile and malleable but at a purity of higher than 99%, produced through a high temperature process, it becomes brittle and hard [8]. Amorphous zirconium powder is bluish-black. It has an atomic mass of 91.22 and a density of 6.5107 g/cm^3 at 25°C with melting and boiling temperatures of 2125 and 4577°C respectively. Through the process of hot-working, zirconium metal ingots can be re-shaped into bars and rods without the negative property of strain hardening that normally occurs, this being done to maintain beneficial hardness and ductility properties. Like aluminium, zirconium forms a protective oxide layer [8]. Without this layer zirconium plate ignites spontaneously in oxygen at pressures of around 2 MPa and pure zirconium powder ignites easily upon contact with oxygen unless preconditioned. The metal zirconium is ranked as the 19th most abundant element found in the earth's crust with an average content of 0.026% in igneous rocks.

As an element or in compounds, zirconium is generally non-toxic as it generally exists as the dioxide under pH conditions associated with biological activity. ZrO_2 is insoluble in water and thus is physiologically inert [13]. The metal powder, however, does present a danger in that it can be extremely flammable and even pyrophoric when not treated properly before exposure to an oxygen-containing atmosphere. Very fine zirconium dust has been known to ignite upon contact with air and unexpected ignitions have occurred resulting in fatal flash burns to those working with the material.

Zirconium's high resistance to corrosion is attributed to the dense oxide layer found on its surface under ordinary conditions [13]. This layer is resistant to chemical attack by water, steam, organic acids, most mineral acids, strong alkalis, molten salts and salt solutions. An exception to this is acids and salts containing fluorides which readily attack the metal and its oxide to form fluorozirconates. Other halide acids have little to no effect, however, and even with the addition of oxidising agents, cupric or ferric ions for instance, only pitting is observed. Zirconium exhibits complete resistance to boiling sulphuric acid in concentrations as high as 70 wt%. Similarly nitric acid has no effect in concentrations up to 98 wt% and temperatures below 250°C. It is completely unaffected by caustics up to boiling temperatures and is resistant to molten sodium hydroxide up to temperatures of 600°C. Zirconium also exhibits complete resistance to organic acid attack and has been used for periods of over twenty years as a construction material in urea production plants.

Table 2-3: Selected examples of zirconium compounds in various oxidation states [37]

Oxidation state	Example
0	**metal**, $Zr(CO)_7$, **$Zr(2,2'\text{-bipyridyl})_3$**, $[Zr(SnMe_3)_2(CO)_5]^{2-}$, **$[K(15\text{-crown-}5)_2]_2[Zr(SnMe_3)_2(CO)_5]$**, $Zr(MeNCH_2CH_2)_3(CO)_4$
+2	ZrI_2, **$ZrCl_2$** [1], $Zr_2I_4(\eta^6\text{-}PhPMe_2)_2(PMe_2Ph)_2$, **$Zr_6Cl_{12}(PMe_2Ph)_6$**, $Zr(C_5H_5BPh)_2(PMe_3)_2$, **$[Pr^n{}_4N]_2[Zr(SnPh_3)_4(CO)_4]$**
+3	ZrN, **ZrI_3**, $ZrBr_3$, **$ZrCl_3(NH_3)_6$**, $Zr_2Cl_6(Ph_2PCH_2CH_2PPh_2)_2$**,** **$[Zr(NH_3)_6]Br_3$**, $Zr_2I_6(PMe_2Ph)_4$, $Zr_2Cl_6(PMe_3)_4$
+4	ZrO_2, **$ZrOCl_2$**, ZrF_4, **$ZrCl_4(PMe_3)_2$**, $Zr(NMe_2)_3[Si(SiMe_3)_3]$, **$Zr(BH_3Me)_4$**, $[Ph_4P][ZrCl_5(NCMe)]$, **K_2ZrS_4**, $Zr[TeSi(SiMe_3)_3]_4(Me_2PCH_2CH_2PMe_2)_2$

The chemistry of both zirconium and hafnium is dominated by the 4+ oxidation state with neither forming simple cationic species. This is due to the $[Kr]4d^25s^2$ electron configuration of zirconium and the $[Xe]4f^{14}5d^26s^2$ configuration of hafnium as well as their almost identical atomic radii, a result of lanthanide contraction of hafnium. The loss of four electrons, 2 d and 2 s, allows these metals to assume noble gas electron configurations with the smallest net charge [38], explaining the prevalence of the 4+ state. Oxidation states higher than this require the removal of electrons from completely filled orbitals. Complexes with other oxidation numbers, i.e. 0, 2+ and 3+ have been characterised [39] but very few of those with the 3+ state and lower have been isolated [37]. The low oxidation state compounds are dominated by various organometallic zirconium complexes including bis(arenes), bipyridines and biphosphinines [40]. Several known compounds of zirconium in various oxidation states can be seen in **Table 2-3**.

The most common zirconium compounds used today are those containing oxygen, halogens, ammonia, water, carbonates and sulphates [38]. A large number of organometallic compounds with nitrogen and oxygen donor atoms have also been characterised. The most well-known and characterised complexes are generally *tetrakis* coordinated showing a large degree of diversity in coordination geometry. A

small number of complexes containing arsenic, phosphorus and carbon bonding atoms are known.

Industrially the most commonly found zirconium chemicals are zirconia (ZrO_2), zirconium oxychloride ($ZrOCl_2 \cdot 8H_2O$), zirconium basic sulphate ($Zr_5O_8(SO_4) \cdot xH_2O$), zirconium basic carbonate ($ZrOCO_3 \cdot xH_2O$), ammonium zirconium carbonate ($(NH_4)_2ZrO(CO_3)$) zirconium acetate ($H_2ZrO_2(C_2H_2O_2)_2$) and potassium hexafluorozirconate (K_2ZrF_6) [2]. Some of these chemicals can be used in the production of the metal sponge by a reduction process. They can also be used as precursors for creating a more pure zirconia by calcining in an oxygen-containing environment.

At elevated temperatures zirconium becomes highly reactive towards water, carbon, oxygen and nitrogen, easily forming the relevant oxide, carbide or nitride at temperatures above 500°C [1]. Contamination, even in small quantities, by these elements causes the crystal structure of metallic zirconium to change from a hexagonal close-packed crystal to a face-centred cubic type. In this state the physical and chemical properties of the metal become almost indistinguishable from those of zirconium carbide.

In aqueous solution, zirconium is always found to be in the 4+ state [13]. Zirconium compounds in aqueous solutions form polymeric substructures due to its high coordination numbers and slow hydrolysis equilibrium.

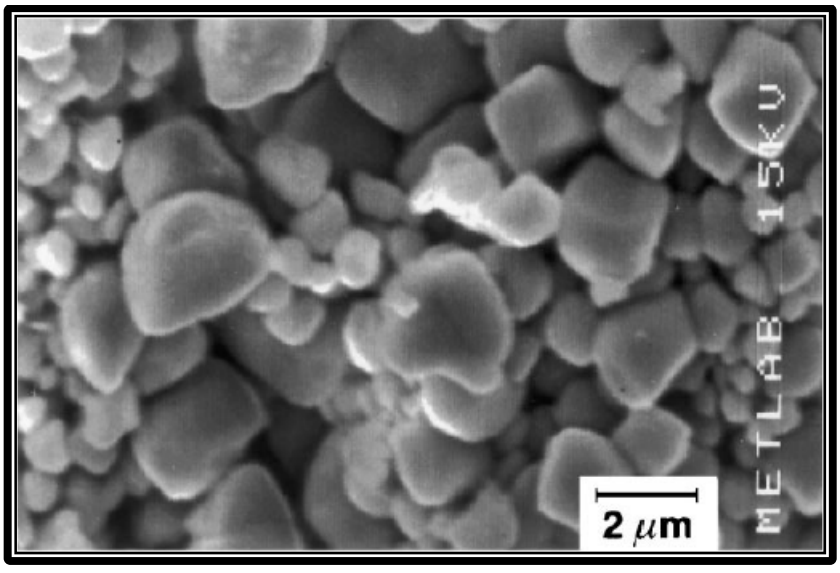

Figure 2-11: SEM micrograph of the surface of a ZrB_2 ceramic [41]

Zirconium- and hafnium-based ceramics, specifically the carbides, nitrides and borides (see **Figure 2-11**), display several unique properties such as high thermal and electrical conductivity, in addition to the extreme hardness and thermal stability exhibited by most zirconium materials [41]. This identifies these materials as potential candidates in several high temperature structural applications such as high temperature shielding, furnace elements, cutting tools, plasma arc electrodes, hypersonic vehicles (**Figure 2-12**) and engines.

Zirconium hydride forms rapidly by the reversible absorption and desorption of hydrogen into highly porous zirconium sponge at temperatures exceeding 400°C [41]. This process takes place very slowly at temperatures below 250°C. Zirconium hydride does not have a fixed stoichiometry but rather exhibits a series of crystalline phases, ranging from composition $ZrH_{0.9}$ to ZrH_2. When the metal hydride content exceeds 40 wt% at room temperature the material becomes brittle and exhibits no tensile ductility. This behaviour and the reversible nature of the hydride reaction are mainly exploited in the preparation of zirconium alloy powders.

Figure 2-12: Concept for a hypersonic aerospace vehicle [42]

Zirconium carbide is typically produced by reduction, in the presence of carbon, in an induction-heated vacuum furnace. Zirconium carbide, like the hydride, does not have a fixed stoichiometry and exists as a defect compound with a composition generally ranging from $ZrC_{0.6}$ to $ZrC_{0.98}$. It is inert to most reagents other than hydrofluoric or hot sulphuric acid and solutions containing nitrate or peroxide ions. At high temperatures

it reacts exothermically with halogens and oxidisers to form tetrahalides or the dioxide respectively.

Cubic zirconium nitride is a brittle, yellow solid which can be prepared by heating zirconium metal sponge to 1100-1500°C in a nitrogen or ammonia atmosphere [41]. The reaction is relatively slow as the process first forms a protective nitride layer which retards the diffusion of nitrogen. Complete conversion to the nitride compound requires either long reaction times or significantly higher temperatures. An alternative means of manufacturing this compound is the heating of zirconium tetrachloride in a nitrogen and hydrogen atmosphere to temperatures above 1000°C. This process yields either a film or a powder as the final product.

Zirconium readily forms tetravalent halides, such as ZrF_4, $ZrCl_4$, $ZrBr_4$ and ZrI_4, with a wide variety of methods available for their production [41]. They can generally be synthesised by the direct action of the halides with zirconium metal or zirconium carbide. Lower valent halides, such as $ZrCl_3$, can also be formed by reacting stoichiometric amounts of the elements in sealed tantalum tubes at 500-700°C but these require several days to reach equilibrium.

Certain zirconium organometallic compounds can be useful as catalysts. Their catalytic properties and their ability to be bound to relatively inert substrates make them well suited to this role. Zirconium readily forms carboxylates and other organic complexes simplifying production of these catalytic materials.

2.6. CONCLUSION

Zirconium is found in a vast array of materials, compounds and processes in modern industry and on the consumer market. As some of these compounds can be toxic or pyrophoric in nature their detection can be an important safety concern. Similarly the quantity of zirconium in a material can have a significant impact on the physical and chemical properties of that material, thus determining whether it would be “fit for purpose”. The development of analytical procedures for the rapid and accurate detection and quantification of zirconium is therefore of critical importance.

Chapter 3: The Quantitative Chemical Analysis of Zirconium and Related Products - A Literature Survey

3.1. INTRODUCTION

The great variety of zirconium-containing materials found in industry today makes it necessary to gain an understanding of the various methods and procedures previously employed in the dissolution of zirconium minerals, chemicals and metallic materials in their pure or alloyed forms. Several broad types of dissolution were identified including acid dissolution, flux fusion and microwave-assisted acid digestion. Pellet pressing procedures for techniques requiring solid samples were also identified and investigated.

While proper sample dissolution is vital for the quantitative analysis of any material, this must be paired with an appropriate analytical detection technique. A wide array of instrumental techniques is available to the modern analytical chemist, the most common of which rely on various types of spectrometry [43, pp. 839-865]. For the most part these methods employ different wavelengths of electromagnetic radiation and their interaction with or emission from analytes of interest. UV-Vis spectrophotometry relies on the analyte absorbing characteristic wavelengths of light either on its own or in conjunction with a chromophore. Similarly atomic absorption spectrometry relies on the absorption by metals in their elemental form when excited in a high temperature flame or by electrothermal processes. ICP-OES, GD-OES and XRF methods, on the other hand, rely on the excited emission of photons by an analyte, either by exposure to a high temperature plasma or by bombardment with X-ray radiation. In contrast ICP-MS, while similar in many regards to ICP-OES, makes use of mass spectrometry which is not dependant on electromagnetic radiation, improving detection limits at the expense of linear dynamic range. A wide variety of other instrumental techniques exist, however these few were focused on due to the availability of the instruments.

3.2. SAMPLE PREPARATION OF ZIRCONIUM MINERALS, METALS AND COMPLEXES

3.2.1 ACID DISSOLUTION AND EXTRACTION

A method for the gravimetric analysis of zirconium mandelate [44], and thus zirconium, was initially published in 1966. This method required the dissolution of zirconium metal and metal powder. This was achieved by digestion in a mixture of 15 mL of water, 10 mL of 1:1 sulphuric acid, 5 mL of nitric acid and 2 mL of perchloric acid with the gradual addition of 5 mL hydrofluoric acid in aliquots of approximately 0.5 mL at one minute intervals. The sample was then allowed to stand until dissolution was complete, a process which took approximately five minutes.

In a method for the determination of calcium in zirconium powder [45] it was reported that the metal powder (0.4 g) was dissolved using a mixture of hydrofluoric and sulphuric acids which was then evaporated until only sulphuric acid remained as solvent. The zirconium was then removed from the solution by precipitation using ammonium chloride and the calcium was determined with murexide (structure seen in **Figure 3-1**).

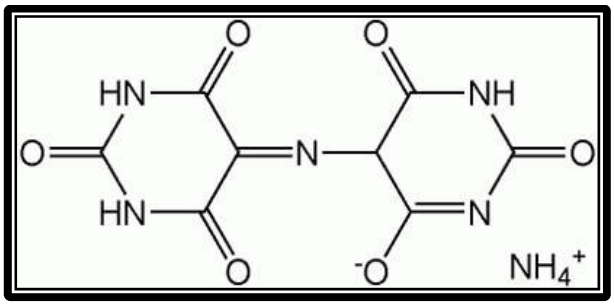

Figure 3-1: Structure of murexide [46]

In the presence of niobium or tantalum the zirconium sample material was dissolved with a 10 M hydrofluoric, 6 M sulphuric acid mixture. The bulk of the niobium or tantalum was then removed by extraction with hexone from the acid solution [47]. The zirconium was subsequently separated by precipitation using ammonium hydroxide and hydrogen peroxide. Under these conditions the zirconium was completely precipitated while any niobium or tantalum remained in solution as soluble peroxy complexes. The zirconium precipitate was then separated by filtration, re-dissolved in hydrochloric acid and determined by titration with ethylenediaminetetraacetic acid (EDTA).

Zirconium metal alloys, specifically Zr-2.5Nb and Zircaloy, can be dissolved directly by the action of hydrofluoric acid [48]. This was performed in a method for the determination of trace phosphorus in the metal. Selective fluoride complexation of zirconium can be achieved by maintaining fluoride concentration in the presence of boric acid which serves to complex excess fluoride ions. This was done in order to facilitate the selective extraction of phosphorus into *n*-butyl acetate by complexation with ammonium molybdate and crystal violet. After separation the phosphorus complex was analysed quantitatively at 582 nm by spectrophotometry.

A method has been reported for the determination of trace amounts of iron in zirconium metal by isotope dilution-thermal ionization mass spectrometry [49]. In this method the zirconium metal was first cleaned by gentle heating with 4 M hydrochloric acid in a Teflon beaker so as to remove any surface iron contamination. The metal was then rinsed with Milli-Q water, dried, and after accurate weighing, dissolved in 8 M nitric acid / 3 M hydrofluoric acid without heating. Zirconium was removed from the samples by a two-step procedure with an initial ion exchange and a subsequent micro-solvent extraction step. This was done as zirconium was found to suppress the iron ionisation signal.

Digestion of marine sediment reference material samples was undertaken to demonstrate the improved applicability of high pressure digestion vessels (HPDVs) over previously utilised screw-top polytetrafluoroethylene (PTFE) jars [50]. These materials contained chemically resistant minerals such as zircons which were not digested completely by the conventional method. These new HPDVs were fabricated from “virgin” PTFE rods and cleaned by immersion in *aqua regia* overnight at 70ºC. During use these “bombs” were enclosed in aluminium rings with their caps held in place with a stainless steel disk, see **Figure 3-2**. Samples of approximately 0.1 g were initially digested by a mixture of nitric and hydrofluoric acids in the HPDVs which were sealed and placed in a conventional oven at 200ºC. Subsequently the sample vessels were opened and heated to dryness and two cycles of dissolution by nitric acid at 70ºC in the closed vessels followed. This procedure took approximately 3 days to complete, a significant improvement over the 8 days required by the conventional method. The samples produced by both methods were compared by inductively coupled plasma mass spectrometry (ICP-MS) and recoveries for elements such as zirconium, yttrium, niobium, hafnium and uranium were seen to be better in the samples produced in the high pressure digestion vessels, indicating more complete digestion.

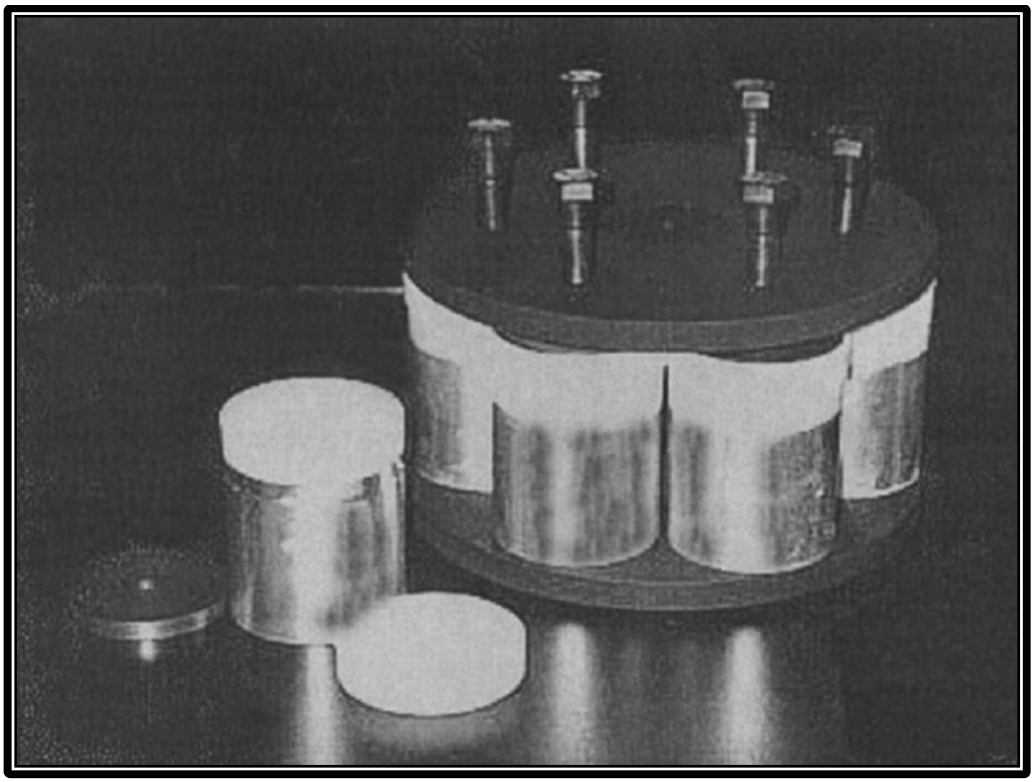

Figure 3-2: A high pressure digestion vessel assembly [50]

3.2.2 FLUX FUSION DIGESTION

Lithium tetraborate may be used as a fluxing agent and has been found to be effective in the digestion of zircon ore as well as plasma dissociated zircon [21]. Depending on the quantity and particle size of the sample material the fusion can take several hours to complete. A clear glass is eventually produced which can be dissolved by the action of dilute nitric acid. For the purposes of determining rare earth elements (REEs) by inductively coupled plasma mass spectrometry (ICP-MS) the same fusion has been used [51] to create glass beads. These beads were pulverized in an agate mortar before decomposition in a mixture of nitric, hydrofluoric and perchloric acids.

A mixture of boracic acid and sodium carbonate in a 2:1 ratio has been used to dissolve corundum samples containing zirconium, amongst other materials such as silicon, iron, titanium, calcium and magnesium [52]. Samples were then dissolved with hydrochloric acid and analysed by inductively coupled plasma optical emission spectrometry (ICP-OES). The method was found to have detection limits of between 0.0003 and 0.0051% and a relative standard deviation of between 0.88 and 4.78%.

Zirconium dioxide has been successfully digested by fusion using either lithium metaborate/boric acid [53] or ammonium sulphate/sulphuric acid mixtures [29]. These

methods however require reagent excesses of in the order of thirty to forty times the sample mass which limits their application. The high salt content of samples decomposed by these methods hinders accurate analysis by most methods. Specific analytical results making use of these digestions were not reported.

A method for the digestion of geological samples including zircon using ammonium fluoride as digestion medium has been reported [54]. This procedure has been applied to a series of international geological reference materials including igneous and sedimentary rocks. The optimum reagent ratio was found to be 6 parts ammonium fluoride to 1 part sample. As such 300 mg of ammonium fluoride powder was added, along with 50 mg powdered rock sample, to a 7 mL perfluoroalkoxy (PFA) vial and this mixture was wetted with a few drops of water. These vials were capped and heated to 250ºC in a conventional electric oven for 2 hours. After cooling, 1.5 mL of nitric acid was added and the solution evaporated to dryness. This was done twice before the sample was re-dissolved in 1 mL nitric acid, 1 mL milliQ water and 1 mL internal standard solution. This solution was then heated at 120ºC for a further 6 hours to obtain a clear solution. The solution was then diluted to volume with dilute nitric acid before analysis. This method has the advantage of dissolving samples much like hydrofluoric acid but with added safety benefits. The excess reagent can be easily removed by evaporation and does not contaminate the sample with a large quantity of salts the way other fusion techniques do. A similar open vessel digestion method using ammonium bifluoride was also developed and applied to reference materials, some containing zircons [55]. It was found that less digestion reagent was required with a reagent to sample ratio of 4:1 instead of 6:1, achieving dissolution in 3 hours rather than 2.

3.2.3 MICROWAVE-ASSISTED ACID DIGESTION

A comparison of traditional multi-step sequential extraction versus several modern variants, including microwave-assisted and ultrasonic extraction, was performed with emphasis on comparative extraction percentage and extraction time [56]. **Figure 3-3** shows an example of a modern microwave-assisted digestion unit.

Figure 3-3: An Anton Paar Multiwave 3000 microwave reaction system [57]

It was found that where the traditional sequential standard procedure took in excess of 50 hours the use of microwave-assisted extraction could reduce this time to a few minutes with actual time under microwave irradiation being in the order of 60-120 seconds. This significant increase in extraction speed came at the cost of a slight reduction in percentage recovery. This reduction was in the order of approximately 3% for cadmium, chromium, copper, lead and zinc but nearly 15% for nickel. However, other work [58] has shown that the microwave-assisted extraction of

nickel can reach 100.4% in a similar matrix indicating that the extraction is significantly dependant on sample matrix and extraction reagents.

Digestion of ceramic glazes using microwave-assisted acid dissolution for ICP-OES analysis has been described in a procedure including zirconium oxychloride as a free fluoride scavenger [59]. Many elements found in these glazes form insoluble (barium, calcium, magnesium, lead and strontium) or volatile fluorides (silicon and boron) when digested in a hydrofluoric acid medium. This complicates their analysis by ICP-OES which normally requires aqueous samples. To circumvent this, an ion with a high affinity for fluoride can be added to preferentially complex free fluoride during microwave-assisted acid digestion. In the method presented, a 40 mg sample of ceramic glaze was digested in a PTFE vessel containing 3 mL nitric acid, 3 mL hydrochloric acid and 2 mL hydrofluoric acid. The heating cycle consisted of four 10-minute periods with 250 W of microwave energy applied in the first and third of these. The vessels were cooled in a water bath for 30 minutes before being opened to add 20 mL of a 0.72 M zirconium solution. The samples were then again subjected to microwave heating at 250 W for 10 minutes. Upon completion this sample was transferred to a plastic volumetric flask and diluted to 100.0 mL. The sample was then analysed by ICP-OES. Analysed and theoretical results were the same at the 95% significance level with relative standard deviations of generally below 2%. These results demonstrated the high accuracy and precision of the method.

A study into the development of a microwave-assisted acid digestion procedure applicable to biomorphic ceramic samples was reported [30]. In this study a biomorphic ceramic composed of zirconium dioxide was decomposed using microwave-assisted acid digestion. Several factors influencing the digestion efficiency were investigated, including volume of nitric acid, hydrofluoric acid and irradiation time. Samples of approximately 10 mg were accurately weighed and to these varying quantities of acid reagent (2-6 mL HF and 4-8 mL HNO_3) were added. The samples were sealed in PTFE vessels and subjected to microwave irradiation for periods of time varying between 3 and 7 minutes. Results were evaluated by both ICP-MS and flame atomic absorption spectroscopy. The optimum dissolution conditions for the recovery of the zirconium in the biomorphic ceramic were found to be 8 mL nitric and 3.6 mL hydrofluoric acids with an irradiation time of 3 minutes at 560 W of power.

Polypropylene fibrous filters are used in the monitoring of radionuclides in the atmosphere [60]. The analysis of these filters after exposure is often done by non-destructive γ-spectrometry. As an alternative, an ICP-OES method was developed to determine several elements after complete digestion of the filters by microwave-assisted acid digestion. In this procedure a sample filter was decomposed in a 230 mL digestion cup containing 6 mL of concentrated nitric acid. The cup was sealed and subjected to microwave heating at 1.25 MPa for 10 minutes. After this procedure if the solution was not clear a further 2 mL of acid was added and the sample was irradiated again for 5 minutes. The sample was then analysed by ICP-OES. Recoveries were good for strontium, barium, molybdenum, lanthanum, cerium and neodymium. Zirconium recoveries, however, were unsatisfactory as nitric acid was used as dissolution medium and zirconium oxide is dissolved only by hydrofluoric and sulphuric acid.

3.2.4 SOLID PELLET PRESSING

Zirconium oxide pellets for use in XRF analysis of iron have been created using boric acid as a binding agent [61]. Zirconium was purified by anion exchange chromatography in a 1 M sulphuric-6 M hydrochloric acid solution. To this a known quantity of iron was added and the total solution was then precipitated in the presence of ammonium hydroxide. The precipitate was then calcined at 750ºC to yield the dry oxide and ground down to smaller than 325 mesh average particle size. This was then either mixed thoroughly with boric acid or sprayed onto a layer of boric acid to form a dual layer disc with the binder acting as a substrate. This was then pressed at a pressure of 150 kg cm^{-2} to yield a sufficiently strong disc for XRF analysis.

For the purposes of GD-OES it is useful to have pellets which are electrically conductive, many zirconium materials (such as zirconium dioxide) are however not electrically conductive. For the analysis of the non-conducting plutonium dioxide powder by GD-OES it was necessary for the sample to be pressed into a solid, conducting pellet [62]. This was achieved by mixing the samples with silver, titanium or tantalum powders of high purity (> 99.9% pure) as a binding matrix before compaction in a hydraulic press. Samples were mixed in a 1:3 ratio of sample to binder and pressed under 8 tons of pressure for 5 minutes. This resulted in conductive sample discs of 13 mm diameter that were suitable for use with the DC lamp of the GD-OES instrument.

3.3. THE SPECTROMETRIC TECHNIQUES IN THE ANALYSIS OF ZIRCONIUM-CONTAINING COMPOUNDS

3.3.1 SPECTROPHOTOMETRIC METHODS AND TECHNIQUES

The spectrophotometric analysis of zirconium and hafnium by use of reverse-phase liquid chromatography was accomplished with the use of 2-(5-bromo-2-pyridylazo)-5-diethylaminophenol in the presence of fluoride or acetate ions [63]. The fluoride containing complexes of zirconium and hafnium have absorption maxima at 582 and 581 nm respectively while the acetate complexes both absorb at 585 nm. In the fluoride complex the molar extinction coefficient (ε) of the zirconium and hafnium complexes differs by only 0.3 x 10^4 L mol^{-1} cm^{-1} (14.6 and 14.9 x 10^4 l mol^{-1} cm^{-1} respectively). However, two complexes showed a slightly greater variation (12.5 and 13.2 x 10^4 L mol^{-1} cm^{-1} respectively). Due to the almost identical optical characteristics of these complexes, they were separated with the use of reverse-phase liquid chromatography. A mixture of 55/45 v/v acetonitrile and water containing 1.5 x 10^{-4} M sodium fluoride and perchloric acid (one drop in 250 mL) was adjusted to pH 4.2 ± 0.3 and used as eluent in all cases. A C18 column was used as the stationary phase. Effective calibration ranges for the two complexes were found to be between 1 and 200 µg l^{-1} (Hf) or 0.8 and 160 µg l^{-1} (Zr) with peak area vs. concentration graphs being linear in these regions.

A method for the determination of oxalic acid using zirconium (as Zr(IV) 3-(2,6-dibromo-4-sulfophenylazo)-6-(2-arsenophenylazo)-4,5-dihydroxynaphthalene-2,7-disulfonic acid, abbreviated Zr(IV) (DBS-ASA)) takes advantage of a hyperchromic effect observed at 520 nm [64]. The complex obeys Beer's Law in the concentration range between 9.0 x 10^{-6} and 5.0 x 10^{-4} M oxalic acid and the calibration is proportional to the concentration of oxalic acid present with a correlation coefficient of 0.9995. Apparent molar absorptivity of the complex is 1.16 x 10^3 L mol^{-1} cm^{-1}.

A simple, sensitive and selective method for the trace analysis of zirconium in water is based on the complexation of zirconium with 4-chloro-N-(2,6-dimethylphenyl)-2-hydroxy-5-sulfamoylbenzamide (xipamide) [65] (structure seen in **Figure 3-4**). The complex forms effectively at pH 8, has an absorption maximum at 333 nm and obeys Beer's Law in the concentration range of 0.2 – 3.6 µg mL^{-1}. The molar absorptivity of the complex was reported as 5.60 x 10^4 L mol^{-1} cm^{-1} with the correlation coefficient of the calibration graph being 0.9998. Recoveries of between 99.1 and 99.8% were

obtained with relative standard deviations of between 0.32 and 0.71% in all determinations carried out. All determinations were performed in sextuplicate. The method does suffer from the interferences of some elements, the most significant of these being cobalt, copper, iron, titanium, lead, nickel and hafnium which have a tolerance limit of 100 µg mL^{-1}.

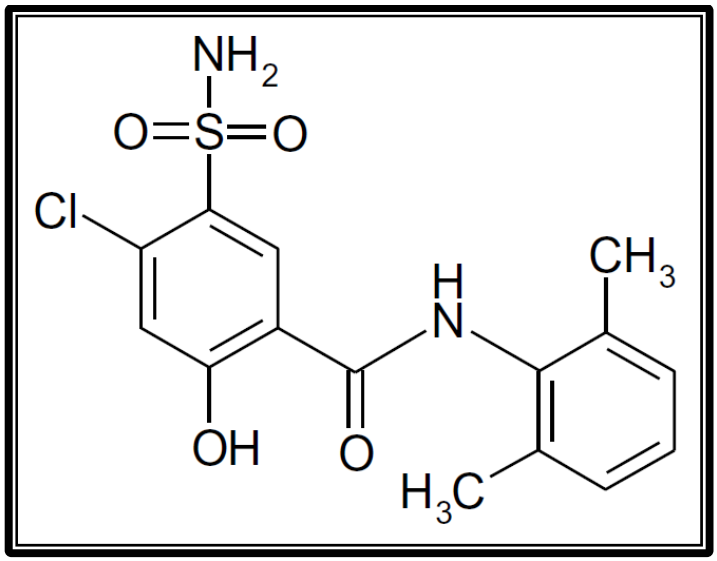

Figure 3-4: Structure of 4-chloro-*N*-(2,6-dimethylphenyl)-2-hydroxy-5-sulfamoylbenzamide (xipamide) [65]

The red complex formed by the reaction between zirconium and 2-(5-bromo-2-pyridylazo)-5-diethylaminophenol in a pH range of between 3.8 and 5.8 obeys Beer's Law over a concentration range of between 0.02 and 0.44 µg mL^{-1} [66]. The stable complex has a 1:3 metal to ligand ratio and a molar absorptivity of 1.54 x 10^5 L mol^{-1} cm^{-1} at 585 nm. EDTA, gallium, indium, titanium and vanadium have been identified as serious interferences.

Alizarin Red S (ARS; 1,2-dihydroxyanthraquinone-3-sulfonic acid, sodium salt) was one of the first reagents used in the spectrophotometric analysis of zirconium and hafnium [67]. Unfortunately the reagent has a very low selectivity between the two metals and their absorption profiles are extremely similar, overlapping over most of their absorption range. Maxima for the two elements complexed with ARS are found at 540 (zirconium) and 527 (hafnium) nm. This slight difference allows for simultaneous analysis using principle component analysis using a neural network (PC-ANN). PC-ANN is a non-linear computational technique in which a neural network is trained with a learning algorithm on a prediction set of calibration data using synthetic samples.

The results based on the prediction set yielded apparent recoveries of between 88.89 and 112.429% (average of 101(5)% for zirconium) and between 97.33 and 110.00% (average of 100(2)% for hafnium). In the validation set of results recoveries ranged between 87.57 and 144.00% (average of 101(11)%) for zirconium and between 80.00 and 108.78% (average of 99(6)%) for hafnium. The error on the average recovery, between 2 and 11%, is high but the accuracy was considered acceptable. When taking into account the almost complete overlap of the two spectrums the method appears to be surprisingly effective.

Trace quantities of zirconium have been measured in water using xylenol orange as chromophore [68]. Pre-concentration was performed using a variety of chelating resins synthesised from 8-hydroxyquinoline (oxine), formaldehyde, fufuraldehyde, benzaldehyde, resorcinol and hydroquinone. These resins were synthesised in an attempt to improve on previously reported oxine-containing resins with regard to their low metal exchange capacities and instability in high (> 2M) acid concentration. Zirconium extracted in this manner was subsequently reacted with xylenol orange and quantified using a UV-Vis spectrometer at 535 nm. Correlation coefficients of the calibration curves were 0.9990(8).

The recently synthesised reagent diacetylmonoxime salicyloylhydrazone (DMSH) has been used to spectrophotometrically determine both zirconium and vanadium in acetic acid medium. The technique has been successfully applied to alloy steel, mineral and soil samples [69]. The technique requires no separation of the analyte elements as derivative spectrophotometry was employed due to the significant overlap of their spectra in the 360 to 460 nm range when complexed with the DMSH ligand. The first order derivative of the absorbance spectra with regard to wavelength yielded the best results in terms of sensitivity and detection limits. Zero-crossing points for the zirconium (380 nm) and vanadium (405 nm) complexes were observed, see **Figure 3-5**. As such the zero-crossing measurement technique was employed. Molar absorptivity for these complexes was determined to be 1.30×10^4 L mol^{-1} cm^{-1} and 1.82×10^4 L mol^{-1} cm^{-1} for the vanadium and zirconium complexes respectively with Beer's Law being obeyed in the ranges 0.26 – 2.80 µg mL^{-1} (V) and 0.30 – 3.20 µg mL^{-1} (Zr).

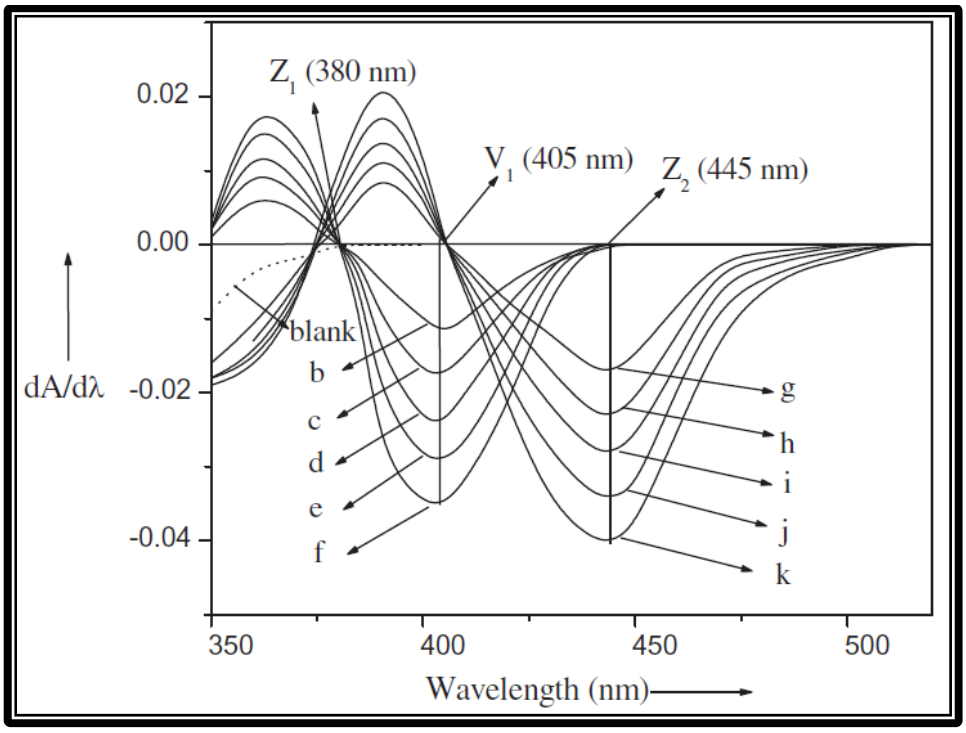

Figure 3-5: First order derivative spectra showing zero crossing points at Z_1, V_1 and Z_2 [69]

Arsenazo III has been successfully used in the determination of uranium, thorium and zirconium present in water samples and ceramics [70]. Ceramic samples were dissolved in the presence of hydrofluoric, sulphuric and perchloric acids in a platinum crucible at 150ºC. The residue was subsequently dissolved in 50 mL of 0.1 mol L^{-1} hydrochloric acid and diluted to 100.0 mL. This, along with samples of sea water, tap water and well water, were pre-concentrated on an Amberlite XAD-2000 resin column (loaded with α-benzoin oxime) with an enrichment factor of 100. The simultaneous determination of all analyte elements was achieved with Arsenazo III as chromogenic reagent using an orthogonal signal correction partial least squares method. Detection limits were found to be 0.50, 0.54 and 0.48 µg L^{-1} respectively for uranium, thorium and zirconium. The relative standard deviation of the method was found to be better than 4% for all elements analysed.

3.3.2 *Atomic Absorption Spectrometry (AAS)*

The analysis of silicon in niobium, titanium and zirconium oxides was carried out using electrothermal (graphite furnace) atomic absorption spectroscopy [71]. These materials are generally digested with the aid of hydrofluoric acid. This has the drawback that highly volatile silicon tetrafluoride is formed which is then lost during digestion, separation and even determination steps. Attempts have been made to circumvent this problem using techniques such as spark source mass spectrometry (SSMS), X-ray fluorescence spectrometry (XRF), laser excited atomic fluorescence spectrometry (LEAFS) and slurry nebulisation. These techniques were coupled with either inductively coupled plasma optical emission spectrometry (ICP-OES) or atomic absorption spectrometry (AAS). The drawbacks of these techniques include high detection limits, in the 10 μg g^{-1} range, and a requirement that the sample be in a very fine powdered form. Furthermore only relatively small sample sizes are supported in the slurry AAS method, another factor negatively impacting achievable detection limits. To avoid these issues a method of solid sampling electrothermal AAS was used wherein the solid sample (maximum of 15 mg zirconium dioxide) was directly added to the graphite pyrolysis tube of the instrument, along with a matrix modifier consisting of equal parts palladium metal and magnesium nitrate. A heating program was reported as seen in **Table 3-1**.

Table 3-1: Electrothermal atomisation heating program

Heating step	Temperature (ºC)	Heating rate (ºC s^{-1})	Hold time (s)	Argon flow (mL min^{-1})
Drying	130	200	2-60	2300
Pyrolysis	1200	200	10	2300
Auto-zero	1200	-	8	100
Atomisation	2600	3000	8-10	100
Cleaning	2600	-	3	-

The silicon hollow cathode lamp (HCL) current was set to 14 mA with a spectral bandwidth of 0.2 nm. Silicon was measured at both 251.6 and 221.7 nm for the zirconium dioxide samples. The instrument was calibrated using standard solutions containing a similar matrix as the solid samples. This method obviated the need for time consuming and difficult sample preparation procedures. It also provided excellent

detection limits, in the order of 100 ng g^{-1} for the less intense 221.7 nm absorption line and 20 ng g^{-1} for the more intense 251.6 nm line. These results showed a 100-fold improvement as compared to the slurry electrothermal method and 1000-fold improvement over slurry flame-AAS.

Graphite furnace atomic absorption spectroscopy (GFAAS) has also been successfully applied to the analysis of zirconium in geological and soil samples [72]. The ligand 25,26,27,28-tetrahydroxy-5,11,17,23-tetrakis (*N*-*p*-chlorophenyl) calix[4]arene hydroxamic acid (CPCHA) (**Figure 3-6**) was used in a liquid-liquid extraction as a pre-concentration procedure prior to determination by GFAAS. The samples were prepared either by hydrofluoric acid digestion, in the case of the geological samples, or by extraction with concentrated hydrochloric acid in the case of the soil samples. In both cases the samples were evaporated to dryness and re-dissolved with dilute hydrochloric acid and diluted with distilled water. The samples were then transferred to a separating funnel where the zirconium was extracted using the CPCHA ligand dissolved in ethyl acetate (0.2% CPCHA solution). The extract was dried over 1 g anhydrous sodium sulphate, which was subsequently washed with more ethyl acetate to ensure no analyte was lost. The combined, dried extract was diluted to a fixed volume with more ethyl acetate and injected into the GFAAS furnace. Zirconium was detected in the spectrometer at 360.1 nm with a spectral width of 0.2 nm and lamp current of 15 mA. A detection limit of 0.1 µg cm^{-3} zirconium was achieved using 100 µl sample volume. Values were confirmed by UV-Vis spectrophotometry wherein potassium thiocyanate was added to the extract to give the coloured Zr(IV)-CPCHA-SCN complex which was found to have a reproducible maximum absorbance at 447 nm. Molar absorptivity of this complex at the specified wavelength was determined to be 9.4 $x10^3$ L mol^{-1} cm^{-1} and Beer's Law was obeyed in the range 1.0 – 9.5 ppm.

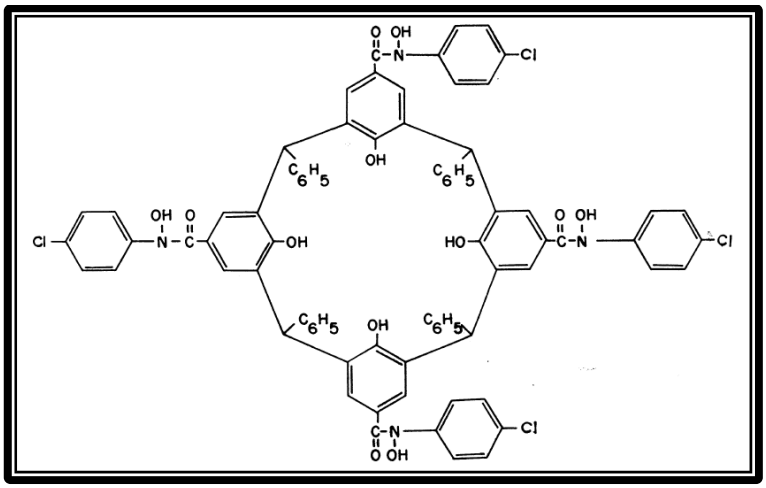

Figure 3-6: Structure of 25,26,27,28-tetrahydroxy-5,11,17,23-tetrakis (*N-p*-chlorophenyl) calix[4]arene hydroxamic acid (CPCHA) [72]

Electrothermal atomic absorption spectrometry has been used to analyse for trace elements in zirconium dioxide and yttrium stabilised zirconium dioxide [29]. Zirconium dioxide samples were prepared by digestion in hydrofluoric acid at 220 ºC for six hours in PTFE-lined pressurised containers before dilution. The yttrium stabilised samples required 8 hours for complete dissolution as well as the addition of nitric and sulphuric acids. Slurries were prepared by sonication by an ultrasonic probe of 10 mg sample in 10 mL water. Significantly improved limits of detection were obtained using the slurry sample preparation method as opposed to the total dissolution method with some elements being determinable as low as 5 ng g^{-1} (Mg).

3.3.3 Inductively Coupled Plasma Optical Emission Spectrometry (ICP-OES)

A procedure reported for the pre-concentration, extraction and subsequent analysis of trace zirconium and hafnium in aqueous solution made use of a cloud point extraction procedure [73] (see **Figure 3-7**). Quinalizarine (1,2,5,8-tetrahydroxyanthraquinone) was added as a chelating agent to a solution containing the trace metals along with octyl phenoxypolyethoxy ethanol (Triton X-114) as a non-ionic surfactant. After phase separation the enriched organic phase was diluted with 30% v/v propanol/water with a concentration of 1 M nitric acid in order to allow for effective nebulisation in the ICP-OES instrument. The instrument was calibrated in the 0.5 – 1000 µg L^{-1} range. Linearity was confirmed with a calibration coefficient of 0.9960 and 0.9971 for hafnium (282.023 nm) and zirconium (343.823 nm) respectively. RF power applied to the plasma was set to 1.65 kW with a frequency of 40 MHz. Detection limits for the two elements were found to be 0.31 (hafnium) and 0.26 (zirconium) µg L^{-1} with enrichment

factors from the pre-concentration step being between 35.8 (hafnium) and 38.9 (zirconium). Percentage recovery in real samples of the analyte elements ranged between 60.9% and 99.8% depending on the purity of the starting aqueous solution. The low 60.9% (hafnium) and 78.6% (zirconium) recovery was obtained from analysis of water sourced from the Caspian Sea which contained large quantities of salt [73]. The interference of the high ionic concentration was mitigated somewhat by the use of a standard addition method which resulted in recoveries of 95.0% (hafnium) and 96.0% (zirconium). Relative standard deviations, as determined from eight replicate synthetic samples, were 2.9 and 2.6% respectively for zirconium and hafnium.

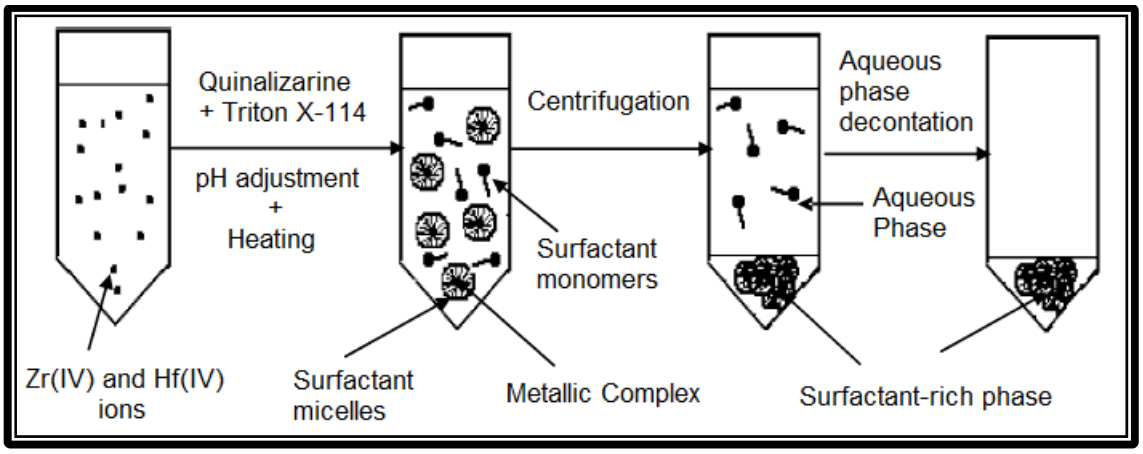

Figure 3-7: Experimental scheme for the cloud point extraction and pre-concentration of zirconium and hafnium [73]

Elemental hafnium, chemically almost identical to zirconium, has been found to be toxic in respiratory and alimentary tracts [74]. Its LD_{50} in mice has been found to be 76 mg kg^{-1}. Exposure to hafnium tetrachloride, which has an LD_{50} of 2000 mg kg^{-1} in rats, results in renal degeneration and inflammation of the small intestine. A study conducted in Poland, where the threshold limit value for total hafnium in air has been proposed as 0.5 mg m^{-3}, used nitrocellulose membrane filters to sample volumes of 400 litres of air at a flow rate of 20 L min^{-1}. After exposure these filters and their contents were “mineralised” and decomposed by successive exposure to mixtures of and pure concentrated nitric, hydrofluoric and perchloric acids with drying steps in between. The final residue was dissolved in 3 to 5 mL 5% hydrofluoric acid and diluted with the same acid to 50 mL. Due to its precision and tolerance to interferences, a characteristic wavelength of 282.022 nm was selected as analytical line using a single point background correction. RF power was set to 1.0 kilowatts with an integration time of 2 seconds and observation height of 12 mm. Gas flow and sample uptake rates were

12.0 L min^{-1} coolant, 1.0 L min^{-1} plasma and 1.0 L min^{-1} carrier gas with 1.3 mL min^{-1} sample flow rate. The instrument was calibrated with matrix matched standards between 1.0 and 10.0 ppm and samples were analysed directly. Due to a lack of certified reference materials the recovery test was based on filters which had a known quantity of hafnium added to them in the form of a standard solution. The recovery was found to be in the range of 98 to 102% with a standard deviation of 2% in all cases. The method was found to be effective in the range of 0.125 to 1.25 mg m^{-3} with minimal interference.

The ablation properties and analytical behaviour of an alloy of zirconium and uranium were investigated using a tandem laser ablation inductively coupled plasma optical emission spectrometer (LA-ICP-OES) [75]. The analyte consisted of a rod of metallic uranium/zirconium alloy enclosed in a stainless steel jacket which had been sectioned by a low speed saw. In this system the composition of the laser ablation aerosol was investigated by comparing it with conventionally aspirated liquid standards. Direct chemical analysis of the ablation product was also performed. Samples were captured both on a silver membrane and a cellulose membrane filter. After collection these filters were digested in a high pressure PTFE bomb with nitric and hydrofluoric acid at 365 K overnight. The effect of laser wavelength and energy were also investigated. It was found that the composition of the laser ablation aerosol appeared to vary depending on laser power, but not wavelength. Power density in the 15-40 GW cm^{-2} range produced results indistinguishable from those obtained from the aqueous samples. Results from power densities below 15 GW cm^{-2} appeared to be deficient in zirconium while the opposite was true at densities higher than 40 GW cm^{-2}. Bulk analysis of the captured aerosol on the membranes, however, showed that this was not the case and the aerosol contained zirconium to uranium ratios identical to those in the alloy at all ablation power densities. The apparent difference in chemical composition at different laser intensities was believed to be an artefact of the spectrochemistry of the ICP. It was hypothesised that this was due to different atomisation efficiencies of the analytes at the different power densities investigated. The only apparent difference related to laser wavelength appeared to be the mechanism of ablation. A laser wavelength of 1064 nm was shown to interact indirectly with the surface via a laser micro-plasma while at 532 nm direct coupling of the laser light into the surface was observed.

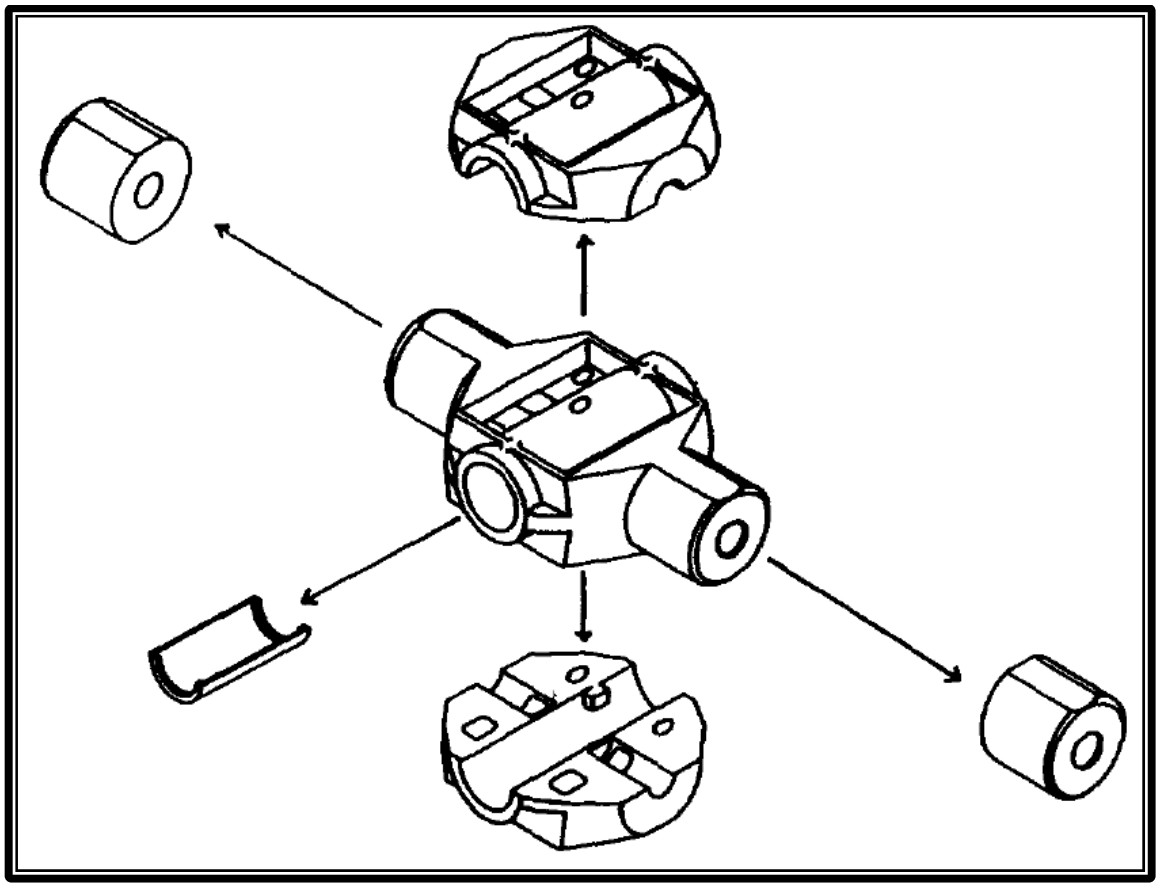

Figure 3-8: Transversely heated graphite furnace atomiser [29]

An ICP-OES method for the analysis of trace rare earth elements in zirconium dioxide has been developed using electrothermal vaporisation [76]. Due to matrix effects caused by excess zirconium it was desirable to remove the bulk of the sample matrix prior to analysis. This was achieved by volatilisation of zirconium as ZrF_4 by electrothermal vaporisation. A small quantity of the analyte was dissolved by heating in the presence of ammonium sulphate and concentrated sulphuric acid. This solution was then evaporated to dryness and re-dissolved in 6 M nitric acid. A small volume of 60% PTFE slurry was added to the solution to serve as a source of fluorides. This solution was diluted to volume and dispersed with an ultrasonic vibrator. 20 µL of this solution was deposited in a graphite furnace (**Figure 3-8**) attached to the ICP-OES, dried, ashed, vaporised and carried into the plasma by the argon carrier gas. Careful selection of ashing temperature allowed for the removal of the ZrF_4 without the loss of the rare earth elements of interest. This was due to the relatively low evaporation temperature of the zirconium fluoride as compared to the fluorides of the other elements. Element recoveries were found to be in good agreement with those obtained by previously defined methods and detection limits of less than 25 ng mL^{-1} were obtained for all elements of interest.

3.3.4 Inductively Coupled Plasma Mass Spectrometry (ICP-MS)

The determination of zirconium and hafnium in seawater was carried out, after pre-concentration, by inductively coupled plasma mass spectrometry (ICP-MS) [77]. Samples were obtained from the subarctic North Pacific Ocean containing an approximately 0.5 M NaCl matrix. Despite the instrument's zirconium detection limit of 2 $x10^{-10}$ M, the low zirconium and hafnium concentration of the seawater necessitated the use of a pre-concentration step before analysis. This was carried out by a chelating ion-exchange procedure using Chelex-100 ion-exchange resin. The resin was prepared by batch-soaking in 2 M nitric acid for 3 days. This was repeated 5 successive times with deionised water rinses in between. Fresh resin was used in each extraction as the elution step was non-quantitative, leaving a small quantity of zirconium and hafnium on the resin. One litre of seawater was pumped through 1 mL of resin at a rate of 0.5 g min^{-1} after which the 5 mL of pH adjusted deionised water was passed through the column to remove any remaining seawater. The resin was then eluted three times with 10 mL of a 2 M nitric acid solution, again at 0.5 g min^{-1}, after which the three fractions were combined. One hundred nanograms of indium were added to each of these samples before the samples were weighed to determine the exact mass of eluent and from this the concentration of internal standard was determined. Each sample was prepared in triplicate with a blank. The ICP-MS instrument was calibrated with standards ranging between 1 and 20 parts per billion (ppb) with an indium internal standard concentration of 10 ppb. Precision of the method was reported as increasing with sample concentration where 42 pmol kg^{-1} of zirconium would have a precision of 7% while at 280 pmol kg^{-1} the precision improved to 2.5%. Accuracy of the method could not be accurately gauged as no certified reference materials were available for this type of sample but values obtained were similar to those obtained in the literature of the time [78].

A method for the determination of low levels of zirconium, hafnium, tantalum and niobium in geological samples has been reporting using ICP-MS [79]. Prior to their analysis the samples were digested and the 4 analytes were separated from their matrix by extraction chromatography. This was achieved by dissolving 0.1 g of sample rock with a mixture of nitric, hydrofluoric and perchloric acid. This mixture was heated in a sealed PFA vial for four hours. The vial was then opened and the excess silicon tetrafluoride and hydrofluoric acid was removed by evaporation. The remaining sample solution was subsequently heated to almost dryness, 1 mL perchloric acid was added

and then slowly heated to dryness again over a period of two to three hours. This “perchloric acid fuming treatment” was carried out in order to remove as much fluoride as possible. The sample was then re-dissolved in 2 mL 4 M hydrochloric acid prior to column separation. The chromatographic resin used in the extraction was prepared by loading 5 g of analytical grade *N*-benzoyl-*N*-phenylhydroxylamine (BPHA) in chloroform onto 10 g of Amberchrom CG-71md resin. The chloroform was removed by evaporation. The sample was then loaded onto the resin, followed by 10 mL of 4 M hydrochloric acid for rinsing and removal of aluminium, iron, potassium, calcium, and magnesium. The titanium in the sample was then eluted with 2 M sulphuric acid containing 1% hydrogen peroxide. After the removal of the titanium the column was once again rinsed with hydrochloric acid. The analytes were finally eluted with 10 mL of 0.5 M oxalic acid-0.2 M hydrofluoric acid, collected, evaporated to near dryness and diluted to volume with 1 M nitric acid containing yttrium, rhodium, rhenium and thulium as internal standards. The ICP-MS was calibrated in the ranges 0-200 ppb (zirconium), 0-80 ppb (hafnium) and 0-20 ppb (niobium and tantalum). The internal standards were monoisotopic and added in such quantities that the final samples contained 20 ppb for yttrium, rhodium and thulium and 60 ppb rhenium. The percentage recovery of zirconium (99.8 – 106%) from the mineral was heavily influenced by the concentration of the hydrofluoric acid (1 – 5 M) used to strip the resin. Hafnium appeared to be fairly insensitive to this effect though while niobium and tantalum showed the opposite trend. The most extreme of these was tantalum which gave between 0 and 100% recovery across the hydrofluoric acid concentration range. Detection limits of between 2 and 30 parts per billion were determined for the method.

3.3.5 X-RAY FLUORESCENCE (XRF)

X-ray fluorescence spectrometry (XRF) has been used to determine the iron content of zirconium oxide in the range 10 to 2500 μg g^{-1} [61]. Iron is an important component of nuclear grade zirconium alloys as a replacement for nickel to regain the steam corrosion resistance properties given by this element [61]. Although nickel has beneficial alloying properties it also increases the uptake of hydrogen into the zirconium metal. This results in the formation $ZrH_{1.5}$, lowering the ductility of the metal and making it brittle. The iron content of the zirconium beneficiation intermediates, starting from the zircon ore, must thus be carefully monitored. In cases where a pellet sample is required, these can be produced using boric acid as a binder or substrate. The method was calibrated using iron-free zirconium to which was added a known quantity of iron. The standards were evaluated using atomic absorption spectrometry and spectrophotometry using 1, 10-phenanthroline to confirm their iron content. The iron was then evaluated at its first order K α line (0.1938 nm) and the zirconium at its second order K α line (0.0790 nm). The instrument was set at 50 kV and 50 mA with a counting time of 60 seconds. Iron was measured at 6.37 keV and 2θ angle of 57.545º while the zirconium was measured at 15.683 keV and 2θ angle of 46.22º. This method, as compared to the traditional 1, 10-phenanthroline atomic absorption method, yielded recoveries of 99(2)% for iron. A comparison with the XRF method using powder and pellet samples yielded a standard deviation of 4.43%. A drawback of this method is that XRF is a surface, and not bulk, analysis procedure. Hence the particle size and packing density may have an adverse effect on the quality of the analysis. This effect can be compensated for by using internal standards such as copper and cobalt although this creates a new set of problems. Gravity segregation, particle size differences and non-homogenous samples are all hazards when introducing an internal standard to this method and these must be negated or accounted for in the method.

Energy dispersive X-ray fluorescence (EDXRF) has been used for the determination of zirconium and hafnium after pre-concentration [80]. This pre-concentration can be achieved both by a liquid-solid extraction procedure using an anionic exchange resin modified with xylenol orange or by precipitation in the presence of lanthanum. There was no need for further sample preparation after the pre-concentration steps as both yielded a solid material, either the loaded resin in the first case or the solid precipitate in the latter. The remaining analyte in the filtrate was heated to almost dryness,

dissolved in 0.3 mol L^{-1} hydrochloric acid and analysed spectrophotometrically at 550 nm using xylenol orange as chromogenic agent. EDXRF calibration curves for the resin extraction procedure were linear in the range 10 – 800 µg for zirconium and 50 – 800 µg for hafnium with correlation coefficients of better than 0.999. The lanthanum precipitation yielded a linear range of between 300 and 1000 µg mL^{-1} with similar linearity. In synthetic samples both methods yielded standard deviations of 4% or better. A high degree of coherence with the true value was also observed with average differences of 1.5 (Zr) and 3.4% (Hf) for the resin method and 0.8 (Zr) and 1.5% (Hf) for the lanthanum precipitation method.

3.3.6 Glow Discharge Optical Emission Spectrometry and Mass Spectrometry (GD-OES / GD-MS)

Glow discharge has, until the last decade or two, not been widely accepted in the field of surface analysis [81]. It was available as early as the 1960s as an analytical tool but only recent advances have made surface analysis by GD viable. There is relatively little literature on analytical procedures specifically for the method and most of these take the form of comparisons with older, better characterised methods such as scanning and transmission electron microscopies (SEM and TEM). A representative summary of the literature that is available follows below.

GD-MS has been utilised for the bulk analysis of trace elements in iron and chromium based powders [82]. Synthetic samples were pressed onto a 99.9999% pure indium sheet at 50 kg cm^{-2} pressure for 5 seconds and contained 21 and 14 trace impurities for the iron and chromium powders respectively. The grains of sample that did not adhere tightly enough to the metal sheet were blown away by pure, dry nitrogen gas. The composition of the synthetic powders was confirmed by chemical methods and compared to the GD-MS results. As could be expected the relative percentage error improved markedly as the concentration of the trace elements increased. With errors of 24.2% (in the 1 to 19 ppm range), 6.2% (in the 100 ppm to 0.1% range) and 1% (in the 10 – 100% range) the correlation between GD-MS and chemical analysis was highly consistent. The higher relative error at lower concentrations was a result of the very small quantities being determined where even a small difference in reported value produced a large percentage error. With a relative percentage error of less than 30% the method described appears to be highly effective in the analysis of these types of powders.

GD-OES analysis of several multi-layer systems was evaluated by comparison to results obtained from scanning and transmission electron microscopies (SEM and TEM) as well as tactile profilometry and atom probe tomography (APT) [83]. The ability of GD-OES to easily quantify light elements such as carbon, nitrogen, oxygen and hydrogen was of particular interest for the determination of the stoichiometry of several thin film samples. These samples included a silicon wafer with alternating layers of chromium and titanium, an alumina layer on a silicon substrate, an alumina passivation coating on zinc and a Ti_3SiC_2 coating on silicon. Solid calibration standards were prepared prior to analysis by polishing them to a mirror finish with silicon carbide grinding paper followed by washing with ethanol. **Figure 3-9** shows the GD-OES data captured in five seconds from a chromium/titanium multilayer sample on a silicon substrate. Ten chromium and ten titanium layers of approximately 10 nanometers (confirmed by TEM) are clearly visible. The GD-OES results showed slight variations in thickness ranging from 11 to 23 nanometers at the silicon interface. This was attributed to loss of resolution caused by the sputtering of material from the same layer at different depths. Detection of carbon contamination at the interface between the aluminium and silicon in a synthetically contaminated sample was also achieved. TEM results showed a disturbed area at the interface indicating carbon diffusion and this was identified and easily quantified by GD-OES. A passivation coating consisting of alumina nanoparticles on a rough zinc substrate was also characterised by GD-OES and showed a clear accumulation of alumina particles near the layer surface and this was again confirmed by TEM analysis. The ability of GD-OES to quantify lighter elements and provide information for the confirmation of stoichiometry was also demonstrated by the analysis of a MAX-phase Ti_3SiC_2 coating on a silicon substrate. MAX-phase materials are compounds exhibiting the best traits of both metals (electrical and thermal conductivity) and ceramics (thermal stability and resistance to oxidation). These properties are highly dependent on their chemical composition and crystalline structure, and growing thin films of these materials is decidedly non-trivial. Thus the characterisation of these layers is critical when preparing materials using these compounds as protective coatings. A clear distinction was visible in the GD-OES depth profile between the MAX-phase layer (155 nm), the interstitial silicon nitride and oxide layers (200 and 10 nm respectively) and the silicon substrate. The stoichiometry of the thin layer was easily confirmed from these results.

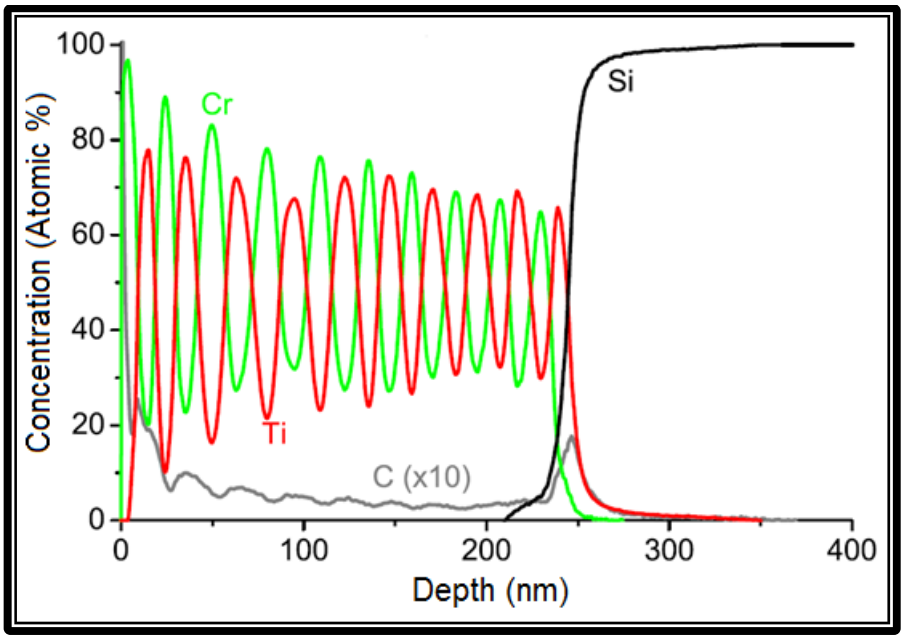

Figure 3-9: Graph showing alternating chromium and titanium layers on a silicon substrate

GD-OES is one of only a few techniques capable of quantifying hydrogen contamination and is the only method for quantification in the sub-ppm range and at depths of more than ten microns [83]. A challenge in this however is calibration as very few certified reference materials are available due to poor stability of hydrogen concentrations in standards. The presence of hydrogen in the glow discharge plasma also has an effect on line intensities as well as on the form of the GD crater formed. These factors must be taken into account for accurate quantification. In steel, the presence of even small hydrogen contamination may cause a reduction of ductility and mechanical strength which leads to hydrogen embrittlement [83]. A synthetic sample (multiple layers of vanadium and iron loaded onto a sapphire substrate with a defined quantity of hydrogen) was prepared to demonstrate the potential and limitations of GD-OES to characterise this type of material. As expected the hydrogen contamination was clearly observed almost exclusively in the vanadium layers due to hydrogen's significantly greater solubility in vanadium than in iron. These results were confirmed by APT [83].

The analysis of ultra-thin layers on materials such as a hard disk, a thin anodic alumina layer and the oxide film on stainless steel was undertaken using radio frequency glow discharge optical emission spectrometry (RF-GD-OES) [84]. This was done to showcase the potential of GD-OES for the characterisation of material layers of less than 10 nm thickness. In this field Auger Electron Spectroscopy (AES) and Secondary

Ion Mass Spectrometry (SIMS) have traditionally been the primary techniques. In the first example, a hard disk consisting of successive layers of aluminium, amorphous nickel-phosphorus, chromium, cobalt chromium magnetic alloy, diamond-like carbon and a thin layer of carbon-based lubricant was analysed by both GD-OES and transmission electron tomography (TEM). As with the TEM the layers of materials were clearly distinguishable with the GD apparatus; an added advantage was the identification of several impurities, such as lead, zinc, iron and sodium, present due to the manufacturing process of the disk. The matrix effect influencing SIMS analysis is absent in GD-OES. The anodic alumina films were chosen so as to assess the depth resolution of the technique as the layers are of a highly uniform thickness. This uniformity is a result of being grown by anodic oxidation over electropolished, high purity aluminium substrates. Again a sample was first analysed by TEM, see **Figure 3-10**, showing a clear boundary between the alumina (top) and aluminium (bottom) layers at a depth of 360 nm.

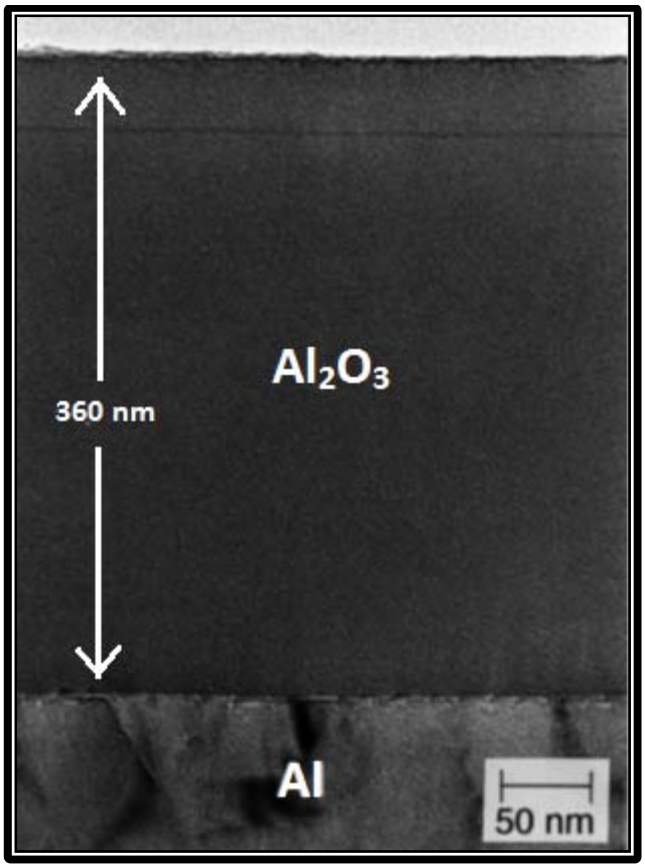

Figure 3-10: TEM image of 360 nm thick alumina film

Once again GD-OES results were comparable (see **Figure 3-11**) with a clear differentiation between the two layers at approximately 360 nm with the GD-OES

showing a transition zone of approximately 6 nm. For purposes of reproducibility a thin, sputter-deposited stainless steel film on a mirror-polished silicon wafer was used rather than bulk stainless steel sheet. The stainless steel layer was then air-oxidised to form an outer oxide layer. This layer is easily characterised both by SIMS and RF-GD-OES with the iron oxide being clearly observable immediately before the chromium and then nickel layers are seen.

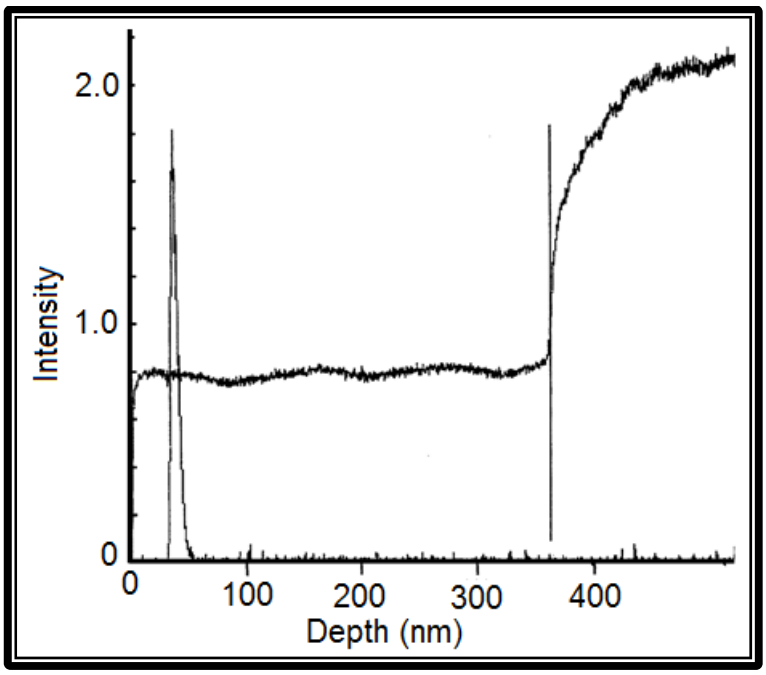

Figure 3-11: GD-OES graph showing Depth (nm) vs. Intensity (Al 396 nm) of a 360 nm thick alumina film with a Cr impurity seen at approximately 40 nm

The effect of GD sputtering was investigated with regard to element enrichment and oxidation state after analysis [85]. Two coating types, specifically an iron oxide film deposited on a silicon substrate and a chromate conversion coating on a galvanized steel substrate, were analysed by RF-GD-OES. The thickness of the films was determined first by SEM analysis while the composition, morphology and homogeneity were confirmed by X-ray diffraction (XRD), Auger electron spectroscopy (AES) and atomic force microscopy (AFM). The oxygen ratios of the layers were evaluated in quantitative depth profiles (QDP) in order to determine the oxidation states of the metals, before and after sputtering. It was found that the sputtering process led to an enrichment of metal atoms relative to oxygen at the sputtered surface. This was confirmed by X-ray photoelectron spectroscopy (XPS) both at the original surface layer and at the bottom of the GD crater. This effect was attributed to preferential sputtering of oxygen atoms from the surface, leading to the reduction in oxidation state of the

remaining metal atoms, e.g. Cr^{6+} to Cr^{3+}. The species of iron oxide, whether Fe_3O_4 or Fe_2O_3, was easily determinable by GD analysis with the chromium oxide being slightly more difficult due to already mixed oxidation states. A change in metal to oxide ratio was clearly observed by XPS with as much as 39% of the iron content having been reduced in the case of the Fe_2O_3 and all surface Cr^{6+} being reduced to lower oxidation states in the chromite samples. The element ratios and layer depth, as determined by GD-OES, were in line with the results obtained from the more commonly accepted SEM technique's results.

Lead zirconate-titanate (PZT) thin films deposited by chemical deposition on a platinum-coated silicon substrate have been characterised by GD-OES [31]. Thin film layers of this type are of interest in the electronics field in the development of micro-electromechanical systems (MEMSs) as well as dynamic access and ferroelectric random access memories (DRAMs and FERAMs). GD-OES was used to profile lead, silicon, titanium, oxygen, hydrogen, nitrogen and carbon in order to characterise the layer and determine the stoichiometry of the compounds formed. Platinum and zirconium were not determined due to the instrument not being configured for their detection. The composition of these 350 nm PZT layers was accomplished with sufficient resolution to identify the stoichiometry of the materials at various depths and also to observe expected segregation and migration behaviors expected of the materials from previous work and theory.

Boron in zirconium-niobium alloys for nuclear application has been measured by GD-MS [86]. Being a strong neutron absorber it is critical that the quantity of the boron in these materials be accurately analysed down to trace and ultra-trace levels. The GD instrument was calibrated using both Zircaloy and NIST steel certified reference materials. The steel standards were useful in that they contained certified values for boron and zirconium at lower concentrations than found in the Zircaloy standards. Once calibrated, the boron recovery was compared to both the reference value as well as values obtained using DC arc atomic emission spectrometry. The results were found to be in fairly close agreement with values ranging from 0.10 to 10.45 mg kg^{-1}. Percentage relative standard deviations between four replicate analyses were found to be between 1.3 and 9.6%. The detection limit for the method was determined to be 13 µg kg^{-1}.

3.4. CONCLUSION

As demonstrated in this chapter, there are a large number of both sample preparation and detection methods for various zirconium–containing materials. These are, however, generally fairly specific in their application and not suitable for general analysis of industrial products. Most methods seem particularly focused on trace level quantities of zirconium and are thus not ideal for the quantification of zirconium in industrial zirconium products. These methods must therefore be adapted or new methods developed in order to serve the needs of this study.

Chapter 4: Selection of Analytical Techniques

4.1. INTRODUCTION

The selection of appropriate digestion, sample preparation and instrumental techniques is crucial when undertaking the analysis of any material. Most instrumental techniques require that samples be in a compatible state before they can be analysed. Conversion to this compatible state may entail breaking down the material's structure and solvation in order to attain a homogenous solution, although this is not always the case. It is also necessary to select an appropriate instrumental technique as some are better suited than others to specific types of materials. In this section various forms of sample preparation as well as quantification techniques are discussed.

4.2. EVALUATION OF DIGESTION TECHNIQUES

In order to prepare a sample for analysis it must often be broken down into soluble components. There are several techniques which can be used in order to achieve this destruction of the sample matrix. These include acid dissolution/extraction (also known as wet-ashing), dry-ashing, fusion with a molten salt, and microwave digestion [43]. Dry-ashing is applicable primarily to organic materials such as plant matter and is thus outside of the scope of this study. Some instruments require that samples must be in solid phase and in those cases the production of a homogenous, solid pellet is sometimes necessary.

4.2.1 ACID DISSOLUTION AND EXTRACTION

There are several modes of action by which acids solubilise insoluble materials. These include neutralisation (acid-base or chemical exchange), decomposition, rearrangement, redox (reduction/oxidation), complexation or a combination of these reactions [87]. An example of both neutralisation and subsequent decomposition is the reaction between calcium carbonate and hydrochloric acid.

$$CaCO_3+2HCl \rightarrow CaCl_2+H_2CO_3 \qquad \textbf{4-1}$$

In this reaction the basic carbonate ion reacts with acid protons to yield carbonic acid (**Equation 4-1**). This process also exchanges the H^+ with the Ca^{2+} cations.

$$H_2CO_3 \rightarrow CO_2 + H_2O \qquad \textbf{4-2}$$

The carbonic acid then decomposes into carbon dioxide and water which drives the reaction forward in accordance with Le Chatelier's principle (**Equation 4-2**). This gives the net reaction seen in **Equation 4-3**.

$$CaCO_3 + 2HCl \rightarrow CaCl_2 + CO_2 + H_2O \qquad \textbf{4-3}$$

An example of a rearrangement reaction can be seen in the fusion reaction (discussed in more detail in **section 4.2.2**) between zirconia and sodium pyrosulphate (**Equation 4-4**) [87].

$$ZrO_2 + 2Na_2S_2O_7 \rightarrow 2Na_2SO_4 + Zr(SO_4)_2 \qquad \textbf{4-4}$$

In this reaction the insoluble zirconia is converted into the soluble zirconium sulphate by an ion exchange reaction and rearrangement of oxygen atoms.

Redox reactions occur when electron density is transferred from one species to another, resulting in a change in oxidation state. This is often encountered when using oxidising acids, such as nitric and perchloric acids. Here an analyte metal is oxidised to a higher, stable oxidation state by the simultaneous reduction of the reagent. An example of this is seen in **Equation 4-5** where uranium metal is oxidised to the +6 oxidation state [87].

$$U + 8HNO_3 \rightarrow UO_2(NO_3)_2 + 6NO_2 + 4H_2O \qquad \textbf{4-5}$$

The corresponding reduction process takes place as nitrate anions are reduced to nitrogen dioxide.

Complexation reactions take place when metal cations form complex ions with the anions provided by the acid reagent. The dissolving power of strong complexing acids, such as hydrochloric and hydrofluoric acids, is dependent on the ability of the analyte metal to form stable, water soluble complexes with the available anions. An example of this can be seen in **Equation 4-6** where the zirconium in zirconia (ZrO_2) complexes with fluoride anions to form the ZrF_6^{2-} species [88].

$$ZrO_2 + 6HF \rightarrow H_2ZrF_6 + 2H_2O \qquad \textbf{4-6}$$

It is important to note that this is also a redox reaction wherein the zirconium is oxidised to its highest, stable oxidation state by the reduction of hydrogen from the acid. Hydrogen gas is then removed by volatilisation, again driving the reaction forward. This serves to emphasise that few acid solubilisation reactions fall into a single one of the categories discussed. Most act by several processes to achieve the desired effect.

The most common dissolution media for inorganic materials are the mineral acids [43, pp. 1042-1044]. For many materials this can be achieved simply by heating in the presence of mineral acids in an open vessel. Agitation by swirling or the generation of gases such as hydrogen can accelerate this process. The rate of dissolution also increases inversely with sample particle size. Fine powders (with a large surface area) may dissolve quickly while large, solid pieces take significantly longer. Dissolution is considered complete when no solid phase sample is left in solution. If this does not occur the process is referred to as extraction. It is generally advisable to perform this kind of dissolution in a fume hood as many of these acids exist as dissolved gases, which are evolved upon heating.

Hydrochloric and hydrofluoric acids

In the case of hydrochloric acid (12 M), HCl gas is evolved upon boiling until the concentration is reduced to 6 M. This acid is more useful in the dissolution of inorganic samples than organic ones and is widely used in the dissolution of metal oxides. It is a very widely used acid in digestion as most metals, alloys and ores will eventually be dissolved, given sufficient time [89, pp. 70-78]. The dissolution by hydrochloric acid often is dependent on the stability of the chloride complexes or salts of the analyte elements. Most metals, including iron, zinc, cadmium, aluminium and gallium dissolve readily but in some cases a small quantity of mercury can be added, as a catalyst, to accelerate the oxidation process. Ores such as carbonates, sulfides, borates, phosphates, limestone and dolomite dissolve as well, mainly due to neutralisation. Certain oxides of iron, aluminium, zirconium, beryllium and others are resistant to hydrochloric acid attack, however. For specific applications other non-acidic oxidising agents are sometimes added to hydrochloric acid. For instance bromine, stannous chloride, ammonium chloride and boric acid assist in the dissolution of lead and antimony alloys, zinc ore, cement and fluorspar respectively. When subjected to high pressure and elevated temperatures, even chemically inert materials can be digested quickly with hydrochloric acid, as discussed later in **section 4.2.3**.

Hydrofluoric acid is most often used in the dissolution of silicate samples. Like hydrochloric acid it is mainly a non-oxidising, complexing dissolution agent. Its ability to aggressively attack siliceous materials such as glasses, quartz and refractories is unique. It is generally used to analyse species other than silicon, as a product of this dissolution is the volatile silicon tetrafluoride. When dissolving silicates it is generally most effective when used alone, but for other materials it is much more efficient when mixed with other acids. Mixed with hydrochloric acid it can be used to dissolve cement, various ores, and titanium and zirconium alloys. Similarly to hydrochloric acid it forms many fluoride metal complexes of varying stability, solubility and coordination numbers. Some of the most stable complexes are those of zirconium, boron and beryllium. Fluoride ions are notoriously difficult to remove from solution because of the formation of these extremely stable, soluble complexes. For this reason it is often avoided as dissolution reagent when a precipitation procedure is part of the analysis. Insoluble fluoride salts can also be formed, such as those of magnesium, calcium, barium and strontium. For this reason care must be taken when preparing samples with these elements.

Figure 4-1: Images of a burn resulting from exposure to hydrofluoric acid [90]

The high toxicity of hydrofluoric acid is also a prohibiting factor in its use. The results of hydrofluoric acid burns can be seen in **Figure 4-1**. When the acid makes contact with skin it must be immediately washed off, followed by application of a complexing agent such as calcium gluconate. Regardless of first aid measures taken even moderate contact must always be treated as serious and the subject must seek medical help as soon as possible.

Nitric acid

Hot, concentrated nitric acid is a powerful oxidising agent in addition to its acidic properties. This makes it ideal as a reagent in the decomposition of organic material, converting the organics into carbon dioxide and water. If this decomposition is performed in an open vessel, however, non-metals such as halogens and sulphur are often lost through volatilisation. Nitric acid (either concentrated or dilute) readily dissolves many metals, including bismuth, copper, cobalt, nickel, mercury, silver, lead, selenium, zinc and cadmium. Unfortunately other metals form a resistant, oxide passivation layer. These include aluminium, zirconium, chromium, titanium, hafnium, gallium, indium, niobium, tantalum, boron and thorium. Nitric acid's primary mode of action is by oxidation and these metals form layers of highly stable oxides, protecting the rest of the metal. Very few elements form stable nitrate complexes (gold and thorium being exceptions), thus nitric acid is a weak complexing agent in contrast to hydrochloric and hydrofluoric acids. When nitric acid is used for the wet-ashing of organic materials there is a risk of the formation of explosive organic nitrates. For this reason care must be taken when performing these digestions as well as in the storage of the concentrated acid [91].

Aqua regia

Mixtures of mineral acids, such as *aqua regia*, are often more effective in the rapid dissolution of samples [87]. The reaction between these acids can be seen in **Equation 4-7** but the interaction of these acids is more complex than is immediately apparent [87].

$$3HCl+HNO_3 \rightarrow NOCl+Cl_2+2H_2O \qquad \textbf{4-7}$$

The elemental chlorine, nitrosyl chloride and various unstable (highly reactive) intermediate products evolved exhibit oxidising properties. The chlorine and nitrosyl chloride also have a catalytic effect in addition to their complexing power. As such this mixture in equilibrium can act by redox (reduction of chlorine or hydrogen), complexation (chlorine and chloride), chemical exchange (chloride), neutralisation (hydronium ion) and oxidation (nitric acid, chlorine and nitrosyl chloride) pathways. The addition of other oxidising agents to acids, such as bromine and hydrogen peroxide, has a similar enhancing effect. This does, however, come with risk involved. In the case of mixed nitric and perchloric acid, severe explosions can occur if all the nitric

acid evaporates before oxidation of the organic material is complete. The process of oxidative decomposition of organic materials by mineral acids is often referred to as wet-ashing. **Table 4-1** shows a number of mineral acids and their most common uses.

Table 4-1: Examples of acid used for wet-ashing [87]

Acid	Typical Uses
Hydrofluoric Acid (HF)	Removal of silicon and destruction of silicates; dissolves oxides of Nb, Ta, Ti, and Zr, and Nb, and Ta ores.
Hydrochloric Acid (HCl)	Dissolves many carbonates, oxides, hydroxides, phosphates, borates, and sulfides; dissolves cement.
Hydrobromic Acid (HBr)	Distillation of bromides (e.g., As, Sb, Sn, Se).
Hydroiodic Acid (HI)	Effective reducing agent; dissolves Sn^{+4} oxide and Hg^{+2} sulfide.
Sulphuric Acid (H_2SO_4)	Dissolves oxides, hydroxides, carbonates, and various sulfide ores; hot concentrated acid will oxidise most organic compounds.
Phosphoric Acid (H_3PO_4)	Dissolves Al_2O_3, chrome ores, iron oxide ores, and slag.
Nitric Acid (HNO_3)	Oxidises many metals and alloys to soluble nitrates; organic material oxidised slowly.
Perchloric Acid ($HClO_4$)	Extremely strong oxidiser; reacts violently or explosively to oxidise organic compounds; attacks nearly all metals.

Sulphuric acid

Sulphuric acid is not a dissolved gas and much of its effectiveness as a solvent can be attributed to its high boiling point (340ºC). It is a powerful dehydrating agent and at this temperature most organic materials are oxidised, leaving only carbon dioxide and water vapour behind. Dehydration of organic materials by sulphuric acid is achieved by removing OH^- and H^+ groups from adjacent carbon atoms with subsequent neutralisation [87]. Hot, concentrated sulphuric acid is mildly oxidising allowing it to dissolve metals like lead- and tin-based alloys. When diluted it is capable of rapidly dissolving iron-based alloys such as ferrotitanium and ferrochromium, as well as

aluminium, beryllium, chromium and titanium. The addition of a mercury (II) salt can accelerate the process by forming a mercury amalgam. This addition also makes the dissolution of copper metal possible. It is sometimes used in the dissolution of minerals as well, such as cryolite, fluorspar and monazite. Stable cyanides formed in the processing of precious metals are destroyed by fuming with sulphuric acid. This process does, however, evolve cyanide gas.

Perchloric acid

Like sulphuric acid, perchloric acid also has a relatively high boiling point (203ºC). It is often used in the dissolution of steels and other iron alloys which are not affected by other acids. Hot, concentrated perchloric acid is highly explosive, however, and special care must be taken in its use. It must never be allowed to come into contact with organic material or easily oxidisable inorganic samples. The cold, concentrated and hot dilute acid is not explosive however. Hot, concentrated perchloric acid does, however, dissolve all metals (with the exception of gold and some platinum group metals), making it fairly useful. It is also able to dissolve certain ores though these are generally limited to those containing sulfides and fluorides.

Phosphoric acid

Phosphoric acid is able to dissolve alumina, chromium ores, iron oxide ores and slags. Despite this it is seldom used in sample digestion as the phosphates interfere with many separation procedures. In addition it attacks glass at temperatures exceeding 300ºC. It has been used to selectively dissolve silicates without digesting quartz [87].

In some cases the addition of pressure can enhance the action of acid on a given sample [87]. Materials that do not normally digest completely in open vessels can sometimes be dissolved in a high pressure digestion “bomb”. Inside one of these bombs the digestion medium can achieve temperatures well above its normal boiling point, greatly enhancing its efficacy. These bombs are usually lined with polytetrafluoroethylene (PTFE or Teflon™) and the bomb is always left with sufficient vapour space (at least one third of the total volume) above the contents. Care must be

taken, however, as the use of this method can increase the likelihood of explosion. This concept is further explored in **section 4.2.3**.

4.2.2 FLUX FUSION

Insoluble or partially soluble substances, usually oxides, can be brought into acid or basic solution by fusion with a molten salt such as anhydrous sodium carbonate, amongst others [92]. Fusions are effective by virtue of the high reaction temperatures used (typically between 300 and 1000ºC) as well as the large reagent concentrations brought into contact with the sample [43, pp. 1049-1050]. They act by mechanisms analogous to dissolution by acid with oxidation and neutralisation (acid/base or chemical exchange) processes occurring. The specific processes are based on each individual reagent's oxidation potential and Lewis acidity. For certain fluxes complexation reactions may also occur. The nature of the flux must therefore be carefully selected to be compatible with the sample matrix. An acidic flux will generally be preferable when digesting a basic sample, for instance. **Figure 4-2** shows a number of flux fusion reagents arranged according to their Lewis acid/base properties and oxidising potential. All fusions begin by creating an intimate mixture of sample and fusion reagent. Both materials must be in a fine powder form to ensure sufficient mixing. The weight ratio is generally of crucial importance but this varies between applications. The mixture is then heated, either by a gas burner or muffle furnace, to slightly above the reagent's melting point [87]. A sand or oil bath may also be used but it is difficult to maintain higher temperatures with this approach [87].

When using a gas burner the difficulty in achieving even heating is a drawback. Muffle furnaces provide both even heating and high temperatures but it is difficult to manipulate or monitor samples during fusion. The temperature at which a fusion is performed varies considerably by application but excessive temperatures should be avoided as much as possible. This is done to avoid attack on the crucible by and decomposition of the flux. The fusion process can take anywhere between several minutes and a few hours, depending on the flux and the sample. During digestion it is often necessary to swirl the molten salt mixture to ensure complete dissolution. A fusion is considered complete when all visible sample material is gone. Generally a clear melt is a good indicator of complete dissolution. Upon cooling the melt is generally dissolved or leached into water and then acidified. This can also be done directly with the addition of dilute acid.

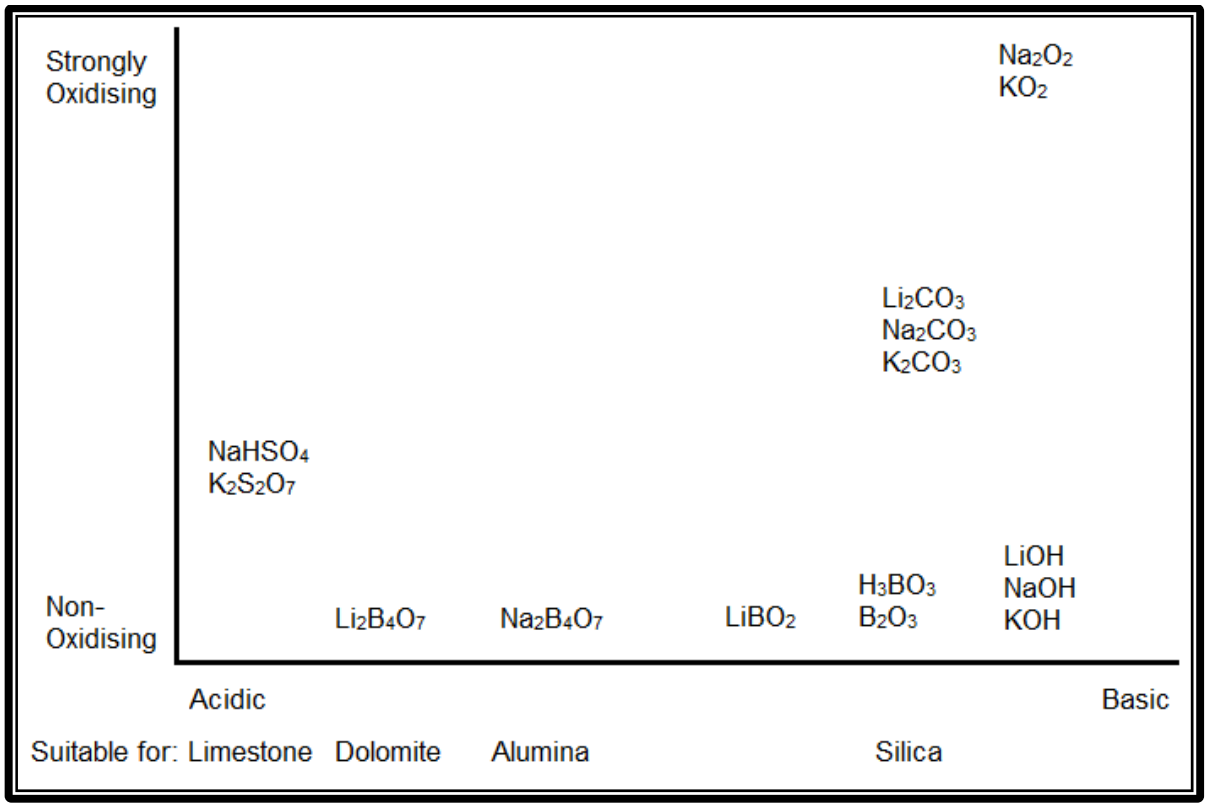

Figure 4-2: Diagram ordering fluxing reagents by their oxidising potential and Lewis acidity [89, p. 84]

Sodium carbonate

Sodium carbonate is an extremely popular fluxing agent [89, pp. 82-88]. It is capable of the complete dissolution of a wide range of materials including, but not limited to, silica and siliceous compounds, alumina, asbestos, beryl, bauxite, feldspar, apatite, titanium boride, tungsten and iron ores as well as most refractories and ceramics. A major advantage of this reagent is that, upon dissolution in acidic medium, the carbonate is evolved as carbon dioxide, removing the flux anion from the matrix. The addition of an equal quantity of potassium carbonate creates a mixture that melts at a temperature significantly lower than either compound alone (710°C). This mix is often used for high-alumina silicates as well as molybdenum and tungsten ores. Alkali carbonates are often used in combination with other reagents. The addition of sodium tetraborate allows for the dissolution of corundum and zirconia, amongst others. A 1:1 mixture with elemental sulphur is used in the “Freiberger decomposition” from which soluble species of several elements (vanadium, tin, palladium, iridium etc.) can be leached. This process leaves behind insoluble sulfides of lead, iron, bismuth and

cadmium amongst others. Carbonate fusions are often performed in platinum crucibles despite the loss of a small amount of platinum (1 to 2 mg per fusion) [87]. This can be minimised though by using a crucible lid or performing the fusion in an inert atmosphere.

Borates

Another popular group of fusion reagents are the borates [87]. These include boric acid, sodium tetraborate, lithium tetraborate and lithium metaborate. Boric acid is often used when determining alkali metals. Boric acid itself has a low melting point (169ºC) but decomposes to boron trioxide (by loss of water), which has a significantly higher melting point (580ºC). Boric acid is often used in the fusion of blast furnace slag, zircon, siliceous and aluminous minerals and barium titanate.

Sodium tetraborate (borax) is non-oxidising and is not particularly acidic or basic. This reagent alone has many drawbacks so it is generally used in combination with other fluxes. These drawbacks include a tendency towards making viscous melts, volatilisation of mercury, thallium, selenium and arsenic, and reduction of certain metals (copper, iron, bismuth etc.) which then alloy with the crucible. It is thus most often used in conjunction with sodium carbonate. A wide range of materials can be dissolved by varying the composition of the sodium carbonate/tetraborate mixture. Granite, chromite, spinel, and bauxite are a few of these. Lithium tetraborate is frequently used in the production of glass disks for use with X-ray fluorescence spectroscopy as it is less hygroscopic than sodium tetraborate. It is quite viscous, however, and special platinum/gold alloy crucibles must be used to avoid “wetting” by the flux. It is an acidic flux making it well suited to the dissolution of basic compounds such as zirconia, magnesite, limestone and dolomite. It is also less effective in dissolving high silica content materials due to their increased acidic nature.

By contrast lithium metaborate is quite basic, making it ideal for the dissolution of high silica-containing samples. As melts which are formed with this reagent are easily soluble in dilute acids it is often used in sample preparation techniques for ICP, AA and wet chemical analyses. A mixture of lithium tetraborate and metaborate in a 1:4 ratio has been found to be more effective across a wider range of samples than either one alone. Lithium metaborate and tetraborate have another marked advantage in the analysis of silica in that upon dissolution of the melt in acid, it does not form insoluble silicates.

Pyrosulphate and Peroxides

Potassium pyrosulphate and sodium bisulphate are very similar oxidising fluxes and, as such, are among the few fluxes that are able to fuse metals directly. Alloys like steel, brass, bronze, monel and various lead alloys are all dissolved by fusion with these reagents. As such it is often used as an alternative to acid dissolution where acid treatment may result in chemical interferences. Sodium peroxide is another powerful fluxing agent, so much so that only highly resistant zirconium metal is considered as a good crucible material when these peroxides are used as fluxing agents. Use of this reagent does carry an element of risk, as it can be explosive, but with proper precautions it may be used to great effect. It may be used for many “difficult” materials such as chromium ores, monazite, wolframite, ilmenite and other tungsten ores.

Alkali hydroxides

Seldom-used fluxes include the basic sodium, potassium and lithium hydroxides. These are used almost exclusively in the digestion of minerals such as silicates, slags, fluorite, mica, diaspora, serpentine and feldspar, among others. Fusions with these fluxes are generally rapid (15 to 20 minutes) and the melts are easily dissolved in water [87]. As the temperature of fusion is comparatively low (450 to 500ºC) there are also fewer losses of desired analytes due to volatility.

Crucible selection

The choice of crucible in which the fusion is performed is also important as many fluxes are capable of damaging and even destroying the specific metal or metal oxide materials from which the crucibles are constructed. **Table 4-2** contains a list of some popular fluxes, crucible materials and applications. Platinum crucibles are used when the fluxing agent is sodium carbonate, lithium metaborate, lithium tetraborate or potassium pyrosulphate. It is the material of choice for most applications as it is almost entirely unaffected by most mineral acids, including hydrofluoric acid. It is only attacked by very hot phosphoric acid and *aqua regia*. Gold, silver, nickel or iron crucibles can be used for sodium carbonate or sodium peroxide while only nickel can be used for potassium nitrate. Other crucible materials include zirconium, graphite, alumina and porcelain [87].

Table 4-2: Table of popular fluxing reagents, appropriate crucible materials, conditions and analyte types [93]

Flux	Crucible	Flux: Sample ratio and Temperature (°C)	Most Popular Applications
$K_2S_2O_7$	Pt	20:1 ; 500 °C	TiO_2, ZrO_2, Nb_2O_5, Ta_2O_5
Lithium Borates	Pt + Au	10:1 ; 1200 °C	SiO_2, Al_2O_3, alumino-silicates
NaOH or KOH	Ag or Ni	20:1 ; 750 °C	Silicates (glass, porcelain, kaolin etc.)
(7:1) KOH:KNO_3	Ag or Ni	10:1 ; 650 °C	Ruthenium, chromite, "Organics"*
Na_2CO_3	Pt	20:1 ; 1000 °C	Minerals, silicates, refractories, insoluble metal fluorides

Graphite crucibles are often used as an inexpensive alternative to metal ones. They have the added advantage of being disposable, eliminating the need for cleaning and chance of cross-contamination. Although they do oxidise slowly at temperatures in excess of 430ºC, for the most part they are chemically inert and heat-resistant. Graphite crucibles also have the advantage of removing the possibility of metal contamination from the slow digestion of the crucible. It has been claimed that graphite crucibles are also effective when using lithium metaborate as fluxing agent but platinum crucibles are more commonly used.

4.2.3 Microwave-assisted Acid Digestion

With the widespread introduction of microwave ovens in homes in the last century it was only a matter of time before they were used in chemical laboratories [94]. As the speed and efficiency of chemical analysis instrumentation increased, sample preparation was fast becoming the slowest step in analytical methodology. Since the first reported use of a microwave oven for sample preparation in 1975, this technology has revolutionised sample preparation and synthetic procedures by greatly reducing sample preparation time and allowing a vast range of new procedures to be developed. A basic design for a microwave heating system can be seen in **Figure 4-3**. Microwave-assisted sample preparation is applicable to such vastly different sample matrices as ceramics, minerals, biological materials, plant and food samples. Microwave heating

offers many advantages over conventional heating [95]. These include but are not limited to non-contact heating, energy transfer rather than heat transfer, rapid heating, material selective heating and a higher level of safety and automation. Loading time of the instrument must always be taken into account, however, and can mitigate or negate any gains in dissolution speed [89, p. 80]. As the method is still essentially an acid dissolution, mineral acids are still used in a similar manner to those described in **section 4.2.1**. Care, however, must be taken to avoid potentially explosive mixtures when using high pressure vessels. An example of this would be the use of a strongly oxidising dissolution medium (such as nitric acid, for instance) with an organic sample. This may result in the formation of explosive nitrates in a heated, pressurised vessel. If this were performed with sufficient material it would almost certainly result in an explosion.

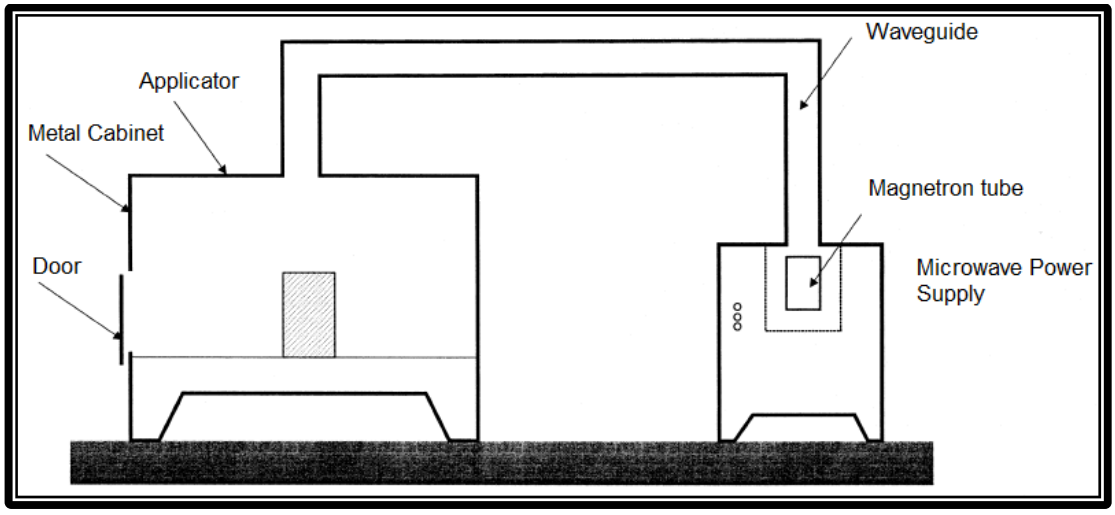

Figure 4-3: Basic layout of a microwave heating system [95]

4.2.4 SOLID PELLET PREPARATION

In cases where a solid sample is required by the instrumental technique it is often necessary to press a pellet, especially when the sample is in powder form [62]. This is a relatively simple procedure wherein a mass of sample is weighed off and compressed, usually by a pneumatic or hydraulic press. In cases where the sample alone does not yield a solid pellet, a binding agent may be required. Depending on the analytical technique to be applied, different binding materials may be required. Boric acid may be used as a binder [61], acting either as a substrate or with the sample mixed thoroughly into it. Other examples of binder are waxes, methylcellulose and organic polymerisation agents [96, p. 98]. These polymerisation agents may require heating as well as pressure to form a suitable pellet. If a conductive pellet is required

it may be pressed with a metal powder such as silver, tantalum or titanium. Depending on application, pressed pellets may or may not require polishing. Particle size of both the analyte and binder are of great importance with regard to homogeneity. If the particles are too big, or there is too great a discrepancy in particle size between analyte and binder, the sample mixture will exhibit poor homogeneity, resulting in poor analytical results. This lack of homogeneity has a significantly adverse effect on accuracy and precision of measurement in most analytical techniques. Thorough grinding or other refining methods are often required prior to pellet pressing.

4.3. EVALUATION OF SPECTROMETRIC TECHNIQUES

Depending on the analyte of interest and nature of the sample matrix, various instrumental methods may be of use. Many modern instruments rely on the absorption or emission of electromagnetic radiation by the analyte. These include UV/VIS, AAS, ICP-OES, XRF and GD-OES [97]. Others, like ICP-MS and other MS techniques, selectively detect charged ions. These methods have significant advantages over older techniques like titrimetry and gravimetric methods in terms of speed, cost and interferences.

4.3.1 UV/VIS SPECTROPHOTOMETRY

The spectrophotometer, often referred to as an ultra-violet/visible light (UV/VIS) spectrophotometer, is a staple of analytical chemistry. These instruments typically detect electromagnetic radiation in the near UV (185-400 nm), visible (400-700 nm) and very near infrared (700-1100 nm) regions of the spectrum [98, pp. 167-202]. The first commercial models were used in labs as early as the 1950s [43, pp. 771-775] and newer instruments are still one of the most common fixtures in any laboratory. There are many variations on the basic design but all contain the basic elements of a high stability, broad spectrum light source, a monochromator (or filter) and some form of transducer. The instrument operates on the principle of absorption of light at characteristic wavelengths by an analyte. The light source must thus be capable of producing light across the entire visible and near ultra-violet spectrums. An example of a light source would be a tungsten lamp, often used in older instruments. This light is then passed through a monochromator to select for specific wavelengths before being passed through the analyte solution. An advantage of this system is that the wavelength can be varied continuously, making it possible to record an entire spectrum. The light is then passed through the sample where some of it is absorbed

by the analyte. The light which is not absorbed is then detected and quantified by an electronic transducer, often a photomultiplier tube (PMT) or charge-coupled device (CCD). In many instruments the light is split into two beams, one of which passes through the analyte while the other passes through a reference cell. These are known as double-beam instruments.

The ratio of light passing through the analyte solution vs. that passing through a blank solution or reference cell gives both the transmittance (**Equation 4-8**) and absorbance (**Equation 4-9**) of an analyte solution at any specific wavelength [43, pp. 718-724].

$$T = \frac{P}{P_0} \qquad \textbf{4-8}$$

In **Equation 4-8** *T* represents transmittance while P_0 and *P* are the measured beam intensities (arbitrary units) before and after absorption respectively.

$$A = -\log T = \log \frac{P_0}{P} \approx \log \frac{P_{Solvent}}{P_{Solution}} \qquad \textbf{4-9}$$

In **Equation 4-9** *T*, P_0 and *P* have the same values as in **Equation 4-8**, *A* represents absorbance while $P_{Solvent}$ and $P_{Solution}$ are roughly equivalent to P_0 and *P*. They are only roughly equivalent as they suffer losses from scattering in solution and reflection at the interfaces between mediums. In most cases these include air-glass and glass-solution interfaces.

$$A = \log \frac{P_0}{P} = \varepsilon bc \qquad \textbf{4-10}$$

The Beer-Lambert Law (**Equation 4-10**) is often referred to simply as Beer's Law. It relates the amount of attenuation of the beam power ($\frac{P_0}{P}$) to the concentration of the analyte and the path length along which this process occurs. This is done by making use of the proportionality constant *ε*. The concentration of the analyte (*c*) is expressed in molarity while the path length (*b*) is expressed in centimetres. *ε* is defined as the molar extinction coefficient with units (L mol^{-1} cm^{-1}) such that *A* is unitless.

Sources of error when measuring the absorbance of a solution can be attributed to several factors such as cuvette absorption, physical obstruction of the light beam, and operator error [96, pp. 108-111]. When measuring in the UV range, a quartz cuvette must be used as glass absorbs light in this region of the spectrum. Dust in the sample, a cloudy solution, sample temperature effects or dirt on the cuvette wall will also cause

errors. Operator error, such as incorrect line selection, and instrument limitations such as insufficient resolving power, will also lead to poor results.

Spectrophotometric methods have a distinct advantage in that they are rugged, tend towards simplicity, are low cost, exhibit sample flexibility and the required instrumentation is present in almost any chemical laboratory [48]. Disadvantages are the generally small linear dynamic range presented in accordance with Beer's Law and the fact that most of these methods are time and labour intensive. The small linear dynamic range is a result of hydrogen bonding, solute-solute and solute-solvent interactions occurring at higher concentrations (usually >0.01 M) [97, pp. 336-339]. At these concentrations the interactions mentioned can alter the analyte species' ability to absorb specific wavelengths of radiation. The limitation that samples must be in solution and must absorb light in the UV/VIS spectrum requires that samples must often first be dissolved and, if not already coloured, must then be complexed with a colouring agent. An example of this is the determination of iron using thiocyanate as a colouring agent. This produces iron thiocyanate ($Fe(SCN)^{2+}$ in solution) which absorbs light in a large portion of the green area of the visible spectrum (460–500 nm) making it appear a deep red [43, p. 725].

4.3.2 Atomic Absorption Spectrometry (AAS)

Atomic absorption spectrometry was introduced in 1955 and the first commercial spectrometer became available in 1959 [43, pp. 839-865]. The technique relies on the ability of the analyte element to absorb characteristic light wavelengths. Up until this time the method had not been viable as ordinary monochromators with a continuum source were not able to produce radiation bands narrow enough to be completely absorbed by the analyte. This problem was solved by the use of hollow cathode lamps (HCL) with filaments made from or coated with the same material as the analyte. These lamps are generally filled with an inert gas at a pressure of between 1 and 5 torr. When sufficient current is applied the gas ionises and these ions strike the cathode. This results in the "sputtering" of the cathode material with some of this material being in an excited state. This process produces an atomic cloud which emits the characteristic wavelengths desired. Due to the difference in conditions between the lamp and sample (temperature, pressure) the bands generated are not only of the same wavelength as those absorbed by the analyte but narrower as well. Some modern instruments now use high-resolution monochromators with a continuum source rather than HCLs. The

design of a modern AA instrument using a continuum source with a high-resolution monochromator can be seen in **Figure 4-4**.

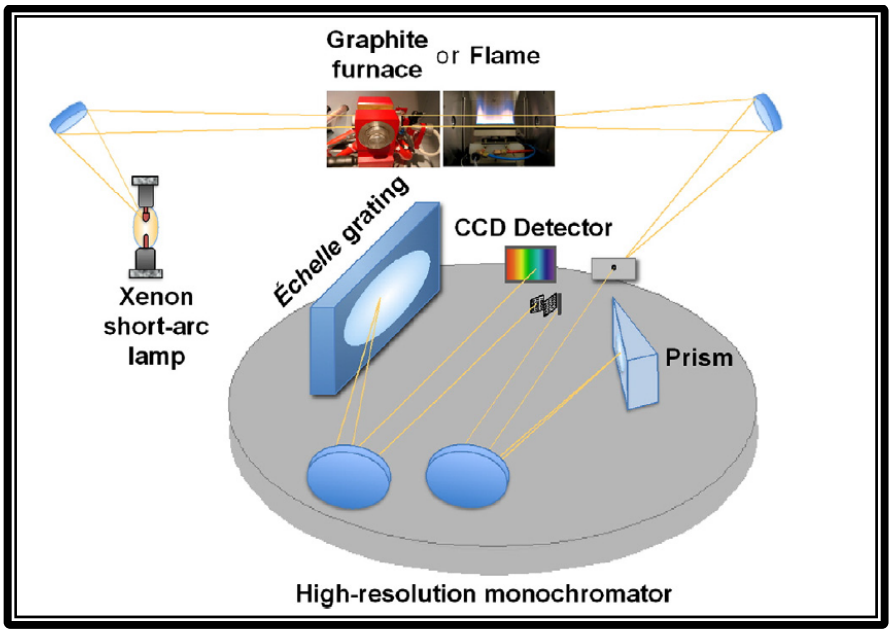

Figure 4-4: Configuration of an atomic absorption spectrometer using a high-resolution continuum source [99]

The construction of an AA spectrometer is fairly similar in concept to a UV/VIS spectrophotometer. The primary difference is in the light source and sampling system. As discussed an element-specific HCL serves as the light source. This light is then passed through the sample. In flame AA light from the HCL is passed through the nebulised and excited analyte in an acetylene flame. Depending on fuel mixtures the temperature in a flame atomiser can range anywhere between 1700ºC (air/propane) and 2800ºC (acetylene/nitrous oxide). Alternatively a graphite furnace may be used to atomise the sample when higher temperatures are required. Graphite furnaces (electrothermal atomisers) allow for a greater degree of control over the heating process. Graphite furnace methods generally include several steps including drying (110ºC to remove water), ashing (300 – 1200ºC to remove carbon) and atomisation (2000 – 3000ºC for analysis). The amount of light absorbed by the analyte is proportional to the concentration of the analyte in the sample in accordance with Beer's Law (**Equation 4-10**). The residual light is then detected with a PMT, CCD or similar device and the absorbance calculated. As the method is still an absorption technique it is still subject to the limitations of Beer's Law. This means that the detection range of the technique is limited and tends to occupy the low parts per million (ppm) concentration range for flame AA and the parts per billion (ppb) range when using a

graphite furnace. Another limitation of the standard AA instrument is the requirement of the element-specific HCLs themselves. As only a single line source is available at any one time, the quantification of multiple elements can be time consuming. This makes the technique a relatively inexpensive and rapid method for applications requiring high sample throughput, but limits its usefulness when multiple elements must be quantified, such as in a research lab.

4.3.3 Inductively Coupled Plasma Optical Emission Spectrometry (ICP-OES)

ICP-OES is superficially similar in concept to AAS. Both techniques use similar detectors, atomise samples by the application of extreme heat and require that samples be in solution. However, instead of relying on absorption, the OES instrument measures the emission of light from excited atoms and ions [43, pp. 839-865]. This is achieved by nebulisation of the analyte sample and excitation in a very high temperature plasma (6000ºC) [100], see **Figure 4-5**.

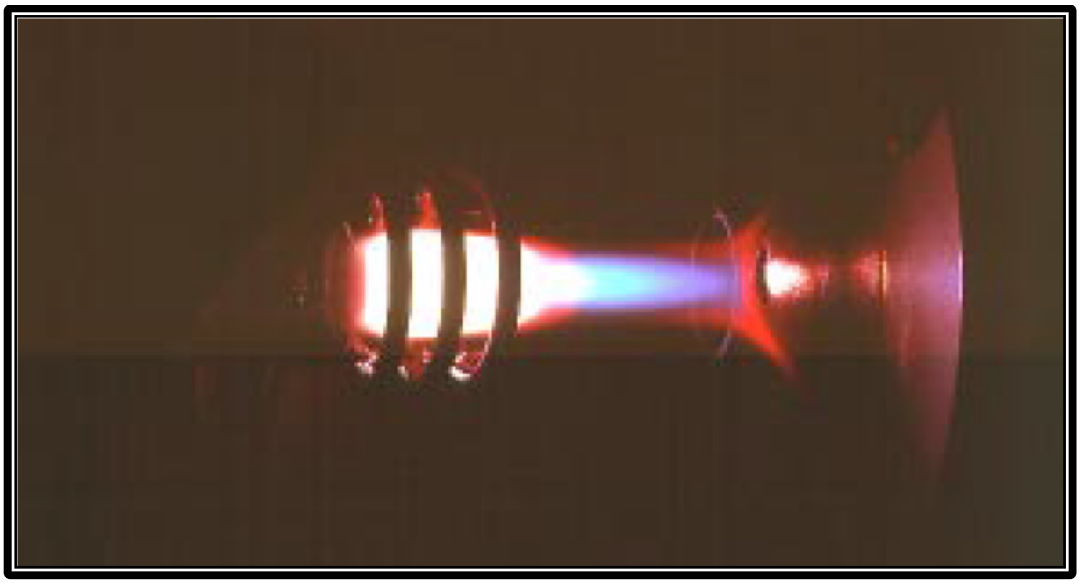

Figure 4-5: An inductively coupled plasma in an ICP-OES system [101]

Sample introduction systems vary between instruments but most have a similar construction, seen in **Figure 4-6**. Sample solution is pumped into a nebuliser specifically by a peristaltic pump in order to minimise pulsing. One of the most popular nebulisers is the concentric nebuliser which has a central capillary through which sample is pumped and an outer channel through which a carrier gas (usually argon) flows [97, pp. 254-269].

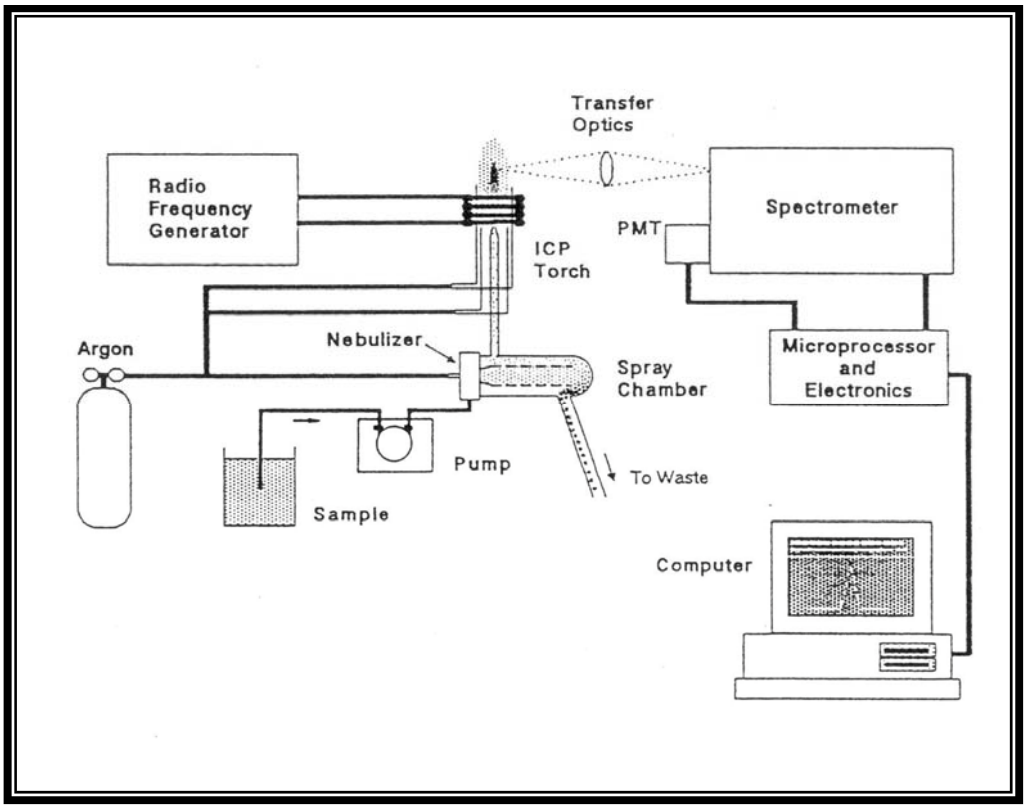

Figure 4-6: Diagrammatic representation of the components of an ICP-OES instrument [100]

Once the sample reaches the end of the inner tube the carrier gas flow nebulises it into a fine mist which is then carried into the spray chamber. This nebuliser has the drawback that it is easily clogged by high salt concentrations in the sample matrix. In cases where this is unavoidable a V-groove nebuliser may be used instead, as it does not suffer this problem but is less efficient than the concentric nebuliser. As with the nebuliser, various types of spray chambers are available for use with ICP-OES. The purpose of the spray chamber is to remove large droplets formed during nebulisation and channel only the fine mist into the ICP torch. Cyclonic (**Figure 4-7**) and Scott-type double pass (**Figure 4-8**) spray chambers are the most commonly found varieties.

Figure 4-7: A cyclonic spray chamber [57]

The ideal particle size for the nebulised solution has been determined to be approximately 10 µm [102, pp. 44-47]. Other sample introduction systems exist, such as laser ablation, slurry and direct introduction. Instruments able to make use of these methods are, however, not nearly as commonly available as those using the solution nebulisation method described.

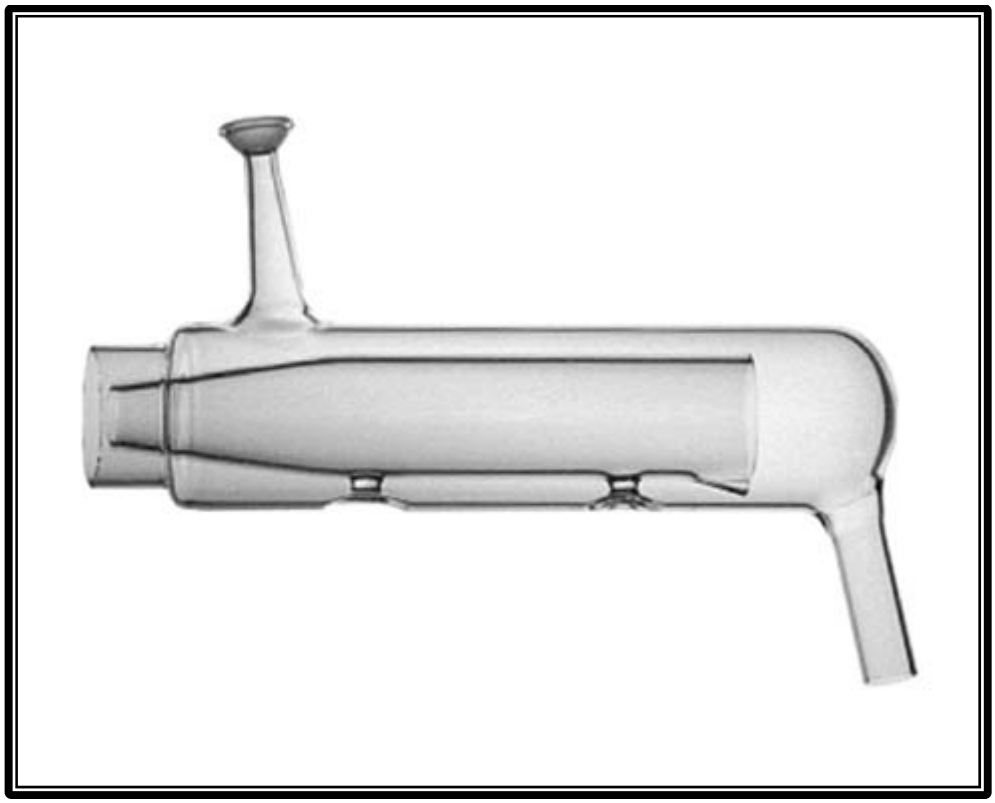

Figure 4-8: A Scott-type double pass spray chamber [103]

The torch itself is where the sample solution (a specialised torch is required for organic solvents) is atomised and excited by the inductively coupled plasma. It is constructed of three concentric tubes, generally made of quartz [96, pp. 92-98]. The inner tube carries the sample aerosol into the plasma by means of the carrier gas flow. The plasma flow is carried by the middle tube and is the primary flow involved in the generation of the inductively coupled plasma. This is generated by the action of the radio-frequency (RF) field, generated by an RF generator and applied to the plasma gas by an RF coil. The plasma is initiated by a spark, creating the initial ionisation of the argon gas. Once this is achieved the RF field accelerates the free electrons along a circular path inside the torch while simultaneously accelerating the positive argon ions in the opposite direction. The friction thus created generates heat as well as ionising more argon atoms, perpetuating the reaction. The outer tube carries the auxiliary or coolant gas. The role of this flow is to assist in the generation of the plasma and protect the torch itself from the intense heat thus generated.

Once the sample enters the plasma the intense heat breaks it down completely into excited atoms and ions. Upon returning to their ground state these then emit light of characteristic wavelengths. This process can be seen in **Figure 4-9** where **a** and **b**

represent excitation, **c** represents ionisation, **d** shows both ionisation and excitation, **e** is ion emission, and **f**, **g** and **h** are all atomic emission.

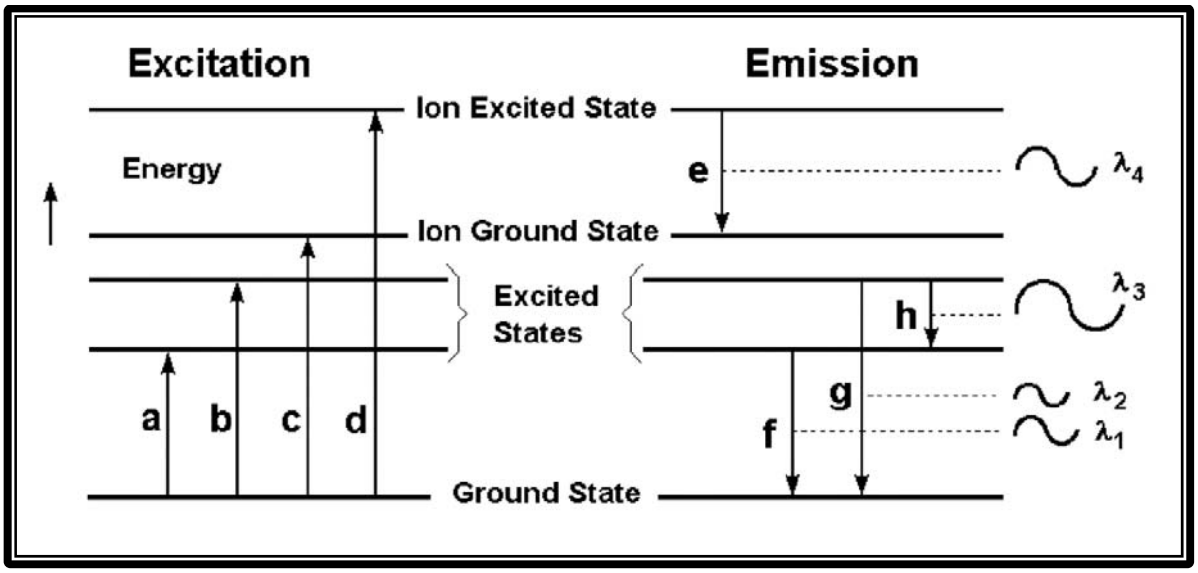

Figure 4-9: Energy level diagram depicting energy transitions [100, pp. 1-3]

The light emitted is proportional to the concentration of the analyte in the sample. The torch and detector may be mounted so that the light from the plasma is read either radially or axially (**Figure 4-10**). Axial viewing allows the detector to collect the light produced at all heights within the plasma simultaneously, allowing for improved detection limits [43, pp. 839-865]. Radial viewing, on the other hand, allows for the selective viewing of only a specific area within the plasma which improves stability and precision. Depending on the sample and matrix, one or the other viewing type may be preferable.

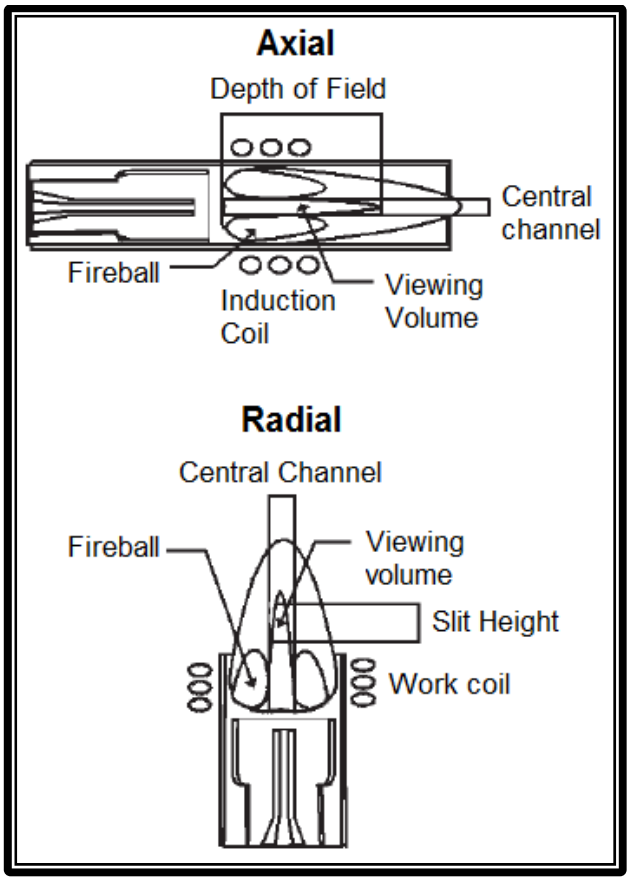

Figure 4-10: Schematic diagram of axially and radially viewed inductively coupled plasmas (ICP) [101]

The light is detected by a high-resolution spectrometer [98, pp. 309-324]. Instruments with simultaneous or sequential spectrometers are available. Simultaneous spectrometers have the advantage of capturing multiple wavelength intensities at once, which is useful in industrial applications when high sample throughput rate and multi-element analysis are required. They are, however, limited to the specific wavelengths for which they are configured which may severely limit their adaptability. Sequential spectrometers, on the other hand, are able to scan through a wide spectrum of wavelengths which makes them far more adaptable and therefore ideal for research labs.

Emission techniques such as ICP-OES are unaffected by Beer's Law, allowing for a vastly greater linear dynamic range of operation. Theoretically calibration curves covering several orders of magnitude are possible. Complicating factors such as matrix effects, however, make this less likely in practice. Matrix effects on the plasma intensity, usually by easily ionised elements, can generally be compensated for by matrix matching. OES techniques are also unaffected by most kinds of interference

(e.g. chemical interference) with only spectral interferences being of major importance. This is due to the extreme temperature (6000 – 10000 K) of, as well as relatively long residence time in, the plasma which effectively destroys all chemical bonds. The plasma is also effectively a chemically inert environment, inhibiting the formation of interfering species. The characteristic emission lines are also largely specific to each element. This yields the advantage that if an interference is discovered on one line the issue can be resolved by simply switching to another.

4.3.4 INDUCTIVELY COUPLED PLASMA MASS SPECTROMETRY (ICP-MS)

Inductively coupled plasma mass spectrometry generally uses the same sampling system as ICP-OES. The difference is that where the OES technique makes use of an optical spectrometer, the mass spectrometer measures the quantity of ionised analyte directly [43, pp. 839-871]. The first coupling of an ICP source with a MS detector was reported in 1980 [102, pp. 89-122]. This was done to replace the capillary arc plasma source, first reported in 1974, due to its limitations as a plasma source. The biggest challenge in the design of these instruments is pressure difference across the interface between the ICP plasma and the spectrometer. The plasma operates at atmospheric pressure while the spectrometer operates at pressures below 10^{-6} torr. As such the construction of the interface is crucial in order to allow a substantial amount of the ions produced in the plasma into the mass analyser. Generally the interface consists of two consecutive metal cones, the sampler and the skimmer. These each have small (approximately 1 mm) holes to allow ions to pass into the ion optics which in turn guide them to the mass analyser. These cones allow passage between three distinct pressure zones. The outer zone contains the plasma source, the middle zone exists between the cones and the inner zone contains the spectrometer (**Figure 4-11**). These zones are kept at atmospheric pressure, moderate vacuum and high vacuum respectively.

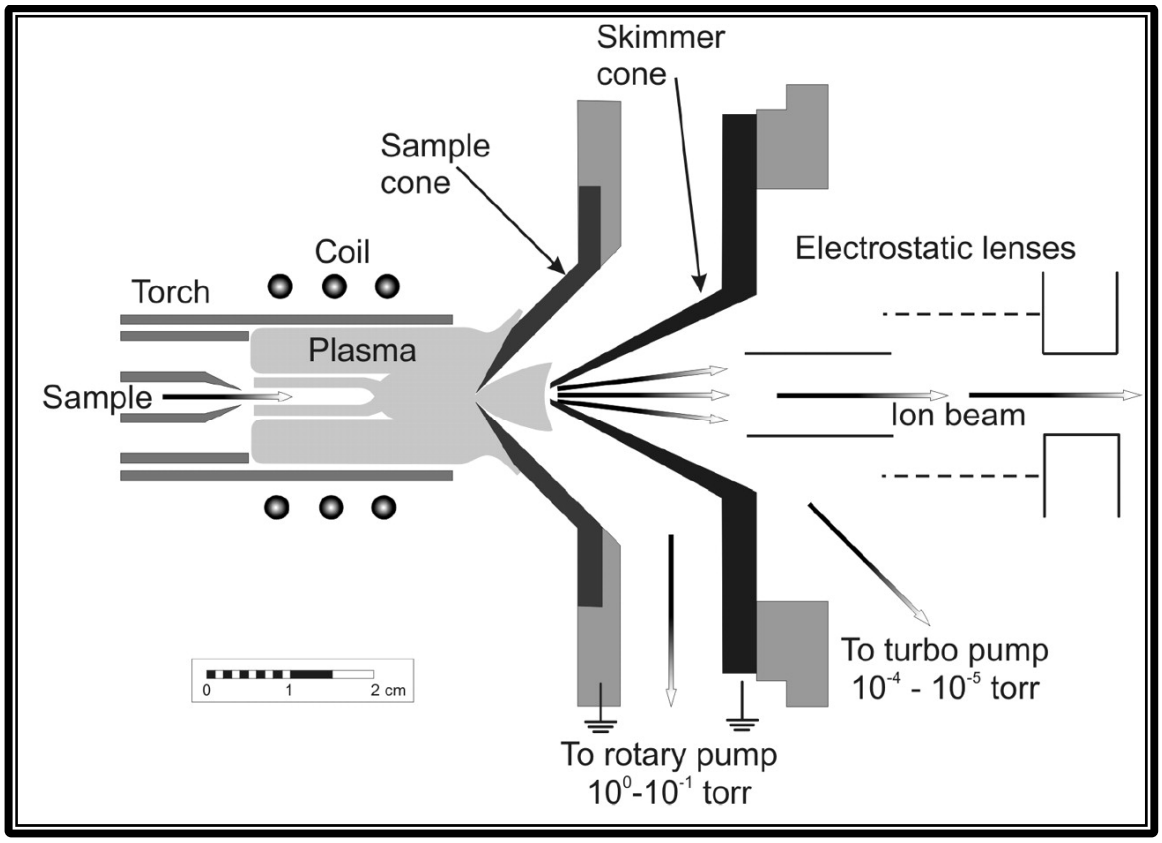

Figure 4-11: Diagram of the interface between an ICP plasma and a mass spectrometer [104]

Several types of MS exist and can be paired with the ICP sampling technique. Common examples of these are the quadrupole (**Figure 4-12**), magnetic sector (**Figure 4-13**) and double-focusing (also called sector-field) spectrometers although time of flight detectors have also been used. A quadrupole MS consists of four cylindrical rods arranged along the axis of the ion beam. Rods opposite each other are connected to the same DC voltages with RF voltages superimposed on them [98, pp. 369-386].

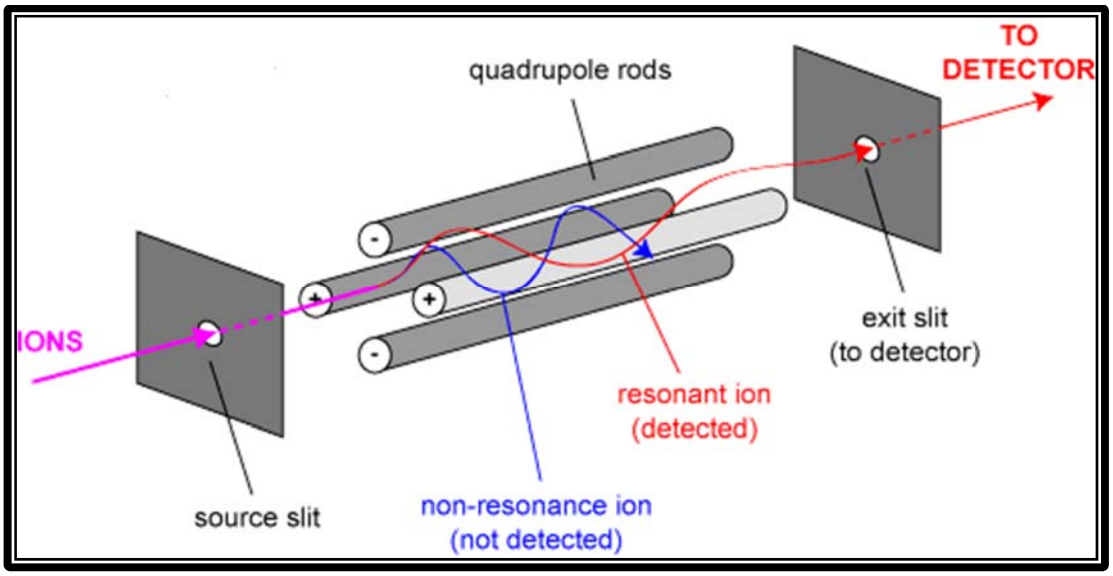

Figure 4-12: Diagram of a quadrupole mass spectrometer [105]

This creates an electric field which acts as a mass filter, allowing a stable, helical path only for the ions with the mass per charge (*m/z*) of interest. The paths of any other ions are simultaneously de-stabilised, stopping them from reaching the detector. Adjustment of the voltages applied to the rods allows the instrument to scan through these *m/z* values, creating the mass spectrum. Quadrupole instruments are known to have a relatively high throughput but suffer from poor resolution as compared to other mass spectrometers. This resolution is expressed in atomic mass units (amu) or Daltons (Da). The resolution of a typical quadrupole instrument is 1 Da [97, pp. 281-302]. In a magnetic sector instrument the ion path is deflected by a magnetic field running perpendicular to the direction of travel of the ion flow.

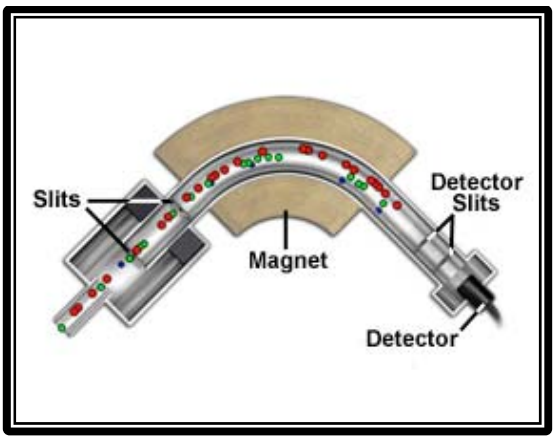

Figure 4-13: Diagram of a magnetic sector mass spectrometer [106]

This takes place in metal tube containing a section bent at an obtuse angle. The magnetic field is applied across this bend, adjusting the flight path of the ions. The

degree of deflection is dependent on the *m/z* of the ions as well as the strength of the magnetic field. This results in the ions with the correct *m/z* having their flight path bent to the same degree as the bend in the tube. Varying the power of the magnetic field allows the instrument to scan through which *m/z* values are allowed to reach the detector [96, pp. 124-127]. Double-focusing instruments add an electric field sector before the magnetic sector. This is done in order to pre-select ions with only a narrow range of kinetic energy before the beam enters the magnetic sector. This allows for significantly greater resolution with some double-focusing instruments having a resolving power 10,000 times that of a typical quadrupole spectrometer. This improved resolution comes at a significantly increased monetary cost, however. These three techniques analyse a continuous beam of ions from the plasma source. This beam is accelerated from the source to the detector by an applied electric field. Another approach is seen in time of flight (TOF) spectrometers. Here a packet of ions with nearly identical kinetic energies is rapidly sampled. These enter a field-free region and the time required for them to reach the detector is measured. Ions with low *m/z* reach the detector more quickly than those with higher *m/z*. Each *m/z* value is detected sequentially along with their magnitude. Analysis times are generally measured in microseconds.

The most common detector used in mass spectrometry is the electron multiplier (**Figure 4-14**), which functions on much the same principle as a photomultiplier, with electrons striking a cathode to emit secondary electrons. These then strike multiple successive dynodes at sequentially higher positive charges, with the same effect. Some transducers of this type are capable of multiplying the signal by a factor of 10^7.

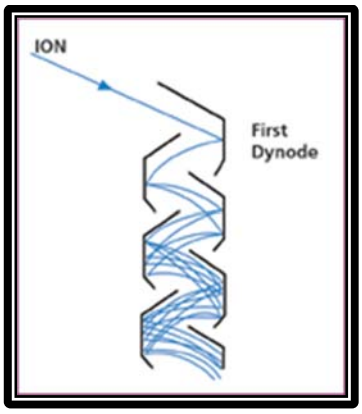

Figure 4-14: Diagrammatic representation of an electron multiplier [107]

The use of a mass spectrometer increases the detection limits achievable by the instrument as compared to OES. This comes at the cost of linear dynamic range though as these detectors are easily over-ranged by even relatively low analyte concentrations. Large concentrations of matrix elements also have a detrimental effect on the analysis and can even damage the detector. Unlike the OES technique, mass spectrometers have the ability to differentiate isotopes of the same element, making them useful for a variety of purposes, including certain radio-dating techniques [108]. A common interference seen in ICP-MS is caused by polyatomic compounds of argon having the same *m/z* ratio as an analyte species [109]. An example of this would be $^{38}Ar^{1}H^{+}$ interfering with $^{39}K^{+}$. Other compounds containing carbon, nitrogen or oxygen may also form and give rise to a similar effect. Interference can also occur when an ion has a double electric charge, halving its *m/z* ratio. Isobaric interferences are caused by overlapping isotopes of different elements [110]. The severity of these interferences is affected by the natural abundance of these isotopes.

4.3.5 X-RAY FLUORESCENCE (XRF)

X-ray fluorescence is a non-destructive analytical technique wherein a solid sample is bombarded with high energy (0.1 to 100 keV) electromagnetic (usually X-ray) radiation [96, pp. 98-103]. This radiation can cause the expulsion of an electron from one of the inner electron shells of higher atomic number elements. Electrons from higher orbitals subsequently fill the vacancies created releasing characteristic K, L and M X-ray spectral lines (**Figure 4-15**). These correspond to the innermost (K) and higher (L and M) electron shells. This process is known as fluorescence.

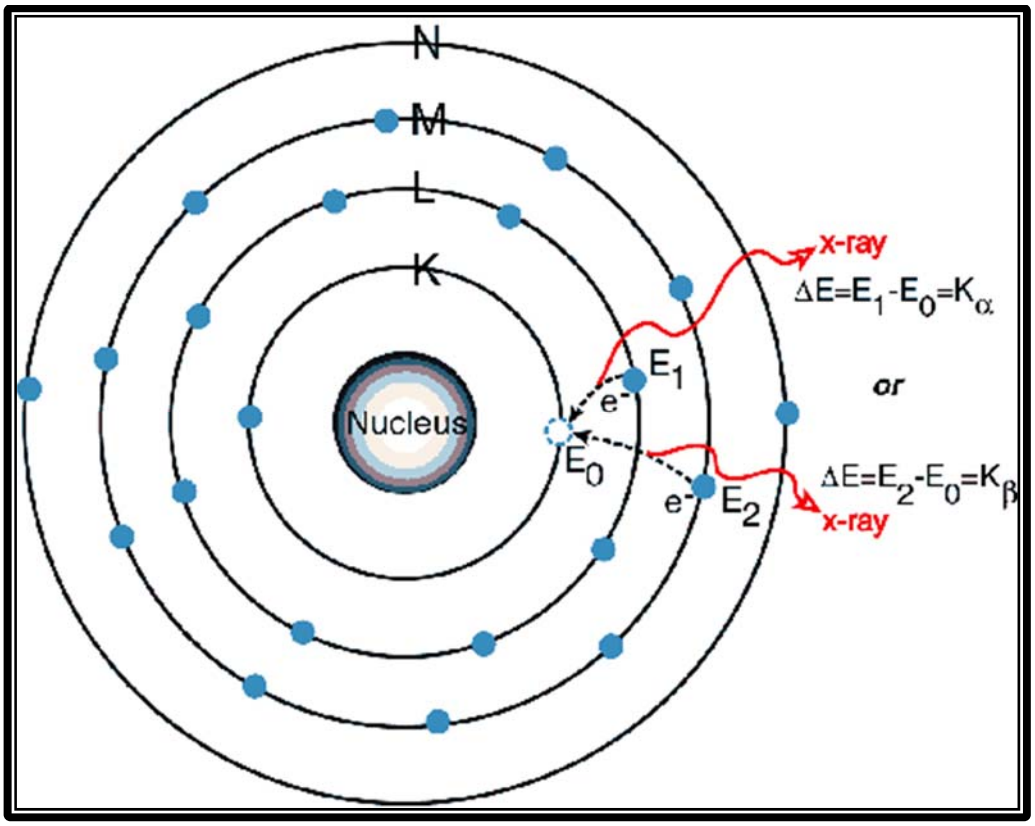

Figure 4-15: A diagram depicting emission of K line X-rays [111]

The radiation thus emitted from a given element in a sample is of specific wavelengths corresponding to the energy difference between the electron orbitals of that element. The intensity of the emitted radiation is proportional to the quantity of the element present.

Two types of XRF instruments are in general use. These are wavelength dispersive (WDXRF) and energy dispersive (EDXRF) instruments and are differentiated by their method of manipulating the emitted X-rays before detection. In an energy dispersive instrument, the radiation quanta are directly converted by a semiconductor detector into energy-proportional electrical signals. In these instruments a sample is irradiated from an X-ray source and the resulting fluorescence is detected directly without further manipulation. Wavelength dispersive instruments (**Figure 4-16**) separate the fluorescence radiation by wavelength, requiring a more complex configuration.

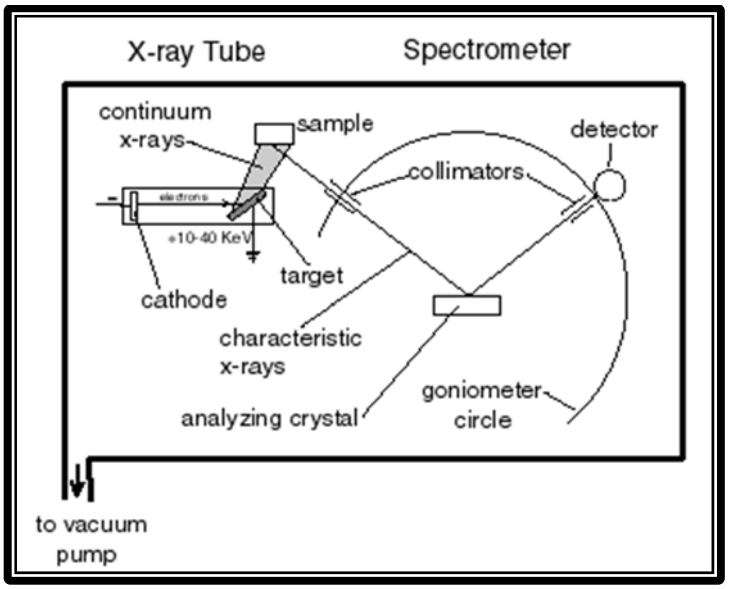

Figure 4-16: Diagrammatic representation of a wavelength dispersive X-ray fluorescence spectrometer [112]

As in EDXRF the sample is excited by high energy radiation. Unlike EDXRF though, this radiation is then diffracted off an analyser crystal with known interplanar spacing. This allows the angle of diffraction of specific wavelengths to be known in accordance with Bragg's Law (**Equation 4-11**).

$$n\lambda = 2d \sin\theta \qquad \textbf{4-11}$$

This analyser crystal is mounted on a goniometer, allowing the instrument to scan through the wavelengths allowed to reach the detector. Alternately the analyser crystal can be fixed and the detector moved to detect the dispersed wavelengths [98, pp. 263-281]. Collimators are mounted both before and after the analyser crystal on the radiation path to minimise the effect of scattered radiation. While the EDXRF instrument is limited to using a semiconductor detector, the WDXRD may use that, a scintillation counter or a counter tube detector. All of these detectors convert the incident X-ray radiation into an electrical signal which can be measured and quantified. The EDXRF configuration exhibits greater sensitivity while WDXRF instruments possess better resolution. A limitation of this technique is its insensitivity to the lighter elements [97, pp. 317-325]. As very light elements do not have filled higher electron shells they are not able to fluoresce and thus are not detectable by this technique. Slightly heavier elements (those lighter than vanadium) also give difficulty due to the competing process of Auger emission.

Sample preparation for XRF is comparatively simple. Generally samples must be in solid phase with a flat surface. Metals must be ground and polished and powders must be pressed into a flat-surfaced pellet, sometimes with a binder material. With powders the particle size can play a role in sample homogeneity and must thus be ground down to less than 50 μm. The homogeneity of the sample affects the accuracy and precision of the method. Examples of binding materials are methylcellulose, organic polymers and waxes. Glass discs formed by fusion with lithium borate may also be used.

4.3.6 GLOW DISCHARGE OPTICAL EMISSION SPECTROSCOPY

Glow discharge optical emission spectroscopy (GD-OES) is a semi-destructive analytical technique often used in the analysis of metal samples [113]. Though primarily useful as a depth profiling technique on samples with varying layers of both conducting and non-conducting materials [84], it is also capable of rapid bulk analysis of homogenous, solid samples (both conducting and non-conducting). In GD-OES analysis, when using a direct current (DC) lamp source, a potential difference (in the order of 1 kV) is applied between two electrodes in a cell containing a gas at low pressure, usually argon, at around 1 Torr [114]. This causes the gas to “break down” into electrons and positive ions, forming the plasma. The electrons are accelerated towards the anode which sustains the plasma and generates more positive ions while these positive ions are accelerated towards the cathode, the sample material. This bombardment causes the sample material to “sputter”, essentially knocking free atoms or molecules of analyte material which are then drawn into the plasma where they too are excited. A diagram of these processes can be seen in **Figure 4-17**.

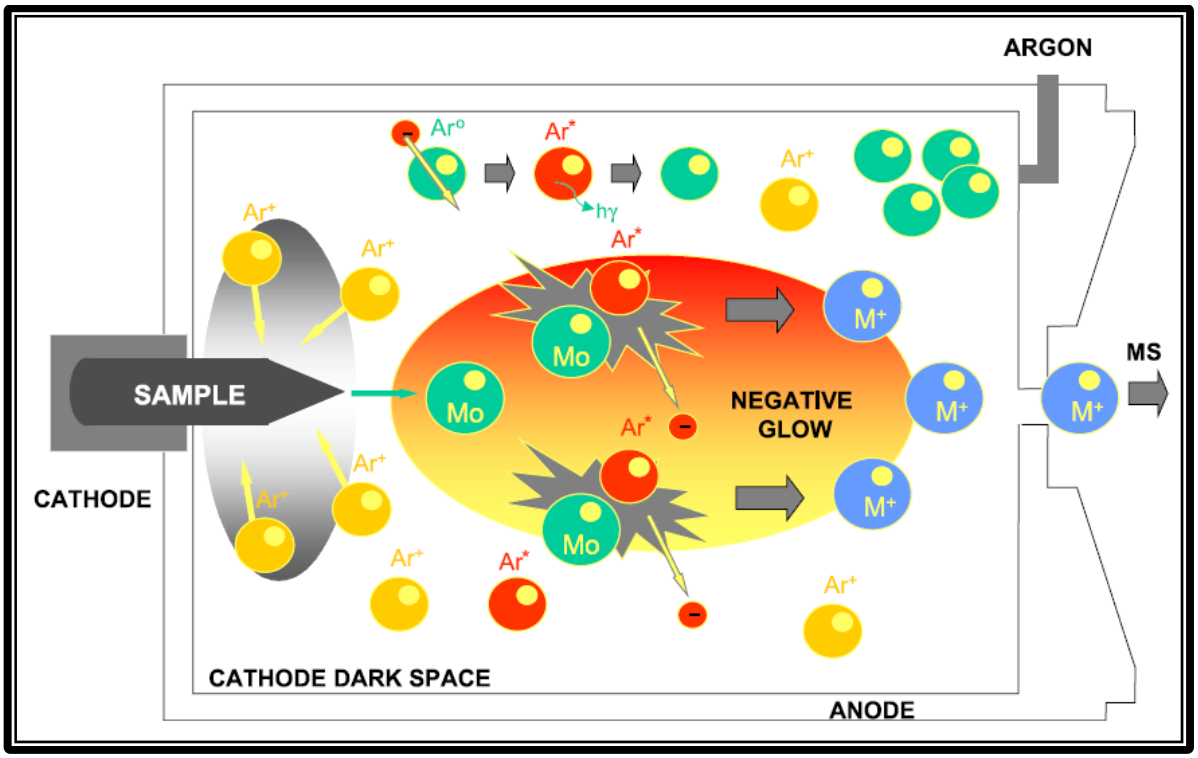

Figure 4-17: Schematic of the various processes occurring during glow discharge (GD) [115]

A radio frequency (RF) lamp may also be used for non-conducting samples [81], see **Figure 4-18**. In GD-OES the light emitted by this excitation is then diffracted to separate the wavelengths emitted by specific elements and detected by a spectrophotometer using either a charge-coupled device (CCD) or a photomultiplier tube (PMT). The intensity of the signal is directly proportional to the quantity of analyte element present in the sample, allowing simple calibration and quantitative determination of elements. Technological improvements made in the past twenty years or so have significantly increased the usefulness of GD-OES for surface analysis [113]. Faster plasma stabilisation and start-up allow for the quantification of surface layers as thin as one nanometer. Sputter rates have been accurately measured for many common materials, allowing them to be built into software libraries in the instrument's control software. This dramatically expands the usefulness of this software. Improvements in calibration systems allow for the changing of instrumental conditions without the need to completely recalibrate, saving time and effort.

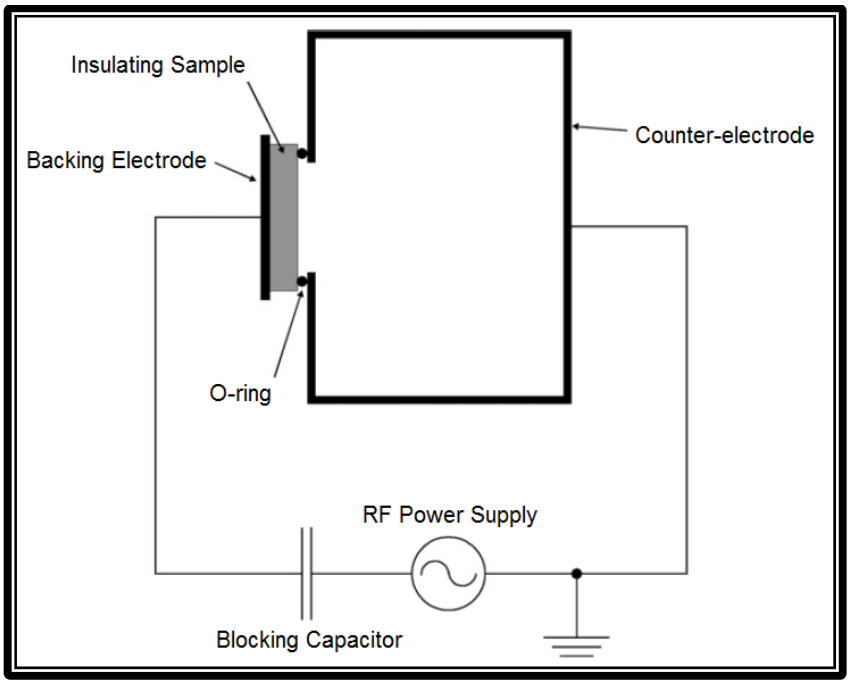

Figure 4-18: Conceptual diagram of a radio frequency glow discharge device (RF GD) [81]

In glow discharge mass spectrometry (GD-MS), a mass spectrometer is used rather than an optical detector with the GD source. This allows for a much lower limit of detection at the cost of linear dynamic range. The instrument is otherwise essentially the same as a GD-OES. The use of a collision cell between the glow discharge plasma and mass spectrometer can minimise interference from polyatomic species formed in the plasma. As GD-MS still makes use of a GD sampling system it shares the relevant advantages and limitations of the GD-OES. Depending on the type of mass spectrometer (discussed in **section 4.3.4**), a GD-MS may have monetary cost or resolution limitations.

4.4. CONCLUSION

The various techniques outlined in this section were selected based on their applicability to the sample matrix under investigation as well as availability of materials and instruments for use. Techniques were evaluated in terms of their applicability both to the samples and their usefulness in an industrial setting.

Acid dissolution allows for the complete dissolution of most samples without overly complicating the sample matrix. This is ideal for most spectrometric techniques that require samples in solution, such as AA and ICP-OES. It is however not always

applicable and must sometimes be augmented with other techniques, such as flux fusion or microwave assistance.

Flux fusion of samples is most often used for the digestion of minerals and oxides. It is generally a rapid, simple method capable of dissolving materials that acid digestion alone cannot. Once complete the melt may be dissolved in acid medium for analysis by ICP or AA or left as a glass for XRF or GD-OES. A drawback of this technique is its limited applicability in terms of sample types and extreme contamination of the sample by the reagent.

Microwave-assisted acid digestion makes use of microwave radiation to rapidly heat samples under relatively high pressure. This has several advantages over open vessel digestion, the most notable of these being reduced time of reaction. It also minimises the loss of sample due to volatilisation. The only drawbacks of the method are that the equipment is expensive and explosions may occur if the operator is not careful.

Solid pellets are required for techniques like XRF and GD-OES. As such the other dissolution techniques are not taken into account for these two methods. The only variables when preparing these samples are pressure, time and whether or not to include a binding material.

Of the instrumental techniques, UV/VIS spectrophotometry has seen the widest use according to literature but has several limitations. Its highly limited linear dynamic range and labour intensive sample preparation procedures are drawbacks. Zirconium analysis by this technique is also subject to a range of interferences, the most significant of these being hafnium.

Atomic absorption spectroscopy encounters similar difficulties in terms of detection range as it is also an absorption technique. It is less subject to interference, however, but may require matrix modifiers, resulting in increased sample preparation complexity.

ICP-OES exhibits several desirable attributes. It is an emission technique which means that it has a very large dynamic range. It is subject to few interferences and sample preparation is generally straightforward. Depending on the type of spectrometer installed, it is also highly flexible as it is optimisable for throughput or research. It is, however, a fairly expensive instrument when compared to AAS and especially UV/VIS. This may limit its industrial availability and application.

ICP-MS has many of the same advantages as ICP-OES owing to the two techniques sharing a sampling system. The difference in detectors is what drastically separates the two. A standard quadrupole MS trades detection range and resolution for lower detection limits and higher throughput as compared to an OES instrument. MS instruments with different mass spectrometer types are available but are generally prohibitively expensive.

XRF has the advantage of being nominally non-destructive. Sample preparation can be time-consuming, however, as grinding of samples is often necessary. Comparatively long detection times make the method even slower. Instruments are also generally quite expensive and suffer from interferences such as self-absorption by the sample.

GD-OES combines the detection range, speed and lack of interferences of ICP-OES with the solid sampling of XRF techniques. It is also able to perform depth profiles of materials that contain layers of varying composition and thickness. This allows the analyst not only to quantify a sample but to evaluate its composition in terms of homogeneity. This is extremely useful when one considers the required sample preparation process. Drawbacks of the method are that it is not yet as well established as other techniques in the field and the instruments are expensive. It also requires conducting samples to be at its most effective.

Chapter 5: Experimental Aspects and Troubleshooting in Relation to Instrumentation

5.1. INTRODUCTION

A thorough understanding of the potential and limitations of the instruments with which one performs analyses is essential in producing the best results possible with said instruments. This understanding must not only cover the general theory behind the operation of an instrument (discussed in **Chapter 4**) but also the specific, practical use thereof. In this study a Shimadzu ICPS-7510, a Shimadzu ICPM-8500 and a LECO GDS850A were used to gather data. These instruments are examples of an ICP-OES, an ICP-MS and a GD-OES respectively.

5.2. RUNNING ASPECTS

When working with complex instruments like those used in this study one must be aware of the many requirements of the instruments in terms of environment and operation. An instrument cannot perform to its full potential when operating outside its design parameters. In this section the specific requirements of the instruments used in the sample analyses in this study are discussed.

5.2.1 ICP-OES

Figure 5-1: A Shimadzu ICPS-7510 [116]

The Shimadzu ICPS-7510 (**Figure 5-1**) consists of a sequential scanning optical spectrometer with an inductively coupled plasma source. To best understand its operation it is helpful to begin from the sample introduction system and proceed systematically towards the detector.

The sample in aqueous solution is first pumped from whatever vessel it is contained in towards the nebuliser by a peristaltic pump. The section of tubing that passes through this pump is both thicker and more flexible than the rest of the tubing transferring the sample from its container (volumetric flask, test tube or similar) to the nebuliser. This is because the tubing is compressed in moving sections by the peristaltic pump (**Figure 5-2**) to press the solution forward without pulsing. When not in use this tubing must be removed from the pump as the tension and compression applied by the pump leads to loss of elasticity of said tubing. This deterioration is inevitable but the life of the tubing is significantly prolonged in this manner. All the tubing in the sample introduction system is somewhat resistant to acid attack although dilute acids may be tolerated indefinitely. Large concentrations of acid, however, are capable of damaging the material and must thus be avoided whenever possible. A similar restriction on basic solutions also applies. Most metal samples must be in acid solution to avoid precipitation. Despite this matrix some elements adhere strongly to the walls of the tubing causing memory effects. As such certain analyses require longer rinse or sample pre-spray times. This is done to avoid sample cross contamination and a consistent sample concentration introduced into the plasma.

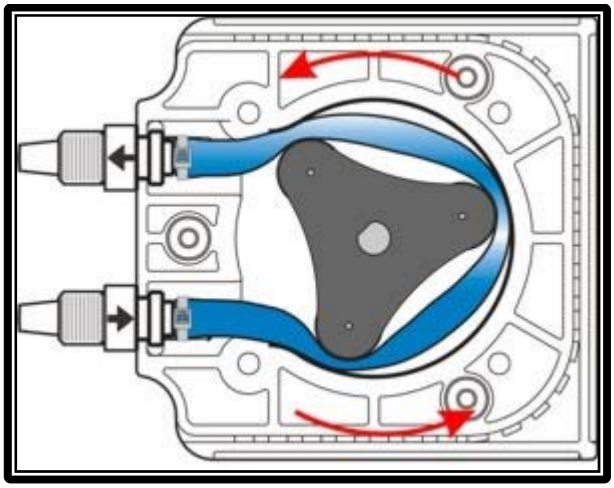

Figure 5-2: Diagram of a peristaltic pump [117]

The ICPS-7510 makes use of a concentric nebuliser (**Figure 5-3**) which is vulnerable to clogging. The opening of the inner tube is both extremely narrow and fragile. As such it is necessary to ensure that all solutions be completely free of solid material. It can also be blocked by the precipitation of high concentrations of sample and matrix materials upon nebulisation. This precipitation is not only able to block the nebuliser but may also lead to co-precipitation of the analyte. Precipitation can be minimised by

diluting the sample or by use of a “bubbler”. This bubbler passes the argon carrier gas flow through water before it reaches the nebuliser in order to “wet” the gas. When the instrument is not in use the sample introduction tube must be removed from the nebuliser as well as from the the rinsing water. This is done because, when there is no argon pressure in the carrier gas line, the solution in the tubing can flow back through the outer nebuliser tube and into the gas flow line. This can damage the valves that control the gas flow if the solution reaches them.

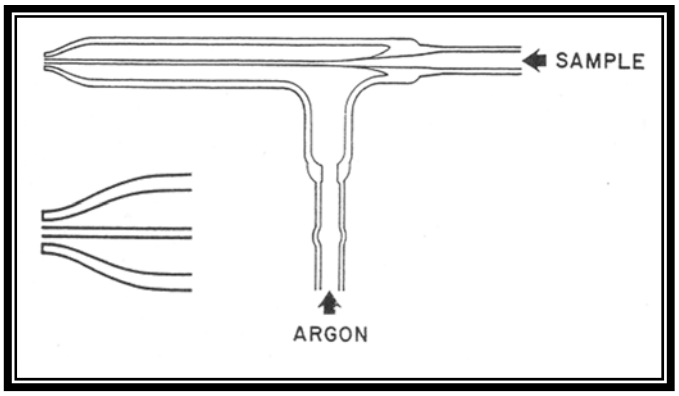

Figure 5-3: Diagram of a concentric nebuliser

The glass nebuliser, glass spray chamber and quartz torch are all composed of silica and thus are vulnerable to attack by hydrofluoric acid and high concentrations of fluoride ions. This must be taken into account when sample preparation procedures include dissolution by these reagents. If these reagents cannot be avoided then the samples must be diluted to the point that damage is negligible or an HF-resistant sample system must be installed.

The cyclonic spray chamber needs little attention as it is simply an empty cylinder with the sample mist and carrier gas entering at an angle. This causes the larger droplets from the nebuliser to impact the walls of the spray chamber from where they run to the waste outlet. This waste outlet has a U bend which must be filled with water before ignition of the plasma to provide back-pressure. The only other consideration in terms of the spray chamber is ensuring that it is aligned properly with the torch to ensure maximum transfer of the analyte aerosol into the plasma.

The torch itself is subject to relatively few problems. It must be firmly mounted at the correct height within the RF coil otherwise the plasma will not ignite. Sufficient gas flow must be available to ensure proper cooling around the mouth of the torch. If this is not available the plasma will melt the torch, destroying it (**Figure 5-4**). A nominal gas

pressure of 350 kPa and flow of 22 litres per minute is required to sustain the plasma. At this flow rate a gas bottle containing 17.4 kg of argon can be emptied in approximately 8 hours. As the plasma requires approximately fifteen minutes in order to properly stabilise for consistent emission, during which time quantitative measurement is not advisable, it is preferable to wait until a relatively large number of samples can be run sequentially. This reduces unnecessary operating costs.

Figure 5-4: Melted Torch from Axial Leeman PS-1000

The RF coil that helps generate the plasma is cooled by water pumped from a reservoir inside the instrument. The water level in this reservoir should be monitored frequently but as the system is fairly tightly sealed it is seldom necessary to refill it. Power to this coil is supplied by the RF generator which is located at the base of the machine, underneath the plasma chamber. It is air-cooled by a number of fans due to the large amount of heat it generates. Care must be taken that any dust sucked in by these fans is removed periodically to ensure proper cooling and avoid burning out the electronics.

The electromagnetic radiation emitted by the analytes in the plasma can be passed into the spectrometer in two ways. The default system reads the emissions radially at one of two heights. These are denoted as “High” and “Low” in the software. An axial viewing attachment allows for viewing of the plasma along the central axis of the torch. This attachment fits over the viewing window of the spectrometer and reflects the light from the plasma into it by means of a simple mirror. As the light entry hole is actually positioned inside the tip of the plasma cone the attachment is constructed mostly of copper and water cooled by a chiller unit (Eyela CA-1112). This design avoids the extreme heat of the plasma melting the attachment. As there is no shear gas some of the analyte can strike the mirror inside the attachment and over time this builds up a deposit. This deposit gradually reduces the mirror’s ability to reflect the light from the plasma, consequently reducing the detection limits of the instrument. The mirror must thus be cleaned periodically with a cotton swab and methanol.

Once inside the spectrometer the light is reflected from two concave mirrors and two Echelle diffraction gratings between them onto a photomultiplier tube (PMT). This is done in order to increase the path length of the spectrometer and split the light into a spectrum. The Echelle gratings are mounted on a goniometer to allow the spectrometer to scan through all available wavelengths (160 to 850 nm). As path length is a crucial factor in determining which light wavelength eventually reaches the PMT, the entire spectrometer is kept at a constant 40ºC as it is mounted inside a large aluminium tank. A wavelength calibration must be performed at least once a month or whenever the instrument receives a significant physical shock. This is done as the calibration may drift over time or due to impact. Whenever a sample is to be quantitatively determined it is necessary to calibrate the voltage of the photomultiplier tube at that wavelength. This is done in order to achieve the maximum sensitivity without the risk of flooding the detector and is done automatically during the qualitative test step in the software.

5.2.2 ICP-MS

In many respects the Shimadzu ICPM-8500 (**Figure 5-5**) shares the same components as the ICPS-7510. The sample introduction system is effectively identical with a few minor exceptions. The nebuliser is also concentric but has a smaller aperture at the end of the inner tube, making it even more prone to clogging.

Figure 5-5: A Shimadzu ICPM-8500 [118]

Instead of a cyclonic spray chamber, a Scott double-pass spray chamber (**Figure 4-8**) is used. This spray chamber is water-cooled to 4ºC by an electronic chiller in order to avoid secondary evaporation from its walls. This cooling is done as the instrument is extremely sensitive and, when used for ultra-trace analysis, evaporation may affect the analytical results.

Unlike the ICPS-7510 the plasma torch is mounted horizontally facing the interface to the mass spectrometer. The interface, constructed from copper, is cooled by another, significantly larger chiller set to 12ºC. This is because the interface cone is actually inside the plasma plume during analysis and thus exposed to the intense temperature generated there. As much of the heat from the plasma is thus carried to the chiller rather than being removed through the air extraction system, a lot of heat is transferred into the immediate environment. This particular instrument is situated in a fairly small room which made it necessary to install a very large air-conditioning unit. This was done in order to maintain a room temperature of 23±5ºC, the instrument's optimum operating temperature zone. **Figure 5-6** shows the percentage difference in apparent recovery between analyses performed internally on the same set of samples by both ICP-OES and ICP-MS. This was done before the installation of the air conditioner. The error is effectively linear with time as the ambient heat builds up. The first result already shows some error as the instrument requires some stabilisation time before analyses can be performed. The linearity fails at the tenth run as at this point the instrument was reading below the blank value, approaching zero.

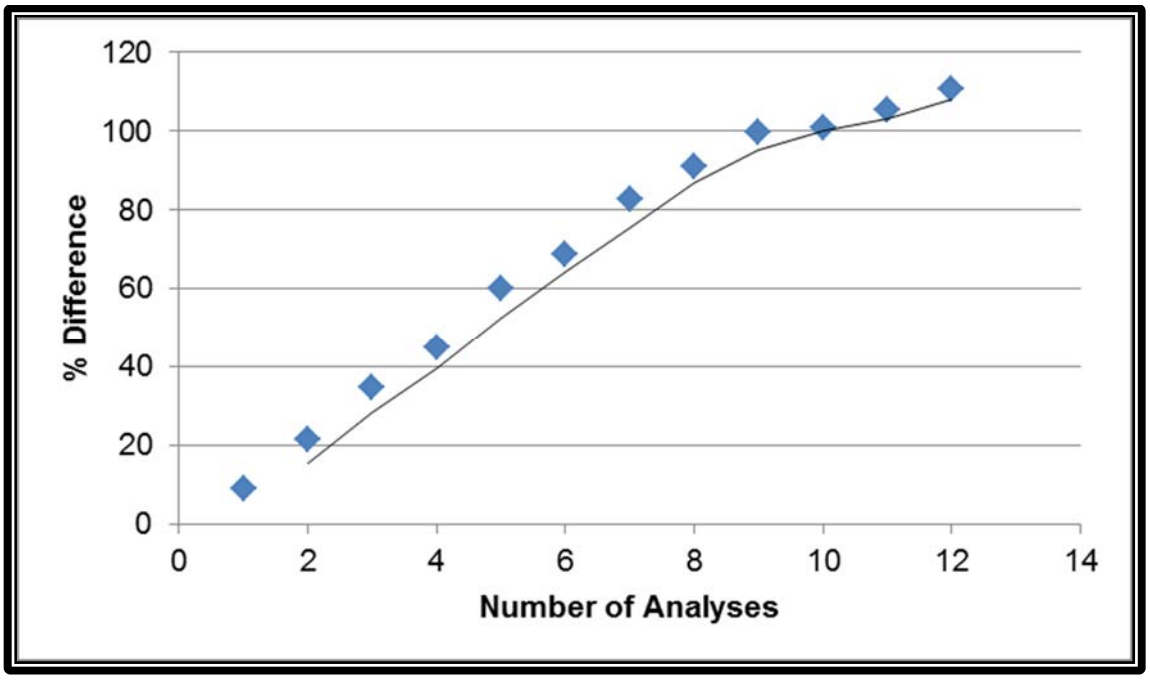

Figure 5-6: Difference in ICP-OES and ICP-MS results due to heat build-up

The track on which the torch is mounted may be adjusted vertically and horizontally to ensure maximum transfer of charged particles into the spectrometer. This is done by means of two knobs accessible through the front panel of the instrument. This generally

need only be performed when maintenance has been performed on the torch or in the torch compartment and sensitivity appears less than optimal.

The ICPM-8500 makes use of a quadrupole mass spectrometer as its detector. This MS must be calibrated regularly to ensure optimum working conditions. A 1 part per billion solution of lithium, indium and bismuth is used to calibrate the spectrometer. The software contains automatic procedures to detect the peaks from these elements striking the detector as well as calibrate the gain on said detector. The instrument has an intermediate “standby” state in which the plasma remains unlit but the primary rotary pump providing vacuum to the spectrometer is active. The two turbo molecular pumps (TMPs) required to provide the extreme vacuum necessary for the operation of the mass spectrometer are also active in this state. Care must be taken to avoid having these TMPs running without the primary “roughing” pump active as this can severely damage them. The instrument does have interlocks that prevent this from occurring as long as there is power to the instrument.

5.2.3 GD-OES

The LECO GDS850A (**Figure 5-7**) is, by comparison, a fairly simple instrument to operate. Once samples are properly prepared, sample introduction consists of placing a sample over the O-ring at the lamp opening and allowing the vacuum to hold it in place. When positioning a sample it is preferable to ensure that no previous GD craters overlap with the surface to be analysed. Care must be taken that samples are non-porous and smooth. If they are not, the vacuum will not be strong enough to form the GD plasma, the instrument will detect this, and the sample will be ejected before analysis can begin. If the seal is tight the sample will then be held in place by the reamer. This reamer serves multiple functions including holding the sample, cleaning the anode between analyses and serving as a conductor to allow the sample to act as cathode (when using the DC lamp). When moving into position the reamer impacts the sample with some force which can break brittle samples.

Figure 5-7: Image of the LECO GDS850A [119]

After the copper anode has been reamed between analyses it is necessary to wipe off the lamp aperture with a thin sponge to remove any metal shavings from the anode. If this is not done, loose shavings may cause arcing between the anode and the sample. If the sample is fairly thin or has a low heat capacity it may be necessary to make use of the cooling puck. This is a water-cooled metal (or Teflon if using the RF lamp) puck that fits between the sample and the reamer, providing cooling for the sample. The generation of the GD plasma causes a great deal of heat in both the sample and the lamp.

The GDS850A supports both a DC and an RF lamp. The RF lamp is intended for use with non-conducting materials and has a lower effective applied power. It was found that using this lamp with the copper anode allowed only for the analysis of very thin, regular non-conducting layers on a conducting substrate. The ceramic anode which would allow for the analysis of thicker materials was unavailable. The DC lamp requires that the sample material be conductive as it must serve as the cathode. This lamp is also able to generate a greater applied power, which increases sensitivity. Both lamps are liquid-cooled.

Vacuum is generated by a rotary pump positioned inside the instrument which must undergo regular maintenance. The water used for cooling the DC lamp and cooling puck is also housed in an internal reservoir and the water level must be monitored.

The GDS850A makes use of a simultaneous optical spectrometer. This spectrometer consists of a Rowland circle (**Figure 5-8**) with PMTs positioned behind slits

corresponding to characteristic emission lines of various elements. The instrument is capable of reading all of these lines simultaneously. This greatly increases sample throughput rate at the cost of the ability to generate a complete spectrum. As there is only a single PMT installed for most elements, this makes the detection of interferences more difficult than with scanning sequential instruments. When developing a method the voltage applied to these PMTs must be calibrated to yield the greatest sensitivity without becoming saturated by high concentration samples. Unlike in the case of the ICPS-7510, however, this need only be performed once, during method creation, and not every time quantitative measurements are performed.

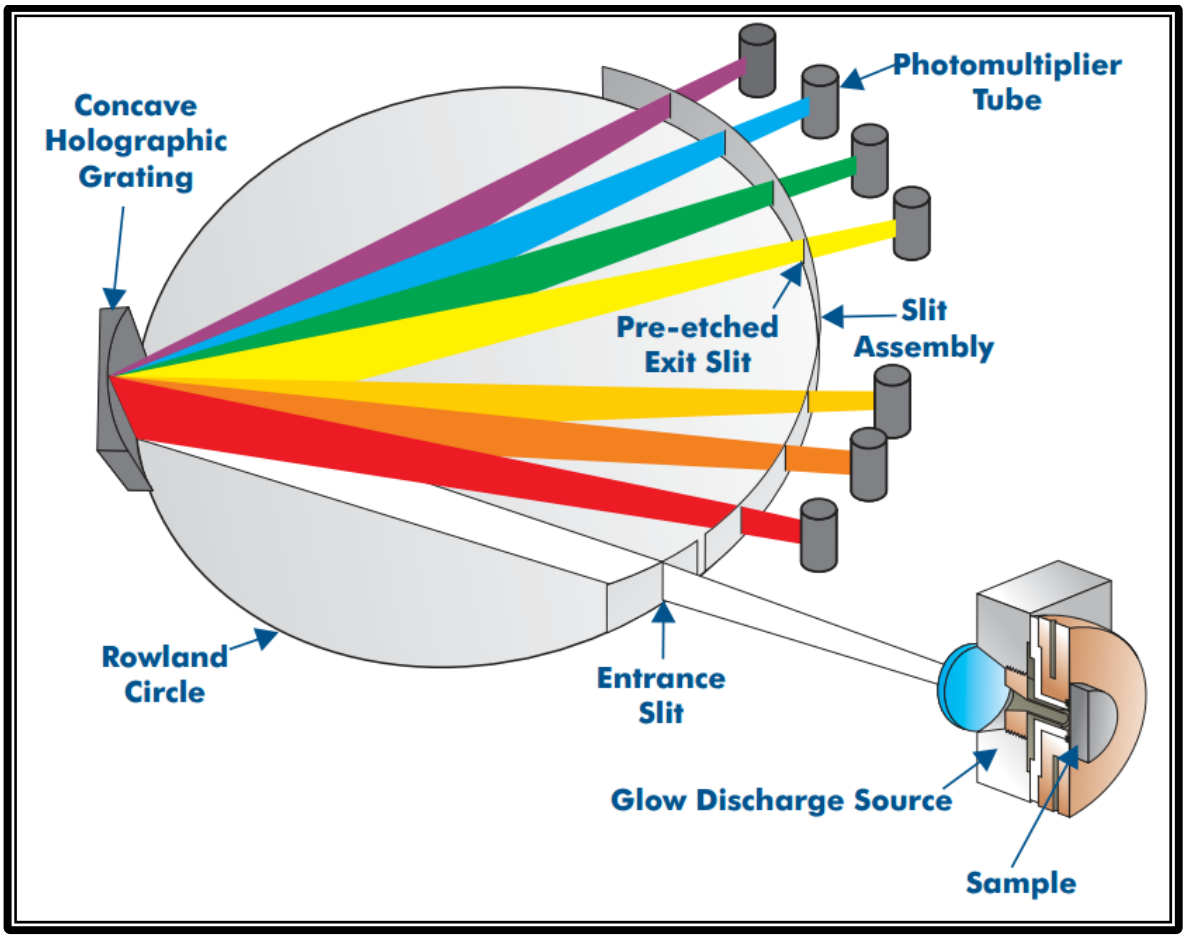

Figure 5-8: Diagram of a Rowland circle used in the LECO GDS850A [119]

The vacuum inside the spectrometer is generated by the rotary pump and a TMP. Care must be taken when first turning on the instrument to wait after activating the rotary pump for the TMP to slow down. The action of the pump causes the TMP to accelerate as gas passes over it. The TMP speed settling back to its minimum value is an indication that there is sufficient vacuum for the TMP to operate safely. At this point the TMP may be switched on.

At the beginning of each working period, usually each day, the lamp must first be “warmed up”. This is done by placing a sample of the same matrix as the intended analytes on the lamp and generating the GD plasma three times. Once this is done the instrument must be “profiled”. Profiling is simply ensuring that the spectrometer is in alignment. This is done by analysing a sample containing iron. The instrument has two PMTs positioned at characteristic iron wavelengths. Detecting these two lines allows the instrument to confirm the position of the spectrometer’s entry slits. As the instrument stores calibration data it is necessary to drift correct a method’s calibration before quantitative analysis. This is performed by analysing standard samples, pre-selected in the method, and adjusting the calibration according to the intensities detected. This drift must be done whenever a different method is used but the warm-up and profiling need only be performed once per working period.

5.3. TROUBLESHOOTING

Unfortunately as the complexity and sensitivity of an instrument increases so does its number of possible points of failure. It is thus extremely important to be able to quickly identify common faults and problems experienced with a specific technique and be well versed in solutions to these problems. Speedy troubleshooting can save on down-time, money and prevent damage to the instrument.

5.3.1 ICP-OES

A particular point of failure in ICP methods is the nebuliser. In the case of the ICPS-7510 the concentric nebuliser can easily become clogged if care is not taken. Should this happen the obstruction can sometimes be cleared by running large quantities of pure water or dilute acid over it. This is only effective, however, when the nebuliser is not completely clogged and a small flow is still possible. If this is not the case then the plasma must be switched off and the nebuliser removed for cleaning. In some cases all that is required to remove an obstruction is to block the outer tube of the nebuliser with the gas flow on and the sample introduction tube removed. This has the effect of forcing argon gas back through the inner tube and with it the obstruction. The nebuliser is then rinsed with distilled water forced in from the front of the nebuliser. If the obstruction is not washed completely out of the nebuliser by this, though, it can simply be pushed back into place upon the resumption of sample flow. If this means of removal is not effective then the entire nebuliser can be removed and placed in an ultrasonic bath. Sonication breaks down the obstruction into small enough pieces to

be easily washed through the nebuliser. This takes longer than simply washing the tube but is sometimes necessary for particularly persistent clogging. Under no circumstances should one attempt to clear an obstruction by manual means, such as by pressing it out with a thin length of wire. This can break the tip of the inner concentric tube, permanently damaging the ability of the nebuliser to create a sufficiently fine mist.

An external cut-off was later installed after the internal gas flow safety of the instrument failed to operate while the instrument was running. This resulted in a melted torch. The cut-off is set to stop all gas flow to the instrument in the event that the gas pressure drops below 600 kPa.

Elements such as sodium, potassium and lithium lose electrons more easily than other metals. As such they are sometimes referred to as easily ionised elements (EIEs) and may pose problems when performing ICP-OES analysis. If the sample matrix contains a large concentration of EIEs they may have a considerable effect on the temperature of the plasma (**Figure 5-9**). This will cause the analyte to emit more or less radiation than it would if these elements were not present. If variation in radiation intensity is not compensated for, the results obtained may be questionable. This can be done by the use of an internal standard or matrix matching the calibration standards.

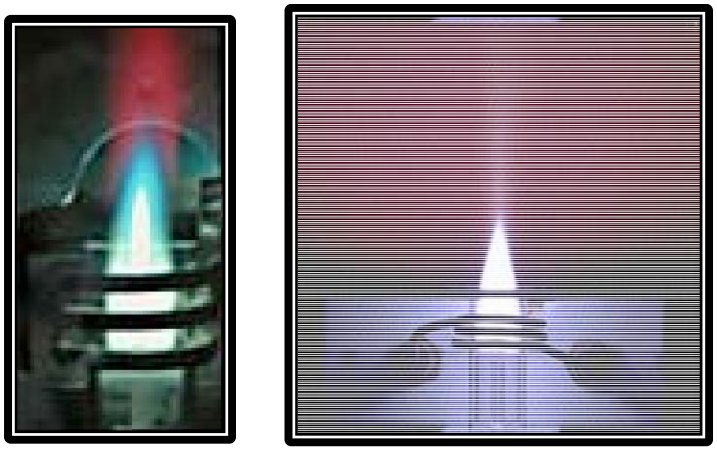

Figure 5-9: An ICP plasma with (left) [120] and without (right) [121] a high EIE content sample

5.3.2 ICP-MS

As the sample introduction system in the ICPM-8500 is essentially identical to that of the ICPS-7510, the problems experienced and solutions to these problems are effectively the same.

In rare cases it is possible that the instrument may be shut down abnormally, such as in the event of a power failure. In such a case the window that seals the mass spectrometer at the interface with the plasma may not close properly. When this occurs the instrument will sound a loud alarm and will not activate into the standby state. Under these circumstances it is necessary to physically open the instrument and manually reset the position of this window to clear the error state.

If the instrument has been used with samples containing excessive quantities of analyte, the detector may become saturated or “dirty”. This has the effect of severely decreasing instrument sensitivity. If this is suspected to have occurred the detector may be “cleaned” by introducing a low ppb-range gold solution and allowing the gold ions to strike the detector.

As was the case with the ICPS-7510 an external cut-off valve was installed after the internal gas pressure safety interlock failed to activate, resulting in a melted torch. As the ICPM-8500 requires a higher gas flow rate the cut-off pressure was set to 1000 kPa.

5.3.3 GD-OES

Failure of a sample to create sufficient vacuum is seldom experienced with solid, metallic samples. When it does occur it is likely due to roughness on the surface and simply polishing the sample will solve the issue. When analysing pressed pellets it may be due to porosity or even a small crack in the sample. If this is the case there is little that can be done and a new pellet must be manufactured. High quantities of oxides appear to cause pressed copper pellets to become brittle and porous very easily although this is dependent on which oxide is used. For instance zirconium oxide causes a greater degree of embrittlement and porosity than chromium oxide does in the same sample to binder mass ratios. A similar effect is seen with other non-conducting materials but not to the same degree. If a metal sample is too thin the heat from the plasma can cause the material to deform which may influence analytical results. It is highly recommended that the cooling puck be used in these cases.

Certain samples may cause a residual particle build-up on the anode. This must be checked for and cleaned as necessary. Failure to do this can cause arcing and therefore unreliable analytical results.

5.4. CONCLUSION

The three machines outlined in this chapter were the primary analytical instruments used in this study. Familiarity with their use and maintenance was crucial in gathering accurate analytical data.

Chapter 6: Characterisation of different zirconium fluoride compounds

6.1. INTRODUCTION

The complete characterisation of reference materials is essential when performing method validation. Without a certified reference material (CRM) it is impossible to gauge the accuracy of any given method. CRMs for a wide variety of materials, including metals and ores, are normally commercially available. These CRMs have been characterised by multiple laboratories using a variety of techniques to ensure that the certified value, supplied with the sample, is as close to the true or experimentally obtained value as possible. Unfortunately certified references are not available for all possible materials. Consequently, while reference materials are available for both the zircon ore (SARM62) and the zirconium metal (commercial alloys and pure metal), in this study none could be found for relevant intermediate beneficiation products. It was decided to produce different stable crystal compounds to be used as reference materials containing the ZrF_6^{2-} ion or similar. The commercially available ZrF_4 is hygroscopic, making it unsuitable to be used as reference material. Crystals are by definition pure substances and if properly prepared and characterised, as well as stable over extended periods of time, may function well as an in-house reference material.

Characterisation, specifically in crystallography, requires a “perfect” crystal in order to successfully resolve a crystal structure. It can therefore be assumed that any crystal from which a structure has been obtained is close to perfect. Such a crystal would, by definition, be a pure substance and thus potentially be ideal as a reference material. Unfortunately growing crystals is widely known to be difficult with many factors influencing successful crystallisation. These factors include ambient temperature, solvent, evaporation rate of the solvent and vibration in the ambient environment. Some materials require highly specialised conditions to avoid precipitation as an amorphous solid while others crystallise relatively quickly and easily under ambient conditions. It was considered to be advantageous to find a zirconium-containing salt which could be synthesised and crystallised quickly and easily. As most samples derived from the Nuclear Energy Corporation of South Africa (Necsa) production process were either metallic or fluorides it was decided that complexes containing the

hexafluorozirconate (ZrF_6^{2-}) anion would be most suitable. A fair number of cations were used in attempts to grow acceptable crystals. These included ammonium (NH_4^+), tetramethylammonium ($N(CH_3)_4^+$), tetraethylammonium ($N(CH_2CH_3)_4^+$), tetrabutylammonium ($N((CH_2)_3CH_3)_4^+$), cesium (Cs), rubidium (Rb), potassium (K), tetraphenylphosphonium (PPh_4^+) and tetraphenylarsonium ($AsPh_4^+$).

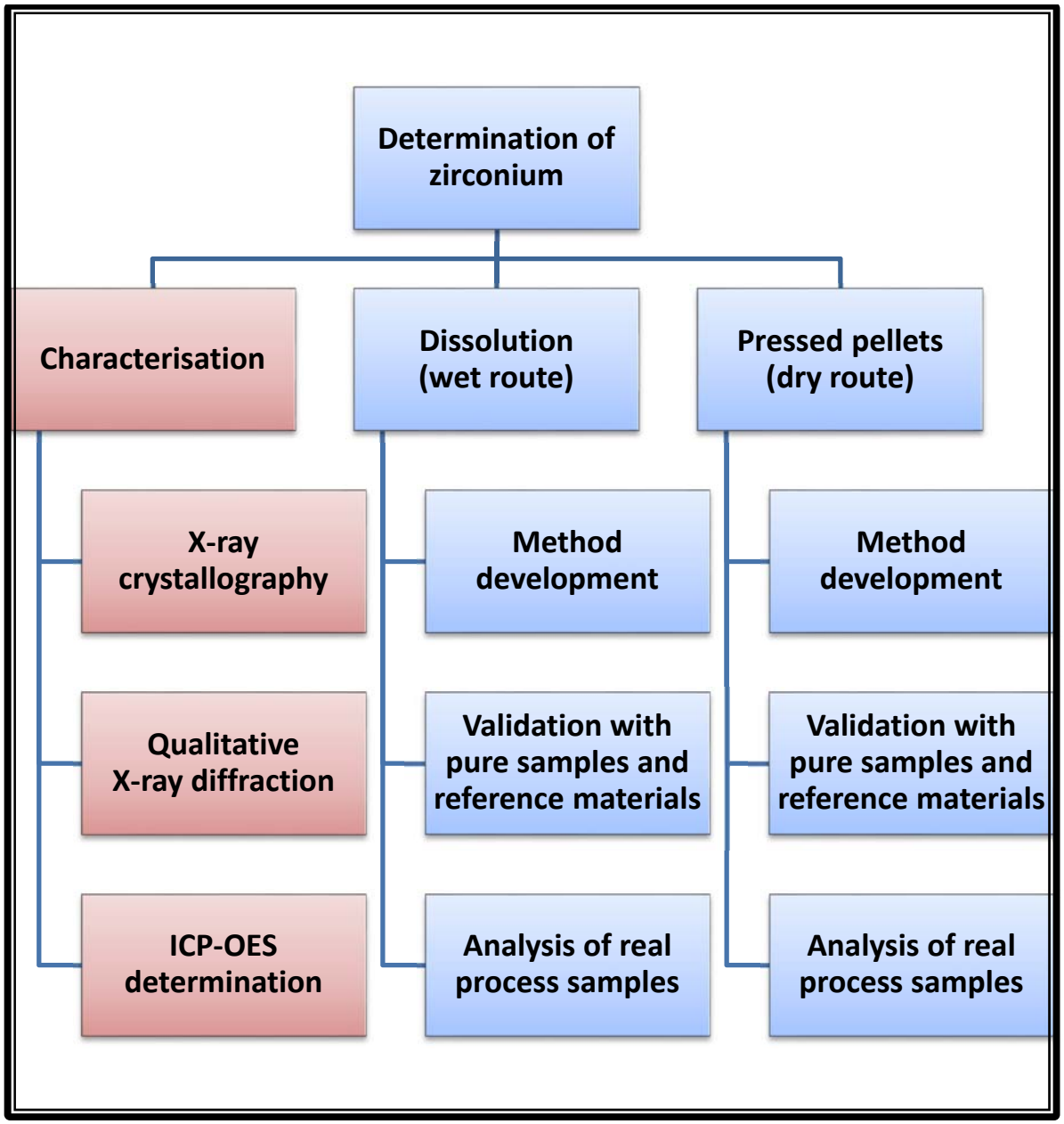

Figure 6-1: Experimental outlay with characterisation and method validation of reference materials highlighted

As seen in **Figure 6-1** the intent was to characterise any potential reference material by X-ray diffraction crystallography (XRD) and qualitative X-ray diffraction before developing and validating an analytical method using ICP-OES. These reference

materials would then be used to ensure traceability when unknown compounds were quantified. ICP analysis has been discussed earlier (**Chapter 4.3**). It was hoped that with a combination of these three techniques a material suitable for use as reference could be identified.

X-ray diffraction (XRD) crystallography relies on the ability of a nearly perfect crystal to diffract incident X-rays in such a way as to cause constructive, destructive and complex interference patterns. These patterns are used to determine atomic positions within a regular crystal lattice (see **Figure 6-2**) [122].

The diffraction pattern alone may also be used for qualitative identification of materials by comparison with patterns for known materials. This allows for the “fingerprinting” of chemical compounds. The peaks obtained for an unknown sample are compared with those for known materials in a database allowing for qualitative identification of the material.

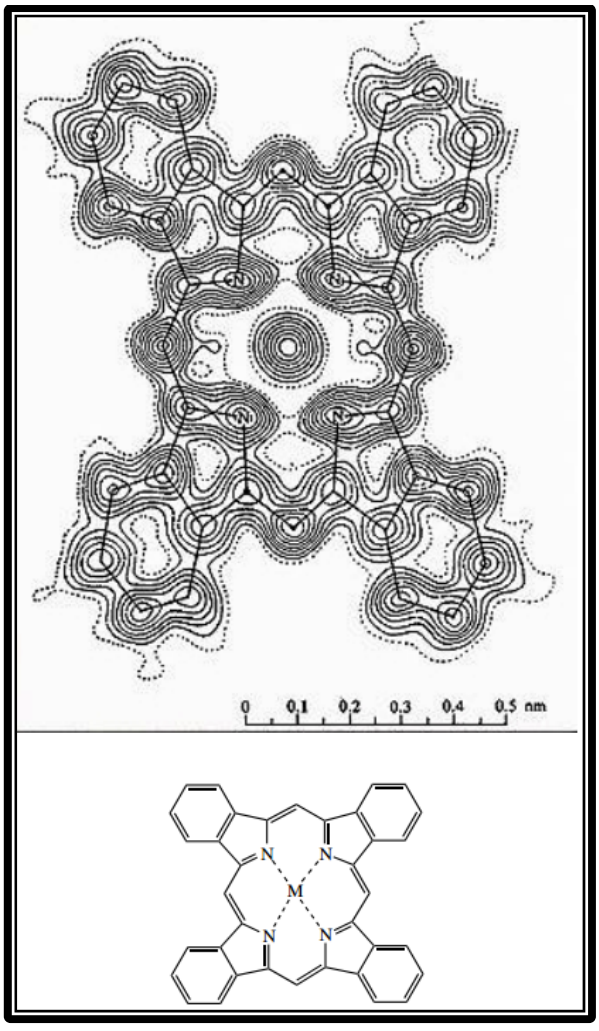

Figure 6-2: Electron density map obtained from XRD [122]

6.2. EXPERIMENTAL

6.2.1 REAGENTS AND EQUIPMENT

Experimental densities were determined using a Micromeritics AccuPyc II 1340 helium gas pycnometer. Zirconium analyses were performed with a Shimadzu ICPS-7510 sequential spectrometer, a Shimadzu ICPM-8500 quadrupole ICP-MS and a Spectro Arcos EOP ICP-OES spectrometer. Cesium analyses were performed with an Agilent 7700cx ICP-MS. Potassium analyses were performed using a Varian AA140 atomic absorption spectrometer. Fluoride determinations were performed with a Thermo Orion Combination Fluoride ion specific electrode. Reagent grade zirconium tetrafluoride, potassium fluoride, cesium fluoride, rubidium carbonate, tetramethylammonium chloride, tetraethylammonium chloride, tetrabutylammonium chloride, tetraphenylphosphonium chloride, tetraphenylarsonium chloride and analytical grade 48% hydrofluoric acid were obtained from Sigma Aldrich. All water used was double distilled.

Table 6-1: ICPS-7510 experimental conditions

Condition	Setting
RF power (kW)	1.2
Coolant gas flow rate (L/min)	14
Plasma gas flow rate (L/min)	1.2
Carrier gas flow rate (L/min)	1.1

Table 6-2: ICPM-8500 experimental conditions

Condition	Setting
RF power (kW)	1.2
Sampling depth (mm)	5.0
Coolant gas flow rate (L/min)	7.0
Plasma gas flow rate (L/min)	1.50
Carrier gas flow rate (L/min)	0.60

Raw experimental data can be found in the attached DVD.

6.2.2 PROCEDURE

Crystallization of zirconium fluorides

$$ZrF_4 + xM^+F^- \rightarrow M_xZrF_{4+x} \quad \textbf{6-1}$$

$$ZrF_4 + xHF + xM^+Y^- \rightarrow M_xZrF_{4+x} + xHY \quad \textbf{6-2}$$

Samples of between 0.1 and 1 g (5.98 and 59.8 mmol) zirconium tetrafluoride starting material were weighed off accurately to 0.1mg and placed in plastic beakers and dissolved in 20.0 mL distilled water and one drop of 48% hydrofluoric acid. The quantity of ZrF_4 was determined by the available quantities of the cation donor material, as several of the compounds were available only in small amounts. To each of the ZrF_4 samples, 2 or 3 equivalents of potassium fluoride, cesium fluoride, rubidium carbonate, tetramethylammonium chloride, tetraethylammonium chloride, tetrabutylammonium chloride, tetraphenylphosphonium chloride or tetraphenylarsonium chloride were added, dissolved in 20.0 mL distilled water and one drop of 48% hydrofluoric acid (**Equation 6-1**). Two equivalents of HF as hydrofluoric acid were added to the samples as a fluoride source where chloride or carbonate salts (**Equation 6-2**) were used. All experimental masses are given in **Table 6-3**. 60.0 mL of distilled water necessary to cause the entire sample to go into solution was added. These samples were allowed to stand for several weeks until crystals or a precipitate formed.

Translucent crystals formed in all cases except the rubidium carbonate, tetramethylammonium chloride and tetrabutylammonium chloride. Of the crystals formed, the potassium hexafluorozirconate proved the quickest and most reliable to produce. In all cases where a crystal formed at least one was selected and sent for crystallographic analysis to the crystallography group at the Nelson Mandela Metropolitan University (NMMU). Of these only the potassium-, cesium- and tetraethylammonium-containing crystals yielded a crystal structure. Only the production of the potassium and cesium crystals was repeatable. A single, large tetraethylammonium-containing crystal was recovered from the mother solution before precipitation began to occur. Despite many further attempts under varying conditions this product could not be crystallised again.

Table 6-3: Experimental conditions used in crystallisation of zirconium reference materials

Intended crystal compound	Cation donor	Mass donor (g)	Mass ZrF_4 (g)	Molar equivalents	Volume 48% HF (mL)
K_2ZrF_6	KF	0.6968	1.0126	2	0.05
K_3ZrF_7	KF	1.0463	1.0060	3	0.05
Rb_2ZrF_6	Rb_2CO_3	0.1923	0.1044	2	0.53
Cs_2ZrF_6	CsF	0.1298	0.1250	2	0.53
$(NH_4)_2ZrF_6$	NH_4F	0.4448	1.0028	2	0.05
$(NH_4)_3ZrF_7$	NH_4F	0.6706	1.0038	3	0.05
$(TPA)_2ZrF_6$	Tetraphenylarsonium chloride	0.0454	0.0101	2	0.53
$(TPP)_2ZrF_6$	Tetraphenylphosphonium chloride	0.0532	0.0105	2	0.53
$(TMA)_2ZrF_6$	Tetramethylammonium chloride	0.1326	0.1001	2	0.53
$(TEA)_2ZrF_6$	tetraethylammonium chloride	0.2011	0.1006	2	0.53
$(TBA)_2ZrF_6$	Tetrabutylammonium chloride	0.3448	0.0998	2	0.53

XRD analysis was performed at the Nelson Mandela Metropolitan University. A Bruker Kappa Apex II X-ray Crystallography System was used to collect the reflection data. The radiation source was a fine-focus sealed tube emitting molybdenum Kα radiation at a wavelength of 0.71073 nm with ω- and φ-scans at 100 K. The radiation monochromator was composed of graphite. All the cell refinements were performed with SAINT-Plus while the data reduction was done with SAINT-Plus and XPREP [123]. The absorption corrections were obtained by the use of the multi-scan technique and the SADABS software package [124]. All of the structures were solved with the use of the SIR-97 package [125], refinement was done with SHELXL-97 [126] and WinGX [127] and the molecular graphics were completed with DIAMOND [128]. The structures are shown with thermal ellipsoids drawn at a 50% probability level and all non-hydrogen atoms were anisotropically refined. Methyl and methylene hydrogen atoms were placed in geometrically idealised positions, C-H = 0.96 Å and 0.97 Å and constrained to ride on their parent atoms, Uiso(H) = 1.5 Ueq(C), 1.2 Ueq(C), 1.2 Ueq(C) and 1.2 Ueq(C) respectively.

6.3. CRYSTALLOGRAPHIC AND QUALITATIVE XRD RESULTS

6.3.1 X-RAY CRYSTALLOGRAPHY

Table 6-4: Table showing crystallographic data and refinement parameters for 3 potential zirconium reference materials

Chemical formula		**K_2ZrF_6**	**Cs_2ZrF_6**	**$C_{16}H_{44}N_2OZr_2F_{10}$**
Compound name		Potassium catena di-μ-fluorido-tetrafluoridozirconate(IV)	Cesium hexafluorido zirconate(IV)	Tetraethyl ammonium catena di-μ-fluorido-bis-(trifluoridozirconate(IV)) monohydrate
Formula weight		283.42	471.04	652.97
Temperature (K)		293(2)	293(2)	200(2)
Wavelength Mo K_α		0.71073	0.71073	0.71073
Crystal system		Monoclinic	Trigonal	Monoclinic
Space group		C2/c	P3m1	C2/c
Cell lengths (Å)	**a**	6.543(5)	6.386(5)	15.8130(4)
	b	11.359(5)	6.386(5)	12.3456(3)
	c	6.926(5)	4.984(5)	13.4704(4)
Cell angles (˚)	**α**	90.00	90.00	90.00
	β	90.774(5)	90.00	109.4660(10)
	γ	90.00	120.00	90.00
Cell volume ($Å^3$)		514.7(6)	176.022	2479.39
Z		4	1	4
Theoretical density (g/cm^3)		3.657	4.444	1.749
Measured density (g/cm^3)		3.68(3)	4.026(3)	-
Crystal size (nm^3)		0.445x0.192x0.137	0.217x0.127x0.106	0.312x0.115x0.089
Absorption coefficient		3.792	11.782	0.926
F(000)		528	204	1328
Theta range for data collection (°)		3.59 to 27.97	3.68 to 27.41	2.39 to 28.31
Index ranges		-8 ≥ h ≥ 7 -14 ≥ k ≥ 12 -9 ≥ l ≥ 9	-6 ≥ h ≥ 5 -4 ≥ k ≥ 8 -6 ≥ l ≥ 5	-21 ≥ h ≥ 21 -14 ≥ k ≥ 16 -17 ≥ l ≥ 13
Reflections collected		1194	172	3090
Independent reflections		1172 [R(int) = 0.0209]	169 [R(int) = 0.0227]	2774 [R(int) = 0.0152]
Refinement method		SHELXL-97	SHELXL-97	SHELXL-97
Data / Restraints / Parameters		1172 / 2 / 66	169 / 0 / 13	2774 / 0 / 144
Goodness of fit on F^2		1.125	1.201	1.042
Final R indices [I ≥2σ(I)]		R_1= 0.0302 wR_2 = 0.0775	R_1= 0.0493 wR_2 = 0.1342	R_1= 0.0162 wR_2 = 0.0454
R indices (all data)		R_1= 0.0306 wR_2 = 0.077	R_1= 0.0495 wR_2 = 0.1345	R_1= 0.0197 wR_2 = 0.0475
Largest diff. peak and hole		0.700 and -2.332	3.496 and -4.462	0.300 and -0.519

6.3.1.1 Crystal structure of potassium catena di-μ-fluorido-tetrafluoridozirconate(IV)

As seen in **Table 6-3**, attempts were made to produce both K_3ZrF_7 and K_2ZrF_6 but under the conditions used, crystallography revealed that both crystal products were K_2ZrF_6. Literature shows a method for producing the K_3ZrF_7 complex [129] with a large excess of KF but these were reported to decompose fairly rapidly. K_2ZrF_6 has also been produced [130] by the addition of stoichiometric quantities of potassium fluoride to zirconium oxide dissolved in 40% hydrofluoric acid. In this study zirconium tetrafluoride was used as starting material (**Equation 6-1**) and only a minimal quantity of hydrofluoric acid was used to bring the reagents into solution. The structure seen in **Figure 6-3** shows the polymeric structure of the potassium catena di-μ-fluorido-tetrafluoridozirconate(IV) crystal. A list of relevant bond lengths is given in **Table 6-5** with bond angles in **Table 6-6**. Bridging fluorine atoms connect alternating zirconium(IV) atoms with the average bridging and terminal zirconium-fluorine bond lengths being approximately 2.06 and 2.17 Å respectively. The bridging fluorine bond lengths between two zirconium atoms are on average approximately 0.1 Å longer than the non-bridging bonds. Potassium-fluorine interaction distances of between 2.62 and 3.00 Å were observed. The 3.776(1) Å distance between the zirconium and potassium atoms is close enough to allow for a degree of interaction, primarily manifesting through the bond lengths and angles of the non-bridging zirconium-fluorine bonds. The zirconium atoms were found to be in the centre of a twisted dodecahedron environment (**Figure 6-5**) with four bridging and four terminal fluorine atoms (coordination number = 8). Each potassium atom, on the other hand, was found in the centre of an irregular polyhedron (coordination number = 8) of interacting fluorine atoms (**Figure 6-6**). The potassium and zirconium appeared to be close enough for a limited amount of interaction. A similar structure found in literature [131] where HF is associated in the crystal had corresponding average bond lengths of 2.02 and 2.18 Å for the bridging and non-bridging zirconium-fluorine bonds respectively, effectively identical to the crystal grown in this study. Potassium-fluorine interaction distances of between 2.62 and 2.88 Å were also in the same range. A structure for γ-zirconium tetrafluoride [132] showed a similarly polymeric character with zirconium-fluorine bond lengths ranging between of 2.03 and 2.20 Å which is very close to those seen in both of the potassium hexafluorozirconate structures. The K_3ZrF_7 structure [129] showed bond lengths of approximately 2.1 and 2.6 Å with and uncertainty of 0.1 Å for the zirconium-fluorine and potassium-fluorine bonds respectively, very much in line with

those seen in the other structures. The structure of the crystal formed from the zirconium oxide starting material [130] showed zirconium-fluorine bond lengths of between 2.0406 and 2.2058 Å with a zirconium coordination polyhedron of a slightly distorted square antiprism in contrast to the twisted dodecahedron seen in this study. With the exception of the slightly different bonding environment and longer zirconium-fluorine bond lengths, the two structures are still quite similar.

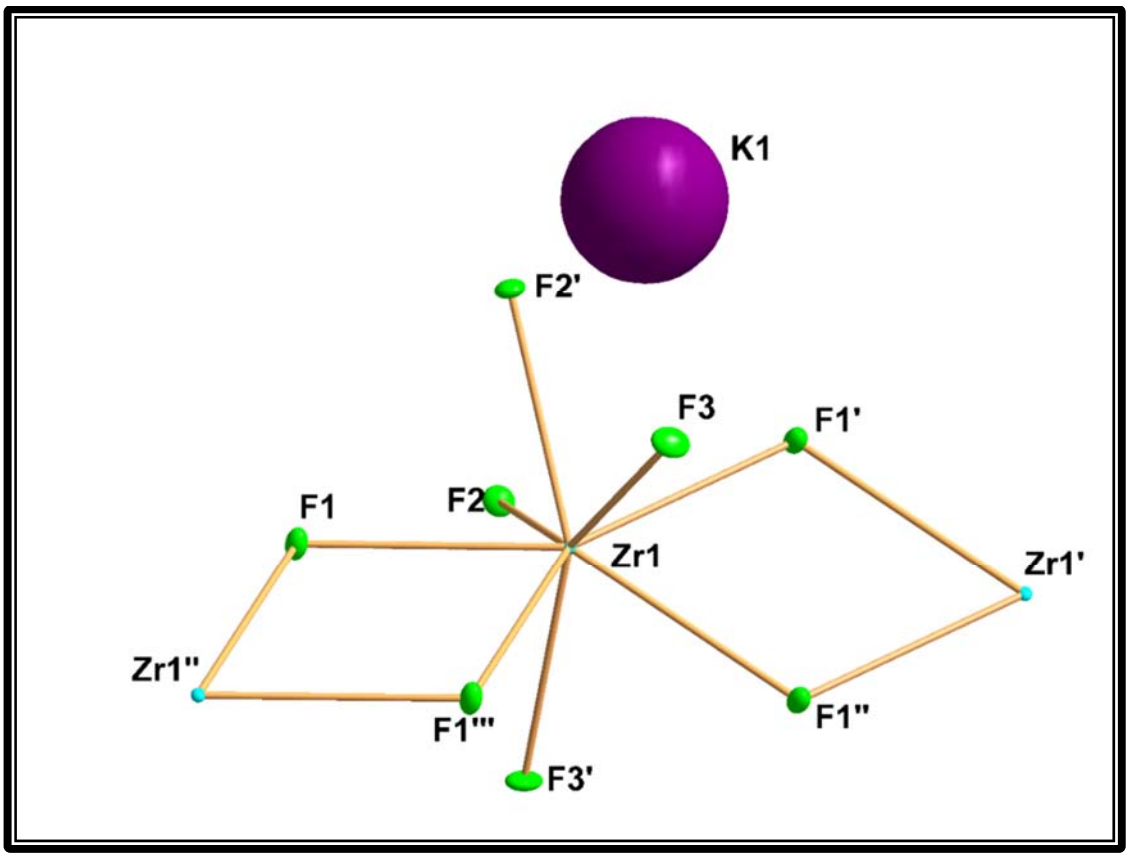

Figure 6-3: Perspective view of the potassium catena di-μ-fluorido-tetrafluoridozirconate(IV) with atomic labelling scheme

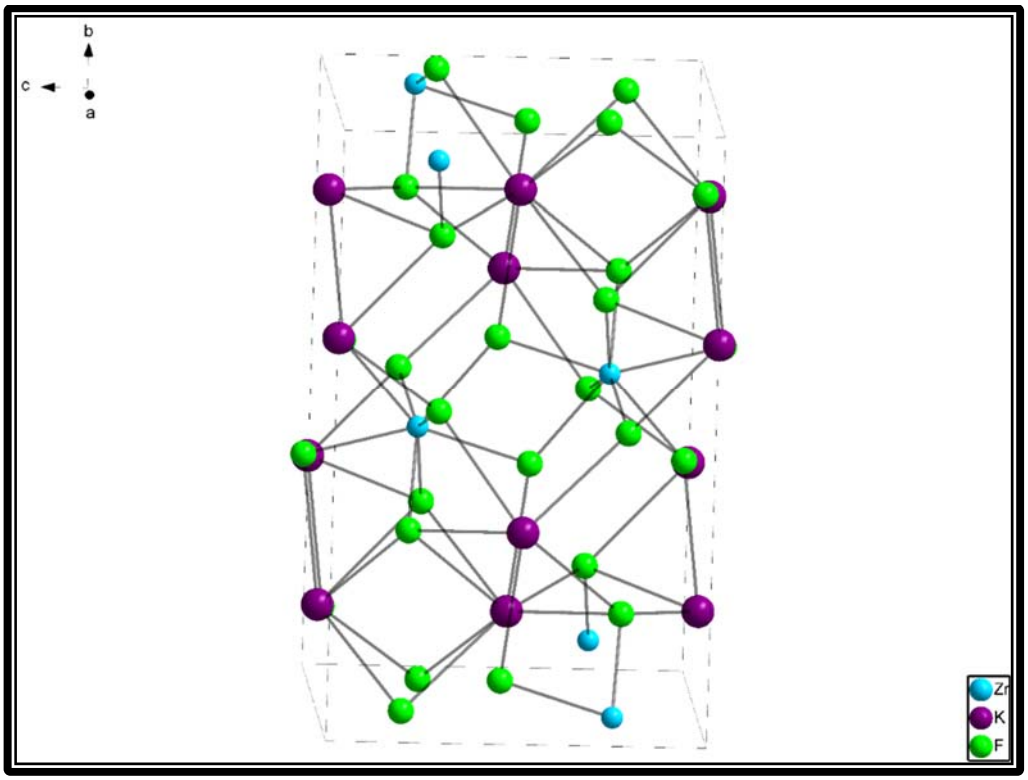

Figure 6-4: Perspective view along the a-axis of packing in the potassium catena di-μ-fluorido-tetrafluoridozirconate(IV) crystal

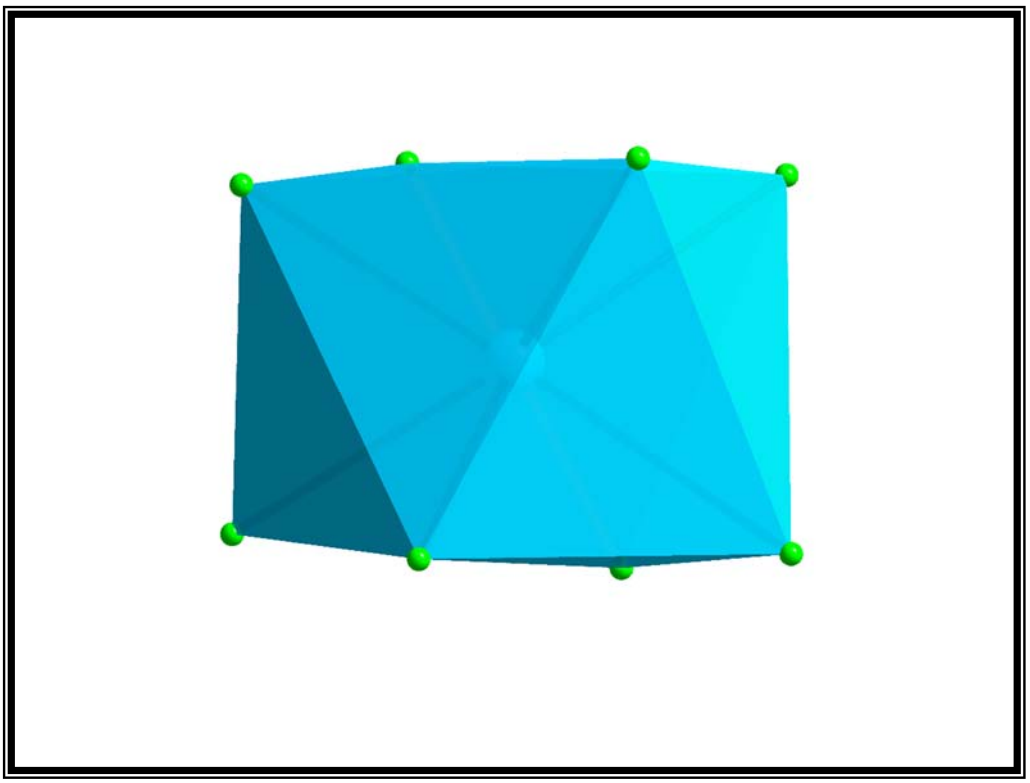

Figure 6-5: Coordination dodecahedron of zirconium in the potassium catena di-μ-fluorido-tetrafluoridozirconate(IV) crystal

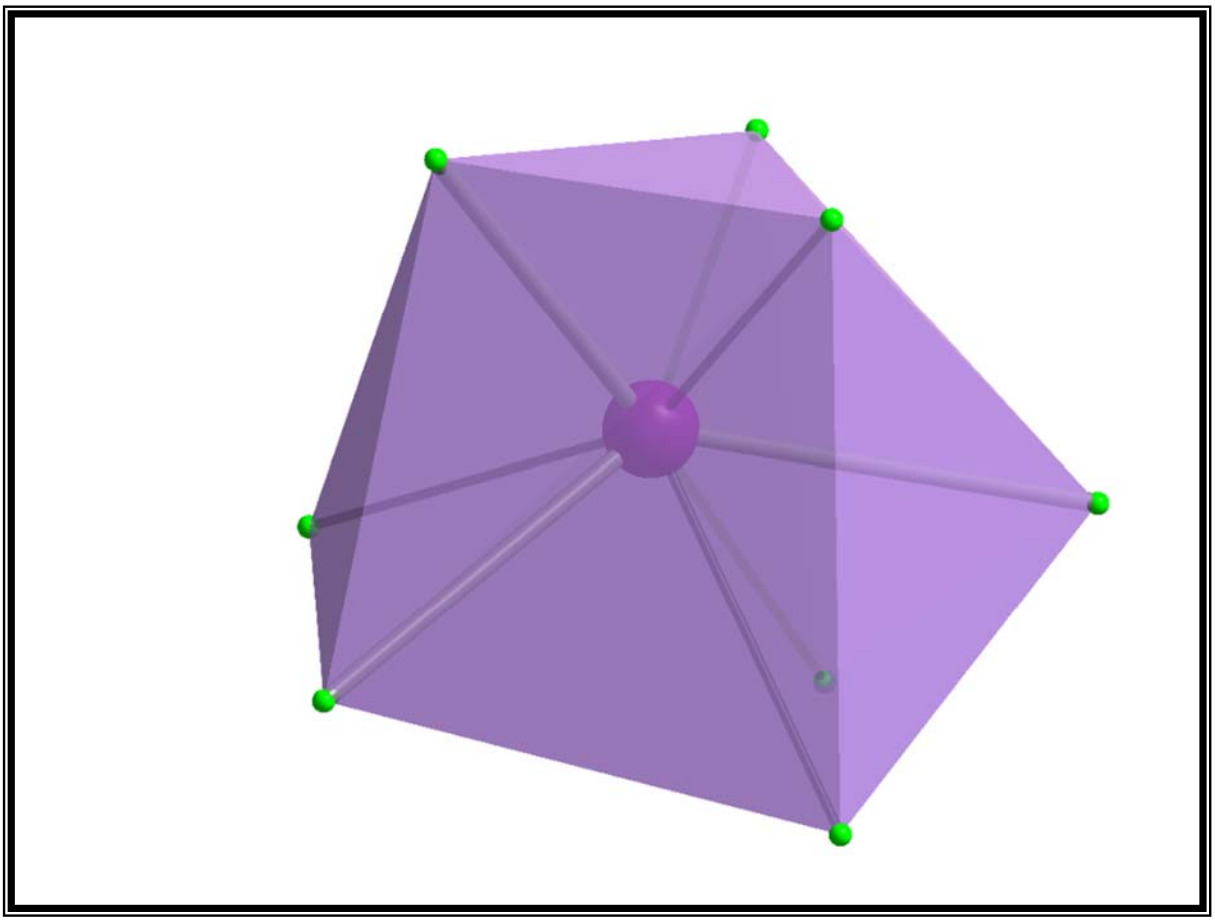

Figure 6-6: Coordination polyhedron of potassium in potassium catena di-μ-fluorido-tetrafluoridozirconate(IV) crystal

Table 6-5: Selected bond distances for potassium catena di-μ-fluorido-tetrafluoridozirconate(IV)

Bond	Distance (Å)	Bond	Distance (Å)
Zr1-F2'	2.030(4)	K1---F1	2.924(4)
Zr1-F1	2.140(4)	K1---F2	2.756(4)
Zr1-F3	2.079(4)	K2---F1'	3.002(4)
Zr1-F1'	2.194(4)	K2---F3	2.679(4)
Zr1-F2	2.060(3)	K2---F1''	2.796(5)
K1---F2'	2.712(4)	K2---F2	2.623(4)
K1---F3	2.787(4)	Zr1---K1	3.776(1)

Table 6-6: Selected bond angles for potassium catena di-μ-fluorido-tetrafluoridozirconate(IV)

Bond	Angle (°)	Bond	Angle (°)
F2'-Zr-F1'	74.0(1)	F3-Zr-F1''	76.9(1)
F2'-Zr-F3	73.4(1)	F3-Zr-F2	145.1(1)
F2'-Zr-F1''	78.6(1)	F3-Zr-F3'	74.7(1)
F2'-Zr-F2	139.5(1)	F1''-Zr-F2	73.3(1)
F2'-Zr-F3'	145.2(1)	F1''-Zr-F3'	77.2(1)
F1'-Zr-F3	79.0(1)	F2-Zr-F3'	75.0(1)
F1'-Zr-F1''	66.7(2)	Zr-F2'-K2	122.7(1)
F1'-Zr-F2	73.6(1)	Zr-F1'-Zr	113.4(2)
F1'-Zr-F3'	76.1(1)	Zr-F3-K3	114.9(2)

6.3.1.2 Crystal structure of cesium hexafluorido zirconate(IV)

In the case of the cesium hexafluorido zirconate(IV) the structure can be seen to be composed of discrete ZrF_6^{2-} with associated cesium cations as seen in **Figure 6-7** with the packing shown in **Figure 6-8**. Similarly to the potassium product, both the intended Cs_3ZrF_7 and Cs_2ZrF_6 proved to be Cs_2ZrF_6 upon crystallographic determination. The zirconium (coordination number = 6) was found in a slightly distorted octahedron (**Figure 6-9**). Fluorine-zirconium-fluorine bond angles between adjacent-coordinated fluorine atoms in the equatorial plane varied between 87.4(2)° and 92.5(2)°, deviating from the expected 90° of a standard octahedron. The cesium was found in an irregular polyhedron (**Figure 6-10**) with no significant interaction between it and the zirconium. In this case the zirconium-fluorine bonds can be seen to be slightly shorter than those seen in the potassium complexes with a constant distance of 2.007 Å (**Table 6-7**) while the cesium-fluorine interaction distances (3.212 Å) are significantly longer than those for the potassium-fluorine interactions seen in **Section 6.3.1.1**. Bond angles are shown in **Table 6-8**. The distance between the zirconium centres and potassium atoms was found to be 3.996(3) Å, indicating a smaller degree of interaction than seen in the the potassium catena di-μ-fluorido-tetrafluoridozirconate (IV) crystal. This greater distance is likely due to the bigger atomic radius of the cesium in comparison to the potassium. Similar zirconium-fluorine bond lengths are seen in literature [133] in a rubidium potassium hexafluorozirconate structure where the bonds ranged from 1.9886 to

2.0958 Å for the bridging fluorine atoms and from 2.1403 to 2.1950 Å for the terminal fluorines. This structure was again produced using zirconium oxide as starting material in contrast to the zirconium tetrafluoride used in this study. Rubidium cadmium heptafluorozirconate [134] was synthesised in the solid state by reacting stoichiometric quantities of the dry metal fluorides in sealed platinum tubes for three days at 600°C. Zirconium-fluoride bond distances again ranged between 1.989 and 2.115 Å, slightly shorter than seen in the rubidium-potassium hexafluorozirconate. The significant difference between the theoretical and experimentally determined density (4.444 and 4.026) will be investigated further.

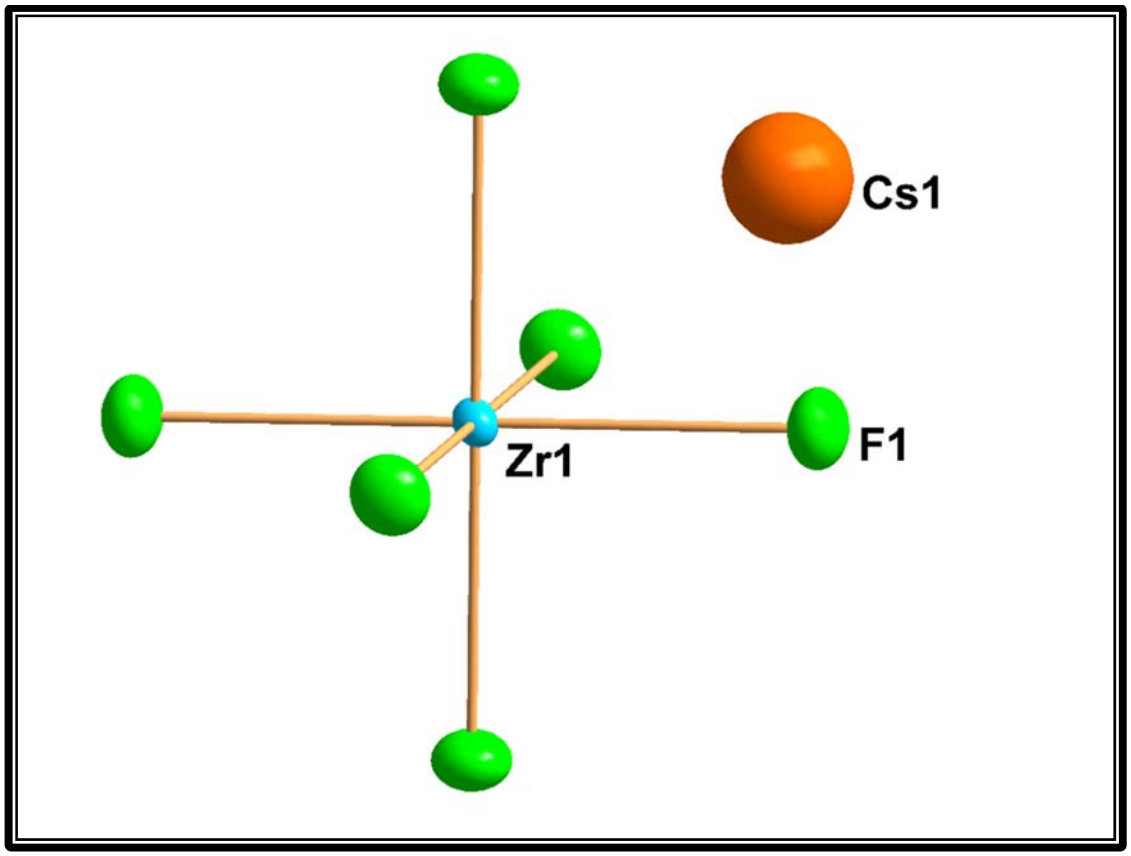

Figure 6-7: Perspective view of the cesium hexafluorido zirconate(IV) crystal with atomic labelling scheme

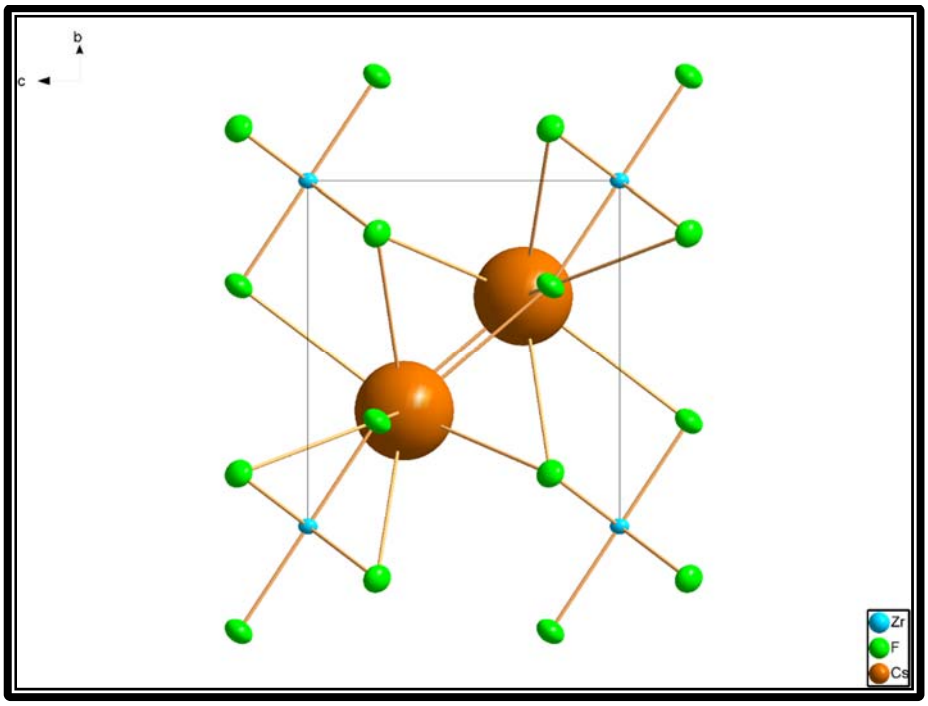

Figure 6-8: Perspective view along the a axis of packing in the cesium hexafluorido zirconate(IV) crystal

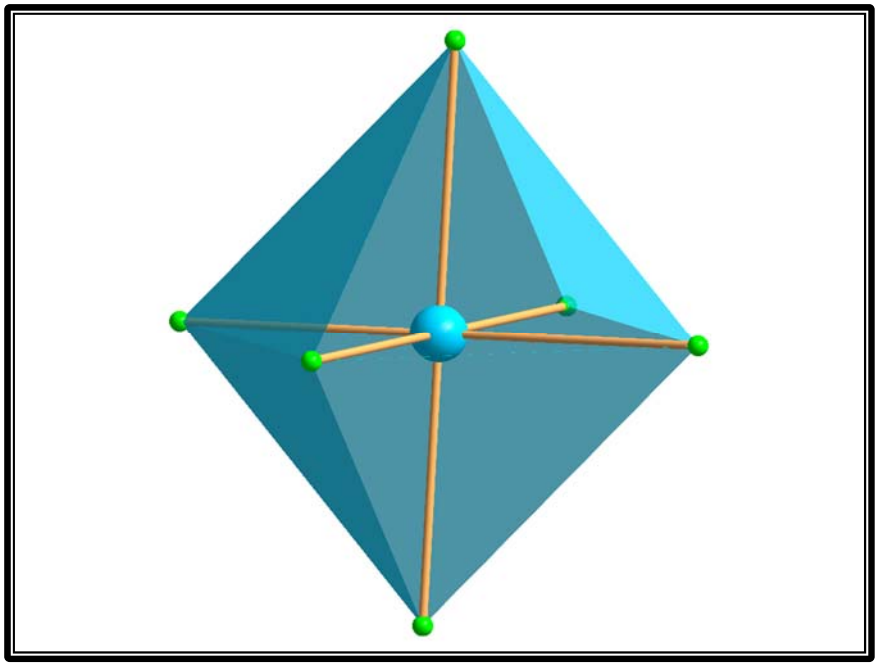

Figure 6-9: Coordination octahedron of zirconium cesium hexafluorido zirconate(IV) crystal

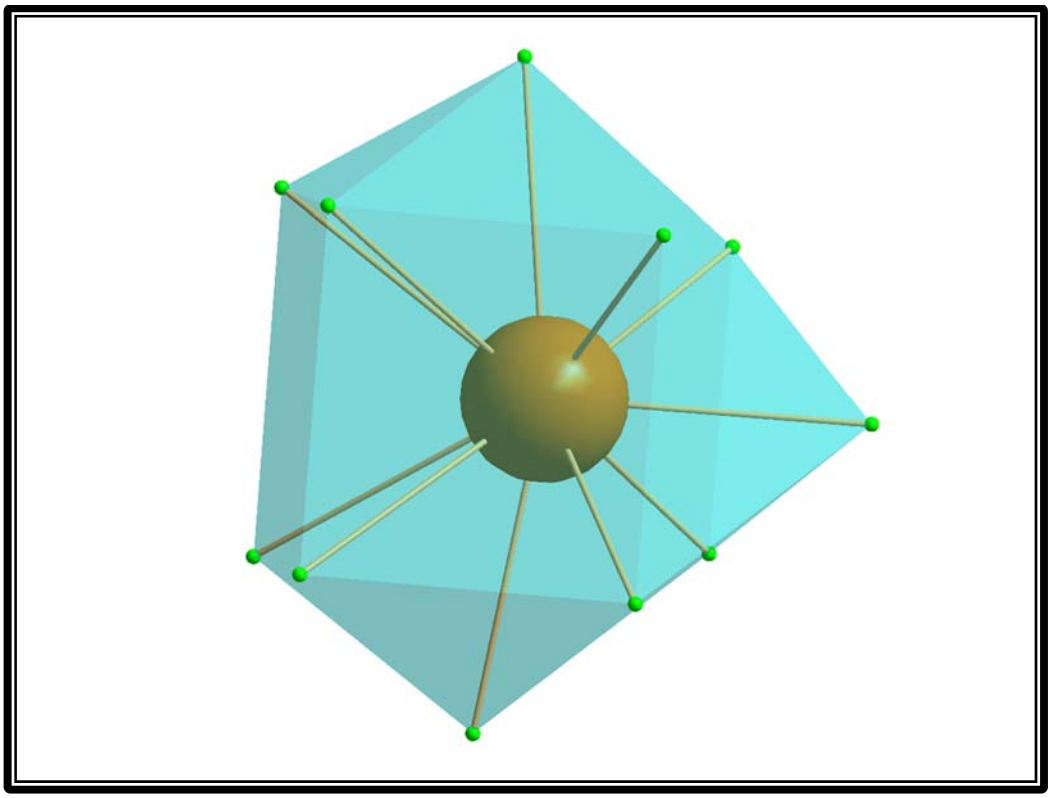

Figure 6-10: Coordination polyhedron of cesium in cesium hexafluorido zirconate(IV) crystal

Table 6-7: Selected bond distances for cesium hexafluorido zirconate(IV)

Bond	Distance (Å)	Bond	Distance (Å)
Zr1-F1*	2.007(6)	**Cs1---F1''**	3.084(5)
Cs1---F1	3.227(8)	**Zr---Cs**	3.996(3)
Cs1---F1'	3.325(5)		

* Zr-F bonds were all 2.007(6) Å in length.

Table 6-8: Selected bond angles for cesium hexafluorido zirconate(IV)

Bond	Angle (°)	Bond	Angle (°)
F1-Zr-F1'	180.0(2)	**Zr-F1-Cs(1)**	164.2(2)
F1-Zr-F1''	87.4(2)	**Zr-F1-Cs(2)**	93.8(1)
F1-Zr-F1'''	92.5(2)	**Zr-F1-Cs(3)**	96.8(2)

6.3.1.3 Crystal structure of tetraethyl ammonium catena di-μ-fluorido-bis-(trifluoridozirconate(IV)) monohydrate

The tetraethyl ammonium catena di-μ-fluorido-bis-(trifluoridozirconate(IV)) monohydrate structure (**Figure 6-11**) shows the zirconium-fluoride chain (**Figure 6-12**) with three single metal to fluoride bonds and four bridging fluorides (coordination

number = 7) with the packing seen in **Figure 6-13**. The terminal zirconium-fluorine average bond distance was 1.97 Å while the bridging bonds' average length was 2.15 Å, very close to that of zirconium tetrafluoride (2.126 Å). The coordination polyhedron around the zirconium is a pentagonal bipyramid. The interaction between the tetraethylammonium cation and the ZrF_5^- chain is likely primarily through hydrogen interaction with the fluoride atoms of the chain. A list of bond angles and distances can be seen in **Table 6-9** and **Table 6-10** respectively.This structure is similar to that seen in literature of $(N_2H_6)_3Zr_2F_{13}$ compound [135] where the associated hydrazinium packs around the Zr_2F_{13} backbone. The zirconium-fluorine bond lengths in this structure vary between 2.031 and 2.212 Å, significantly longer than seen in the tetraethylammonium crystal. The density of the crystal could not be experimentally determined as there was insufficient sample for analysis.

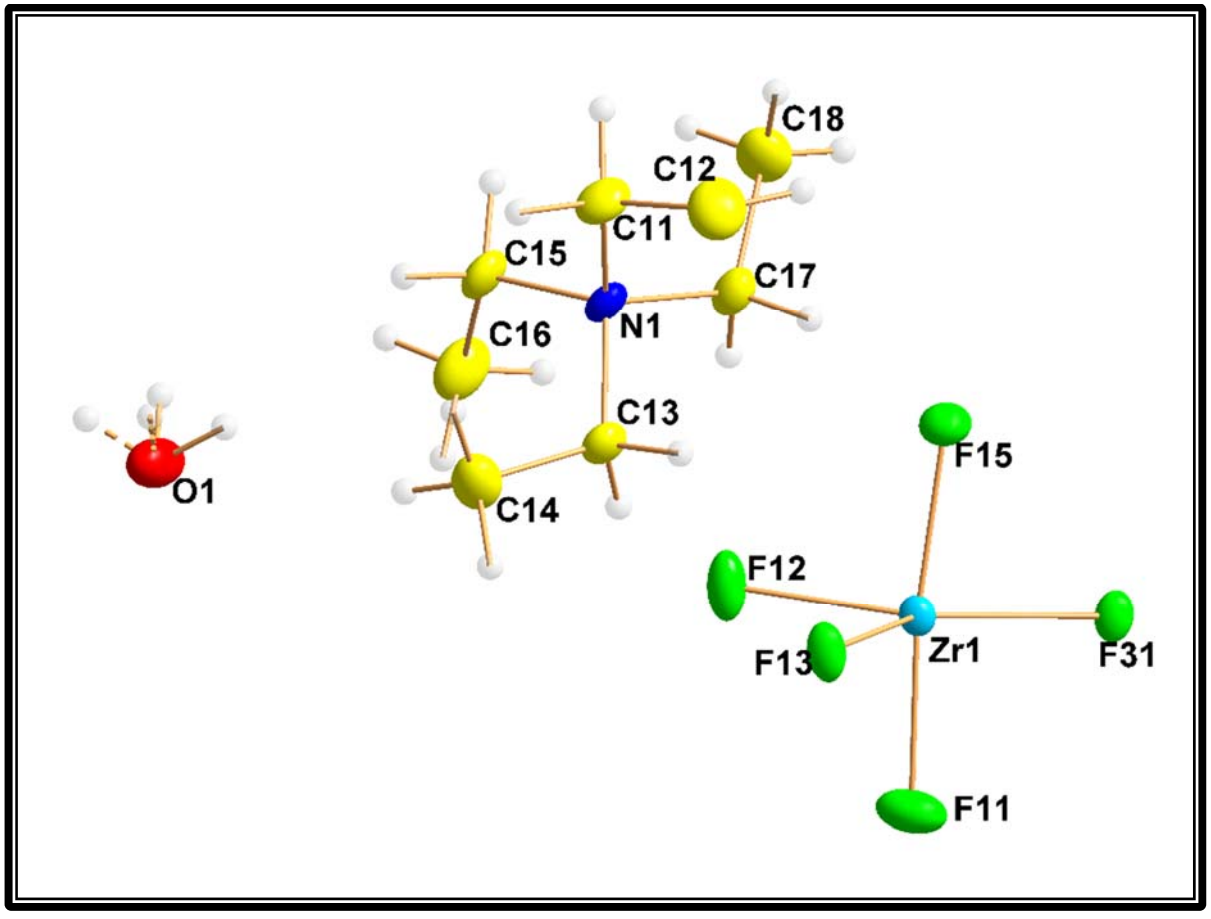

Figure 6-11: Numbering scheme of the tetraethyl ammonium catena di-μ-fluorido-bis-(trifluoridozirconate(IV)) monohydrate

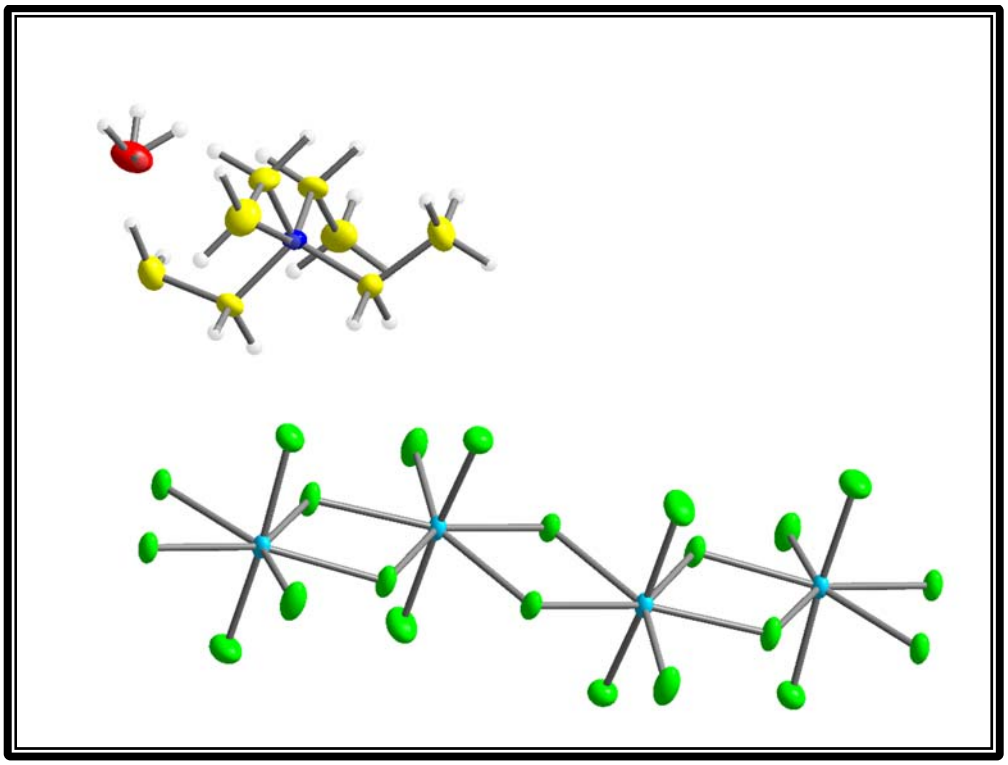

Figure 6-12: Perspective view of the tetraethyl ammonium catena di-μ-fluorido-bis-(trifluoridozirconate(IV)) monohydrate showing the chain structure

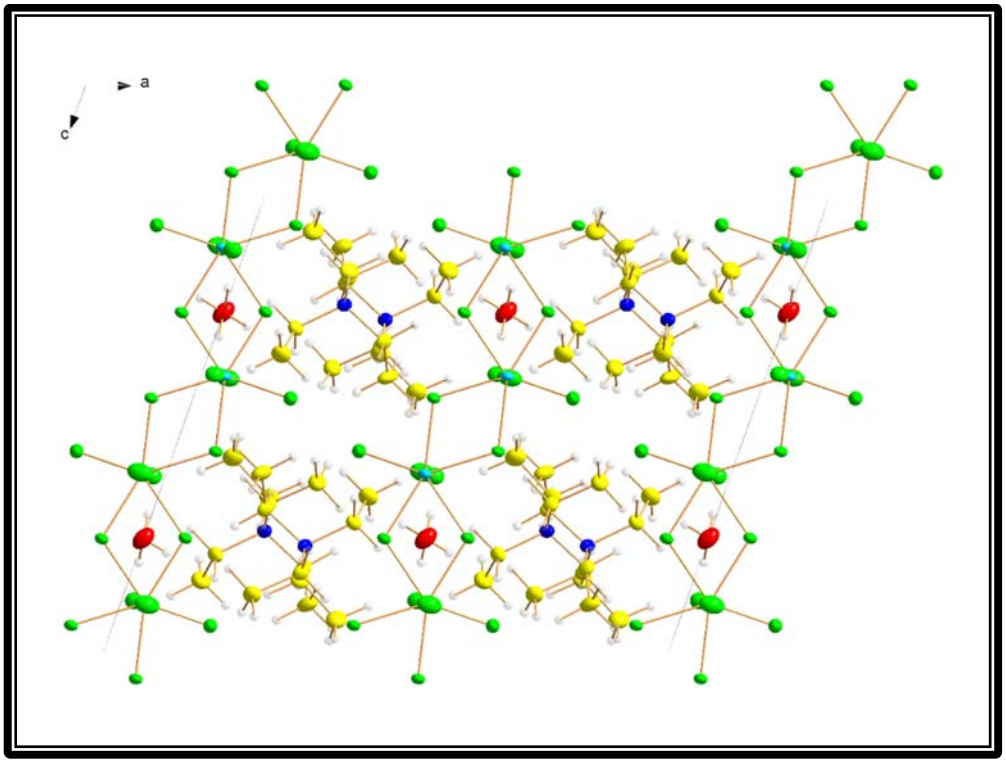

Figure 6-13: Perspective view along the b axis of packing in the tetraethyl ammonium catena di-μ-fluorido-bis-(trifluoridozirconate(IV)) monohydrate crystal

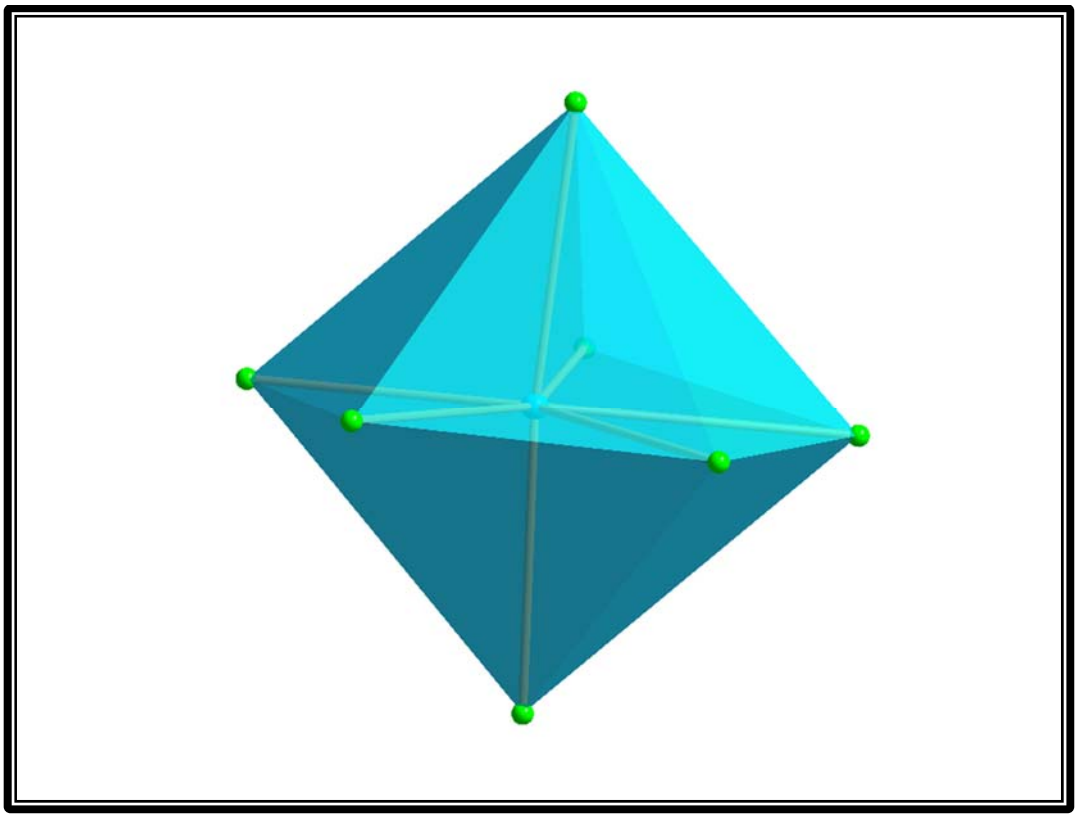

Figure 6-14: Coordination pentagonal bipyramid of zirconium in tetraethyl ammonium catena di-μ-fluorido-bis-(trifluoridozirconate(IV)) monohydrate crystal

Table 6-9: Selected bond distances for tetraethyl ammonium catena di-μ-fluorido-bis-(trifluoridozirconate(IV)) monohydrate

Bond	Distance (Å)	Bond	Distance (Å)
Zr1-F11	1.9785(9)	**Zr1-F31'**	2.1351(8)
Zr1-F12	1.9632(8)	**N1-C11**	1.513(2)
Zr1-F13	2.1401(9)	**N1-C13**	1.516(2)
Zr1-F15	1.9652(8)	**N1-C15**	1.517(2)
Zr1-F31	2.1564(9)	**N1-C17**	1.517(2)
Zr1-F13'	2.1605(7)	**C11-C12**	1.507(2)

Table 6-10: Selected bond angles for tetraethyl ammonium catena di-μ-fluorido-bis-(trifluoridozirconate(IV)) monohydrate

Bond	Angle (°)	Bond	Angle (°)
F11-Zr1-F12	95.29(4)	**Zr1-F13-Zr2**	113.93(4)
F11-Zr1-F13	88.40(4)	**Zr1-F31-Zr2**	113.64(4)
F11-Zr1-F15	173.47(4)	**C11-N1-C13**	110.7(1)
F11-Zr1-F31	87.37(4)	**C11-N1-C15**	106.3(1)
F12-Zr1-F13	77.35(3)	**C11-N1-C17**	111.5(1)
F12-Zr1-F15	91.03(4)	**C13-N1-C17**	105.7(1)
F12-Zr1-F31	77.79(3)	**C15-N1-C17**	111.2(1)
F13-Zr1-F15	85.43(3)	**N1-C11-C12**	115.7(2)
F13-Zr1-F31	72.97(3)	**N1-C13-C14**	114.8(1)
F15-Zr1-F31	86.54(3)		

6.3.2 QUALITATIVE XRD

Qualitative determinations were performed on the K_2ZrF_6 and Cs_2ZrF_6 crystal samples using a Bruker D8 Advance powder diffractometer. Instrument conditions are given in **Table 6-11**. The tetraethylammonium hexafluorozirconate was not analysed as there was insufficient sample available.

Table 6-11: Instrument conditions for qualitative XRD analysis

Diffractometer	D8 Advance
Goniometer	θ-θ
Target tube	Cu
Recording range	15˚ to 120˚
Step size	0.04
Counts/frame	1s

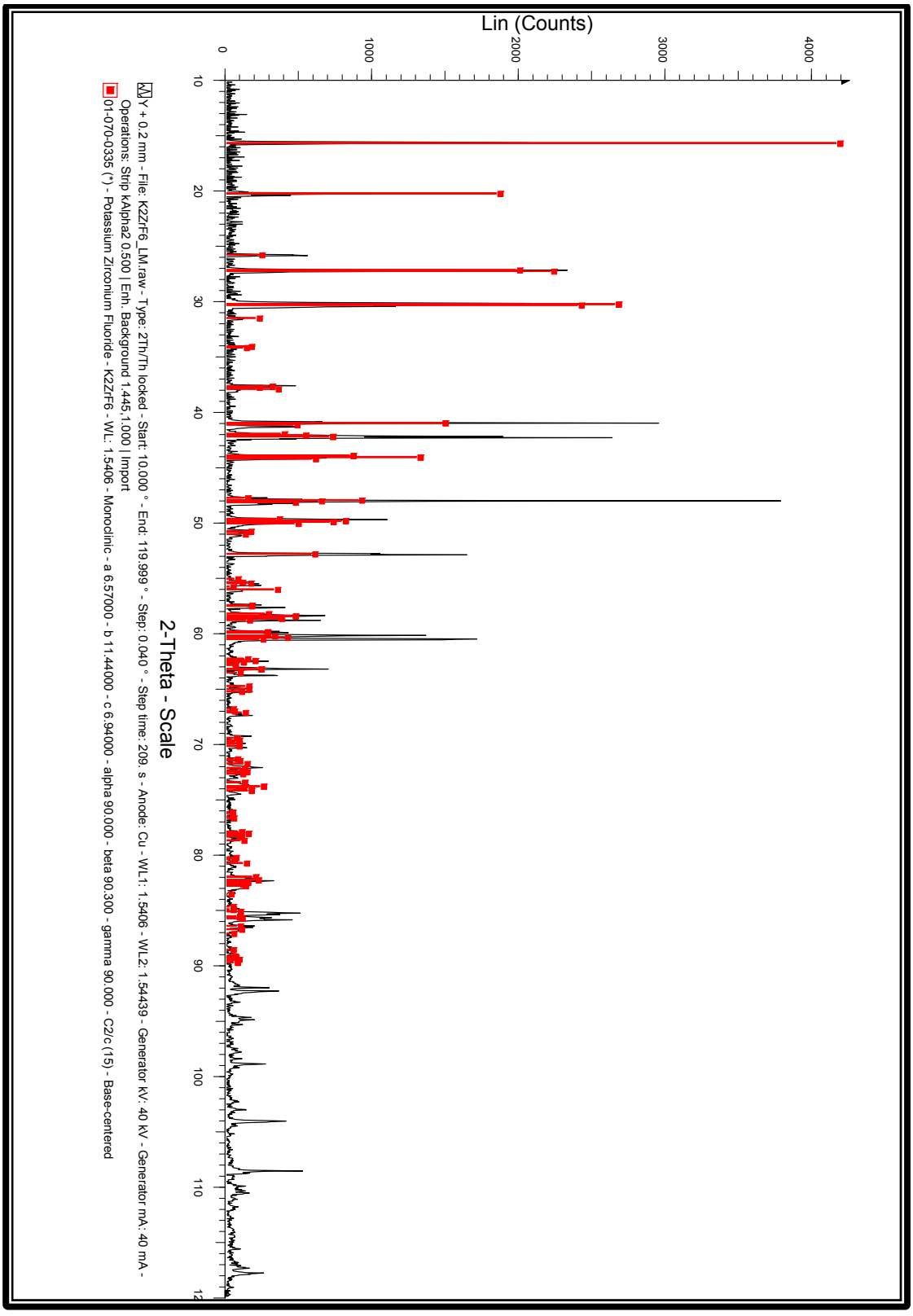

Figure 6-15: XRD spectrum of potassium hexafluorozirconate with theoretical lines superimposed

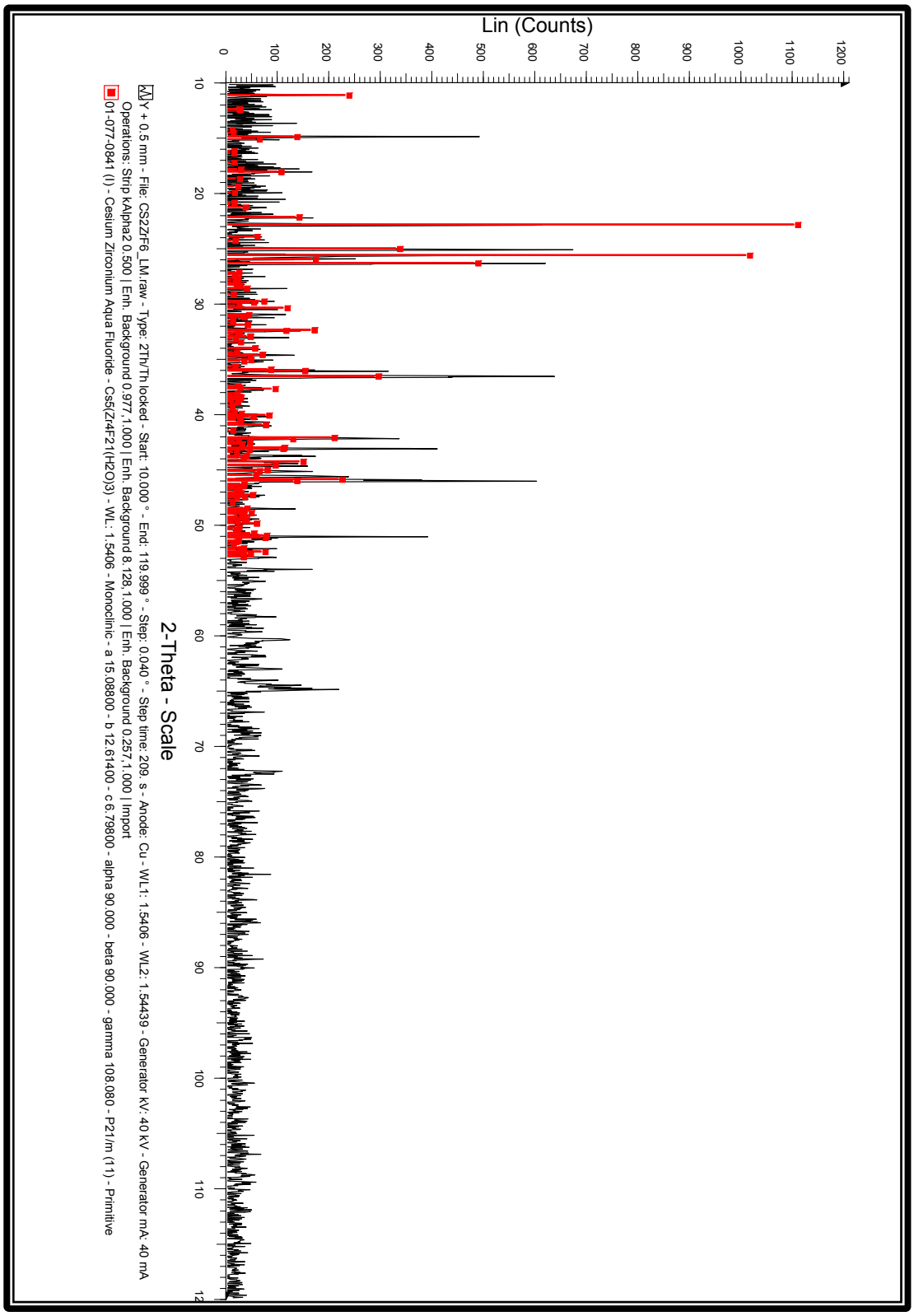

Figure 6-16: XRD spectrum of cesium hexafluorozirconate with theoretical lines superimposed

The diffraction patterns seen in **Figure 6-15** (K_2ZrF_6) and **Figure 6-16** (Cs_2ZrF_6) match the theoretical peak positions almost exactly for the potassium complex and well enough for the cesium to positively identify both compounds. In the case of the cesium

hexafluorozirconate the theoretical spectrum is that of cesium zirconium aquafluoride, a similar compound, as no structure for cesium hexafluorozirconate was available in the database. It is a close enough match however, along with the crystal structure and other determinations, to positively identify the material.

6.4. METHOD DEVELOPMENT AND VALIDATION OF ZIRCONIUM DETERMINATION IN REFERENCE MATERIALS

6.4.1 ICP-OES AND ICP-MS INSTRUMENT CONDITIONS

A Shimadzu ICPS-7510 sequential spectrometer and a Shimadzu ICPM-8500 quadrupole mass spectrometer were used for all ICP measurements. All standards were purchased as 1000 ppm solutions from Merck. These included a cobalt standard which was used as an internal standard.

Prior to use the ICPS-7510 was routinely checked to confirm that it was in good operating condition. The Tygon tubing was checked for elasticity before being mounted on the peristaltic pump. The nebuliser was confirmed to be creating a fine mist and the torch was checked for blockages. A wavelength (OES) or quadrupole (MS) calibration was performed regularly to ensure that the spectrometer was in proper alignment. Plasma conditions were used as tabulated in **Table 6-1**. Linearity and gradient of calibration curves was used as a guideline for confirming consistent instrument response and selectivity was evaluated using the y-intercept of the curve.

6.4.2 CALIBRATION STANDARDS

All working calibration standards for use with ICP instruments were made by dilution from 1000 ppm commercial standard solutions which were traceable to NIST standards. Volumes of between 0.1 and 2.0 mL where pipetted accurately into 100.0 mL volumetric flasks containing 5 mL 65% concentrated analytical grade nitric acid which were then made up to volume with double distilled water. This yielded standards with concentrations in the range of 1 to 20 ppm and all samples were diluted so as to fall within this working range. The formulae used for the calculation of the lower limits of detection and quantification can be found in the appendix (**Section 10.1)**.

As samples were initially analysed in a sulphuric acid matrix and later in a nitric acid matrix, lower limits of detection were determined for both. As can be seen in **Table 6-12** the lower limits of detection for the various elements were very similar despite the difference in matrix. Zirconium was the primary element of interest but

lower limits of detection of others were determined as these elements were deemed to be possible contaminants in the newly processed samples which are also to be analysed at a later stage (See **Section 7.5**). In one set of determinations, 2 ppm cobalt was used as an internal standard (see **Section 7.4.1.1**) and calibration results are seen in **Table 6-13**.

6.4.3 ICPS-7510 INSTRUMENT CALIBRATIONS AND LOWER LIMITS OF DETECTION

ICP-OES detection and quantification limits for various elements in appropriate matrices were determined to be as follows in **Table 6-12**, **Table 6-13**, **Table 6-14** and **Table 6-15**. A representative calibration curve can be seen in **Figure 6-17**. The instrument was re-calibrated before each analysis as flame conditions were not absolutely identical from day to day and small differences could result in large quantification errors.

Table 6-12: Details of zirconium and hafnium calibration curves for ICPS-7510 in 3.25% nitric acid and 9.8% sulphuric acid matrix

Element (Matrix)	*m* gradient	*y* intercept	R^2
Zr (3.25% HNO_3)	9.469	1.0844	0.9990
Zr (9.8% H_2SO_4)	8.2398	0.2271	1.0000
Hf (3.25% HNO_3)	0.3207	0.0041	0.9998
Hf (9.8% H_2SO_4)	0.3574	0.0061	1.0000

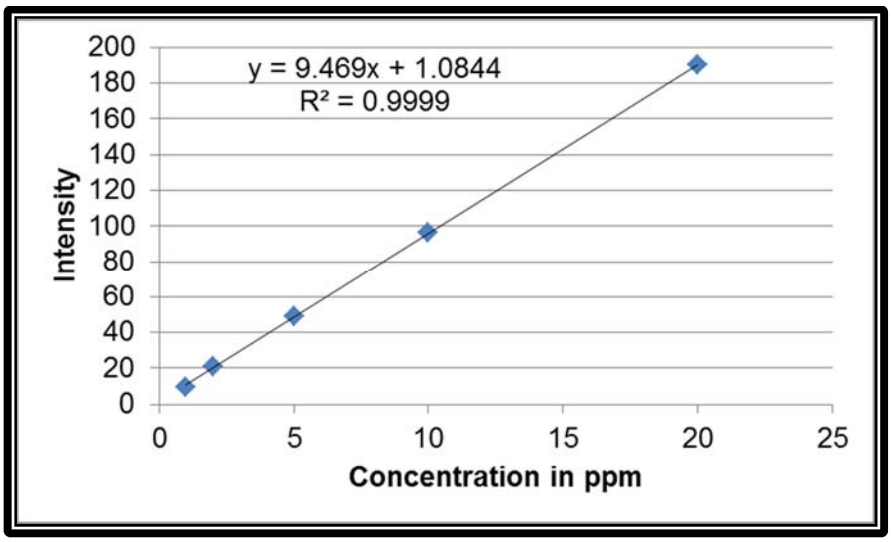

Figure 6-17: Representative ICP-OES zirconium calibration

Table 6-13: Details of zirconium and hafnium calibration curves for ICPS-7510 in 9.8% sulphuric acid matrix with a 2ppm cobalt internal standard

Element	Corrected using internal standard			Calculated from raw intensities		
	m gradient	*y* intercept	R^2	*m* gradient	*y* intercept	R^2
Zirconium	3.4957	0.8993	0.9965	9.8362	1.3246	0.9944
Hafnium	0.1518	0.032	0.998	0.4274	0.0815	0.9915

Table 6-14: Lower limits of detection of several elements in 9.8% sulphuric acid medium

Element	LLOD (ppm)	LLOQ (ppm)
Zr (343.823 nm)	0.001663	0.01663
Hf (277.336 nm)	0.001995	0.019951
Mg (279.553 nm)	0.000801	0.008008
Al (396.153 nm)	0.00297	0.029703
Ca (393.366 nm)	0.001172	0.011721
Cr (267.716 nm)	0.001635	0.016354
Fe (259.940 nm)	0.001094	0.010943

Table 6-15: Lower limits of detection of several elements in 3.25% nitric acid medium

Element	LLOD (ppm)	LLOQ (ppm)
Zr (343.823 nm)	0.001652	0.01652
Zr (339.198 nm)	0.001058	0.01058
Hf (277.336 nm)	0.005798	0.05798
Mg (279.553 nm)	0.000338	0.003378
Al (396.153 nm)	0.002838	0.028382
Ca (393.366 nm)	0.001333	0.013326
Cr (267.716 nm)	0.003095	0.030952
Fe (259.940 nm)	0.000916	0.009162

In all cases lower limits of detection (**Table 6-14** and **Table 6-15**) were found to be in line with those expected of an ICP-OES instrument [136]. A lower limit of detection of 5 ppb is considered normal for zirconium and 50 ppb for hafnium. These levels were exceeded by the values in **Table 6-15**. Calibration linearity (R^2) was less than 0.999 only in the case of calibration standards containing a cobalt internal standard (**Table 6-12** and **Table 6-13**) in their matrix. An internal standard is intended to improve results by compensating for matrix effects. The apparent matrix effect caused by the cobalt presence indicates that cobalt should only be used in the case of severe errors in analysis that cannot be compensated for by other methods. Stability of zirconium in solution was observed over several months by replacing diluted standard solutions individually as they ran out. No change in instrument response between new and old standards was observed, even when standard ages varied by months.

6.4.4 ICPM-8500 INSTRUMENT CALIBRATIONS AND LOWER LIMITS OF DETECTION

Similarly to the ICP-OES, the ICPM-8500 was confirmed to be in good working order by inspection prior to use. Where applicable the same procedures were followed as in **Section 6.4.1.** The mass spectrometer was calibrated using a solution containing 1 ppb each of lithium, indium and bismuth, as required by the calibration software.

Similarly to the ICP-OES results the calibration and lower limits of detection for the MS instrument were in line with those expected for an instrument of this type (0.1 ppb for both [136]). Linearity of the calibration curves (R^2) was acceptable with values in excess of 0.998 (**Table 6-16**). Lower limits of detection in the low parts-per-billion and high parts-per-trillion range are clearly seen in **Table 6-17**.

Table 6-16: Details of zirconium and hafnium calibration curves for ICPM-8500 in 3.25% nitric acid matrix

Element	*m* gradient	*y* intercept	R^2
Zr	311.51	211.64	0.9982
Hf	1028.4	481.32	0.9992

ICP-MS detection and quantification limits for various elements in appropriate matrices were determined to be as follows in **Table 6-17**.

Table 6-17: ICP-MS lower limits of detection and quantification

Element	LLOD (ppb)	LLOQ (ppb)
Zr	0.1473	1.473
Hf	0.02950	0.2950
Mg	0.41124	4.1124
Al	2.14651	21.4651

6.5. Results for ICP-OES Analysis of Crystals

Approximately 0.1 g of crystal sample was weighed accurately to 0.1 mg and transferred quantitatively to a 100.0 mL volumetric flask. 10 mL double distilled water and 5.00 mL analytical grade 65% nitric acid was added to the flask and the crystals were allowed to dissolve. Upon complete dissolution the flask was made up to volume with double distilled water. A 1.00 mL aliquot was transferred to a new 100.0 mL volumetric flask, a further 5.00 mL analytical grade 65% nitric acid was added and the solution was again made up to volume with double distilled water. This solution was then analysed for zirconium by ICP-OES at an emission wavelength of 343.823 nm on a Shimadzu ICPS-7510 sequential spectrometer.

ICP-OES analysis was performed on both the potassium and cesium hexafluorozirconate crystals with results seen in **Table 6-18**. A recovery of 101(1)% for the potassium complex and 100(2)% for the cesium analogue showed that the analytical method was capable of accurately analysing the zirconium content of these materials in this matrix. A Student's *t*-test performed on the data yielded a value of -1.4965 for the potassium complex and -0.1513 for the cesium complex, both of these being less than 4.30, the t_{crit} value at the 95% confidence level for 2 degrees of freedom. This indicates that the result obtained is not statistically different from a 100% recovery. The standard deviations of 1 and 3% for the zirconium recovery in the potassium and cesium crystals respectively were greater than hoped but within the upper range of the expected instrumental error. Samples of the crystals were sent to Pelindaba Analytical Labs (PAL), an ISO accredited analytical laboratory, for potassium, cesium and fluorine content determinations. The potassium was analysed by AAS and the cesium by ICP-MS. Recoveries for these elements were 100(2) and 96(2)% respectively, confirming their composition. The fluoride was analysed by ISE which yielded recoveries of 84.2 and 87.7% respectively with no error reported as only

a single analysis was performed for each compound. The similarly low recovery is likely due to incomplete dissociation of the fluoride from the ZrF_6^{2-} ion in solution. ISE requires that all fluoride ions be dissociated in solution for quantitative determination.

Table 6-18: ICP-OES results for hexafluoride crystals

Sample	% cation recovery	% fluoride recovery*	% zirconium recovery	Zirconium *t*-statistic (t_{crit} 95% = 4.3)
K_2ZrF_6	100(2)	84.2	101(1)	1.4965
Cs_2ZrF_6	96(2)	87.7	100(2)	-0.1513

*Samples analysed by Pelindaba Analytical Laboratories (PAL) by ICP-MS (Cs), Atomic Absorption Spectroscopy (K) and Ion Selective Electrode (F)

The process of preparing an in-house reference material by crystallisation and characterisation by crystallography and qualitative XRD appears to have been successful. The quantitative and reproducible recovery of the analyte of interest can be seen as validation of the analytical method developed and ensures traceability.

6.6. CONCLUSION

A complete elucidation of the crystal structure of the compounds produced in this section was of vital importance in confirming their composition. Their intended use as a reference material required that their exact chemical composition be known beyond any doubt.

As stated earlier in the chapter it is quite a challenge to grow perfect crystals. Considering this the fact that three of the nine cations used yielded crystals of sufficient quality to obtain a crystal structure was found to be quite acceptable. Unfortunately the growing of the tetraethylammonium crystals was found to be far more difficult than for the potassium and cesium ones. The former had a strong tendency to precipitate out rather than form crystals, making the production of crystals for ICP work unfeasible. Fortunately the potassium and cesium hexafluorozirconate crystals formed relatively easily.

Table 6-4 shows the crystal properties of the three crystals successfully characterised by X-ray crystallography and is followed by several tables and figures describing the structure, packing, bond lengths and bond angles of each crystal.

With the ease of production of the potassium complex as well as its amenability to simple, accurate analysis, it is an ideal complex to use as a reference for the zirconium compounds under investigation in the rest of this study. The cesium complex yielded a marginally better analytical result but is significantly more difficult to produce. Once the crystals were formed, however, sample preparation was no more difficult than that of the potassium complex. The positive results seen in **Table 6-18** indicate that the method used is capable of accurately and reproducibly analysing for zirconium in solution.

Chapter 7: ICP-OES and ICP-MS Assay Method Development and Experimental Results

7.1. INTRODUCTION

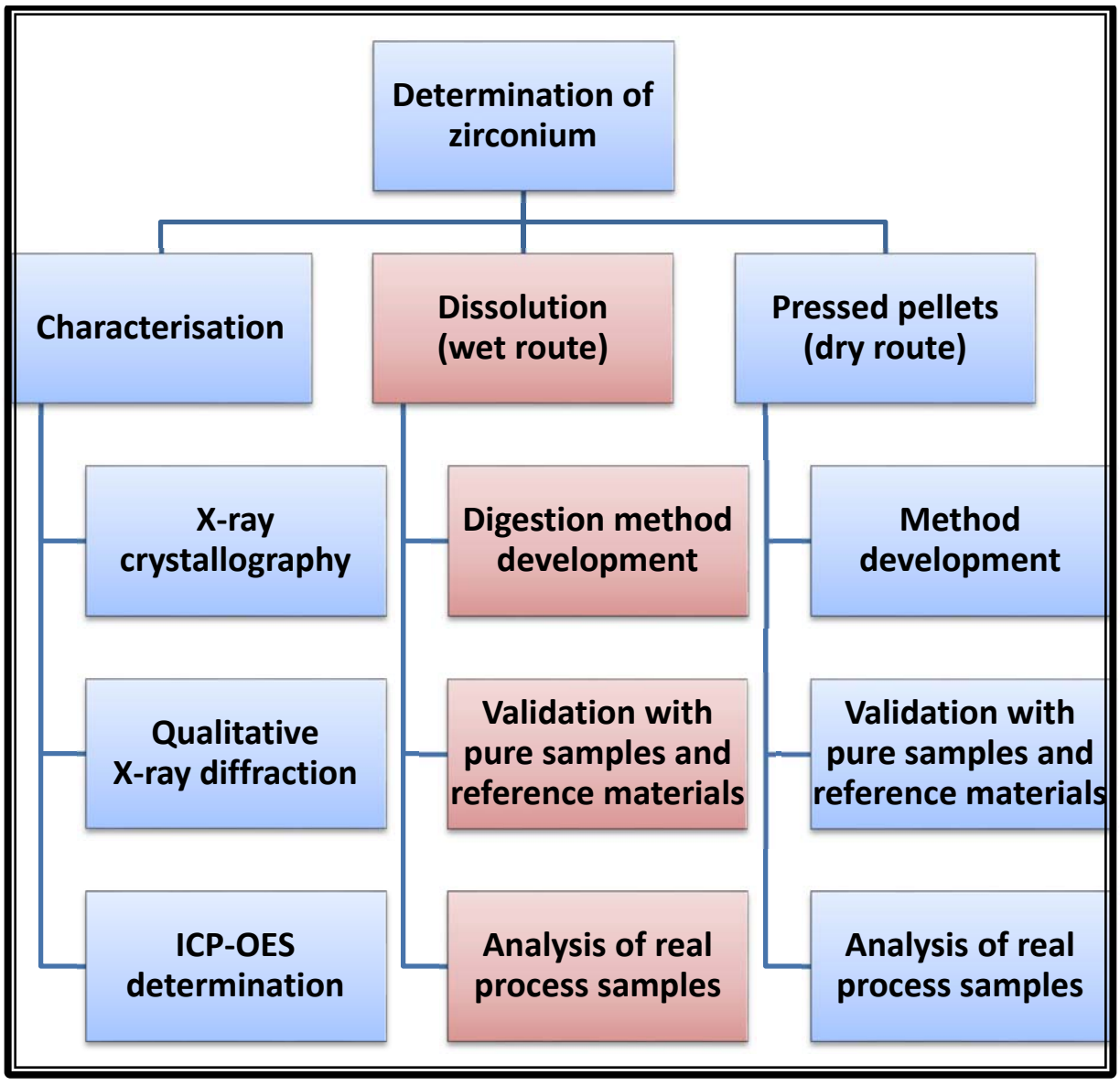

Figure 7-1: Experimental outlay with the dissolution and wet analysis of samples highlighted

As discussed in **Sections 1.2** and **1.3** the analysis of the intermediate and final products of the zirconium beneficiation chain is of vital importance. Of the many characteristics that make zirconium a useful material as fuel cladding in the nuclear industry, its resistance to chemical attack, and thus dissolution, is one of the most

important. Unfortunately this also makes analysis by methods requiring a dissolved sample extremely difficult. Several of the beneficiation products produced in the Necsa process shared this property with the metal and thus development of a dissolution procedure applicable to these materials was critical. Commercial metal samples as well as refractories such as zirconium carbide, nitride and hydride were used as test cases as these were possible products and contaminations of the beneficiation products. The nitride and carbide were the most important of these as nitrogen and carbon could be present during the refinement process, in the plasma and vacuum furnace respectively, as possible contaminants. Furthermore the presence of zirconium nitride and zirconium carbide in the metal has a very detrimental effect on the metallurgy of the final product.

Hafnium is a known contaminant which is always associated with naturally occurring zirconium ores [1]. Its chemical behaviour is almost identical to that of zirconium and as such a dissolution technique applicable to zirconium would undoubtedly be applicable to hafnium as well. Unfortunately many commercial zirconium materials describe their zirconium content as a mass percentage including a poorly specified quantity of hafnium. As such extremely pure zirconium materials, such as the 99.98% zirconium foil, were used to ensure quantitative results.

ICP-OES analysis was chosen as the primary analytical technique based on its large linear dynamic range, ability to scan through multiple characteristic wavelengths, and relatively rapid sample throughput rate. ICP-MS was used for comparison when available as it has a nearly identical sampling system but with a different detector. Detection and quantification of the element zirconium in multiple matrices was the primary focus of all instrumental work. When other elements were expected they were scanned for as well but method validation for every element was not a goal of this project. The section of the experimental outlay relevant to this section is highlighted in **Figure 7-1**.

7.2. General Procedures, Equipment and Reagents

All analyses were performed in triplicate unless otherwise stated. All results are reported to the number of significant figures allowed by the degree of error determined from the standard deviation. All volumes were measured using micro-pipettes which were calibrated monthly. Particular care was taken when working with acidic fluoride solutions such as hydrofluoric acid. Nitrile gloves and protective goggles were worn at

all times when handling the acid and all work requiring hydrofluoric acid was performed in a fume cupboard. Calcium gluconate gel was kept on hand at all times as a first aid measure in the event of an accident. After the completion of any work using hydrofluoric acid the area was checked thoroughly for any spills or droplets as they are visually indistinguishable from water.

A Shimadzu ICPS-7510 sequential spectrometer and a Shimadzu ICPM-8500 quadrupole mass spectrometer were used for all ICP measurements. An Anton Paar Multiwave 3000 microwave reaction system with XF-100 rotor and PTFE-lined pressure vessels was used for microwave-assisted acid digestion. A Mettler Toledo Thermal Analysis System TGA instrument was used for thermal gravimetric analyses. A Eutech CyberScan pH 1500 bench meter was used for pH determinations. All standards were purchased as 1000 ppm solutions from Merck. These included a cobalt standard which was used as an internal standard. Pure zirconium metal (zirconium rod, 99%, zirconium foil 99.98%), zirconium hydride (99%), zirconium carbide (99%) and zirconium nitride (99%) were purchased from Sigma Aldrich. Analytical grade glacial acetic acid, sodium acetate and disodium ethylenediaminetetraacetic acid were also purchased from Sigma Aldrich. SARM62 certified reference material was provided by Necsa and supplied by Industrial Analytical Ltd. A sample of Zircaloy 2, a product of Areva's trademarked range of Zircaloy™ zirconium alloys, was also provided by Necsa. All acids used (nitric, sulphuric and hydrofluoric) were of analytical grade. The $(NH_4)_3ZrF_7$ from PDZ, $(NH_4)_3ZrF_7$ from ZrO_2, $(NH_4)_2ZrF_6$ and several zirconium metal powders of varying degrees of purity were provided by Necsa as representative refinement products in the zirconium beneficiation process.

Raw experimental data can be found in the attached DVD.

7.3. REAGENT CHARACTERISATION

XRD scans were taken of the commercial materials used with a Bruker D8 Advance (**Table 6-11**) as references to confirm their composition. As can be seen in **Figure 7-2**, **Figure 7-3**, **Figure 7-4** and **Figure 7-5** the pure materials exhibit peaks matching their theoretical positions exactly, providing positive confirmation of the composition of the compounds.

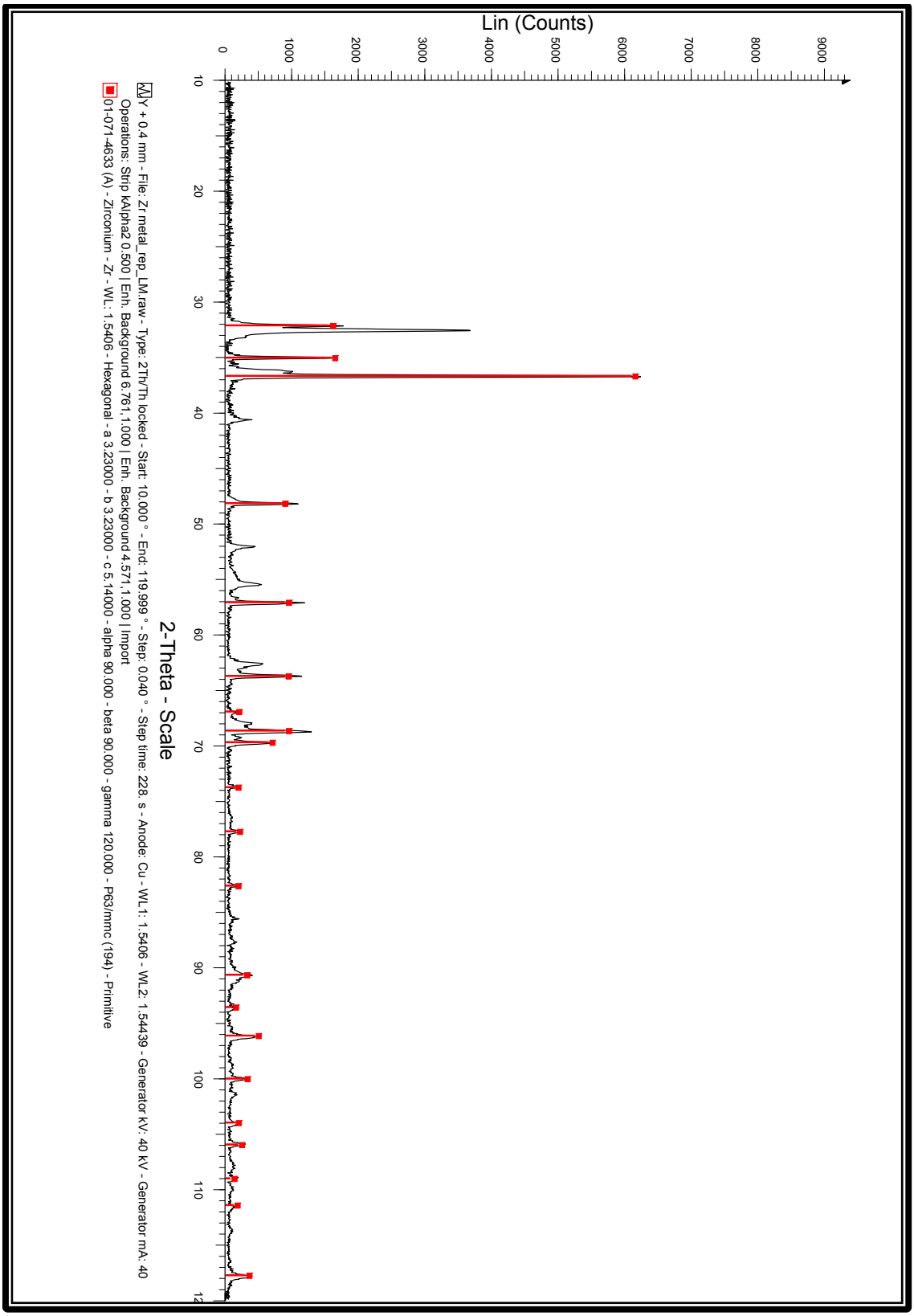

Figure 7-2: XRD spectrum of zirconium metal with theoretical lines for the metal, oxide, nitride and hydride superimposed

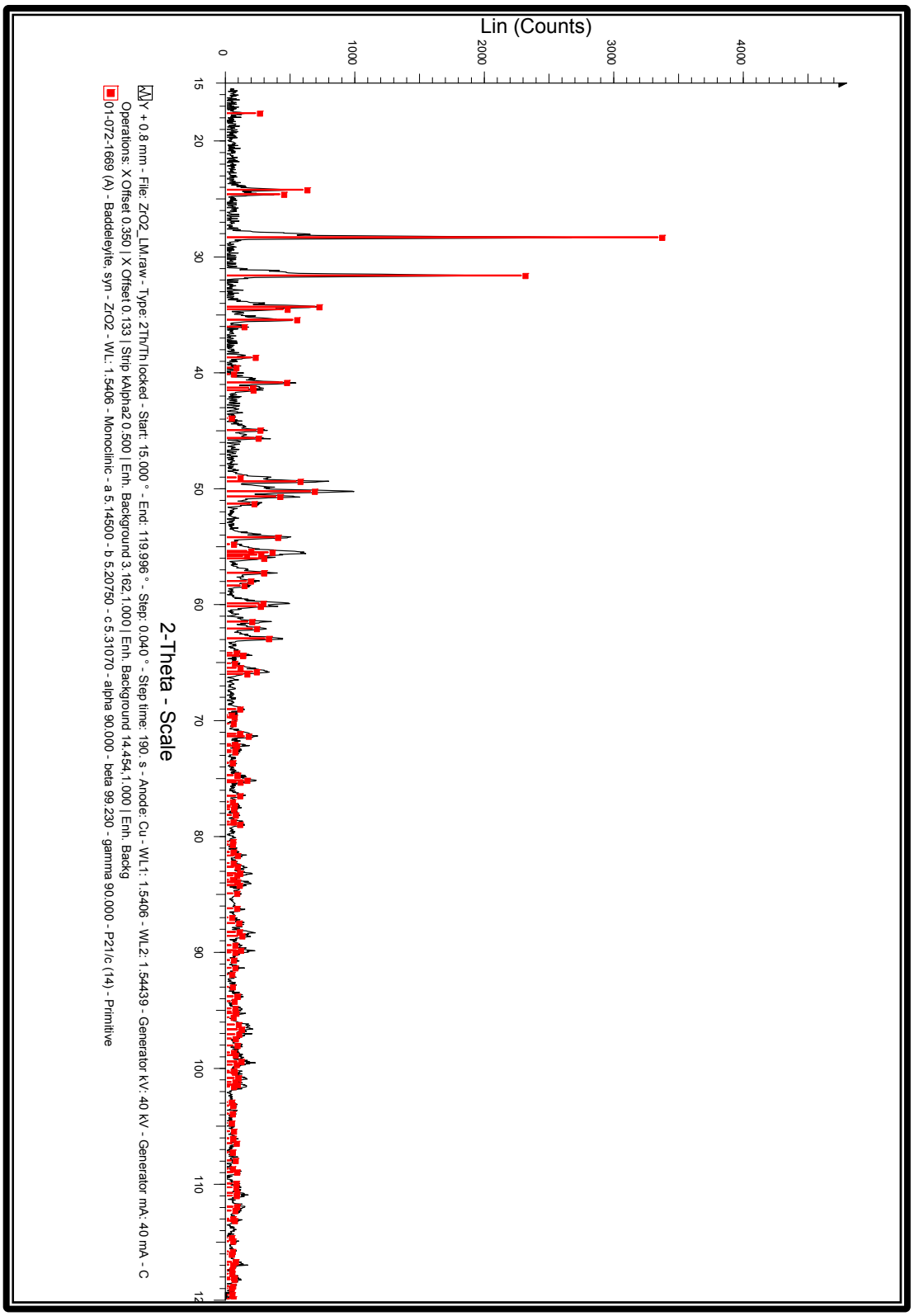

Figure 7-3: XRD spectrum of zirconium oxide with theoretical lines superimposed

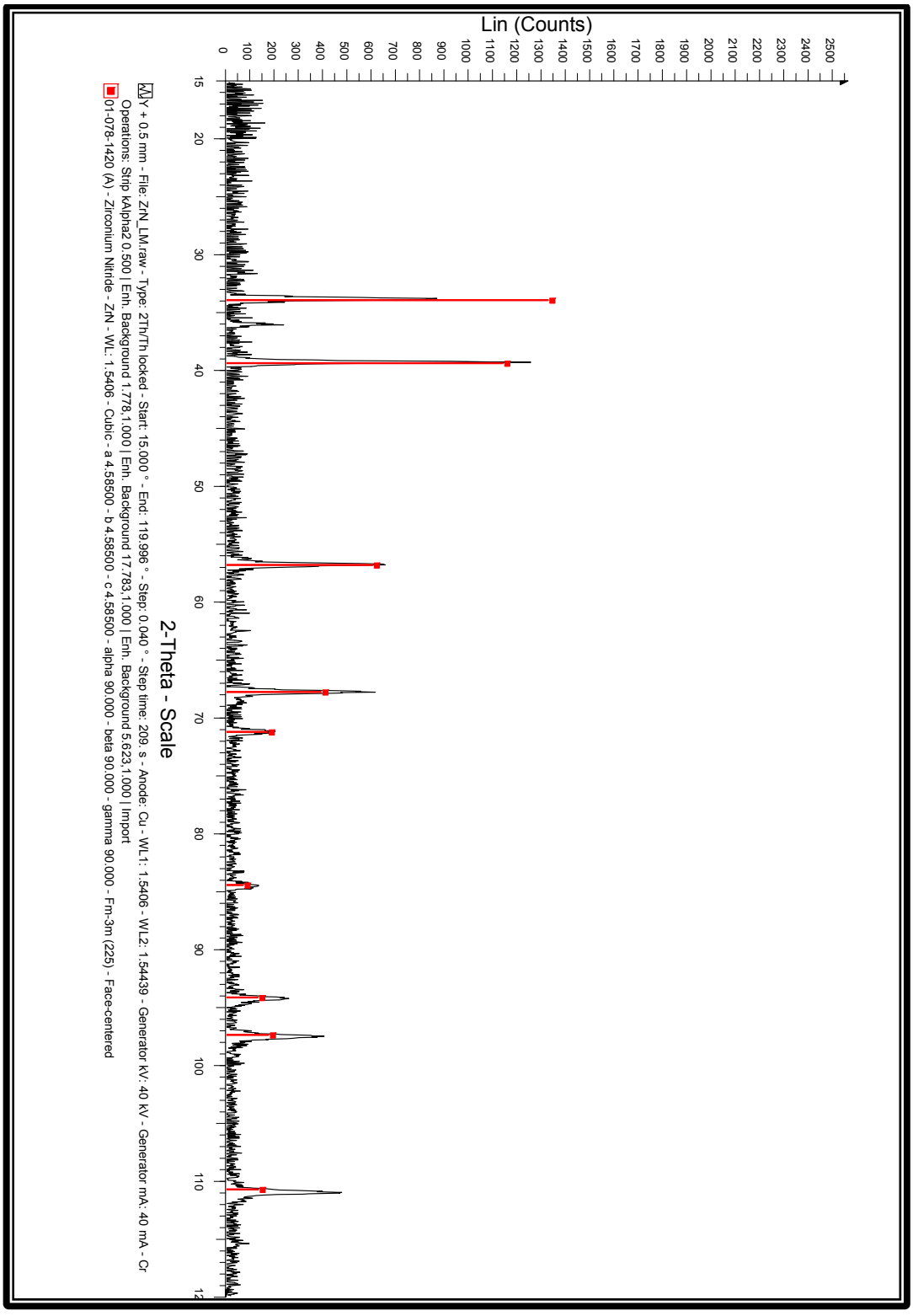

Figure 7-4: XRD spectrum of zirconium nitride with theoretical lines superimposed

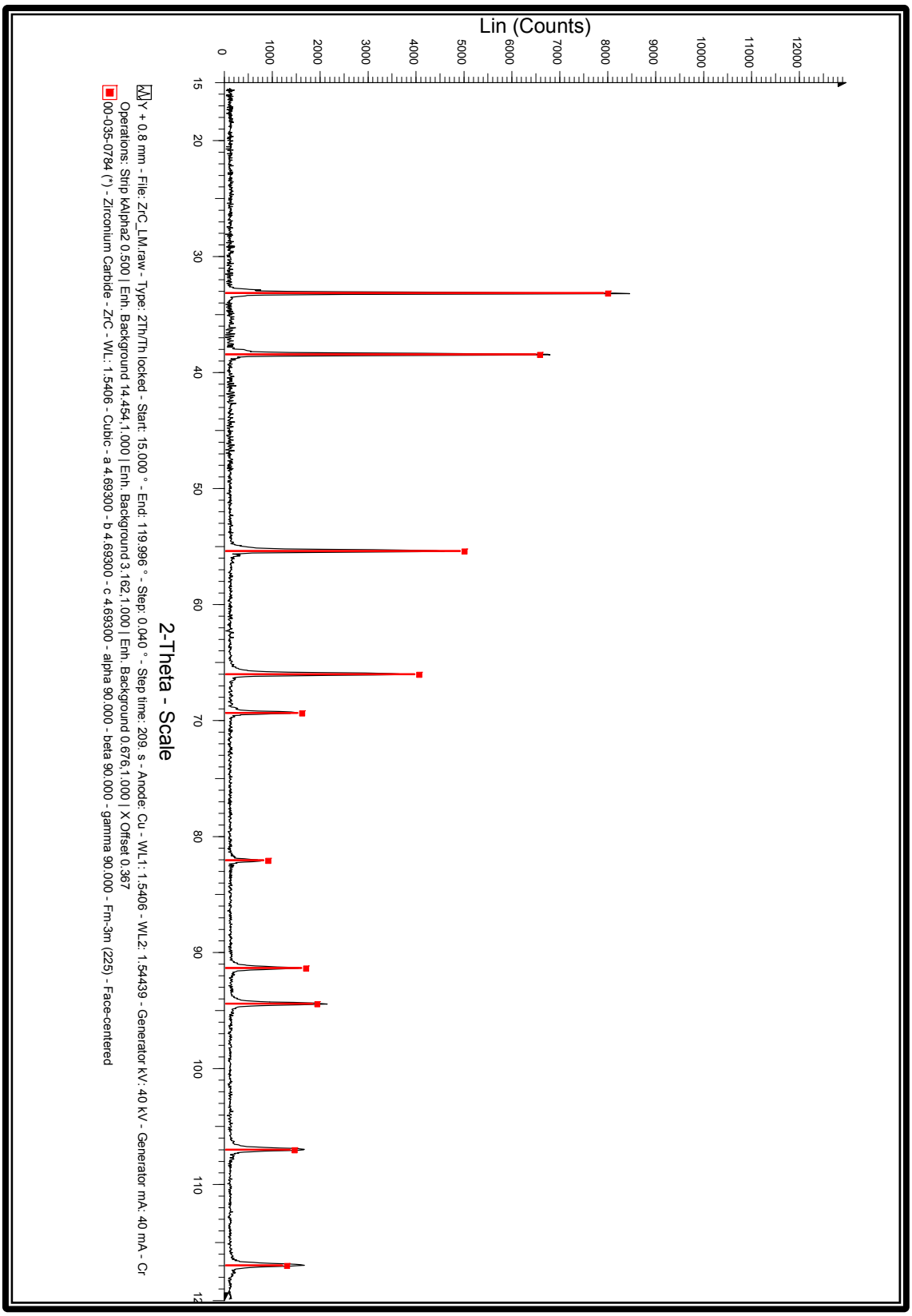

Figure 7-5: XRD spectrum of zirconium carbide with theoretical lines superimposed

7.4. SAMPLE PREPARATION AND METHOD DEVELOPMENT

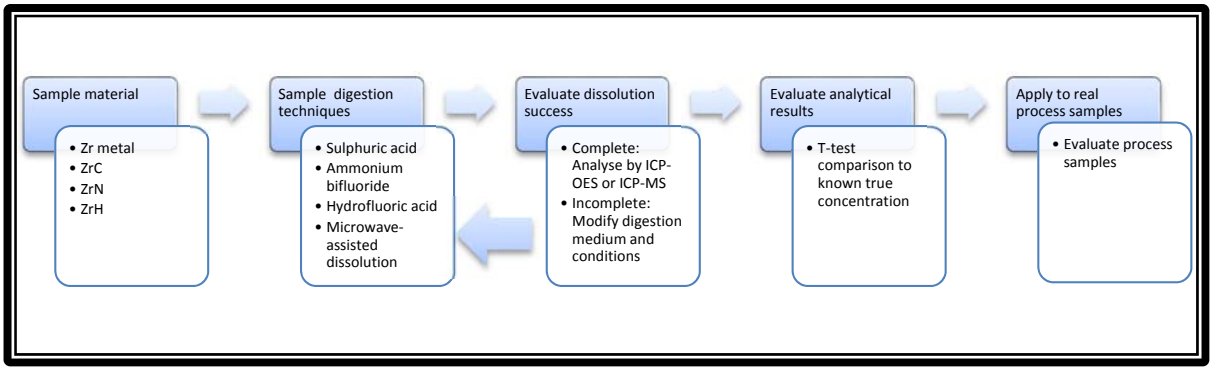

Figure 7-6: Outline of dissolution methodology

Figure 7-6 is a schematic outline of the dissolution process implemented in order to find a sample digestion medium capable of completely dissolving whichever sample was of interest. The detailed methods for digestion follow below.

7.4.1 DISSOLUTION OF ZIRCONIUM METAL

7.4.1.1 Initial sulphuric acid digestion of pure zirconium metal rod

Experimental

The zirconium rod was sectioned using an angle grinder. Approximately 0.1 g of metal rod sample was weighed off accurately to 0.1 mg and added to 10.0 mL 98% sulphuric acid. This was heated to just below boiling with stirring overnight. The solution contained a white precipitate after 18 hours of heating. This solution was allowed to cool and 5.0 mL distilled water was added. This dilution partially dissolved the white suspension and additional heating to the solution's boiling point with stirring yielded a completely translucent solution. This solution was again allowed to cool before being transferred to a volumetric flask whereupon it was diluted to 100.0 mL. A 2.00 mL aliquot of this solution was transferred to another volumetric flask containing 10.0 mL 98% sulphuric acid and again diluted to 100.0 mL. The first (undiluted) solution was designated Hafnium-Sample and used to analyse for hafnium (277.336 nm), while the second was designated Zirconium-Sample and used to analyse for zirconium (343.823 nm). A second, parallel set of samples and standards were prepared where 2 ppm cobalt was added in the final dilutions as an internal standard. These were designated Hafnium-Sample-Co and Zirconium-Sample-Co. The zirconium and hafnium recoveries are reported in **Table 7-1**. All samples were prepared and analysed in triplicate.

Table 7-1: Zirconium metal mass percentage recoveries of samples using initial sulphuric acid digestion

Samples	Zirconium/hafnium percentage recovery	*t* statistic*	*m (calibration gradient)*
Zirconium-Sample	103(2)	2.770	9.7065
Zirconium-Sample-Co	84(1)	-19.67	9.7065
Zirconium-Sample-Co with internal standard calibration	105(2)	5.677	3.4957
Hafnium-Sample	1.08(1)	10.24	0.4205
Hafnium-Sample-Co	0.92(3)	-3.969	0.4205
Hafnium-Sample-Co with internal standard calibration	1.13(2)	10.35	0.01520
Zirconium (99.98% metal foil)	98(3)	-1.013	8.338

**t* statistics were calculated based on the zirconium rod being 99% pure zirconium with the balance being hafnium. Analyses are for the zirconium rod unless otherwise stated.

Discussion

As can be seen from **Table 7-1** attempts to dissolve zirconium metal using sulphuric acid were successful despite the tendency of the hot sulphuric acid to “spit”, with a possible resultant loss of sample material. The white precipitate may have been a zirconium sulphate compound [137] but was not isolated for characterisation. Some zirconium sulphates are known to exhibit moderate solubility in water [138]. The first analyses, using both a direct analysis with an external calibration as well as a separate analysis using cobalt as an internal standard, yielded recoveries of 103(2), 84(1) and 105(2)% respectively. These results showed that the presence of this element in the matrix, even at 2ppm levels, was enough to significantly reduce the accuracy of the method. The use of cobalt was investigated here as it had been seen to be effective in previous analyses performed by external laboratories [21, p. 65]. In the mentioned analysis a flux fusion digestion method was employed to dissolve a zircon certified

reference material (SARM62) as well as a sample of PDZ. The internal analysis yielded a percentage recovery of 102(10)% for zirconium and 131(13)% for hafnium. By contrast the external analysis, which included a cobalt internal standard, yielded a recovery of 100.47 and 101.6% for zirconium and hafnium in the SARM62 respectively. No error was reported so the precision of the method is unknown. From these results the use of a cobalt internal standard was deemed worth investigating.

The Student's *t* test was applied to the experimental data in **Table 7-1** to determine the accuracy of the data collected as compared to a known value. At the 95% confidence level and 2 degrees of freedom (as samples were analysed in triplicate) the t_{crit} value is 4.30. For zirconium only the analysis performed without an internal standard present yielded a *t* statistic lower than this (t = 2.770), indicating that it is not statistically different from the true value. It seemed that, while the cobalt internal standard was effective in improving the analysis of the high salt content samples produced by the flux fusion method, it was not necessary and was in fact detrimental to the analysis of the current sample matrix. Hafnium results were included as it was the only other detectable element present and the result confirmed the composition of the metal sample, i.e. that it contained approximately one percent hafnium. While the *t* statistic value is large (10.24), indicating that the value is statistically different from the expected value of 1%, this value is near enough to the expected range to confirm sample composition. From these results it was concluded that little value was added using cobalt as an internal standard with this analysis. As an internal standard is generally of greater use when the matrix is more complicated and contains salts it was therefore only used in the rest of the study when a more complex matrix was encountered.

Subsequent dissolutions were performed using zirconium foil as it was of a higher purity (99.98% as opposed to 99%) and was far easier to work with. The cutting process was a possible source of contamination as an angle grinder was required whereas the zirconium foil could be cut to appropriate sizes with a clean pair of scissors. Due to the thickness of the rod it also took a significant amount of time to dissolve completely due to the small surface area to volume ratio. The rod was used in initial work primarily due to its availability.

7.4.1.2 Modified sulphuric acid digestion of pure zirconium metal foil

Experimental

Approximately 0.1 g of metal sample was cut from the foil sheet with clean scissors and weighed off accurately to 0.1 mg and **added 5 mL of distilled water** mixed with 10.0 mL 98% sulphuric acid. This was heated to just below boiling with stirring for **2 hours**. The solution contained a white precipitate upon completion. This solution was allowed to cool and **10.0 mL** distilled water was added. This caused the solution to clear rapidly. The solution was stirred until all sample had dissolved and was again allowed to cool and then diluted to 100.0 mL. 2.00 mL of this solution was added to another 10 mL 98% sulphuric acid and again diluted to 100.0 mL. The first solution was used to analyse for hafnium while the second was used to analyse for zirconium.

Discussion

The modified method using slightly diluted sulphuric acid as initial digestion medium was also successful with a recovery of 98(3)% and a *t* value of -1.013 (see **Table 7-1**). This indicated a slightly better agreement with the known value for the foil than the previous dissolution exhibited for the rod. The standard deviation was still fairly significant though. Hafnium results were below the lower limit of detection of the instrument. The minor modification of using slightly diluted sulphuric acid for the digestion reduced dissolution time by an order of magnitude. As hot sulphuric acid is mildly oxidising, this may be analogous to the reaction of concentrated nitric acid with iron metal [139] where the concentrated acid forms a passivation layer. If the passivation layer consisted of zirconium oxide then the slower dissolution of the white precipitate in the initial, undiluted acid may have been the dissolution of the oxide in addition to the zirconium sulphate. As zirconium oxide and zirconium sulphate are both white the two compounds would have been visually indistinguishable.

Ultimately the sulphuric acid route was deemed to be too time consuming due to the long digestion times associated with dissolution. As rapid digestion was a requirement an alternative dissolution route was sought.

7.4.1.3 Dissolution of zirconium metal foil by ammonium bifluoride solution

Experimental

Approximately 0.1 grams of zirconium metal foil was weighed off accurately to 0.1 mg in each replicate analysis. This was dissolved using four different quantities of 1.00 M ammonium bifluoride solution and water such that the dissolution media had a volume of 10 mL and concentrations of 0.005, 0.01, 0.10 and 1.00 M respectively. Any remaining solid was filtered off and the filtrate was then diluted to 100.0 mL in a volumetric flask. A 1.00 mL aliquot was then transferred to another 100.0 mL volumetric flask and again diluted to volume. This solution was then analysed.

Discussion

Initial results showed very poor consistency between analyses and low recovery for the lower concentration digestion solutions. In order to determine if the samples were stable a set of duplicate samples was analysed repeatedly over the course of 3 weeks to determine stability over time. The results can be seen in **Table 7-2** where a good recovery (103(7)%) is achieved using 1 M ammonium bifluoride solution on the day of sample preparation. Recovery decreases rapidly from the second day of analyses to approximately 92% and below. Samples with 0.10 M ammonium bifluoride and lower did not achieve complete dissolution and likewise exhibit poor stability. This decrease is clearly illustrated in **Figure 7-7**. No solid material was observed to form in the digestion vessel as in the case of the sulphuric acid digestion. There was also no defined trend in recoveries for the lower ammonium bifluoride concentration samples.

Table 7-2: Effect of varying ammonium bifluoride concentration and time

Day	**% zirconium recovery**				***m (calibration gradient)***
	0.005 M $NH_4F.HF$	0.01 M $NH_4F.HF$	0.10 M $NH_4F.HF$	1.00 M $NH_4F.HF$	
1	2.5(5)	2.87(9)	28(17)	103(7)	6.919
2	1.5(5)	3.1(1)	43(13)	91.6(4)	7.711
3	2.0(4)	3.9(2)	44(14)	91(2)	6.961
4	2.6(8)	3.7(2)	44(14)	92(3)	7.474
5	2.1(8)	3.2(2)	43(14)	88(3)	7.760
11	2.4(4)	4.1(1)	42(13)	87(2)	7.337
19	3(1)	4.09(5)	41(13)	85(2)	8.610

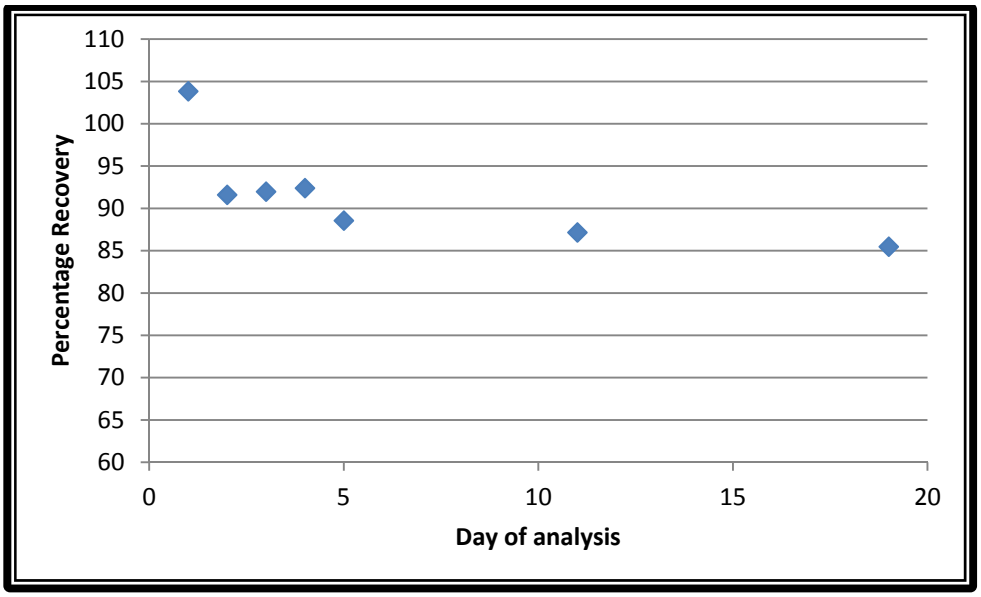

Figure 7-7: Zirconium recovery as a function of time for 1 M ammonium bifluoride digestion

In order to determine the cause of this instability, the same dissolution procedure was applied but with the addition of a complexing agent in the hopes that this would improve sample stability. An alternate zirconium characteristic emission wavelength [140] (339.198 nm) was also investigated in order to rule out spectral interferences. This second line exhibited greater sensitivity, had more known interferences but as no other cations were present in significant quantities this was not a problem at this point of the current study.

7.4.1.4 Dissolution of zirconium metal foil by ammonium bifluoride solution with EDTA as complexing agent and determination at different wavelengths

Experimental

Approximately 0.1 grams of zirconium metal foil was weighed off accurately to 0.1 mg in each replicate analysis. This was dissolved using 10.0 mL of a 1.00 M ammonium bifluoride solution. The solution was then diluted to 100.0 mL in a volumetric flask using pH 3 acetate buffer. A 1.00 mL aliquot was then transferred to another 100.0 mL volumetric flask and again diluted using pH 3 acetate buffer. This solution was then analysed. One set of replicate samples was prepared containing 0.02 M disodium ethylenediaminetetraacetic acid (EDTA) to determine the effect of a complexing agent on sample stability. The pH buffer was required to ensure that the correct pH was maintained for the complexing of zirconium by EDTA. The buffer was added to both sets of samples and standards in order to maintain matched matrices. The analysis

was also performed at both the 343.824 nm and 339.198 nm characteristic emission lines after being allowed to stand for 24 hrs.

Table 7-3: Results of benchtop digestion of zirconium foil using 1M $NH_4F.HF$ and EDTA in a pH 3 solution

Sample	Wavelength (nm)	Zirconium % recovery	*t* statistic	*m (calibration gradient)*
Zirconium foil	343.824	91.1(8)	-23.52	8.610
	339.198	99.2(9)	-2.015	7.012
Zirconium foil (0.02 M EDTA)	343.824	90(1)	-22.31	8.610
	339.198	99.5(3)	-1.275	7.012

Discussion

All samples analysed at the 343.824 nm wavelength (as seen performed in **Section 6.5**) yielded percentage recoveries of approximately 90% (see **Table 7-3**). This was unfortunate but not unexpected despite the modified sample matrix as it had been observed in the previous experiment (**Table 7-2**) after a similar standing time period. The results of both samples at the 339.198 nm wavelength yielded recoveries in the 99% range with *t* values of -2.015 (without EDTA) and -1.275 (with EDTA) respectively. These values indicate that both analyses successfully determined the quantity of zirconium present in solution. From this data it can be concluded that the presence of EDTA at this concentration level has no significant effect on the recovery of zirconium. The improvement seen due to altering the analytical wavelength implies that the ammonium bifluoride has an effect on the sample emission at what is normally the best analytical line, 343.824 nm. The effectiveness of dissolution with 1 M ammonium bifluoride also suggests the use of hydrofluoric acid as digesting medium. As such it was decided to attempt dissolution with simple hydrofluoric acid rather than the dissolved ammonium bifluoride. This would hopefully decrease dissolution time and avoid the introduction of the ammonium ion, a possible reason for the decrease in recovery at the 343.824 nm line. As the recovery was quantitative at the 339.198 nm wavelength the cause of the low recovery must have been spectral and unrelated to the sample introduction system. No literature could be found regarding spectral interference by fluorine, ammonia or nitrogen in this region in an argon plasma but

molecular nitrogen is known to have emission lines in the 325-384 nm region [141] in a nitrogen plasma, the closest one being at 337.13 nm. The formation of a molecular ion with an absorption wavelength in this region was also a possibility. If the removal of the ammonium ion failed to resolve this issue it would indicate that the fluoride ion or another as yet unknown factor was responsible for this effect.

7.4.1.5 Dissolution of zirconium metal foil by hydrofluoric acid

Experimental

Approximately 0.1 grams of zirconium metal foil was weighed off accurately to 0.1 mg in each replicate analysis. This was dissolved using 5.0 mL of 40% hydrofluoric acid was then diluted to 100.0 mL in a high density polyethylene (HDPE) volumetric flask. Dissolution was effectively immediate with the metal dissolving completely upon contact with the hydrofluoric acid. The total time of dissolution was less than 2 seconds. A 1.00 mL aliquot was then transferred to another 100.0 mL volumetric flask and again diluted to volume. This solution was then analysed by ICP-OES.

Discussion

Duplicate samples for this method yielded a zirconium recovery of 98(2)% at the 343.823 nm line and 96(2)% at the 339.198 line. A *t* test on the data yielded a value of -1.02 for the former and -2.77 for the latter indicating that both values were statistically the same as the true value of 99.98%. From these results it could be seen that the low recovery seen in **Table 7-3** using the 343.823 nm line was likely due to the presence of the ammonium ion in solution as no similar effect was observed at the same line in this case. Due to the speed and completeness of digestion and the accuracy of the result at the 343.823 nm line, hydrofluoric acid was judged to be suitable as dissolution medium for further analyses.

As discussed in **Section 4.2.1** hydrofluoric acid is primarily a complexing and secondarily an oxidising acid. This indicates that its ability to dissolve the zirconium metal likely derives from both its acidity and ability to donate fluoride ions. Safe handling of this highly toxic chemical is of the utmost importance (see **Section 7.2**).

7.4.2 HYDROFLUORIC ACID AS DIGESTION AGENT FOR DIFFERENT ZIRCONIUM-CONTAINING SAMPLES

7.4.2.1 *Initial benchtop dissolution of zirconium materials by hydrofluoric acid*

Experimental

Approximately 0.1 grams of sample (ZrH_2, ZrN, ZrC and Zircaloy 2) was weighed off accurately to 0.1 mg in each replicate analysis. This was rapidly dissolved using 5.0 mL of 48% hydrofluoric acid. This was then filtered (Zircaloy 2) diluted to 100.0 mL in a high density polyethylene (HDPE) volumetric flask. A 0.20 mL aliquot was then transferred to a 100.0 mL glass volumetric flask containing 5.0 mL nitric acid and again diluted to the mark. These solutions were then analysed using an external calibration curve set of at least 5 standard solutions between 1 and 5 ppm made using the same matrix as the samples. A detailed description of the preparation of standards can be found in **Section 6.4.1**.

Table 7-4: Various elemental recoveries of Zircaloy 2

Element	Zircaloy 2 specification (%)	Recovery (%)
Zirconium	Balance	94(5)
Tin	1.2 - 1.7	1.51(6)
Chromium	0.05 - 0.15	0.088(3)
Iron	0.07 - 0.20	0.166(7)
Nickel	0.03 – 0.08	0.0028(2)
Hafnium	0.0100	0.0066(2)
Total	-	96(5)

Discussion

The Zircaloy 2 results are tabulated in **Table 7-4**. The ZrH_2 and ZrN samples dissolved rapidly and yielded recoveries of 106(1) and 100(10)% respectively (**Table 7-5**). The ZrC was not significantly dissolved and the Zircaloy 2 required filtration. The Zircaloy 2 was expected to contain several alloying metals and these were determined concurrently with the zirconium. Despite the method not being optimised for these elements, recoveries in the expected ranges [142] was achieved for all the minor components (Cr, Fe, Ni, Sn). The hafnium content was approximately three times the

expected maximum [25] (0.01%) but this was analysed outside of the calibration range and is thus not reliable. The zirconium content of 94(5)% was lower than expected but the high standard deviation makes the accuracy of this determination dubious. This as well as the 6% over-recovery of the hydride and the 10% standard deviation of the nitride indicate that the method of dissolution and quantification was not yet ideal and needed refinement. Microwave digestion was thus investigated and the procedure and results can be seen in **Section 7.4.2.4.**

7.4.2.2 Refined benchtop dissolution of zirconium carbide and Zircaloy 2 by hydrofluoric acid

Experimental

Approximately 0.1 grams (weighed accurately to 0.1 mg) of sample (ZrC or Zircaloy 2) was used in each replicate analysis. **ZrC was subjected to heating at 500ºC in an alumina crucible for a period of not less than 24 hours, changing from a dark grey to white colour.** All samples were placed in **10.0 mL of hydrofluoric acid** in a 100.0 mL plastic (high density polyethylene) volumetric flask. The samples were then diluted to 100.0 mL. A 1.00 mL aliquot was then transferred to a glass 100.0 mL volumetric flask containing 5.0 mL nitric acid and again diluted to the mark. This solution was then analysed by ICP-OES using an external calibration curve set of at least 5 standard solutions between 1 and 50 ppm made using the same matrix as the samples.

Table 7-5: Zirconium percentage recoveries from zirconium hydride, nitride and carbide

Sample	Zirconium % recovery	*t* statistic	*m (calibration gradient)*
ZrH_2*	106(1)	9.63	2.934
ZrN*	100(10)	0.00718	2.934
ZrC**	108(1)	11.5	2.934
Zircaloy 2**	100.2(6)	3.836	3.633

*Initial method

**Refined method

Discussion

The result of this modification can be seen in **Table 7-5**. The increased quantity of hydrofluoric acid appeared to improve the recovery of the Zircaloy 2 significantly (100.2(6)%) with a standard deviation an order of magnitude better than seen in **Table 7-4**. It was found that prolonged heating in an oxygen-rich environment caused the zirconium carbide powder to change colour and become reactive towards hydrofluoric acid. This was thought likely to be due to conversion to zirconium oxide. A thermal gravimetric analysis was done in oxygen to determine if this was the case. The result can be seen in **Figure 7-8**, confirming this hypothesis. The increase in mass was consistent with the expected increase (19.36%) for a conversion from zirconium carbide (M_r 103.23) to zirconium oxide (M_r 123.218). The mass change peaked at approximately 22.15% but then steadily decreased to 21.24% and was still decreasing at the end of the analysis. Only 6 hours were made available for the experiment. Even though the results were over-recoveries of between 6 and 8% it was taken as a big step in the right direction. Another negative aspect of this procedure was that it required in excess of 24 hours of sample preparation time in order for complete oxidation to occur. The use of microwave heating in a pressure vessel was thus investigated as a means to solve both of these problems.

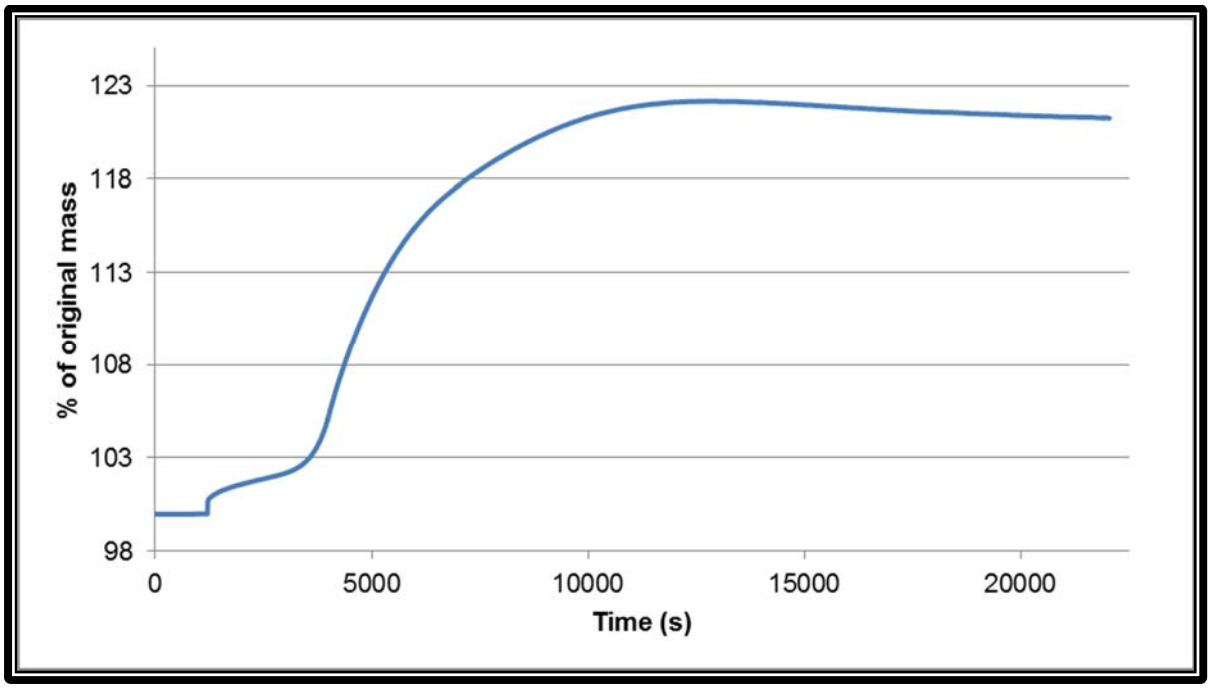

Figure 7-8: TGA graph of ZrC at 500°C in air showing mass increase consistent with conversion from ZrC to ZrO_2

7.4.2.3 *Initial microwave-assisted dissolution of Necsa zirconium metal powder by hydrofluoric acid*

Experimental

Approximately 0.1 grams of the sample was weighed off accurately to 0.1 mg and used in each replicate analysis. This was placed in 8.0 mL of hydrofluoric acid in the XF-100 rotor of the Anton Paar Multiwave 3000 microwave reaction system. The sample was then subjected to increasing digestion time intervals at 900 W of 2.45 GHz microwave energy. Pressure and temperature inside the vessels were limited at 60 Bar and 220ºC respectively. The samples were then filtered and diluted to 100.0 mL in a HDPE volumetric flask. A 0.20 mL aliquot was then transferred to a glass 100.0 mL volumetric flask containing 5.0 mL nitric acid and again diluted to the mark. This solution was then analysed using an external calibration curve set of at least 5 standard solutions between 1 and 5 ppm made using the same matrix as the samples.

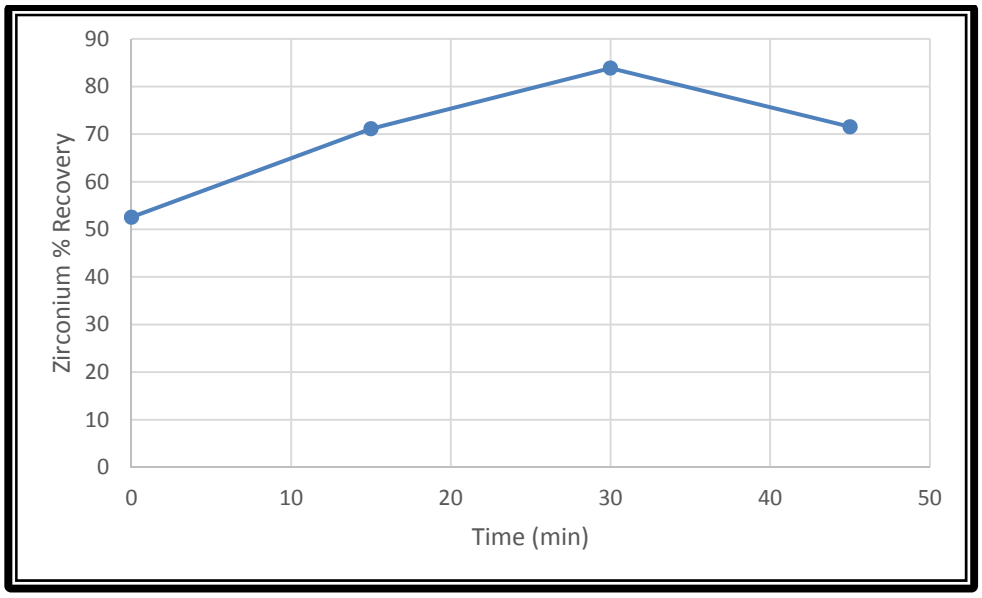

Figure 7-9: Effect of microwave heating on Necsa zirconium powder dissolution. Zero minute point indicates dissolution over 12 hours at benchtop conditions

Discussion

Similar to the zirconium carbide, the Necsa zirconium metal powder was found to be highly resistant to simple digestion by hydrofluoric acid. It was decided that microwave assistance might be useful. This was done in order to possibly bypass the long oven oxidation process. **Figure 7-9** shows the result of attempted dissolution by 48%

hydrofluoric acid for varying times under microwave irradiation. As the highest recovery was only 83.86% and complete sample dissolution was not achieved it was decided that the method required modification.

7.4.2.4 Modified microwave-assisted dissolution of zirconium metal foil and ceramics by hydrofluoric acid

Experimental

Between 0.05 and 0.3 grams (weighed accurately to 0.1 mg) of sample (zirconium metal foil, ZrC, ZrN and ZrH_2) was used in each replicate analysis. All samples were placed in PTFE microwave reaction vessels **8 mL of a mixture of hydrofluoric acid and nitric acid in a ratio of 7:1**. These were then microwaved at 600 Watts power for 45 (zirconium metal foil, ZrN and ZrH_2) and 105 (ZrC) minutes with a ramp time of 15 minutes in both cases. Pressure and temperature inside the vessels were limited at 60 Bar and 220ºC respectively. The samples were allowed to cool and transferred quantitatively to 100.0 mL plastic (high density polyethylene) volumetric flasks. No precipitate or remaining solid was observed. The samples were then diluted to 100.0 mL. A 5.0 mL aliquot was then transferred to a glass 100.0 mL volumetric flask containing 5.0 mL nitric acid and again diluted to the mark. This solution was then analysed by ICP-OES using an external calibration curve set of at least 5 standard solutions between 1 and 50 ppm made using the same matrix as the samples. For ICP-MS analysis the samples and standards were further diluted by a factor of 100 before analysis. The results can be seen in **Table 7-6**. The procedure for the preparation of these standards can be seen in **Section 6.4.1**.

Table 7-6: Zirconium percentage recoveries for ceramic and metallic samples using the modified microwave-assisted dissolution method

Sample	Zirconium percentage recovery*	*t* statistic	*m (calibration gradient)*	Zirconium percentage recovery on MS*	*t* statistic	*m (calibration gradient)*
Zirconium metal foil	102.0(9)%	3.837	3.633	99.9(8)%	-0.2623	13461
ZrN	100(10)	0.007182	3.633	-	-	-
ZrC	100(2)	0.3883	3.633	-	-	-
ZrH_2	101(3)	0.7734	3.633	-	-	-

* Percentage recoveries are reported based on the assumption that the sample used was a pure compound of known composition.

- The ICP-MS was unavailable due to instrument failure and could not be returned to operation within the time constraints of this study.

Discussion

The final dissolution procedure using hydrofluoric acid with microwave assistance was applied to a sample of zirconium foil. This method had been developed to provide rapid dissolution of all available zirconium-containing compounds with the exception of the mineral ore. The results can be seen in **Table 7-6**. Some of the samples were analysed with both ICP-OES and ICP-MS with results of 102.0(9) and 99.9(8)% respectively. The *t* statistic for both of these analyses was below the t_{crit} value indicating that both are accurate at the 95% confidence level.

The accuracy and precision of the results was found to be acceptable in all cases but that of the zirconium nitride, which showed a fairly large standard deviation. The error in the other analyses was in line with what is expected from instrumental error with the error being on the third or fourth significant figure. Very little literature is available on the dissolution and determination of zirconium in zirconium carbides, nitrides and hydrides. Dissolution and determination of trace elements in zirconium carbide and nitride [143] has been reported but the bulk zirconium content was not determined directly. The determination of zirconium carbide in a metallic glass matrix [144] after separation yielded excellent precision (RSD = 0.07%) but dissolution was required by two separate processes and 106% recovery was reported. This serves to illustrate the difficulty involved in this type of analysis and, with this in mind, the results were deemed on the whole to be good enough to accept the method.

7.5. ANALYSIS OF NECSA PLANT SAMPLES

7.5.1 SAMPLE HISTORY

All real samples analysed in this project were produced at Necsa. Several processes were envisioned for the beneficiation of zircon ore to nuclear grade zirconium metal. As discussed in previous chapters the purification of zirconium is a difficult and expensive process and the development of novel methods of refinement is thus desirable.

The first stage of the beneficiation was a plasma dissociation process [21] wherein the crystal structure of raw zircon was destroyed by rapid heating in a high temperature plasma. The material was subsequently rapidly cooled so as to ensure that the silica formed into an amorphous mass rather than returning to the zircon crystal structure. This drastically improved the material's amenability to chemical modification [16].

SARM62 is a zircon certified reference material used for comparison with the Plasma Dissociated Zircon (PDZ) produced in this process.

As part of the study at Necsa ammonium bifluoride [16], amongst other fluorinating compounds, was reacted with the PDZ, as well as pure ZrO_2 for comparison, to form ammonium hexa- and heptafluorozirconates ($(NH_4)_2ZrF_6$ and $(NH_4)_3ZrF_7$). This was done in order to convert the zirconium in the PDZ into a more soluble form for further processing. These complexes were then converted to $ZrCl_4$, first by thermal decomposition to ZrF_4 and then by a proprietary process to $ZrCl_4$. The newly produced $ZrCl_4$ was then used as starting material in the production of the Zr metal in the plasma reactor as indicated in **Figure 7-10**.

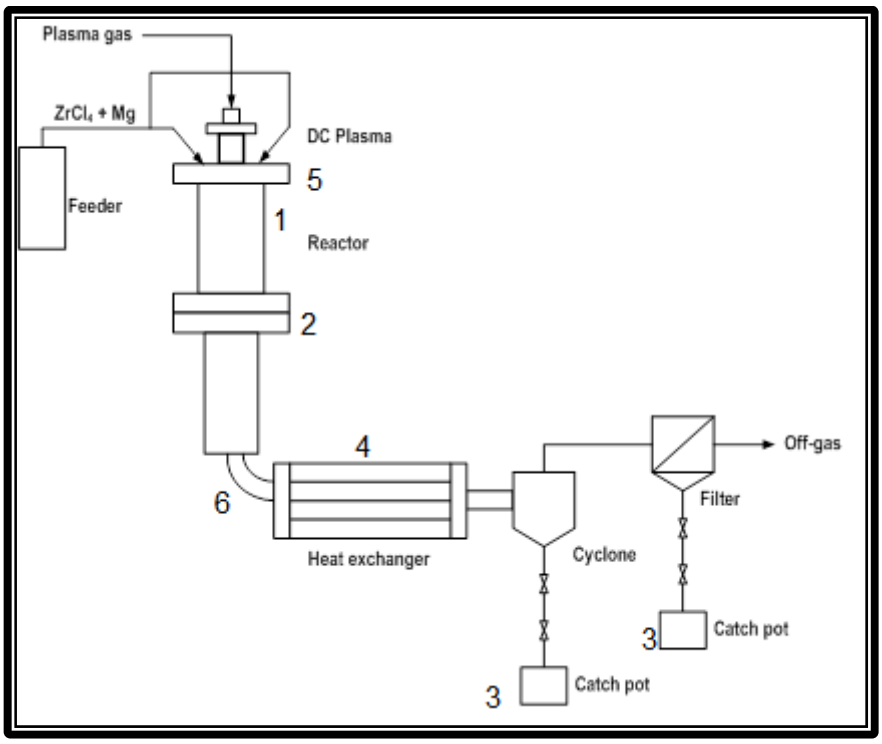

Figure 7-10: Schematic representation of the plasma pilot reactor for the production of zirconium metal [145]

The whole process for the production of zirconium metal can be seen in **Figure 7-10** where zirconium tetrachloride is reacted with magnesium metal as per the Kroll process. An intimate mixture of the two reactants was fed slowly into a nitrogen DC plasma. A mixture of zirconium metal and magnesium chloride was recovered from the catch pot (3 in **Figure 7-10**). Initially magnesium chloride was removed from early batches of newly formed zirconium powder by leaching with 65% nitric acid and washing with water. This process yielded the unwashed zirconium and washed

zirconium samples seen in **Section 7.5.2.5**. Later batches were purified in a vacuum arc furnace at temperatures in excess of 1600˚C. At these temperatures the magnesium chloride sublimated, ideally leaving behind only pure zirconium metal powder. Other samples labelled Reactor Wall (1), Reactor Interface (2), Catch Pot (3), Heat Exchanger (4), Reactor Head (5) and Reactor Bottom Valve (6) were recovered from the corresponding sections inside the reactor. Analytical results for these materials are seen in **Table 7-12.**

Other samples such as $ZrAl_3$ and zirconium sponge were legacy samples, part of previous studies performed at Necsa that were made available as references. Commercial samples zirconium foil (99%), zirconium hydride, zirconium carbide, zirconium nitride and Zircaloy 2 were also used as reference materials.

7.5.2 RESULTS FOR PROCESS SAMPLES

Analysis of the Necsa process samples was performed using applicable procedures as developed in **Section 7.4**.

7.5.2.1 Initial sulphuric acid digestion of zirconium applied to salts from the ammonium bifluoride dissolution of PDZ

Experimental

Approximately 0.1 g of sample ($(NH_4)_3ZrF_7$ from ZrO_2, $(NH_4)_3ZrF_7$ from PDZ and $(NH_4)_2ZrF_6$) was weighed off accurately to 0.1 mg and added to 10.0 mL 98% sulphuric acid. This was heated vigorously with stirring overnight. The solution contained a white precipitate after 18 hours of heating. This solution was allowed to cool and 5.0 mL distilled water was added. This dilution partially dissolved the white suspension and additional heating to the solution's boiling point with stirring yielded a completely translucent solution. This solution was again allowed to cool before being transferred to a volumetric flask whereupon it was diluted to 100.0 mL. A 2.00 mL aliquot of this solution was transferred to another volumetric flask containing 10 mL 98% sulphuric acid and again diluted to 100.0 mL. 2 ppm cobalt was added in the final dilutions as an internal standard. The first solution was used to analyse for hafnium while the second was used to analyse for zirconium.

Table 7-7: Zirconium salt mass percentage recoveries of samples using initial sulphuric acid digestion

Sample	Uncorrected zirconium percentage recovery with IS*	Corrected zirconium percentage recovery with IS*	Uncorrected hafnium percentage content with IS*	Corrected hafnium percentage content with IS*
$(NH_4)_3ZrF_7$ from ZrO_2	81(1)	105(1)	0.575(3)	0.74(3)
$(NH_4)_3ZrF_7$ from PDZ	30(2)	39.4(6)	0.2130(6)	0.280(2)
$(NH_4)_2ZrF_6$	69.5(6)	90.5(7)	0.520(3)	0.670(6)

* IS = Internal Standard

Discussion

The sulphuric acid dissolution method using cobalt as an internal standard was used in the case of the Necsa ammonium fluorozirconate products as they were expected to be soluble by this method, avoiding the use of hydrofluoric acid. The cobalt standard was used as the dissolved products were expected to contain ammonium fluoride and ammonium sulphate, salts which had the potential to affect the analytical recovery. The samples were process products which may still have contained significant quantities of their starting materials such as ZrO_2. As no solid residue was observed after dissolution it was evident that at least no silica remained in the sample prepared from PDZ.

Similarly to the results seen in **Section 7.4.1.1**, there were significant differences between the recoveries obtained using the internal standard method (**Table 7-7**) when calculated with and without the internal standard correction. As the corrected value was seen to be closer to the true value in the earlier analyses, that was taken to be the case here as well. The lower recoveries seen without the correction may also have been due to the ammonium salts in solution. The over-recovery of approximately 5% from the $(NH_4)_3ZrF_7$ from ZrO_2 sample may have been due to the presence of residual ZrO_2 present in the sample. In the case of the $(NH_4)_3ZrF_7$ from PDZ sample only 39.4(6)% of the expected zirconium content was recovered. This may again have been due to residual ZrO_2 in the sample but ammonium fluorosilicate ($(NH_4)_xSiF_{4+x}$), a product of the silica in the PDZ, may also have been present and would have decreased the zirconium recovery. Ammonium fluorosilicate is soluble [146] up to 250 g/L and would easily have dissolved in the digestion medium. The sample simply

labelled $(NH_4)_2ZrF_6$ yielded a zirconium recovery of 90.5(7)%. This was a decomposition product produced by heating of $(NH_4)_3ZrF_7$ and may thus also still have contained residual starting material. The hafnium contents were lower than those seen for the zirconium rod in **Section 7.4.1.1** but still within the calibration range at 0.74(3), 0.280(2) and 0.670(6)% for the $(NH_4)_3ZrF_7$ from ZrO_2, $(NH_4)_3ZrF_7$ from PDZ and $(NH_4)_2ZrF_6$ respectively.

7.5.2.2 Modified sulphuric acid digestion of Necsa zirconium metal samples

Experimental

Approximately 0.1 g of sample (washed Necsa zirconium metal powder and unwashed Necsa zirconium metal powder) was weighed accurately to 0.1 mg and **5 mL of distilled water** mixed with 10.0 mL 98% sulphuric acid was added. This was vigorously heated with stirring for **2 hours**. The solution contained a white precipitate and grey solid upon completion. This solution was allowed to cool and **10.0 mL** distilled water was added. This caused the white precipitate to clear rapidly. The solution was stirred until all sample had dissolved and was again allowed to cool, filtered and then diluted to 100.0 mL. 2.00 mL of this solution was added to another 10.0 mL 98% sulphuric acid and again diluted to 100.0 mL. This solution was analysed for zirconium.

Table 7-8: Zirconium metal mass percentage recoveries of samples using modified sulphuric acid digestion

Sample	Zirconium mass percentage
Necsa unwashed zirconium metal powder	11(7)
Necsa washed zirconium metal powder	34(5)

Discussion

As the washed and unwashed Necsa zirconium metal powders were expected to be a mixture of zirconium metal, unreacted magnesium metal and magnesium chloride (see **Section 7.5.1**) dissolution by sulphuric acid to avoid hydrofluoric acid again seemed feasible. In this case the cobalt internal standard was not used as there was not expected to be a significant salt concentration.

The low zirconium recoveries found in **Table 7-8** are likely due to both incomplete digestion of insoluble zirconium compounds by the sulphuric acid as well as residual magnesium metal and magnesium chloride left over from the plasma reduction

process. As the magnesium metal was added in excess only this and the magnesium chloride product were possible contaminants in the sample. As the washed metal yielded a higher recovery (34(5) versus 11(7)%), it can be surmised that the washing process did in fact remove a large amount of the magnesium chloride. The recovery was very low regardless, and the standard deviations were high indicating that the sulphuric acid digestion method was not very successful in the dissolution and determination of these samples.

7.5.2.3 Dissolution of legacy zirconium metals and alloys by hydrofluoric acid and analysis for major and minor components

Experimental

Between 0.25 and 0.60 g of metallic sample ($ZrAl_3$ and zirconium sponge) was weighed off accurately to 0.1 mg in each replicate analysis. This was dissolved using 5.0 mL of 40% hydrofluoric acid. The filtrate was then diluted to 100.0 mL in a high density polyethylene (HDPE) volumetric flask. A 1.00 mL aliquot was then transferred to another 100.0 mL volumetric flask and again diluted to volume. This solution was then analysed.

Table 7-9: Various elemental recoveries of legacy $ZrAl_3$

	Mass percentage					Mass balance
Sample mass (g)	Cr	Fe	Ni	Al	Zr	
0.2592	0.0213	0.203	0.0158	41.757	58.550	100.55
0.2599	0.00606	0.430	0.00922	47.746	52.022	100.21
0.3166	0.0277	0.201	0.0217	44.921	55.636	100.81
Average	**0.0183**	**0.278**	**0.0156**	**44.808**	**55.403**	**100.52**
Standard deviation	**0.0111**	**0.131**	**0.00626**	**2.996**	**3.270**	**0.298**

Table 7-10: Various elemental recoveries of legacy zirconium sponge

	Mass percentage					Mass balance
Sample mass (g)	Cr	Fe	Ni	Al	Zr	
0.2592	0.0152	0.0705	0.00678	49.689	54.273	104.055
0.2599	0.00250	0.0502	0.00936	48.277	51.827	100.166
0.3166	0.00336	0.0280	0.00883	45.080	55.161	100.281
Average	**0.00702**	**0.0496**	**0.00833**	**47.682**	**53.754**	**101.50**
Standard deviation	**0.00708**	**0.0213**	**0.00136**	**2.362**	**1.727**	**2.212**

Discussion

Two metallic samples provided by Necsa that were not a part of the beneficiation project were analysed. These materials were samples of a previous production process [147] of which there is still a substantial quantity of product present at Necsa. They were manufactured by an aluminothermic reduction process circa 1982 but did not fulfil the specifications for nuclear grade zirconium. As these samples have been stored for over 30 years it was important to determine if the current analytical method would be useful in the identification and quantification of the composition of these compounds. The results can be seen in **Table 7-9** and **Table 7-10**. In these tables the percentage recovery of each element was combined in a mass balance to get an idea of the degree of accuracy. The $ZrAl_3$ material yielded an excellent average mass balance of 100.5(3)%. However the standard deviation on the major components, zirconium and aluminium, was significant. This may be due to the sample lacking homogeneity. The zirconium sponge yielded almost as good a mass balance (101(2)%) and again had a rather large standards deviation. The surprise was that where zirconium sponge is expected to be pure zirconium this sample appeared to have an almost identical chemical composition to the $ZrAl_3$ (48(2)% aluminium). This may be due to mislabelling of the sample before it was stored, or an ineffective separation process. As the samples are not part of the current process the cause for this remains unknown. This unexpected recovery confirms the need for analysis of these legacy products.

7.5.2.4 Refined benchtop dissolution of zirconium materials by hydrofluoric acid

Experimental

Approximately 0.1 grams (weighed accurately to 0.1 mg) of sample (zirconium sponge, $ZrAl_3$, Necsa zirconium metal powder and several ammonium fluorozirconates) was used in each replicate analysis. **ZrC and Necsa Zr powder were subjected to heating at 500ºC in an alumina crucible for a period of not less than 24 hours, changing from a dark grey to white colour.** All samples were placed in 10.0 mL of hydrofluoric acid in a 100.0 mL plastic (high density polyethylene) volumetric flask. The samples were then diluted to 100.0 mL. A 1.00 mL aliquot was then transferred to a glass 100.0 mL volumetric flask containing 5.0 mL nitric acid and again diluted to the mark. This solution was then analysed by ICP-OES using an external calibration curve

set of at least 5 standard solutions between 1 and 50 ppm made using the same matrix as the samples.

Table 7-11: Zirconium percentage recoveries for metallic and fluoride-containing samples

Sample	Zirconium percentage recovery on ICP-OES*	Zirconium percentage recovery on ICP-MS*
Zirconium sponge**	95.4(3)	94(2)%
$ZrAl_3$	102(1)%	99.4(3)%
Necsa zirconium metal powder	98(1)	113(2)
Necsa $(NH_4)_3ZrF_7$ from ZrO_2	92.0(2)	106(1)%
Necsa $(NH_4)_3ZrF_7$ from PDZ	32.3(5)	34.3(5)%
Crystalline $(NH_4)_3ZrF_7$	95(1)	103(1)
Necsa $(NH_4)_2ZrF_6$	81(2)	85(3)%
Crystalline $(NH_4)_2ZrF_6$	90.1(4)	89(7)

* Percentage recoveries are reported based on the theoretical mass percentage of zirconium in the sample.

** Zirconium sponge recovery percentage calculated as though it were $ZrAl_3$ due to its high aluminium content.

Discussion

As the method outlined in **Section 7.4.2.2** yielded excellent results for the Zircaloy 2 alloy, the Zirconium Sponge, $ZrAl_3$ and Necsa zirconium metal powder samples were analysed by this method as well. The Necsa zirconium metal powder proved to be resistant to direct hydrofluoric acid attack and was thus treated in the same manner as the ZrC sample. **Table 7-11** shows zirconium percentage recoveries for the sponge, $ZrAl_3$, and Necsa zirconium metal powder after dissolution by hydrofluoric acid on both ICP-OES and ICP-MS. The zirconium sponge showed a lower than expected recovery (95.4(3)%) but very high precision. However the composition of this sample is suspect and without knowing its history no further conclusions can be drawn. The recoveries on ICP-OES for the other metallic samples were extremely encouraging with $ZrAl_3$ and

the Necsa zirconium metal powder yielding 102(1) and 98(1)% recoveries respectively. The results on MS were significantly more erratic. With results ranging between 89(2) and 113(2)%, the ICP-MS data appeared far less reliable. As the MS is an instrument designed for ultra-trace level analysis, it is not surprising that it is not ideal for the measurement of bulk materials.

A comparison was also performed between ICP-OES and ICP-MS results using the Necsa ammonium hexa- and heptafluorozirconate materials as well as several crystalline samples of similar constitution. As was seen in **Section 6.5** this instrumental method is very accurate for this type of sample. As such it can be seen in **Table 7-11** that the recovery values for these compounds are very similar, but slightly lower than those determined in **Table 7-7**. The Necsa $(NH_4)_3ZrF_7$ from PDZ was determined to contain 32.3(5)% of the expected zirconium content as opposed to 39.4(6)% as determined after dissolution by sulphuric acid. The $(NH_4)_3ZrF_7$ from ZrO_2 sample yielded a recovery of 92.0(2)% of the expected value compared to the 105(1)% determined using the sulphuric acid method. As both methods achieved complete dissolution and the calibration standards were matched to the sample matrices the only difference between the analyses was the presence of cobalt as an internal standard in the sulphuric acid matrix samples. This may indicate that the presence of cobalt alone had a deleterious effect on the analysis of zirconium. The ICP-MS results appear to be in line with several of the ICP-OES results but from previous work it is known that these results are very erratic.

7.5.2.5 Modified microwave-assisted dissolution of zirconium metal products obtained from different positions/places in the reactor by hydrofluoric acid

Experimental

Between 0.05 and 0.3 grams (weighed accurately to 0.1 mg) of sample (Washed Zr, Catch Pot, Reactor Wall, Reactor Interface, Unwashed Zr, Reactor Head, Heat Exchanger, Reactor Bottom Valve, Reactor Wall A, Reactor Wall B and Reactor Wall C) was used in each replicate analysis. All samples were placed in PTFE microwave reaction vessels with **8.0 mL of a mixture of hydrofluoric acid and nitric acid with a ratio of 7:1**. These were then microwaved at 600 Watts power for 105 minutes with a ramp time of 15 minutes. Pressure and temperature inside the vessels were limited at 60 Bar and 220ºC respectively. The samples were allowed to cool and transferred qualitatively to 100.0 mL plastic (high density polyethylene)

volumetric flasks. The samples were then diluted to 100.0 mL. A 5.00 mL aliquot was then transferred to a glass 100.0 mL volumetric flask containing 5 mL nitric acid and again diluted to the mark. This solution was then analysed by ICP-OES using an external calibration curve set of at least 5 standard solutions between 1 and 50 ppm made using the same matrix as the samples. For ICP-MS analysis the samples and standards were further diluted by a factor of 100 before analysis.

Table 7-12: Digestion of process samples from Necsa

Sample	Recovery point in reactor	Zirconium mass percentage recovery (ICP-OES)	Zirconium mass percentage recovery (ICP-MS)
Washed Zr*	3	77.0(4)	71(4)
Catch Pot*	3	27(1)	30(1)
Reactor Wall*	1	33(6)	18.6(7)
Reactor Interface*	2	26(6)	25(14)
Unwashed Zr*	3	14.8(7)	-
Reactor Head	5	46(15)	-
Heat Exchanger	4	19(1)	-
Reactor Bottom Valve	6	15(3)	-
Reactor Wall A	1	32.2(2)	-
Reactor Wall B	1	96(6)	-
Reactor Wall C	1	113(16)	-

*Samples were from an early experiment before significant optimisation had taken place.

- The ICP-MS was unavailable due to instrument failure and could not be returned to operation within the time constraints of this study.

Discussion

Table 7-12 shows the results of the analysis of the plasma metal production process samples received from Necsa. The modified microwave method making use of hydrofluoric acid was attempted to analyse these materials as they were not easily soluble under normal conditions, requiring long periods of heating similar to the ZrC

sample. After sample dissolution they were analysed by ICP-OES and some by ICP-MS when available. As previously though, some of the ICP-MS results differed from the ICP-OES results with the Reactor Wall sample differing significantly. This may not be entirely due to the MS though as these samples were recovered from inside the reactor and may not have been entirely uniform as no purification had yet been performed with the exception of the washed zirconium metal. These samples likely still contained magnesium chloride, a fairly hygrosopic compound, from the production process, complicating analysis. As expected the highest reliable recovery (ICP-OES) was for the washed zirconium product (77.0(4)%) while the other samples varied between 14.8(7) and 113(16)%. These results indicated that there was a significant degree of variation between the composition of samples recovered from different sample points in the reactor. The low recovery of the nominally purified Washed Zr (77.0(4)%) as compared to the Necsa zirconium metal powder (98(1)%) purified by volatilisation in the vacuum furnace indicated that the washing process was significantly less effective than volatilisation.

7.6. CONCLUSION

7.6.1 COMMERCIAL MATERIALS AND METHOD VALIDATION

The basic instrumental technique developed in **Chapter 6** was applied to all the dissolution methods used in this chapter. After digestion samples were diluted down to fit inside the calibration range of the standards as prepared in **Section 6.4.2.** The matrices were matched and the dilutions made with the intention of minimising matrix effects as much as possible. The quantitative recovery of zirconium from the reference crystals (**Table 6-18**) indicated that this method was accurate and acceptably precise provided that the sample was dissolved quantitatively.

Unfortunately, many zirconium-containing materials are highly inert, making quantitative dissolution difficult. This necessitated the development of new methods for the total dissolution of the sample. Modifications of the validated method were made as sparingly as possible with the majority of these being digestion media and conditions, alterations which would have a minimal effect after dilution. Progressively harsher reagents and conditions were required to achieve quantitative dissolution as the Necsa process samples proved to be particularly resistant to acid digestion.

From the data collected here the conclusion can be drawn that the ICP-OES microwave-assisted hydrofluoric acid digestion method is accurate and has a good degree of precision. The final, refined method's primary advantage over the earlier ones is best expressed in terms of time, reliability and applicability. It is significantly faster than the sulphuric acid method. It is more reliable as it is not wavelength dependent as the ammonium bifluoride method appears to be but further investigation is required to determine the exact cause of this observed effect. In terms of applicability it is possible to completely dissolve and analyse all available process samples using this method. Whereas several of the Necsa samples and the zirconium carbide were resistant to other methods, the final, refined dissolution is applicable to all of these inert materials achieving complete dissolution in all cases. The final results for the reference materials indicated that all analyses were statistically the same as the true value, indicating a high degree of accuracy. The standard deviations at the same time were quite low, approximately three orders of magnitude smaller than the mean in almost all cases. This low standard deviation indicates a high degree of reproducibility in the results.

7.6.2 NECSA PRODUCTS

From these results (see **Table 7-12**) it can be concluded that of the several digestion methods identified for the ICP analysis of zirconium-containing materials the use of microwave-assisted hydrofluoric acid digestion is the most effective. The method has the advantages of speed, reliability, robustness and reproducibility with acceptable accuracy and precision. It is reliable and robust in that all samples can be completely dissolved, destroying any pre-existing sample matrix. This simplifies analysis immensely. It also does not require any additives such as an internal standard in order to function correctly.

Chapter 8: GD-OES Assay Method Development and Experimental Results

8.1. INTRODUCTION

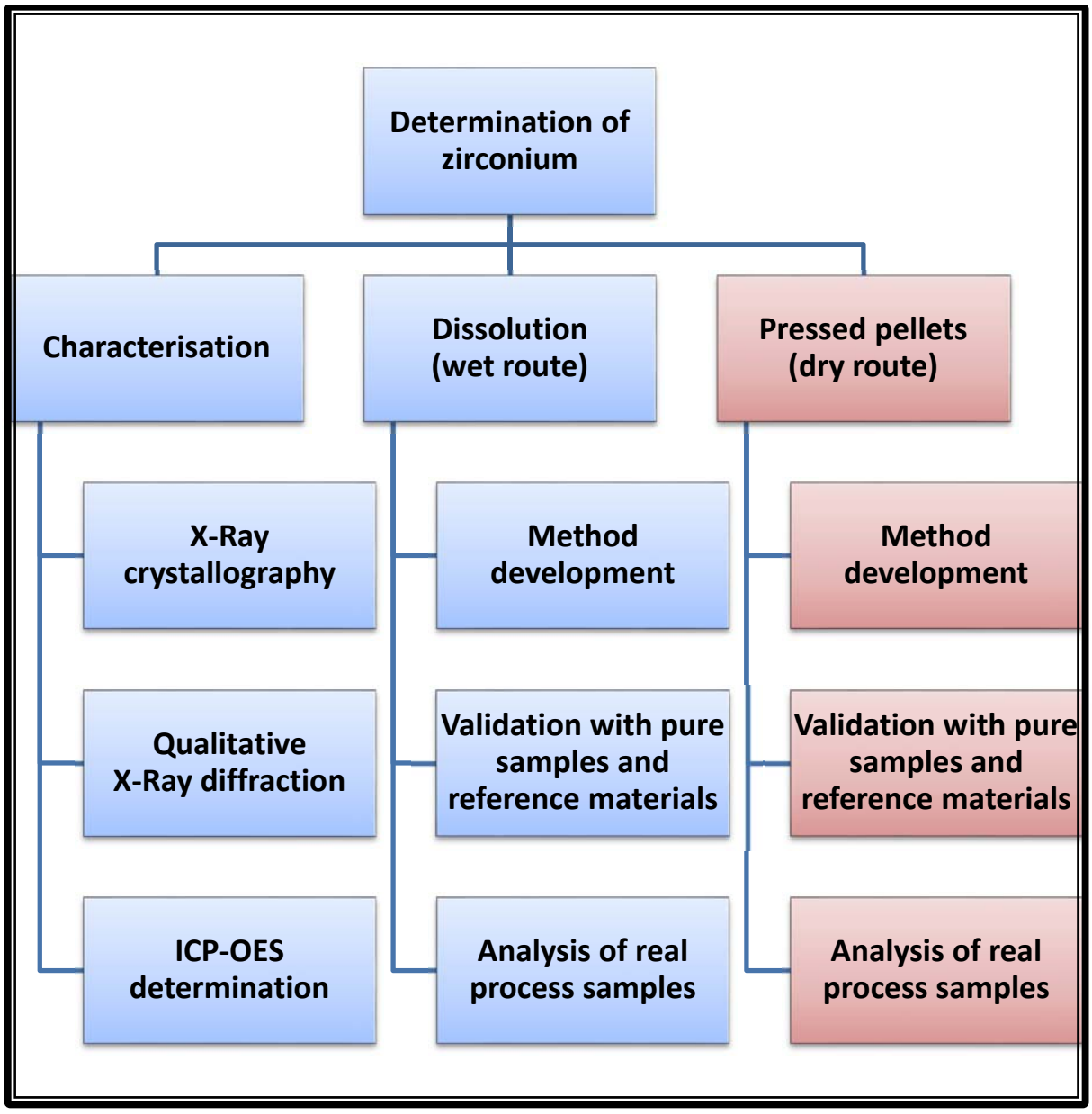

Figure 8-1: Experimental outlay with the pressed pellet and solid state analysis of samples highlighted

As seen in **Chapter 7** the dissolution of zirconium materials ranges widely in difficulty depending on the sample. Some materials dissolve immediately in minerals acids at benchtop conditions while others require specialised equipment (microwave digestion)

and severe conditions (high pressure and temperature). A method of analysis that would not require dissolution would thus be highly useful.

GD-OES has several extremely attractive advantages for bulk analysis over such analytical methods as ICP-OES and XRF. As it makes use of a solid sample there is often need for little or no sample preparation, in contrast with ICP instruments. The GD-OES instrument requires only a solid, flat surface for analysis of a conducting material. This makes it ideal for the analysis of metals but less so for ceramics and powders. This limitation may be circumvented, however, by the production of pressed pellets containing the non-conducting powder of interest in a conducting matrix. As the technique analyses an area of the sample with a diameter of between 4 and 8 mm homogeneity of the sample is not as significant an issue as would be expected, considering the difficulties in mixing powders. In contrast to XRF methods, which also require a solid sample, GD-OES has the advantage of rapid sample analysis. Analyses on GD-OES are orders of magnitude faster than on XRF and have the advantage of being able to perform either bulk analysis, for which the XRF (**Section 4.3.5**) is well suited [96, pp. 98-103], or quantitative depth profiling (**Figure 8-2**), which the XRF is completely incapable of. These depth profiles are also performed far more rapidly and easily than more traditional methods of surface analysis such as secondary ion mass spectrometry (SIMS) or transmission electron tomography (TEM). Development of a method for the quantitative analysis of zirconium materials specific to this project was thus deemed to be highly desirable.

When compared to other surface quantification techniques, such as Auger Electron Spectroscopy (AES), Secondary Ion Mass Spectrometry (SIMS) or X-ray Photoelectron Spectroscopy (XPS), GD-OES also has several advantages [148, pp. 306-307]. Samples of less than 10 nm and up to 15 μm thick can be analysed, the analysis is fast (in the order of a few minutes) and almost all elements are detectable (with the correct experimental conditions). It is also far cheaper than the other mentioned surface methods, provides elemental information and has a high sensitivity (in the ppm range). Disadvantages as compared to the aforementioned methods include poor depth resolution, a lack of lateral resolution, and no chemical information is obtained. These factors make GD-OES a highly useful complementary technique to other surface analysis techniques.GD-OES instruments are also capable of accurately analysing trace elements down to the ppm level [149].

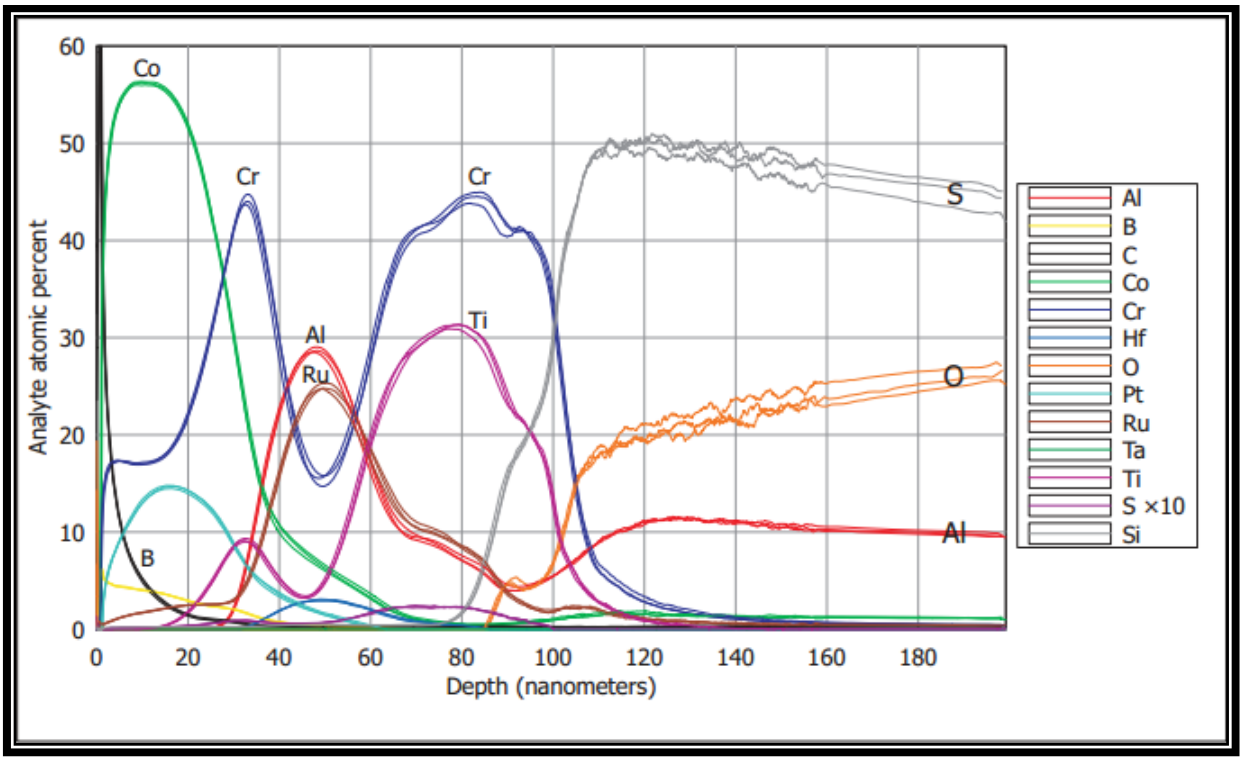

Figure 8-2: GD-OES quantitative depth profile of the surface of a hard disk drive platter [119]

The history of radio frequency glow discharges goes back to the early 1930s when Kennebaker and Clapp observed the effect in a cylindrical glass chamber when a high frequency was applied to two sleeve electrodes in contact with it [150]. It was not until 1989, however, that Marcus and Winchester designed an RF-powered GD source for direct elemental analysis of solid materials. Similar in concept to the Grimm source, emission stabilisation times and temporal stability were found to be better in this new source. The ability to analyse non-conducting layers with this source has renewed interest in the GD-OES method in industry where it has obvious advantages over traditional methods.

8.2. Equipment and Reagents

A LECO GDS850A Glow Discharge Optical Emission Spectrometer with a 4 mm anode and both a Direct Current (DC) and a Radio Frequency (RF) lamp were used for determinations. A FEI Quanta 200 3D SEM was used for scanning electron microscopy and energy dispersive spectroscopy (EDS) analyses. Copper powder (325 mesh, 99.5% purity), graphite powder (20 μm, 99% purity), zirconium nitride, zirconium oxide, spectroscopically pure (SP) zirconium oxide, zirconium metal powder (97%) and zirconium carbide powder (5 micron, 99% purity) were supplied by Sigma Aldrich.

Bakelite powder and PDZ were provided by Necsa. Samples were mixed and milled in a Retsch MM200 mixer mill. A seventy ton hydraulic press with a 200 mm ram provided by Hytec was used to press the solid pellets. The press mould was supplied by Paul Weber. SARM62 and SARM13 were sourced from Mintek through Industrial Analytical.

Raw experimental data can be found in the attached DVD.

8.3. METHOD DEVELOPMENT

8.3.1 SAMPLE PREPARATION METHODS

Initial attempts to create copper pellet disks containing a total of 15 grams of material were met with limited success. These pellets were prone to "tearing" in the plane of the pellet, resulting in porosity. The total sample mass was thus reduced to 7 grams, which alleviated the problem to a large extent. In the case of samples containing oxides (e.g. PDZ and ZrO_2) in quantities greater than 7 mass percent, the pellets were particularly brittle and cracked upon removal from the press. The components of the press mould can be seen in **Figure 8-3** and the assembled mould is shown in **Figure 8-4**. The disks were used without polishing as they were smooth enough to create a good seal and vacuum.

Copper powder was used as other metal powders known to be suitable for the pressing of pellets, like silver and tantalum, were prohibitively expensive.

Figure 8-3: Components of press mould used to make pressed pellets

Samples containing between 5.5 and 7 g of 325 mesh copper powder and between 0.01 and 2.5 g of sample (zirconium carbide, zirconium nitride, zirconium oxide, PDZ, SARM62, SARM13 or zirconium metal powder) were mixed thoroughly using a Retsch automatic shaker with tungsten carbide balls inside stainless steel vessels at a frequency of 20 Hz for 10 minutes. They were then pressed at approximately 1000 MPa pressure for 3 minutes each. These samples were then removed from the

press and analysed directly on the GD-OES using either the DC or the RF lamp. Zirconium tetrafluoride was used as well but was found to make brittle, porous samples at all useful concentrations.

Figure 8-4: Assembled press mould used for production of pressed pellets

An alternative sample matrix was prepared by mixing graphite and Bakelite to a ratio of four to one. Graphite was chosen as an inexpensive conducting powder but alone could not be pressed into a suitable pellet as the resulting sample was not mechanically strong enough to be mounted. The addition of a binding material was required and Bakelite and polytetrafluoroethylene (PTFE) powders were available. The PTFE was found to make too soft a pellet while the Bakelite produced a sufficiently hard and non-porous sample.

Samples containing between approximately 0.69 and 15.4% zirconium were made up using SARM62, SARM13, zirconium metal powder, zirconium oxide, carbide, nitride and tetrafluoride with a mixture of graphite and Bakelite. This mixture consisted of 20%

Bakelite and 80% graphite. These components were mixed thoroughly and pressed under 1000 MPa pressure. All samples were mixed using a Retsch automatic shaker with tungsten carbide balls inside stainless steel vessels at a frequency of 20 Hz. These samples were analysed on both the DC and RF lamps of the GD-OES instrument.

8.4. VARIATION OF INSTRUMENT PARAMETERS

The LECO GDS850A DC GD plasma has three co-dependant variables. These are current (mA), voltage (V) and pressure (torr). Any two of the three can be set within certain safe parameters and the instrument will automatically adjust the third to generate a stable glow discharge. As it is not recommended to control the instrument on pressure only the voltage and current were varied systematically during the study. The RF plasma, by contrast, was controlled on voltage, applied power (W) and pressure. Again the pressure was allowed to be the dependant variable while the other two were adjusted. In both cases the voltage had allowed the greatest range of alteration without causing damage to the instrument so the majority of the conditions used kept the current or applied power constant while varying the voltage.

8.4.1 INITIAL RESULTS

Two distinct regions of instrument response were observed under the default conditions (**Table 8-1**) for a copper matrix containing either zirconium carbide or zirconium nitride. These can be seen in both **Figure 8-6** and **Figure 8-7** respectively. The region above approximately 6% zirconium content shows a markedly lower increase in instrument response with zirconium concentration when compared to the region below said percentage. The excellent linearity (R^2 of 0.9998) in the higher concentration range of the zirconium carbide samples was extremely encouraging but the differences in gradient between samples appeared to be a problem.

Figure 8-5: A representative pellet showing a single glow discharge crater on a copper matrix pellet

Table 8-1: Default conditions of DC GD-OES analyses

Variable	Condition
Lamp	DC
Voltage (V)	700
Current (mA)	35
Sample matrix	Cu
Pre-burn time (min)	1

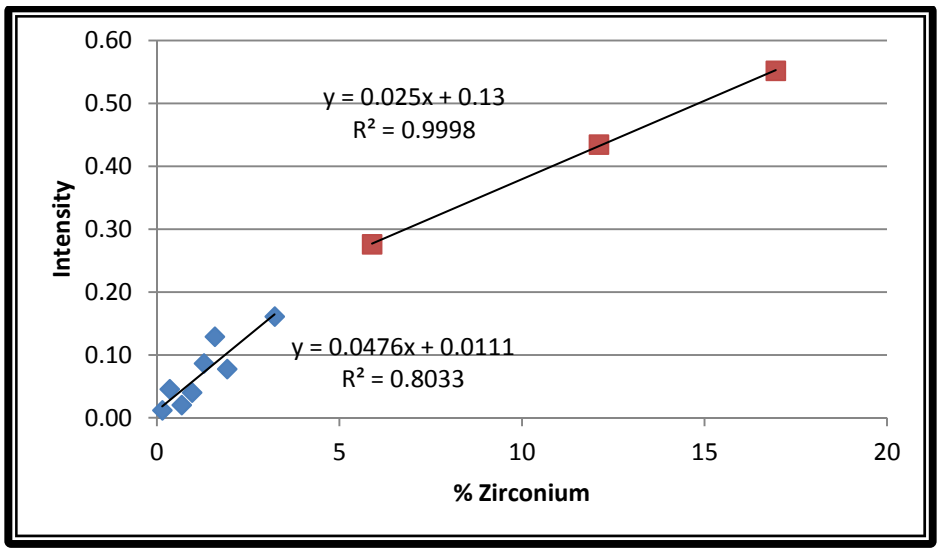

Figure 8-6: Graph showing instrument response for ZrC samples

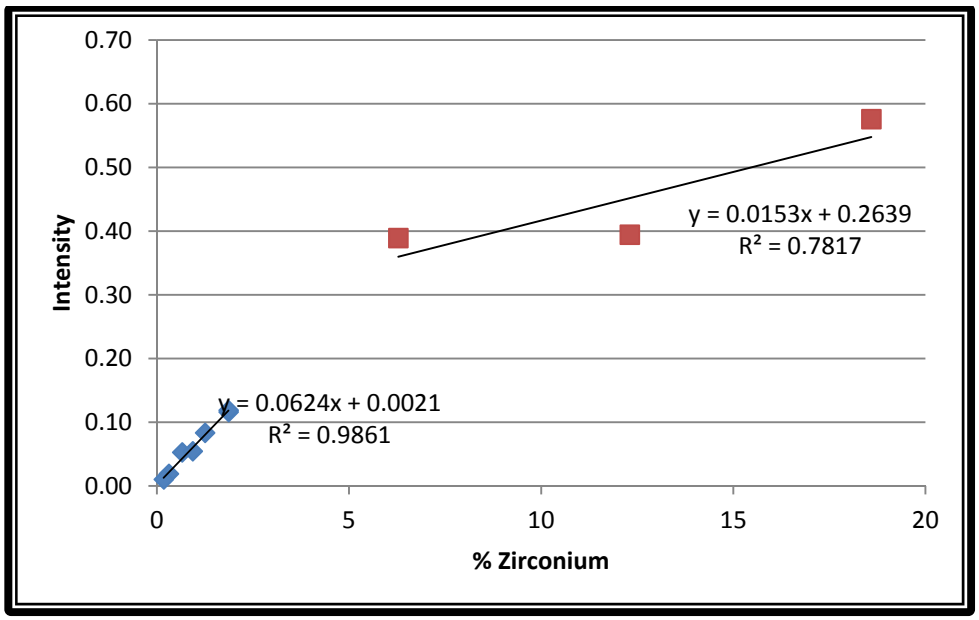

Figure 8-7: Graph showing instrument response for ZrN samples

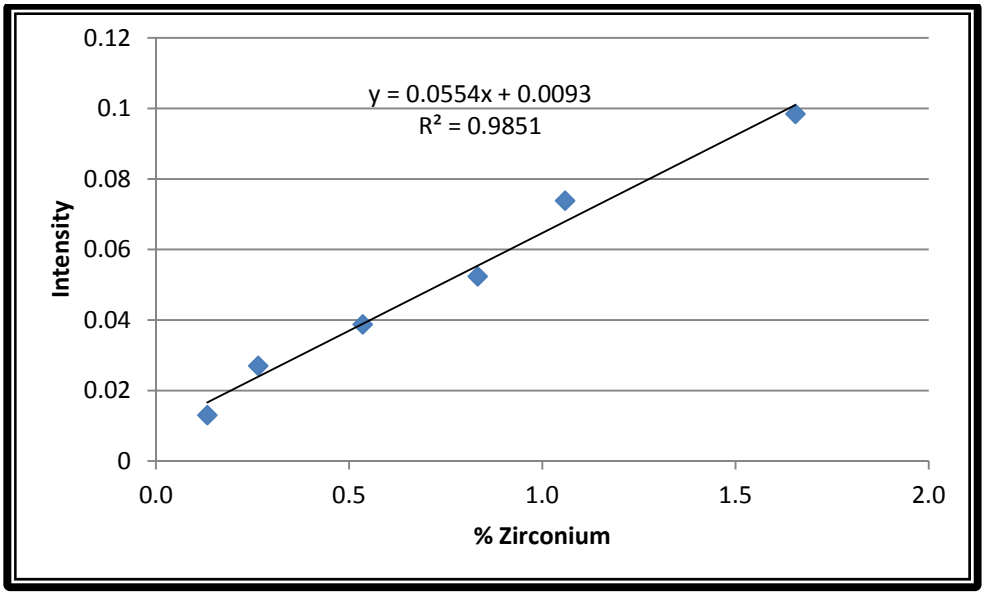

Figure 8-8: Graph showing instrument response for ZrO_2 samples

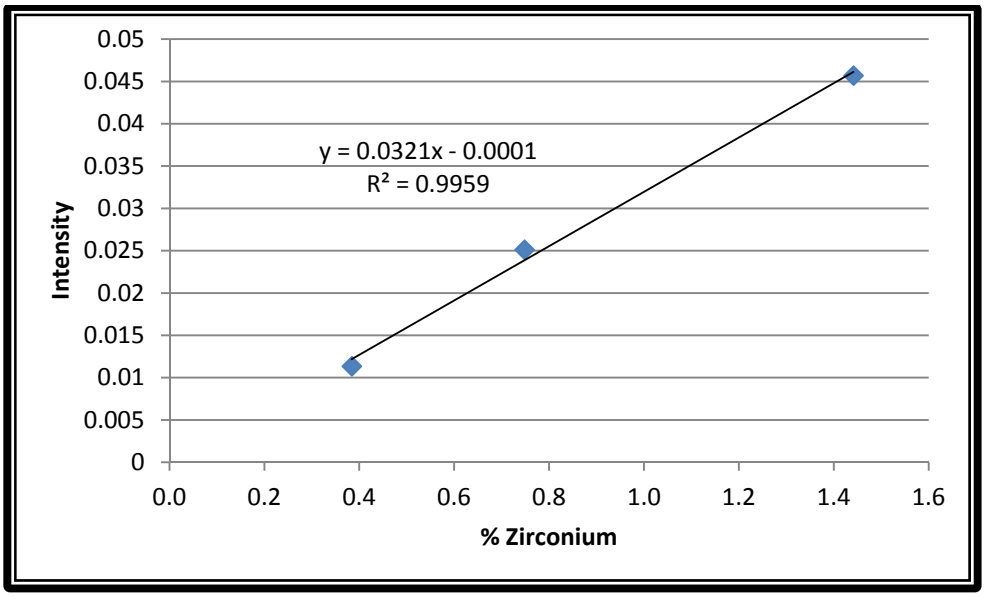

Figure 8-9: Graph showing instrument response for Zr powder samples

The distinct regions were not observed for samples containing zirconium oxide and zirconium metal powder (see **Figure 8-8** and **Figure 8-9** respectively) as their zirconium concentrations were well below the 6% level. It is not known whether a similar effect would be observed with these materials as pellets produced with higher quantities of oxide were too porous or brittle to mount on the GD. Limitations on the amount of zirconium metal powder available also limited the concentrations and number of the pellets containing it. The instrument response for both of these were quite linear (R^2 of 0.9851 and 0.9959 respectively) but the concentration range was quite small, being in the 0.1 to 2% range.

The calibration gradients of the four slopes were different but in the same order in all the lower concentration ranges. This may point towards the sputter rate of the materials being more strongly influenced by the matrix in this region.

8.4.2 Increased Voltage on DC lamp with copper matrix

The SP ZrO_2 (**Figure 8-10**) was a different zirconium oxide, specifically the spectroscopically pure material purchased from Sigma Aldrich. Increasing the applied voltage on the DC lamp did little to improve either linearity or instrument response. This can be seen in **Figure 8-10** and **Figure 8-11** where the instrument response to several different zirconium-containing materials in copper matrix are graphed together. After little change was seen from increasing the voltage to 800 V, a further increase to 900 V was tried to determine if this would remain the case. Only the SARM62, SARM13, ZrO_2 and Zr Metal samples were run as the instrument began to “short”

consistently while attempting the other materials, making further determinations impossible.

It can clearly be seen that the different materials have significantly different responses under the same conditions and the same trend of different instrument response in different concentration ranges is again visible. Under these conditions a real sample would need to be a very close match to the matrix of the calibration standards, requiring knowledge of the exact composition of the sample. As determining this would be the reason for performing the analysis in the first place, this was deemed to be a fairly serious drawback. Applied voltages above 900 V were found to cause damage to the instrument as, instead of forming a glow discharge, an arc would occur, damaging the insulator sleeve between the cathode and anode. This occurred at the lower voltages as well but with much less frequency.

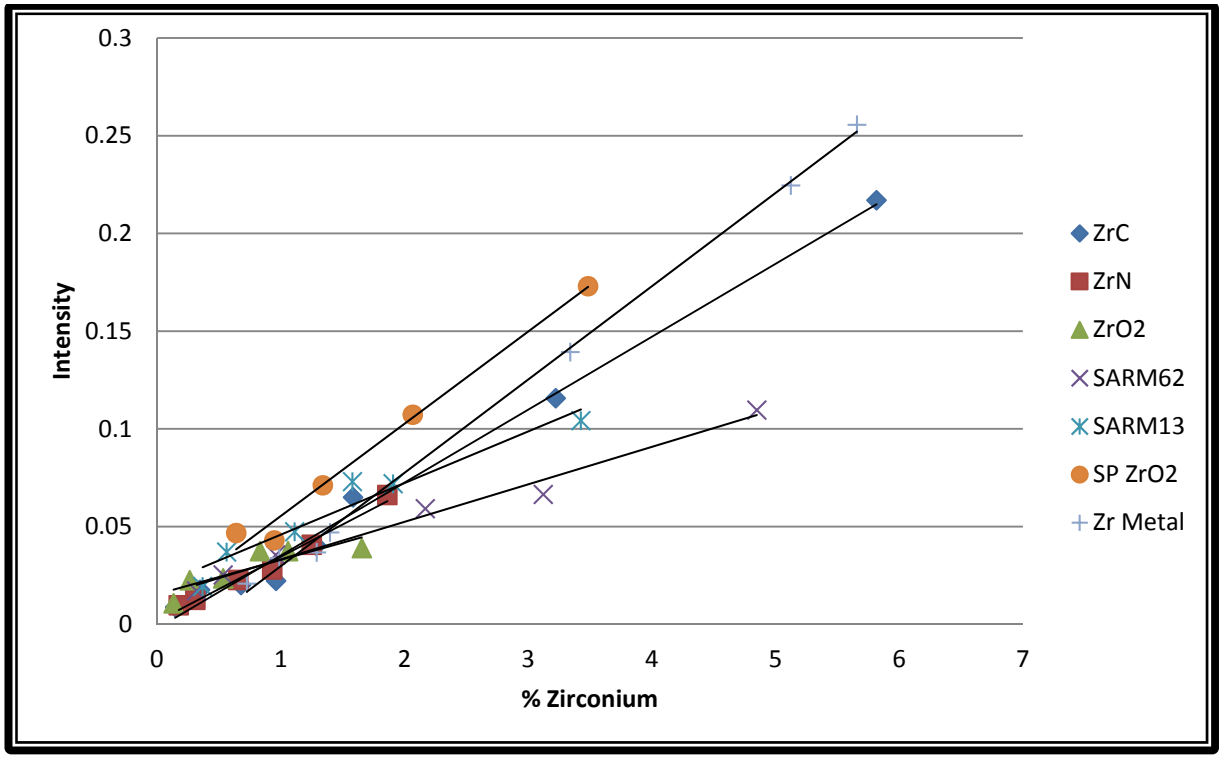

Figure 8-10: Instrument response for several materials plotted together (DC lamp, **800 V**, 35 mA, Cu matrix, 1 min pre-burn)

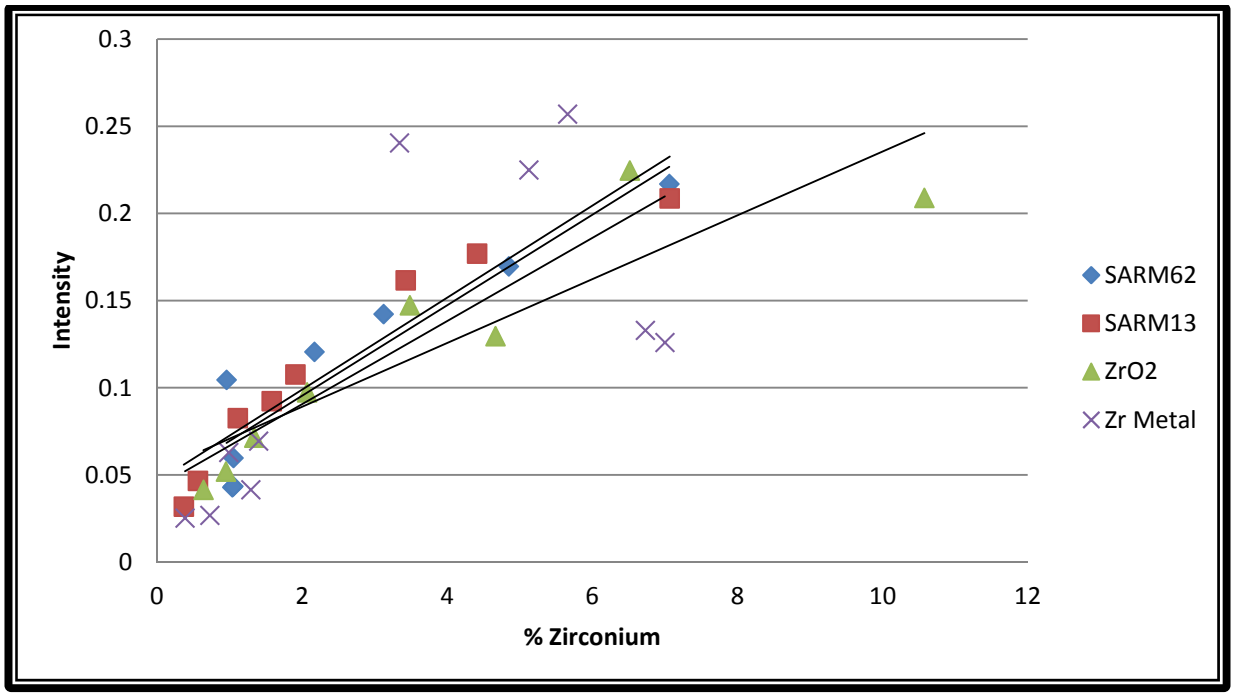

Figure 8-11: Instrument response for several materials plotted together (DC lamp, **900 V**, 35 mA, Cu matrix, 1 min pre-burn)

8.4.3 COPPER MATRIX SAMPLES ANALYSED BY RF LAMP

As it was evident that increasing the voltage did not improve the linearity of instrument response with the DC lamp over the selected concentration range it was decided to switch to the RF GD source to compare the results obtained thus far with results from it. This was also done in order to determine if the change in instrument response in different concentration regions was an artefact of the DC lamp. The same copper samples were analysed at varying voltage settings on the RF lamp but, due to differences in the lamp control systems, the applied power was kept constant at 14W rather than the current as was the case with the DC lamp. Rather than having two zones of linearity as seen in **Section 8.4.1** the instrument response appeared to level off and even decrease after 6%. These results can be seen in **Figure 8-12**, **Figure 8-13** and **Figure 8-14** with the decrease becoming more pronounced with the increase from 700V applied voltage, through 850V and up to 1000V. Due to the scale of these graphs the range below 2% zirconium concentration appears to be linear but magnification shows this not to be the case with different materials giving different instrument responses. Though the RF lamp allowed for higher voltages than the DC lamp, voltages above 1000V again resulted in damage to the instrument's insulating between the "anode" and sample. The word anode is used here to describe the inner tube of the lamp. As the lamp is a radio frequency device it has no true, consistent

anode but using this nomenclature makes for simpler discussion of components. Again the values in the sub 6% range are nominally linear but vary significantly in instrument response to concentration with different zirconium materials.

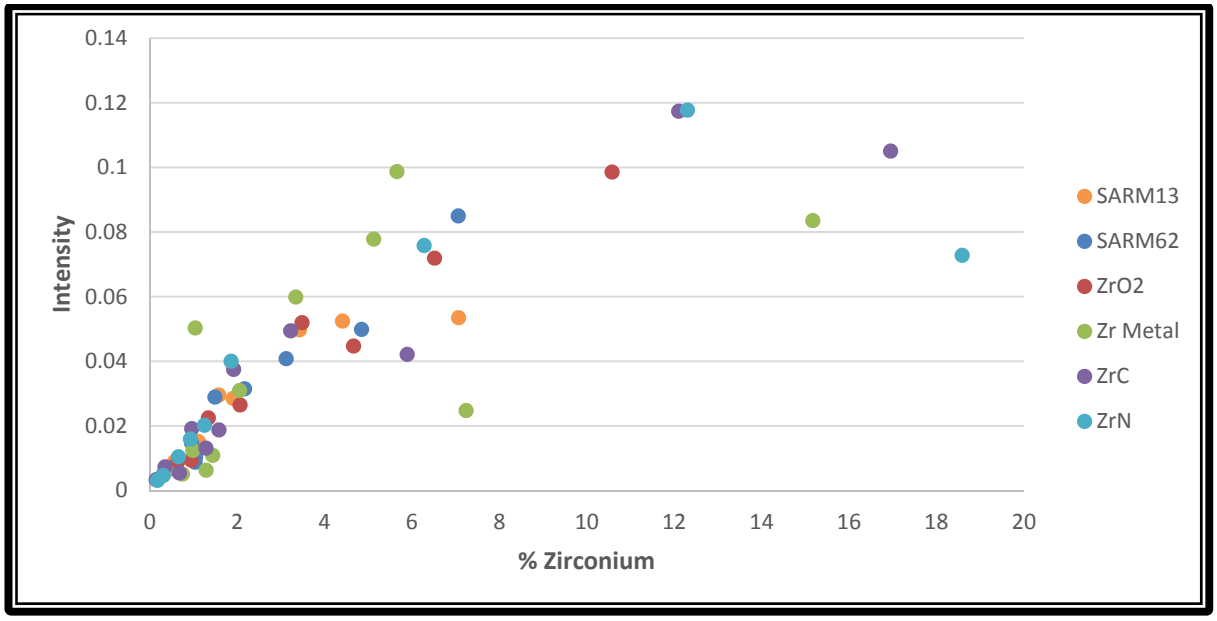

Figure 8-12: Instrument response for several materials plotted together (RF lamp, **700 V**, 14 W, Cu matrix, 1 min pre-burn)

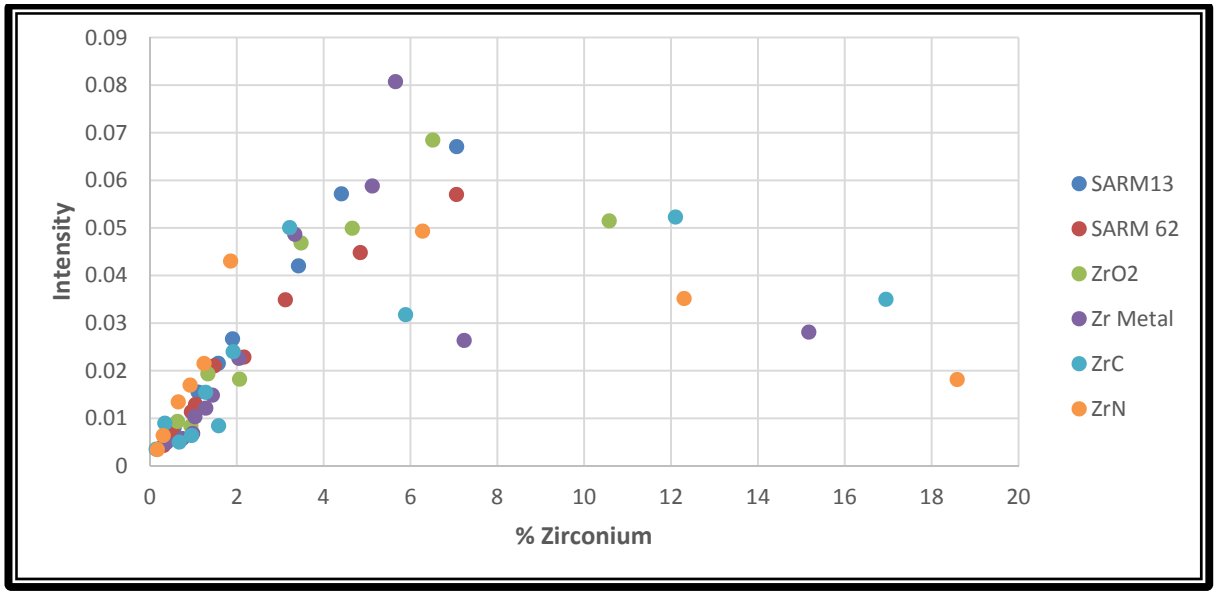

Figure 8-13: Instrument response for several materials plotted together (RF lamp, **850 V**, 14 W, Cu matrix, 1 min pre-burn)

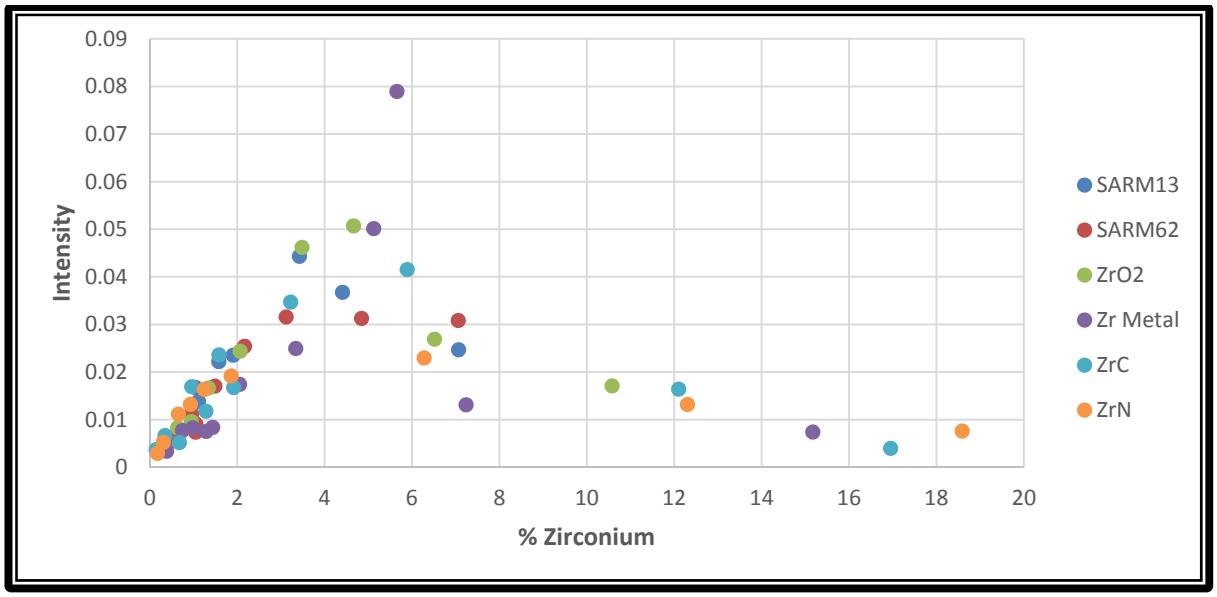

Figure 8-14: Instrument response for several materials plotted together (RF lamp, **1000 V**, 14 W, Cu matrix, 1 min pre-burn)

8.4.4 Samples using Graphite Matrix and RF lamp

In this section the sample matrix was changed as well as continuing to vary the applied voltage. As only a single set of samples was run it was deemed acceptable to increase the voltage past the "safe" 1000V value for the short time the analysis would take. Graphite with a Bakelite binder was used to produce conducting pellets containing zirconium oxide and zirconium tetrafluoride. These two materials were chosen initially as they were the most difficult to form copper pellets with and are also similar to the process samples, the analysis of which which was the ultimate analytical goal.

As seen with the copper pellets, there was an upper and lower region of linearity for the zirconium oxide. The concentrations were made up to try to match those in the copper samples and again the three highest concentration samples showed a different instrument response. Unlike the copper, however, the instrument response gradient appeared to increase after the 6% zirconium content threshold. The difference can be seen in **Figure 8-16** and **Figure 8-17** where the trendline for the 1200 V RF analyses was plotted. This was the condition with the highest instrument response rather than the highest voltage. Excellent linearity was observed for both of these lines ($R^2 > 0.997$). The lower instrument response at 1300 V may have been due to melting occurring in the Bakelite in the sample. The samples were analysed at varying applied power settings with both the DC and RF lamps. Several of the results at lower power

settings overlap considerably and are thus difficult to distinguish in the graphs. Acceptable linear response for most power settings was also obtained with the zirconium tetrafluoride samples (see **Figure 8-18**). Although the zirconium tetrafluoride is known to be hygroscopic, the non-porous nature and pre-burn condition of the analysis was deemed to be sufficient to protect the analysed portion of the sample from moisture. As precautions needed to be taken against moisture during the sample preparation procedure and most of the procedure was open to atmosphere, the samples needed to be prepared individually and moved from weighing to mixing to pressing as quickly as possible. As such, production of these pellets was more time sensitive as all of the instruments needed to be available at once. Thus only three pellets were produced and further research will be required as they do not appear to obey the two-zone rule the other materials exhibit.

In all three graphs it can clearly be seen that an increase in applied voltage yields an increase in instrument response up to 1200V RF. After this the 1300V RF results drop significantly. However, at voltages above 1000V on the RF lamp and 700V on the DC lamp, arcs become common and cause damage to the anode insulating sleeve. As there did not appear to be any increased linearity in the instrument response at these higher voltages the gain in intensity was deemed unnecessary.

With the improved linearity, greater range of voltages, lower likelihood of damage to the insulator sleeve and lower incidence of “shorting”, the RF lamp was selected as the source of choice for all further analyses.

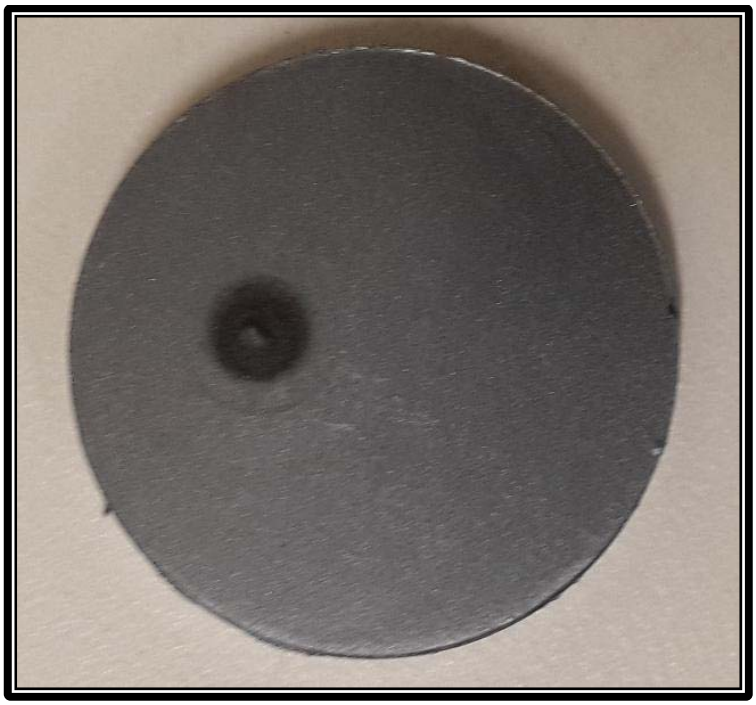

Figure 8-15: A representative pellet showing a single glow discharge crater on a graphite matrix pellet

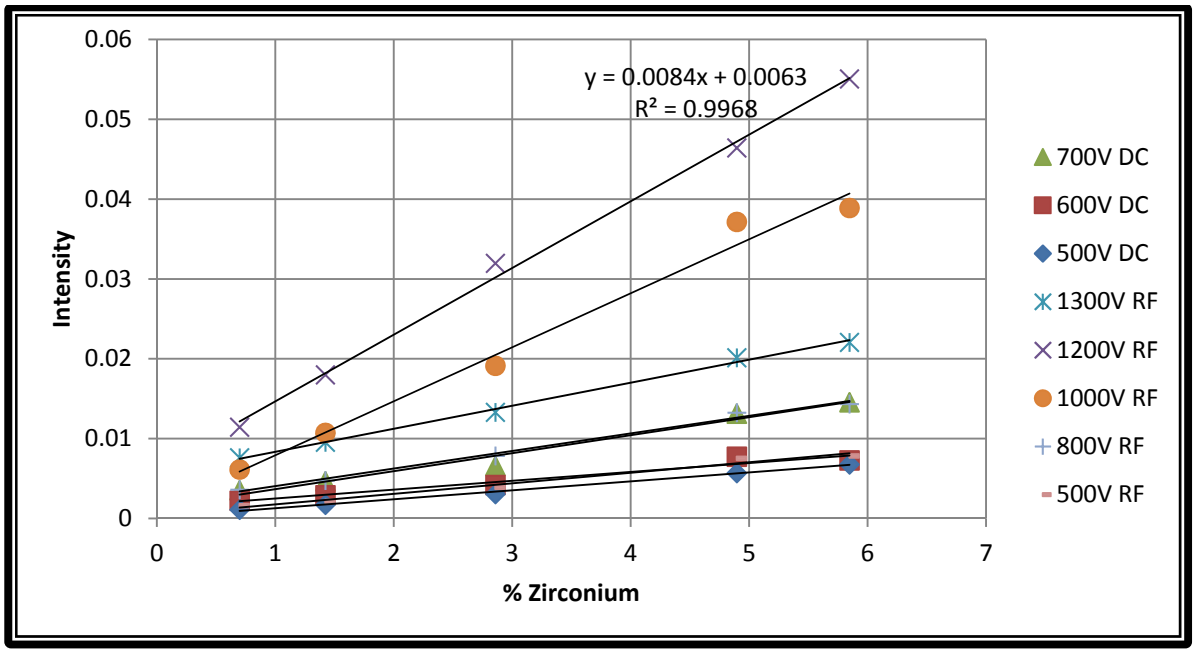

Figure 8-16: Low range instrument response for ZrO_2 at varying applied voltage in a graphite matrix (35 mA DC or 14 W RF, graphite matrix)

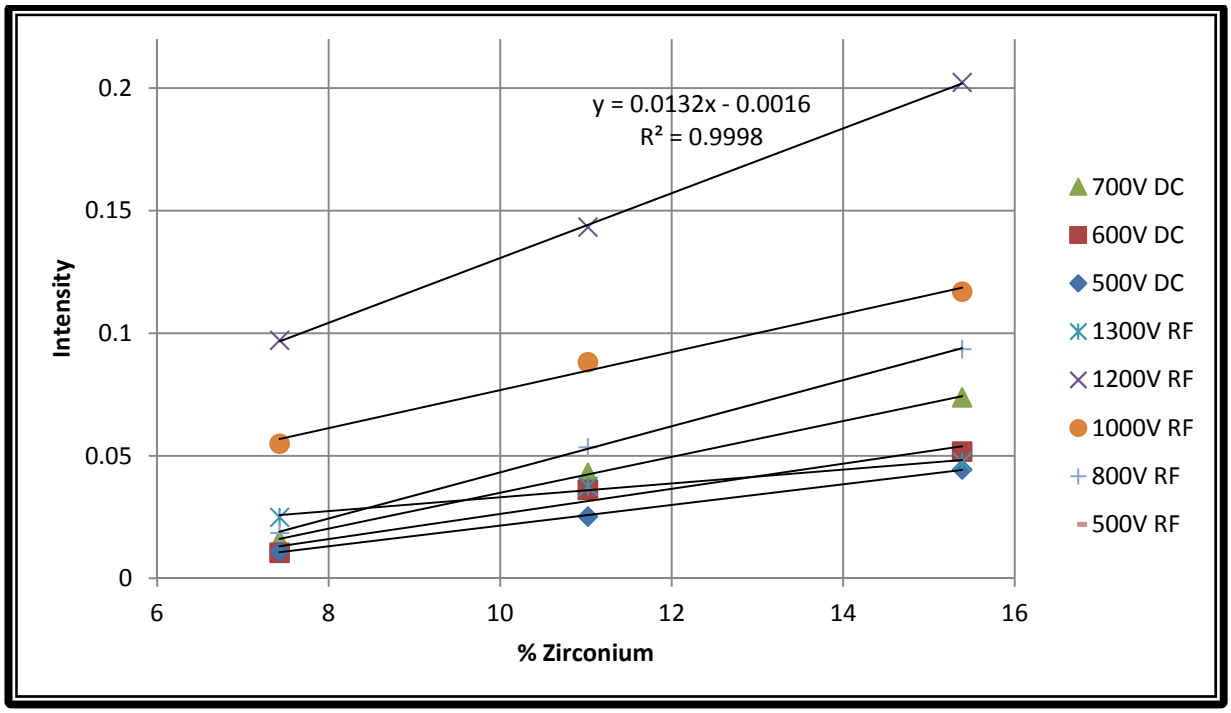

Figure 8-17: High range instrument response for ZrO_2 at varying applied voltage in a graphite matrix (35 mA DC or 14 W RF, graphite matrix)

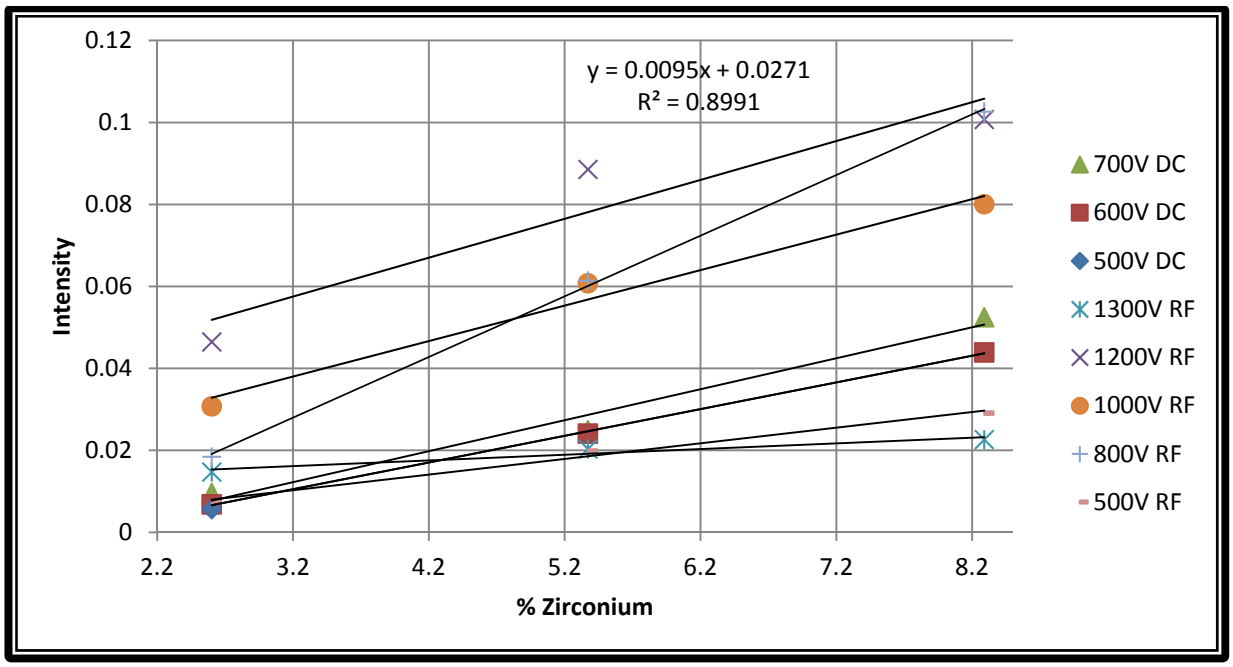

Figure 8-18: Instrument response for ZrF_4 at varying applied voltage in a graphite matrix (35 mA DC or 14 W RF, graphite matrix)

8.4.5 TIME PROFILE OF INSTRUMENT RESPONSE

The cause of the different calibration slopes (one high and one low) under the previous operating conditions of the equipment (sample matrix, voltage and lamp type) could not be determined, thus the following study was undertaken. A quantitative depth

profile was performed on both the copper and the graphite matrix samples at the default settings for the RF lamp. This was done not to determine the depth profile as such as the pellets were intended to be homogenous as far as the GD-OES instrument was concerned, but rather to determine if instrument response was in fact stable after one minute of pre-burn time. As can be seen in **Figure 8-19** this was decidedly not the case and was likely the cause of the differences in calibration gradients for the different zirconium materials. From the graph it was determined that a 5-minute (300 seconds) pre-burn was the minimum burn time for most materials to stabilise. The changing gradients in different concentration regions observed for some compounds was likely due to insufficient stabilisation time. The increased sample content in the pellet likely changed the rate at which stabilisation took place, thus appearing to give two different linear regions.

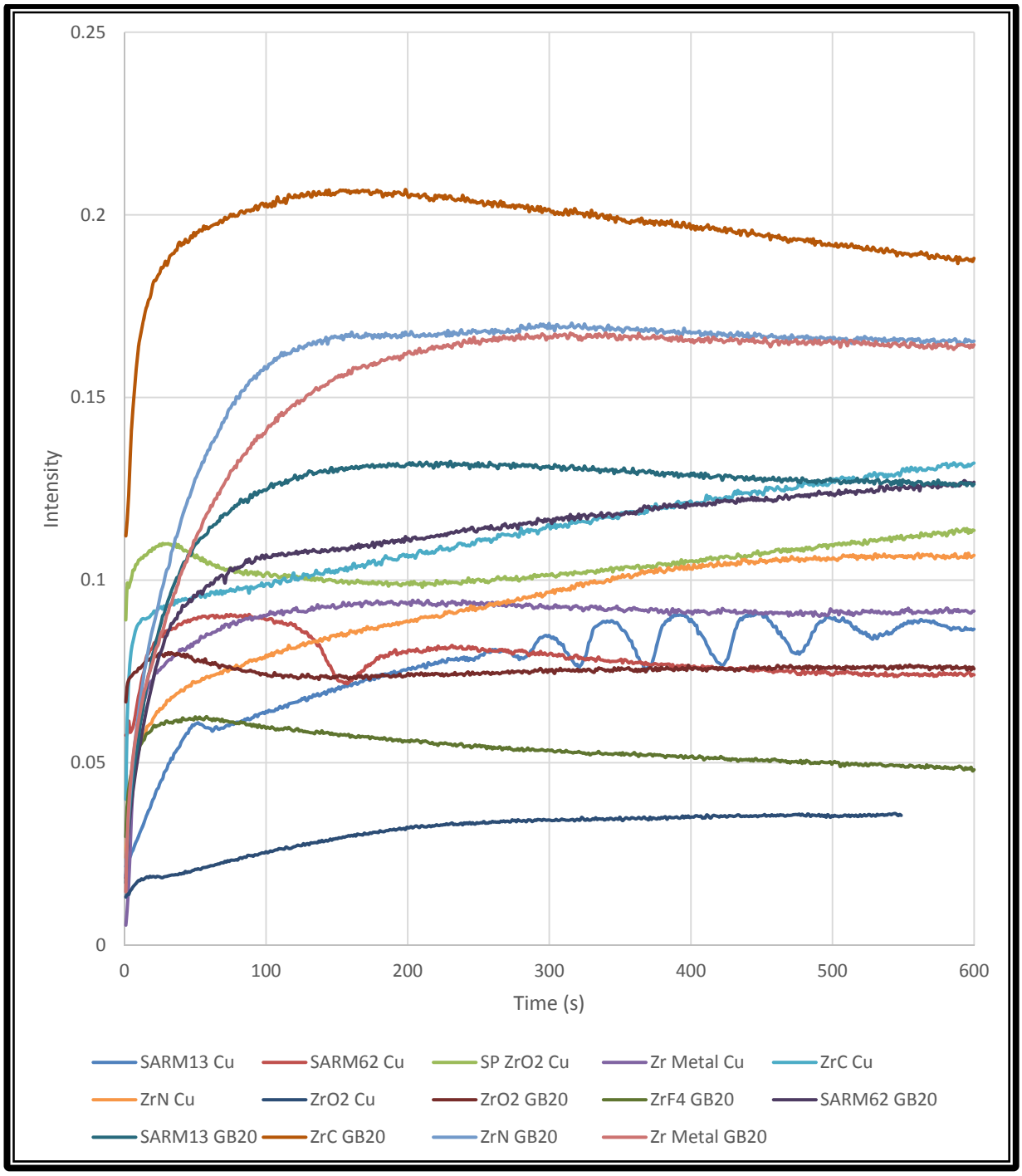

Figure 8-19: Graph showing zirconium instrument response for multiple materials in both the copper and graphite matrices together (RF lamp, 700 V, 14 W)

8.4.6 SEM AND EDS ANALYSIS OF CRATER AND BULK SURFACE COMPOSITION

SEM-EDS is a surface analysis technique capable of showing the surface structure and determining the elemental composition of the surface at a point. This information is complementary to the understanding of the process occurring in and around the GD crater. Samples containing zirconium carbide were analysed as these contained the

greatest percentage zirconium in the hope that they would give a good contrast between the raw and crater surfaces. A clear difference in morphology is evident between the bulk material and the GD crater, designated Area 1 and Area 2 in **Figure 8-20**. The brighter portions correspond with high concentrations of zirconium while the darker areas are mainly copper. The surface within the GD crater is more homogenous than the area outside with a region of apparent zirconium redeposition being evident just inside the edge of the crater. This homogeneity is a result of the action of the glow discharge plasma on the surface and would not affect the chemical composition, and thus instrument response, on its own. The apparent lack of zirconium in the majority of the crater may be caused by the preferential sputtering of said zirconium. This may be due to the zirconium carbide being more loosely bound into the pellet than the copper.

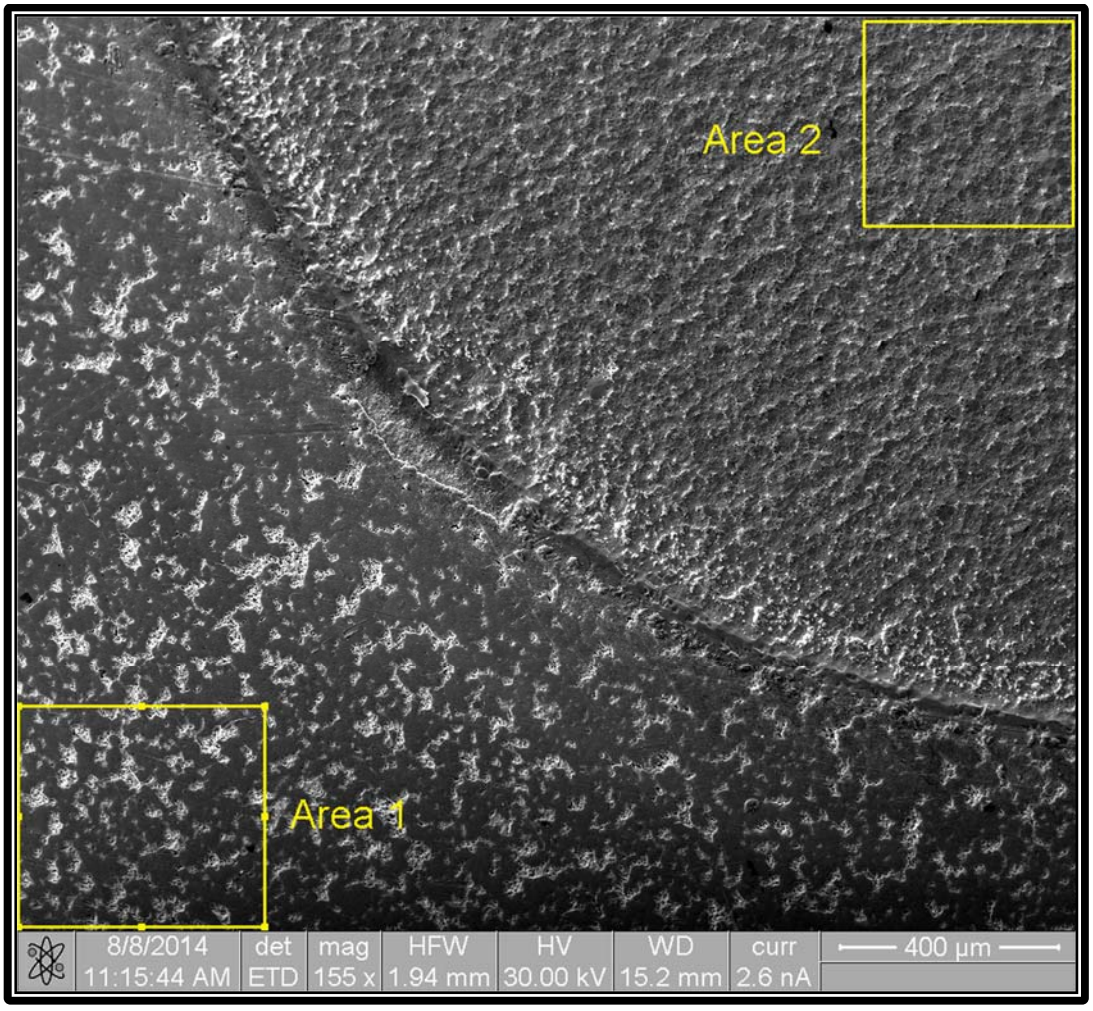

Figure 8-20: SEM image of copper pellet containing ZrC

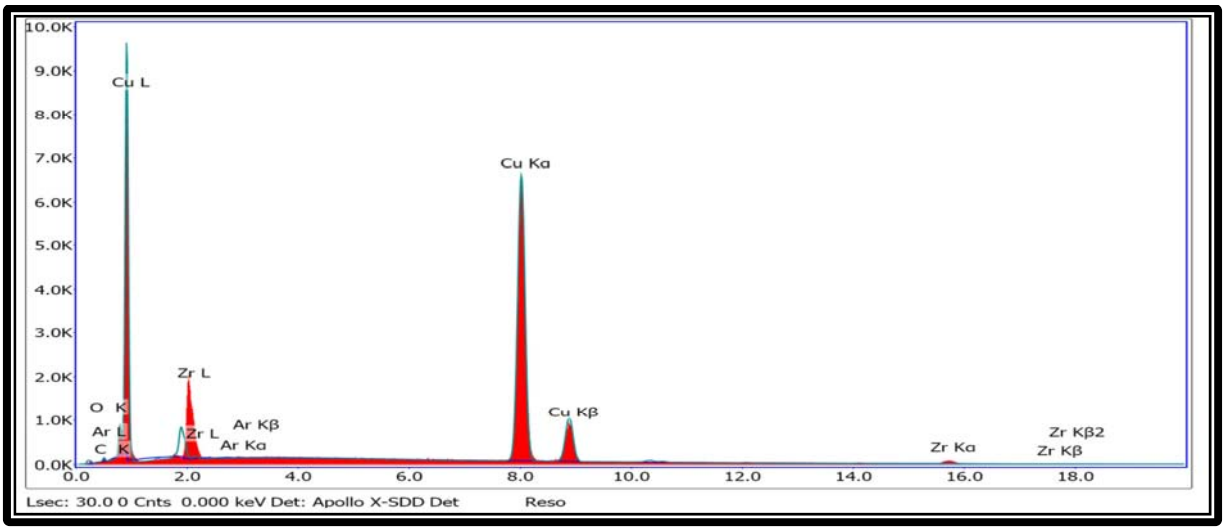

Figure 8-21: EDS spectrum of GD crater in copper matrix

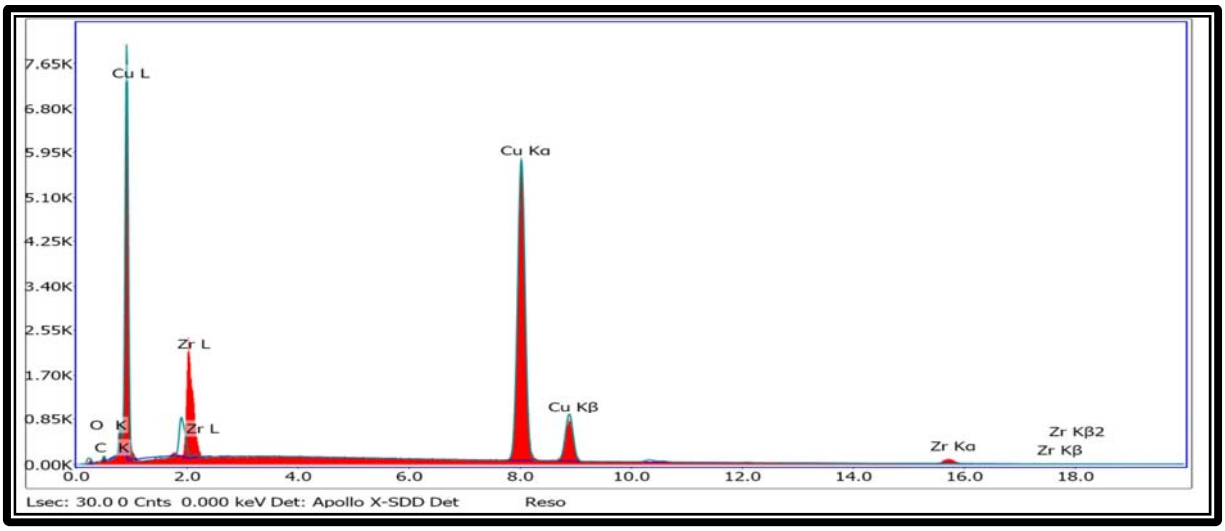

Figure 8-22: EDS spectrum of bulk sample in copper matrix

Looking at the difference in intensities of the EDS spectra of the two regions (**Figure 8-21** and **Figure 8-22**) it can be seen that the zirconium L-peak is slightly smaller for the GD crater area than for the bulk material. This agrees with the visual observation made of the SEM image. Small argon peaks are also visible in only the crater analysis. This is likely due to argon ions being trapped in the matrix after impact from the plasma.

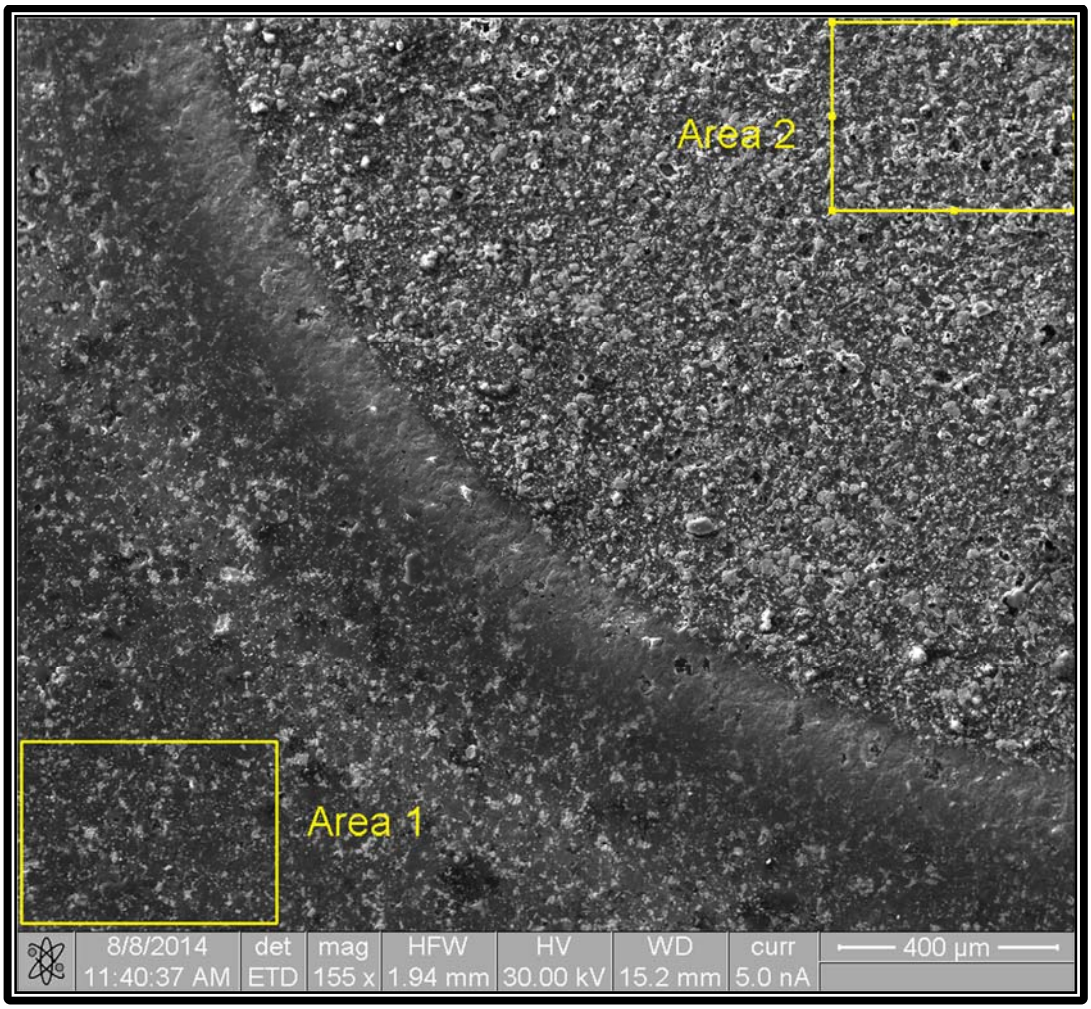

Figure 8-23: SEM image of graphite pellet containing ZrC

A clear difference in sample composition is again seen in the GD crater of a graphite pellet (**Figure 8-23**). As in **Figure 8-20**, Area 1 corresponds to the bulk sample while Area 2 lies within the GD crater. In contrast to the copper matrix more zirconium (bright material) is visible in the GD crater than in the bulk. This is likely due to preferential sputtering of the graphite, the carbon atoms of which are far lighter than those of the zirconium, making them more susceptible to being sputtered by the energetic argon ions.

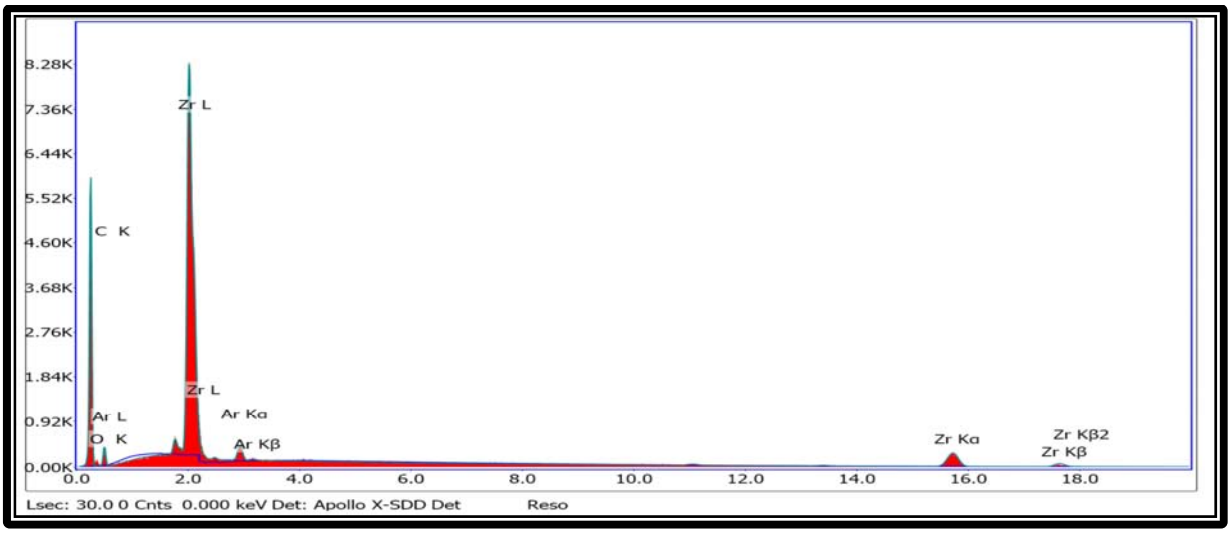

Figure 8-24: EDS spectrum of GD crater in graphite matrix

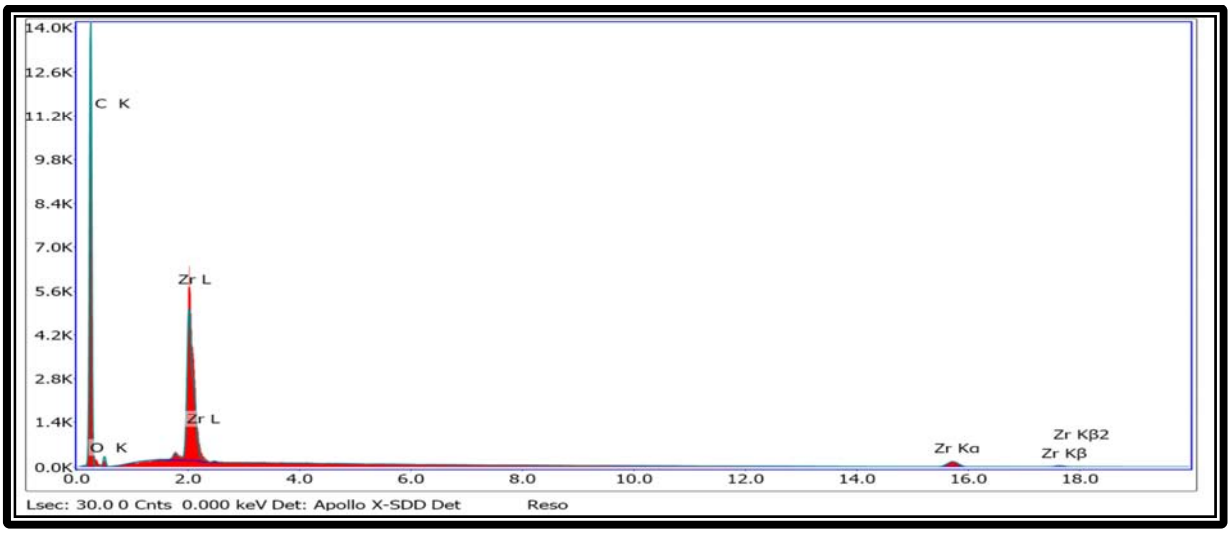

Figure 8-25: EDS spectrum of bulk sample in graphite matrix

The EDS spectra of the two regions of the graphite pellet (**Figure 8-24** and **Figure 8-25**) again bear out the observations made on the SEM image. The zirconium L line peak is in this case markedly smaller in the bulk sample analysis than in the GD crater itself, with argon lines evident only in the crater analysis.

The depletion of zirconium on the surface of the copper pellets and enrichment of the surface of the graphite ones may indicate that preferential sputtering is indeed the cause of the change in slope seen in earlier experiments. At lower concentration ranges the sputter rate may thus be controlled by the matrix while the sample has a greater effect at higher concentrations.

Table 8-2: Table of EDS analysis results for both copper and graphite sample matrices

Element	Graphite pellet crater	Graphite pellet bulk	Graphite pellet crater ridge	Copper pellet crater	Copper pellet bulk	Copper pellet crater ridge
C Kα (%)	67.88	83.48	9.35	2.74	5.19	1.59
O Kα (%)	5.18	3.33	15.63	0.93	1.7	12.64
Ar Kα (%)	0.45	<DL	2.75	0.07	<DL	2.28
Cu Kα (%)	<DL	<DL	<DL	77.11	69.54	63.12
Zr K λ (%)	26.5	13.19	72.27	19.14	23.57	20.37

Percentages reported as given by instrument software in weight percentage.

The semi-quantitative results for each of the areas analysed by EDS is given in **Table 8-2**. As the instrument was not specifically calibrated for this type of sample and the sample preparation of the pellets was not suitable for this kind of analysis the results can only be taken as an indication of difference and are not fully quantitative. As this particular SEM/EDS instrument had difficulty determining elements in the sample with less than 1% concentration, only the major components could be observed and any possible impurities would not have been detected. The observations made from the SEM images and EDS graphs are further confirmed by the apparent concentrations seen in **Table 8-2**. The graphite pellet has nearly double the apparent concentration of zirconium (26.5%) in the GD crater than outside (13.19%) with a large concentration (72.27%) on the crater edge. As there is a similarly large oxygen deposit (15.63%) on this ridge it is likely that zirconium is being redeposited here as ZrO_2 with the oxygen possibly being supplied by the Bakelite binder. Conversely the ridge area of the copper pellet appears to be roughly as depleted of zirconium (20.37%) as the crater itself (19.14%) in comparison to the bulk (23.57%). As these results were obtained using EDS, which has a comparatively small sampling area compared to the GD-OES, the actual quantitative results given in this table cannot be taken to be

representative of the entire surface and are used merely as an indication of the change in the sample surface as a result of the GD analysis.

8.4.7 Instrument response at varying power settings after a 5-minute pre-burn

Based on the results seen in **Figure 8-19** and those in **Section 8.4.6** it became apparent that the signal intensity had not stabilised after the default 1 minute pre-burn time. **Figure 8-19** clearly showed that most of the samples only reached a steady state after at least 5 minutes of pre-burn time. It was decided to alter the conditions of the analysis by increasing the pre-burn to five minutes while varying the voltage from 500 to 900 V with determinations being made in both the copper and the graphite matrices. The following sections demonstrate the gradual improvement in linearity as the conditions are optimised.

8.4.7.1 Voltage setting: 500V

A 5-minute pre-burn using the RF lamp at 500V and 14W was used in the analysis of all of the copper and graphite matrix samples with the results graphed together in **Figure 8-26** for the copper matrix and **Figure 8-27** for the graphite. In the copper matrix the low concentration samples (ZrO_2, SP ZrO_2, ZrN, ZrC, Zr metal powder, SARM13 and SARM62) appeared to respond fairly consistently with the intensity decreasing markedly as the zirconium concentration increased past 6%. From the SEM and EDS data seen in **Section 8.4.6** it can be surmised that this may be due to depletion of the zirconium by a greater degree than is seen for the lower zirconium content samples. It is possible that, due to the difficulties in mixing powders, the higher zirconium-concentration samples are more heterogeneous with larger pockets of analyte in the matrix. Preferential sputtering of these pockets would lead to greater depletion than in a more homogeneous material. A far better correlation can be seen in **Figure 8-27** for the graphite matrix. Under the same conditions there appeared far fewer obvious outliers, especially considering that the graphite samples' range extended past 40% zirconium in the matrix. This was possible as the graphite matrix allowed for the creation of samples with far higher analyte content than was achievable with the copper. The higher concentration graphite-matrix samples appear to increase in instrument response. This may again be explained by the depletion of carbon from the analysed surface but as the carbon is the matrix material here and is present in far greater relative quantities, the effect is not as significant.

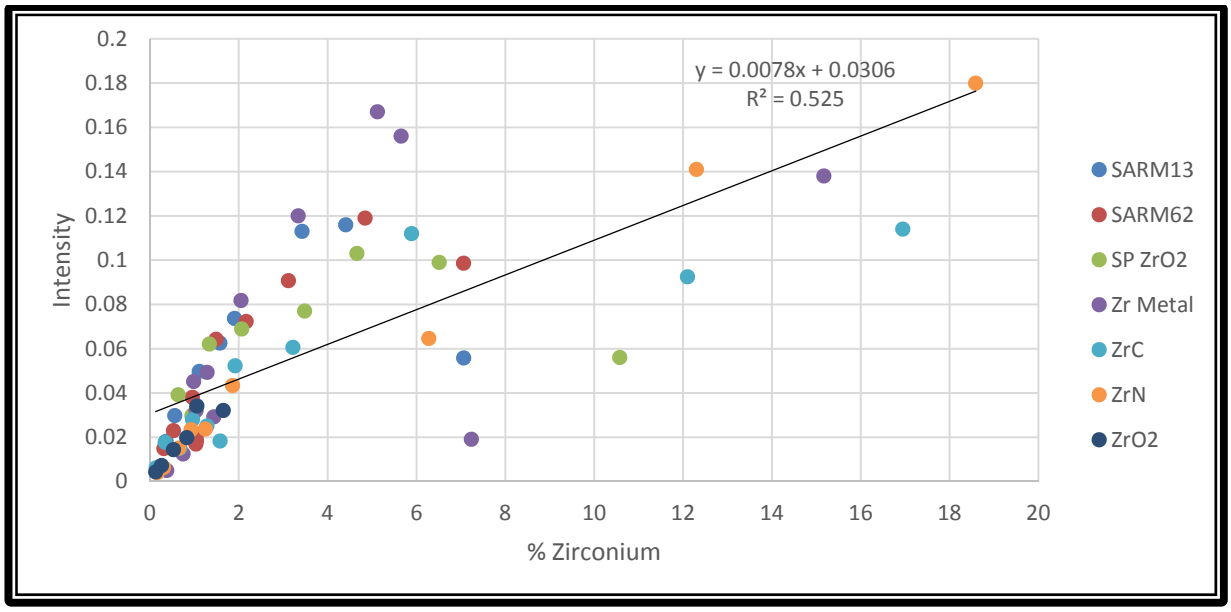

Figure 8-26: Graph showing instrument response for multiple materials in copper matrix together (RF lamp, 500 V, 14 W, 5 min preburn)

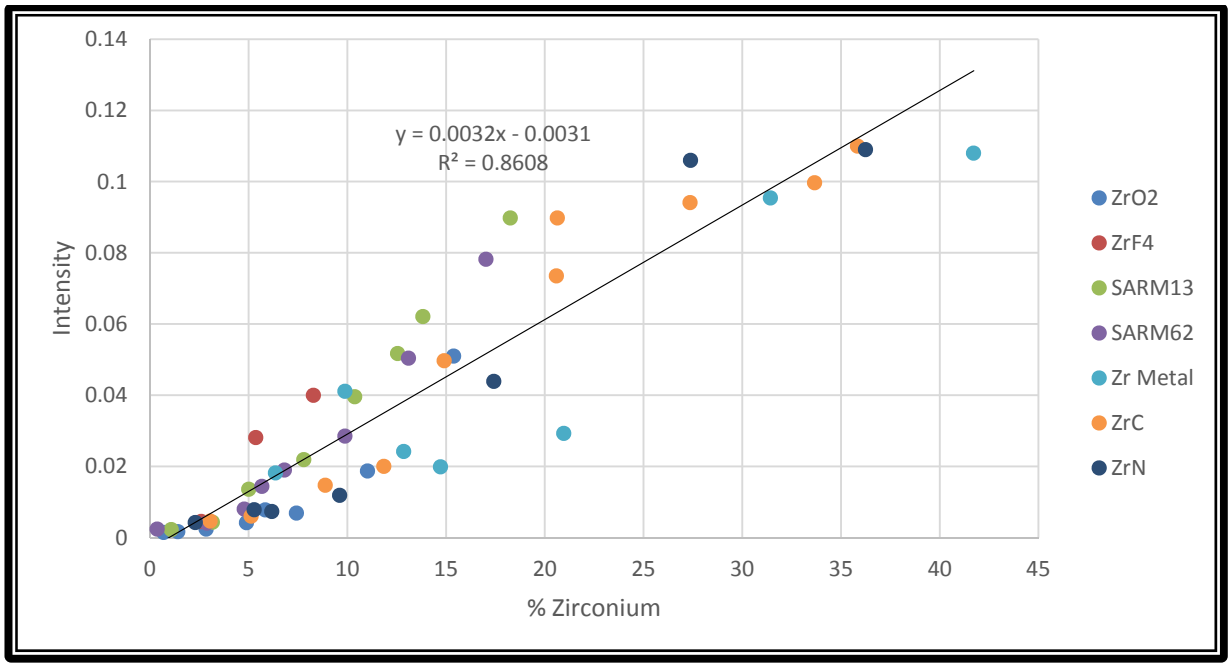

Figure 8-27: Graph showing instrument response for multiple materials in graphite matrix together (RF lamp, 500 V, 14 W, 5 min preburn)

8.4.7.2 Voltage setting: 700V

Increasing the voltage to 700V while keeping all other variables constant yielded improved results, which can be seen in **Figure 8-28** and **Figure 8-29** for copper and graphite matrices respectively. The results for the copper matrix appeared very similar to those in the 500V experiment (**Figure 8-26**) but the results for the graphite matrix

were significantly improved. Without eliminating any outliers the linearity (R^2) of the results for the graphite matrix with all the different zirconium compounds changed from 0.8608 to 0.7866 across the full range of the samples.

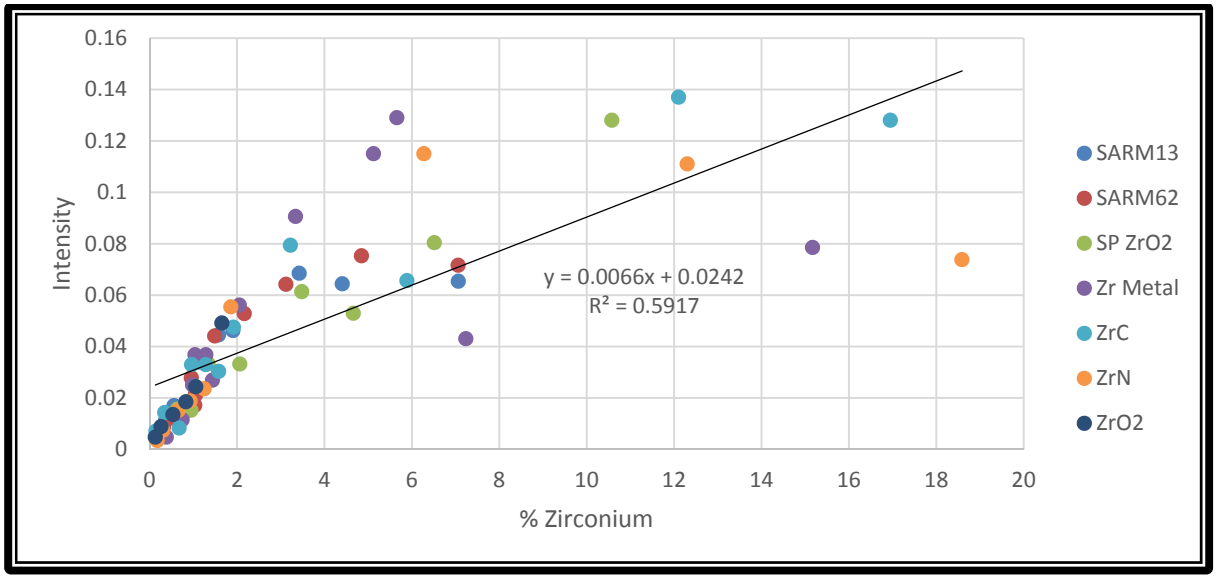

Figure 8-28: Graph showing instrument response for multiple materials in copper matrix together (RF lamp, 700 V, 14 W, 5 min preburn)

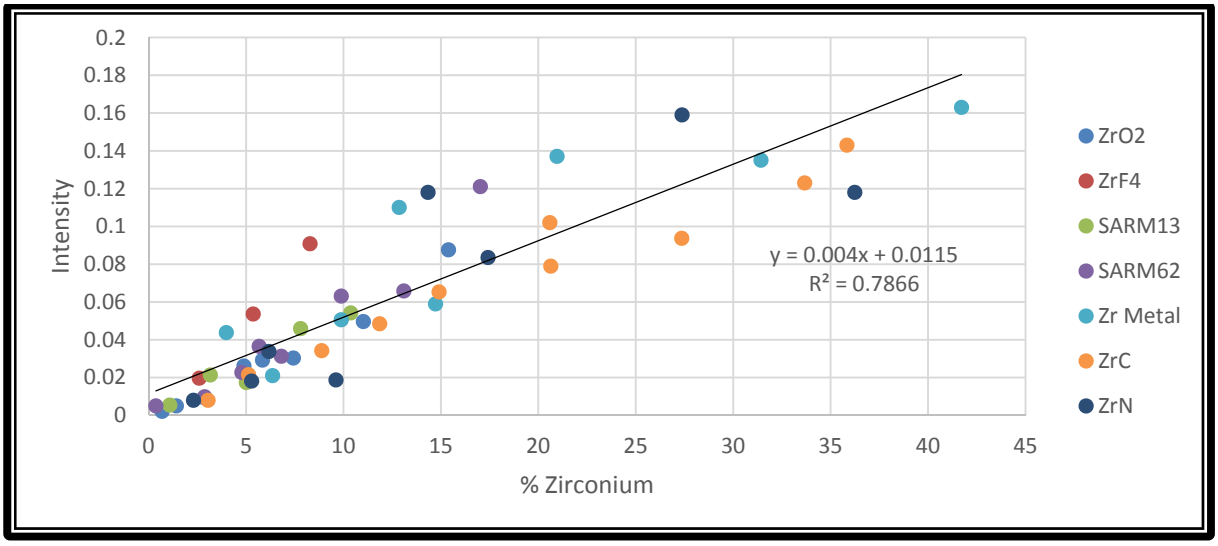

Figure 8-29: Graph showing instrument response for multiple materials in graphite matrix together (RF lamp, 700 V, 14 W, 5 min preburn)

8.4.7.3 Voltage setting: 900V

The applied voltage was finally increased to 900V as this was the upper limit that could be applied safely without damage being caused to the instrument. As before, the copper matrix samples (see **Figure 8-30**) appeared largely the same while the graphite ones (see **Figure 8-31**) yielded a trendline with an R^2 value of 0.8624 across the full

range. The instrument response was especially linear below 14% zirconium concentration. This was deemed acceptable for calibration of the instrument as a linear instrument response across all sample compounds was the objective of this method development process.

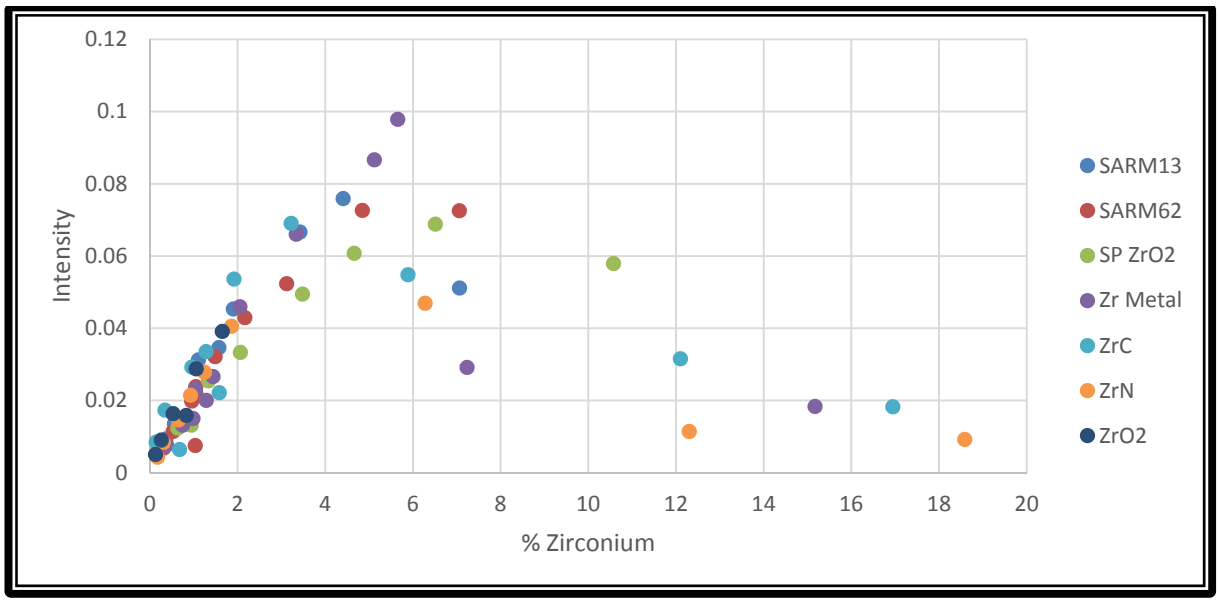

Figure 8-30: Graph showing instrument response for multiple materials in copper matrix (RF lamp, 900 V, 14 W, 5 min preburn)

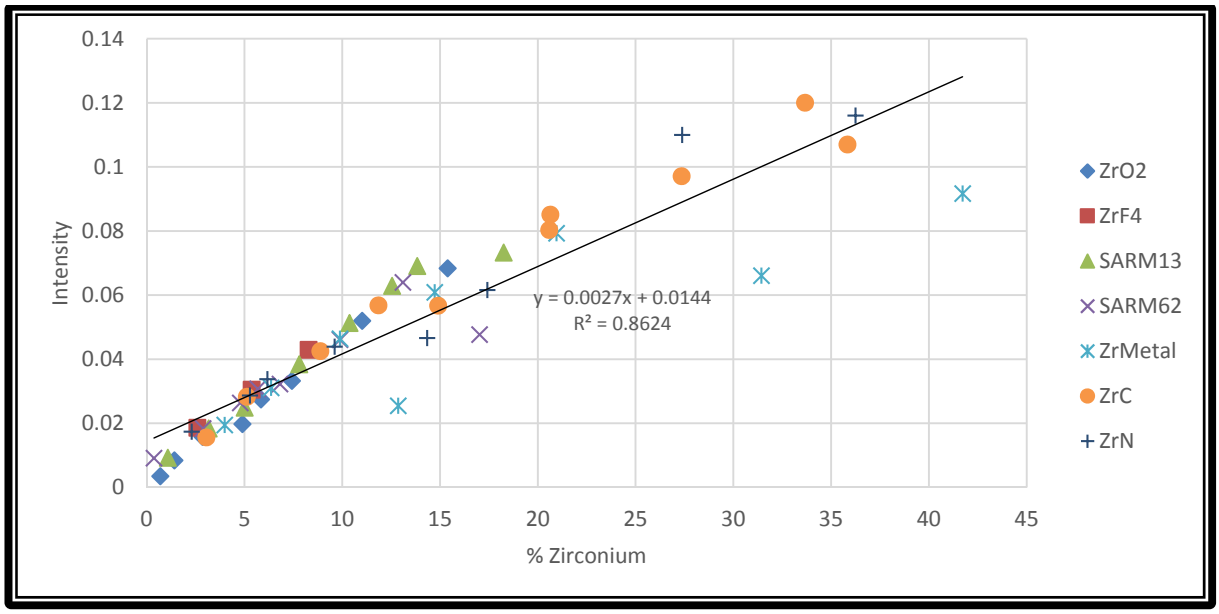

Figure 8-31: Graph showing instrument response for multiple materials in graphite matrix together (RF lamp, 900 V, 14 W, 5 min preburn)

8.4.8 *Instrument Validation and Lower Limits of Detection*

The results in **Figure 8-30** and **Figure 8-31** showed that at the 900 V setting using the RF lamp linear instrument response was achieved over all of the sample materials, at least in the lower concentration ranges. The results using the graphite sample matrix were markedly better across a longer calibration range than those using the copper matrix. These settings and conditions were used going forward.

The best calibration zone achieved using the copper matrix was found to be in the sub 5% zirconium region yielding a correlation coefficient (R^2) of 0.8790 and can be seen in **Figure 8-32**. In contrast the graphite matrix yielded a linear calibration in the region up to 14% zirconium with an R^2 value of 0.9805 as seen in **Figure 8-33**. The calibration gradient for the entire group of compounds in each matrix, as well as for each individual compound is given in **Table 8-3** and **Table 8-4**.

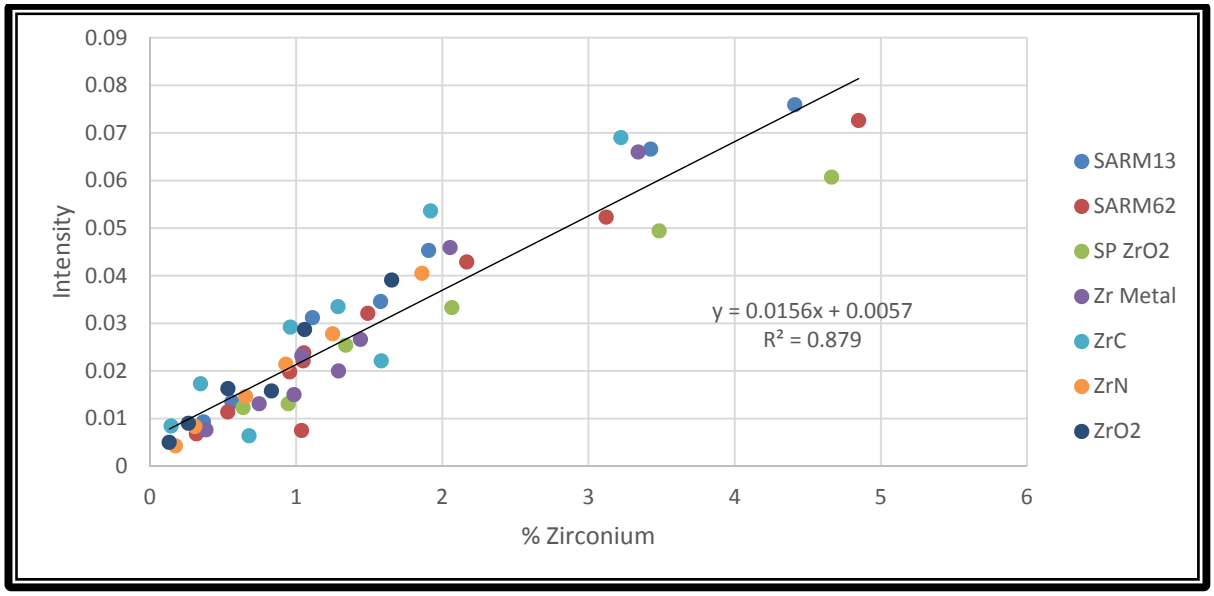

Figure 8-32: Calibration graph using all materials in copper matrix (RF lamp, 900V, 14W, 5 min preburn)

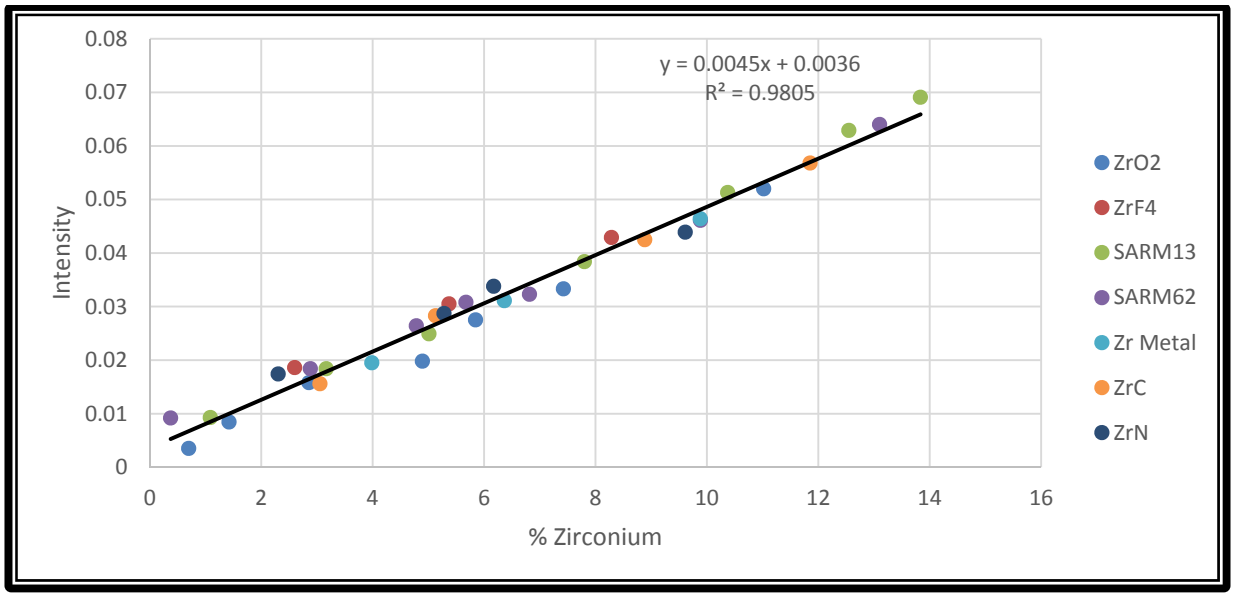

Figure 8-33: Calibration graph using all materials in graphite matrix (RF lamp, 900V, 14W, 5 min preburn)

Table 8-3: Table of detection and quantification limits for various non-conducting samples in copper matrix on GD-OES

Material	Gradient (*m*)	Intercept (*c*)	R^2	LLOD (%)	LLOQ (%)	LLOD (ppm)	LLOQ (ppm)
All Cu	0.0156	0.0057	0.8790	0.0011	0.0114	11.4	114.0
SARM13	0.0187	0.0055	0.9705	0.0010	0.0095	9.51	95.1
SARM62	0.0198	0.0013	0.9919	0.0009	0.0090	8.98	89.8
ZrO_2	0.0123	0.0055	0.9788	0.0014	0.0145	14.46	144.6
Zr Metal	0.0172	0.0022	0.9811	0.0010	0.0103	10.34	103.4
ZrC	0.0196	0.0093	0.9711	0.0009	0.0091	9.08	90.8
ZrN	0.0213	0.0011	0.9986	0.0008	0.0084	8.35	83.5

Table 8-4: Table of detection and quantification limits for various non-conducting samples in graphite matrix on GD-OES

Material	Gradient (*m*)	Intercept (*c*)	R^2	LLOD (%)	LLOQ (%)	LLOD (ppm)	LLOQ (ppm)
All GB20	0.0045	0.0036	0.9805	0.0487	0.4867	486.66	4866.6
SARM13	0.0047	0.0028	0.9974	0.0466	0.4660	465.95	4659.5
SARM62	0.0042	0.0062	0.9902	0.0521	0.5214	521.42	5214.2
Zr Metal	0.0035	0.0087	0.9881	0.0626	0.6257	625.70	6257.0
ZrC	0.0033	0.0116	0.9835	0.0664	0.6636	663.63	6636.29
ZrF_4	0.0043	0.0075	1.0000	0.0509	0.5093	509.30	5093.0
ZrN	0.0031	0.0118	0.9614	0.0706	0.7064	706.44	7064.4
ZrO_2	0.0044	0.0013	0.9941	0.0498	0.4977	497.72	4977.2

The detection and quantification limits calculated for each compound and for the matrix as a whole (see **Table 8-3** and **Table 8-4**) were orders of magnitude better for the copper matrix (LLOD 11.4ppm) than for the graphite (LLOD 487ppm). This is due to the greater instrument response (gradient) and the lower background noise when using the copper matrix. These values are only theoretical, however, and due to problems achieving homogeneity at very low sample concentration analysis outside of the calibrated region, even more dubious than usual. The selectivity of the method appeared to be slightly better for the copper matrix with its greater instrument response (average gradient of 0.0156 in the copper as opposed to 0.0045 in the graphite) but with similar *c* values in both matrices (0.0057 and 0.0036 in copper and graphite respectively). In almost all the individual compound calibrations the linearity (R^2) was better than 0.97 with most approaching 0.99. When plotted together, however, linearity for the copper matrix was only 0.8790 while the graphite samples yielded an R^2 of 0.9805. Despite the slightly improved lower limits of detection seen in the copper matrix (0.0011 vs 0.0487%), it was determined that the graphite matrix was preferable for these sample materials. This decision was taken based on the better R^2 values and the possibility of introducing more sample into a pellet than in the case of the copper matrix.

8.5. RESULTS FOR PROCESS SAMPLES

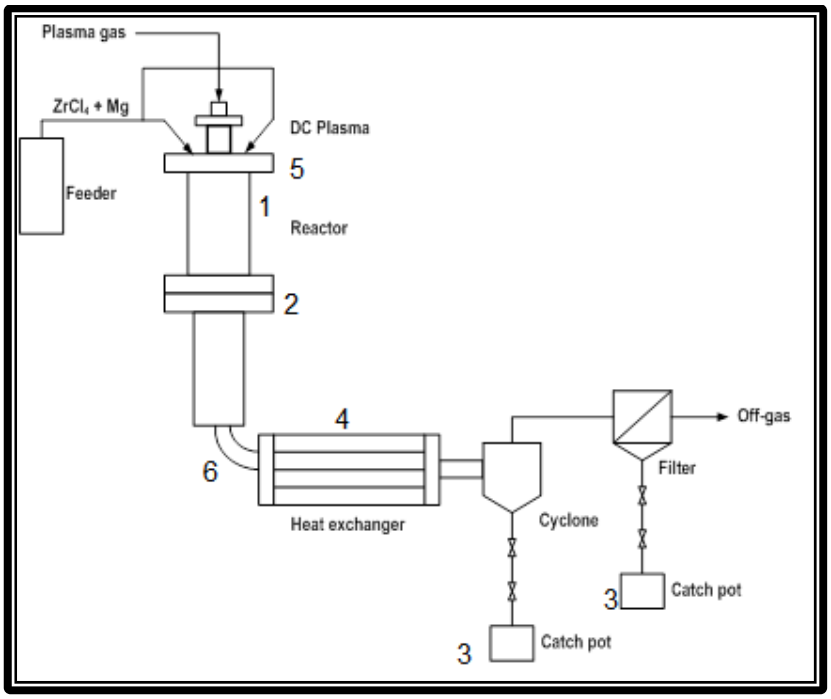

Figure 8-34: Schematic representation of the plasma pilot reactor for the production of zirconium metal [145]

In **Figure 8-34** samples labelled Reactor Wall (1), Reactor Head (5) and Reactor Bottom Valve (6) were recovered from the corresponding sections inside the reactor. The washed and unwashed zirconium metal powders were collected from the Catch Pot (3). Analysis conditions were as shown in **Table 8-5**.

Table 8-5: Instrument conditions for RF GD-OES analyses of Necsa process samples

Variable	Condition
Lamp	RF
Voltage (V)	900
True plasma power (W)	14
Sample matrix	Graphite/Bakelite
Pre-burn time (min)	5

Samples were made up so as to ensure that their concentrations would fall within the working range of the calibration. Sample masses of between 0.05 and 0.3 g were weighed accurately to 0.1 mg. Approximately 1.3 g (weighed to 0.1 mg) of a mixture of 20% Bakelite in graphite was added to each sample whereupon the mixture was transferred quantitatively to a steel vessel with two tungsten carbide milling balls. This vessel was sealed and placed in a mixer mill and shaken at 20 Hz for 10 minutes. The sample was then transferred to a 24 mm press mould and pressed at approximately 1000 MPa for 3 minutes. The pressed pellet was then analysed three times by GD-OES using the calibration seen in **Figure 8-33**.

The low recoveries seen for most samples in **Table 8-6** were disappointing but not completely unexpected. Recoveries as low as -9(1)% and as high as 91.1(1)% were found for the K_2ZrF_6 crystals and Reactor Wall B respectively. The samples recovered directly from the reactor were expected to be erratic as seen in **Chapter 7** as they had not been processed and purified. As was seen throughout the method development process the sputter rate and preferential sputtering have very significant effects on the emission intensities for different sample types. The crystalline, inorganic nature of the hexafluorozirconate complexes may have decreased the sputter rate relative to the other analyte materials as most of the commercial reference materials were ceramics.

Table 8-6: Percentage recovery results for process samples analysed by GD-OES in graphite/Bakelite matrix

Sample	% zirconium recovered (GD-OES)	% zirconium recovered (ICP-OES)
K_2ZrF_6 crystals	-9(1)	101(1)
Cs_2ZrF_6 crystals	-10(1)	100(2)
Plasma dissociated zircon	78.5(6)	100.16*
Necsa ZrF_4	79(1)	78(2)**
Reactor Wall B	38.5(3)	96(6)
Reactor Wall C	91.1(1)	113(16)
Reactor Head	10.8(7)	46(15)
Reactor Bottom Valve	20.4(9)	15(3)
Washed zirconium metal powder	74.1(4)	77.0(4)
Necsa zirconium metal powder	61(1)	98(1)

*Results from previous study [21].

** Sample analysed by Pelindaba Analytical Laboratories (PAL) for sample PS2014-2077X001 produced at Necsa [151].

The 78.5(6)% recovery achieved for the PDZ sample on the other hand may be due to preferential sputtering of the amorphous silicon oxide (glass) over the zirconium oxide crystallites. As the PDZ is known to have the same chemical composition as the SARM CRMs used in the calibration, the difference in structure is the only possible cause for this low recovery.

The Necsa process-produced zirconium tetrafluoride sample also gave a low recovery of 79(1)%. Commercial zirconium fluoride had been used in the standards and was found to have instrument response in line with the other materials used for calibration. While zirconium tetrafluoride is known to be far less hygroscopic than zirconium tetrachloride [19] this sample had been stored for several months in non-anhydrous conditions. The low recovery may thus have been due to the sample gaining moisture from the atmosphere before being pressed into the pellet. The ICP analysis performed

by Pelindaba Analytical Labs as part of the study in which the sample was produced yielded a similar recovery, lending credence to this hypothesis.

The recoveries for the samples taken directly from the zirconium metal powder production reactor (i.e. the reactor walls, head and bottom valve) yielded zirconium contents of between 10.8 and 91.1%. As these samples were not purified or stored under anhydrous conditions, any remaining zirconium tetrachloride or magnesium chloride would have gained moisture rapidly, decreasing the zirconium percentage in the sample. The presence of the magnesium as an easily ionisable element would also have affected the recovery in the same manner that the potassium and cesium did for the crystalline samples.

The washed zirconium metal powder was purified from the reactor product by washing with 65% nitric acid, a strong oxidising agent. As the zirconium recovery was calculated on the assumption that the material was pure zirconium, the percentage recovery can also be said to be the percentage zirconium content. Pure zirconium oxide is approximately 74% zirconium, almost exactly the result determined. The ICP-OES analysis (**Table 7-12**) of the same material yielded a recovery of 77.0(4)% which appeared to confirm that the washing process converted some of the material to zirconium oxide.

Commercial zirconium metal powder was used in the calibration of the instrument and yielded instrument response in line with the other commercial materials under the conditions employed in **Section 8.4.8.** The ICP-OES analysis (see **Table 7-11**) showed that the Necsa zirconium metal powder was approximately 98(1)% zirconium indicating that the low GD-OES recovery cannot be due to the chemical composition. The low recovery must thus be due to a lower sputter rate than that of the commercial zirconium powder. As the production process for the commercial material is unknown a comparison between the two materials cannot be definitively drawn. However, if the commercial zirconium metal powder was produced by a precipitation process, rather than the thermal process employed for the Necsa metal, there may be a difference in sample structure and density. This difference would likely affect the sputter rate and thus the recovery as the strength with which the atoms are bonded to each other in the sample has a direct influence on their sputter rate. Further research into this problem will need to be conducted.

8.6. CONCLUSION

The linear instrument response (R^2 of 0.9805) seen in **Section 8.4.8** indicates that, while the various commercial materials require significant time to stabilise (long pre-burn), the conditions and matrix employed allowed for a single calibration to be created for several zirconium refractories and the pure metal. This should allow for the analysis of various zirconium compounds without the need of initial sample digestion and dissolution. The only necessary preparation would be homogenising a sample and pressing the resultant powder into a pellet with a graphite and Bakelite binding matrix.

Unfortunately the crystal reference materials created and characterised for the express purpose of verifying the developed method proved to be unsuitable for this analytical method. Zirconium percentage recoveries of only 9 and 10% respectively for the potassium and cesium hexafluorozirconates made this abundantly clear. Fortunately the fact that the certified reference materials SARM13 and SARM62 yielded results in line with those of the commercial materials confirms that, for these materials at least, the method has some potential validity but further development is needed to have a validated analytical method and technique. The low recoveries seen in **Table 8-6** can be explained for various reasons but the disagreement between the ICP-OES and GD-OES results for the purified Necsa process zirconium powder alone merits further investigation.

At this point there are several advantages and disadvantages apparent with regard to this method in comparison to the “wet” ICP-OES method. The wet method requires harsh conditions to achieve complete dissolution of all samples. Once this is achieved, however, the original matrix is completely destroyed, removing almost all matrix effects on the analysis. In contrast the GD-OES method does not require dissolution, which simplifies sample preparation significantly but leaves the matrix largely intact which has been seen to cause problems with analysis. In order to matrix-match samples to calibration standards in ICP-OES the samples must be diluted significantly. This would make analysis of trace and ultra-trace components of the sample more difficult. While pressing a sample into a binding material also dilutes the sample, the degree of dilution is far smaller, allowing theoretically for better detection capability. The analysis of minor and trace components was outside of the scope of this study, however. While both methods are quite rapid, the GD-OES method is slightly quicker. Linearity of the GD-OES calibration curve was acceptable but not as good as that found using ICP-OES.

It is difficult to compare the lower limits of detection between the two techniques as sample matrix plays such a major role in the GD-OES method. In the graphite and copper matrices the average lower limit of detection is 486 and 11 ppm respectively, several orders of magnitude higher than that for ICP-OES (1.66 ppb). However the sample is not diluted as severely in the solid pellet, theoretically allowing for comparable capabilities.

The sample preparation method development appears to be largely complete with the graphite matrix standing out as the most promising. The GD-OES method will likely be most useful applied to the products of a manufacturing plant where the samples are of a constant and similar matrix.

Chapter 9: Evaluation of Research

9.1. CURRENT RESEARCH

As stated in **Chapter 1** the aim of this study was to attempt to analyse the reference materials and the Necsa process samples by both a “wet” dissolution (ICP-OES) and a “dry” solid state (GD-OES) method. Factors such as time, safety and environmental friendliness were taken into consideration as ideally these methods would eventually be applied to an industrial process.

The main objective of this study was to develop a robust, rapid and accurate method for the analysis of zirconium materials. The specific aims were:

1. Preparation of reference materials for specific compounds that were not commercially available. Crystallisation of complexes such as K_2ZrF_6, Cs_2ZrF_6, Li_2ZrF_6, Na_2ZrF_6, $CaZrF_6$, tetraethylammonium hexafluorozirconate, tetramethylammonium hexafluorozirconate, tetrabutylammonium hexafluorozirconate, tetraphenylarsonium hexafluorozirconate and tetraphenylphosphonium hexafluorozirconate was attempted as crystals are by definition pure compounds.
2. Thorough characterisation of the newly synthesised crystalline materials mentioned in Point 1 by such methods as X-ray crystallography and X-ray diffraction (XRD).
3. Evaluation of literature methods previously found to be successful in the analysis of various zirconium compounds and materials. Digestion methods such as acid dissolution, flux fusion and microwave-assisted acid digestion as well as quantification methods like atomic absorption spectrometry (AAS), graphite furnace atomic absorption spectrometry (GF-AAS), UV/VIS spectrophotometry, X-ray fluorescence (XRF), inductively coupled plasma mass spectrometry (ICP-MS) and ICP-OES were to be researched.
4. Identification of new analytical methods and techniques in sample preparation and determination such as powder pressing using various matrices and GD-OES with both direct current (DC) and radio frequency (RF) glow discharge lamps. Scanning electron microscopy (SEM) and energy dispersive X-ray spectroscopy (EDS) would be used for the characterisation of the surface of and glow discharge crater on solid pellets.

5. Method development using the most promising techniques identified in Points 3 and 4. Methods would be assessed using certified reference materials, new reference materials characterised and produced in-house as well as commercially available compounds.
6. Statistical evaluation of results for reference materials by evaluation of R^2 values, t-statistics, standard deviations, detection and quantification limits and instrument sensitivity and selectivity.
7. Comparison of these methods and techniques and application to real process samples, with focus on speed, precision, accuracy, robustness and safety.

Crystallisation of pure zirconium-containing compounds, such as potassium hexafluorozirconate amongst others, successfully produced three crystalline compounds. While several possible cations were investigated, only three formed crystals from which a crystal structure to confirm their composition could be obtained, namely those using potassium, cesium and tetraethylammonium. Of these only the potassium and cesium hexafluorozirconates could be produced repeatably.

Both the potassium catena di-μ-fluorido-tetrafluoridozirconate(IV) and the cesium hexafluorido zirconate(IV) were successfully characterised by X-ray crystallography and qualitative XRD. This was sufficient to confirm their elemental composition and make them useful as reference materials. Dissolution of these crystals was simple as the compounds are highly soluble in water making them well suited to ICP-OES, amongst other analytical techniques.

A thorough literature review revealed that, while there are many techniques available for the analysis of small quantities of zirconium, the analysis of primarily zirconium materials is not widely published. While there are many methods for analysing zirconium that is already present in solution there are few that are applicable to materials that are as resistant to dissolution as the samples produced in the Necsa's plasma/fluoride beneficiation process. As such it was necessary to develop new sample preparation procedures. ICP-OES was chosen as the analytical method of choice for the analysis of the dissolved materials due to its accuracy, precision, speed, lack of chemical interferences and long linear dynamic range. Dissolution methods were developed that quantitatively dissolved all of the materials of interest within a reasonable time-frame and allowed for accurate quantification of their zirconium

content, see **Chapter 7**. Analysis with ICP-MS was also undertaken when the instrument was available but was found to be less reliable than the OES.

A method for the analysis of zirconium compounds without dissolution was developed using a GD-OES instrument, see **Chapter 8**. As expected sample preparation was the biggest hurdle as GD-OES requires a solid, conducting sample to act as a cathode while the process samples were almost all powders and most were non-conductive. A new graphite/Bakelite sample matrix was developed which offers improved characteristics over conventional metal powder pressed pellets. Using the RF lamp for the GD-OES instrument, conditions were determined that yielded a linear response with zirconium content across several zirconium compounds including zirconium metal, carbide, nitride and oxide as well as zircon certified reference materials SARM13 and SARM62. Unfortunately the crystalline nature of the in-house reference materials made their analysis by this method unreliable.

All reference and commercial material analytical results were evaluated statistically using standard deviations and the Student's *t* test for precision and accuracy respectively. All calibrations were evaluated by their R^2 values, and detection and quantification limits were calculated.

The objective of developing a reliable and robust method of analysis for zirconium with good accuracy and precision was achieved by the wet route. While the solid sample preparation method was more limited in scope than the wet route, it was still able to achieve linear instrument response with zirconium concentration for all commercial materials. The relative advantages and disadvantages of these two methods was discussed in terms of speed, precision, accuracy, robustness and safety. Necsa process samples were analysed by both methods with comparable, but not identical, results.

9.2. FUTURE RESEARCH

Of concern with the ICP-OES analyses was the slightly higher than expected standard deviation for several of the process samples. Further investigation will be required in order to determine if there are as yet unidentified systematic errors in the analyses. Improved sampling procedures may also improve both accuracy and precision.

Analysis of alloying, minor and trace components in the zirconium matrix was outside of the scope of this study but will need to be undertaken. Determination of neutron

absorbing elements and elements affecting the mechanical properties of zirconium is crucial for producing nuclear grade zirconium metal.

Further research into sample preparation for the GD-OES instrument is certainly warranted. The significant advantages in terms of speed and environmental safety without the disadvantages of difficult sample digestion make the method extremely attractive.

The development of a similar GD-OES procedure for other mineral or process sample matrices may be warranted.

As with the ICP-OES method, determination of alloying, minor and trace elements by GD-OES in the graphite/Bakelite pressed pellets will need to be performed.

Investigation into other sample support matrices, such as other thermoplastic binding materials (poly(methyl methacrylate)) or resins (diallyl phthalate), for the production of pressed pellets may also be undertaken.

Chapter 10: Appendix

10.1. STATISTICS AND CALCULATIONS

The statistical treatment of data in this study was performed using the following calculations.

The average of a set of results was calculated using the formula $\bar{x} = \frac{\sum x_i}{N}$ where $\bar{x}$ is the mean, $\sum x_i$ the sum of all the results and N the number of results.

The sample standard deviation was determined using the equation $SD = \sqrt{\frac{\sum_{I=1}^{N}(x_i - \bar{x})^2}{N-1}}$ where SD is the standard deviation, $\sum_{I=1}^{N}(x_i - \bar{x})^2$ the sum of the deviations and N the number of data points.

Relative standard deviation was determined by the equation $RSD = \frac{SD}{\bar{x}} \times 100$ where RSD is the relative standard deviation, SD the standard deviation and $\bar{x}$ the mean.

Determination of the slope and intercept of a line were determined using Microsoft Excel and checked using a Least-Squares regression [43, pp. 196-201].

The lower limit of detection of the instrument is defined as the minimum concentration necessary for the instrument to be able to clearly distinguish between the analytes' emission and the background. This is critical in determining whether it is in fact possible to determine quantitatively the concentration of an analyte. The lower limit of detections of the instrument for a normal calibration curve were determined by the equation $DL = \frac{3 \times SD_b}{m}$ where DL is the lower limit of detection in ppm, m is the gradient of the calibration

graph and SD_b is the standard deviation of the blank. The quantification limit is defined as 10 times the lower limit of detection.

All Student's *t*-test statistics were calculated using the formula for the small sample *t* test [43, pp. 152-153] where $\bar{x}$ is the mean of the set of data points, μ_0 is the accepted, theoretical or true value, *s* is the standard deviation of the data and $\sqrt{N}$ is the square root of the number of degrees of freedom. The equation was as follows: $t = \frac{\bar{x}-\mu_0}{s/\sqrt{N}}$.

Chapter 11: Bibliography

[1] W. B. Blumenthal, The Chemical Behaviour of Zirconium, New Jersey: D.Van Nostrand Company, 1958.

[2] Roskill Information Services Ltd, Zirconium: Global Industry Markets and Outlook, Thirteenth ed., London: Roskill Information Services Ltd, 2011.

[3] "MetalPrices.com," [Online]. Available: http://www.metalprices.com/metal/zirconium/zirconium-sponge-99-china. [Accessed 6 May 2013].

[4] M. Zhuwakinyu, "Engineering News Online : Govt pursuing heavy mineral sands beneficiation initiatives," Creamer Media (Pty) Ltd, 13 July 2012. [Online]. Available: http://www.engineeringnews.co.za/article/govt-pursuing-heavy-mineral-sands-beneficiation-initiatives-2012-07-13. [Accessed 13 February 2013].

[5] "Zircon," 18 April 2009. [Online]. Available: http://commons.wikimedia.org/wiki/File:Zircon.GIF. [Accessed 6 May 2013].

[6] S. Lubbe, R. Munsami and D. Fourie, "Beneficiation of zircon sand in South Africa," *The Journal of The Southern African Institute of Mining and Metallurgy,* vol. 7A, pp. 583-588, July 2012.

[7] W. Kroll, "The Production of Ductile Titanium," *Transactions of the American Electrochemical Society,* vol. 78, no. 1, pp. 35-47, 1940.

[8] D. M. Considine, Van Nostrand's Scientific Encyclopedia, Fifth ed., Van Nostrand Reinhold Company, 1976.

[9] S. Furukawa, T. Masui and N. Imanaka, "New environment-friendly yellow pigments based on CeO2–ZrO2 solid solutions," *Journal of Alloys and Compounds,* vol. 451, no. 1-2, pp. 640-643, 28 February 2008.

[10] D. I. Chalmers, “Dubbo Zirconia Project,” 6 November 2012. [Online]. Available: http://www.alkane.com.au/projects/nsw/dubbo/. [Accessed 13 February 2013].

[11] Venus Jewellers India, “Venus Jewellers,” [Online]. Available: http://venusjewellers.in/images/WHITE_edited.jpg. [Accessed 25 April 2013].

[12] T. R. Prinsloo, “Spiral Concentrator”. Patent 5,472,096, 5 December 1995.

[13] R. E. Kirk and D. F. Othmer, Encyclopedia of Chemical Technology, Third ed., vol. 24, John Wiley and Sons, 1978, pp. 863-896.

[14] K. Patel, “Shifting sands: substitution and expanding markets,” *Industrial Minerals,* pp. 32-35, July 2014.

[15] A. Kaiser, M. Lobert and R. Telle, “Thermal stability of zircon (ZrSiO4),” *Journal of the European Ceramic Society,* vol. 28, pp. 2199-2211, 2008.

[16] O. S. Monnahela, “Advanced Metals Initiative (AMI) Project Literature Survey,” 2006.

[17] R. Martin, “Micro-mineral images of crystals from Glass Furnaces,” [Online]. Available: http://homepages.ihug.co.nz/~pincha/glassmins.html. [Accessed 06 May 2013].

[18] M. H. Jazini, S. M. Ghoreishi and A. A. Dadkhah, “Modeling of Carbochlorination of Zircon in Fluidized Bed,” *Metallurgical and Materials Transactions B,* vol. 41B, pp. 248-254, February 2010.

[19] O. S. Monnahela, Synthesis of high purity zirconium tetrafluoride for nuclear applications (M.Sc.), Bloemfontein, 2008, p. 29.

[20] A. Manhique, Optimisation of alkali-fusion process for zircon sands: A kinetic study of the Process, Pretoria: University of Pretoria, 2003, pp. 34-52.

[21] S. J. Lötter, W. Purcell, J. Nel and I. M. Potgieter, Identification and quantification of impurities in Zircon, PDZ and other relevant zirconium products (M.Sc.), 2009.

[22] Cameco Fuel Manufacturing Inc., “Cameco.com,” [Online]. Available: http://www.cameco.com/common/images/content/lightbox/img_fm_0610-0616.jpg. [Accessed 7 August 2013].

[23] L. E. Sarbeck, W. A. Crocker, C. T. Goodwin, J. C. Haygarth, L. J. Jacoby and D. R. Lee, “Zirconium-hafnium separation process”. Patent 5176878, 5 January 1993.

[24] D. G. Franklin and R. B. Adamson, Zirconium in the Nuclear Industry, ASTM International, 1984, pp. 24-25.

[25] ASTM International, *Standard Specification for Zirconium and Zirconium Alloy Ingots for Nuclear Application B350/B350M,* 2006.

[26] ATI Wah Chang, “ATI Metals,” 2003. [Online]. Available: http://www.atimetals.com/businesses/business-units/wahchang/products/Documents/Zr%20nuke%20waste%20disposal.pdf. [Accessed 26 02 2013].

[27] L. L. Nkabiti, Method Validation for the Quantification of Impurities in Zirconium Metal and Other Relevant Zr Compounds (M.Sc), Bloemfontein: University of the Free State, 2013.

[28] M. Qian, L. Zheng, D. Graham, M. T. Frost and D. H. StJohn, “Settling of undissolved zirconium particles in pure magnesium melts,” *Journal of Light Metals,* vol. 1, pp. 157-165, 2001.

[29] G. Schneider and V. Krivan, “Slurry and liquid sampling using electrothermal atomic absorption spectrometry for the analysis of zirconium dioxide based materials,” *Spectrochimica Acta Part B,* vol. 50, pp. 1557-1571, 1995.

[30] F. S. Rojas, C. B. Ojeda and J. M. C. Pavón, “Experimental design in the optimization of a microwave acid digestion procedure for the determination of metals in biomorphic ceramic samples by inductively coupled plasma mass spectrometry and atomic absorption spectrometry,” *Microchemical Journal,* vol. 94, pp. 7-13, 2010.

[31] R. K. Marcus and R. W. Schwartz, “Compositional profiling of solution-deposited lead zirconate–titanate thin films by radio-frequency glow discharge

atomic emission spectroscopy (rf-GD-AES)," *Chemical Physics Letters,* vol. 318, pp. 481-487, 2000.

[32] P. Schwaller, A. Fisher, R. Thapliyal, M. Aeberhard, J. Michler and H. J. Hug, "Single-target DC-pulsed deposition of lead zirconate titanate thin films: Investigation of the chemical and mechanical properties by glow-discharge optical emission spectroscopy and nanoindentation," *Surface & Coatings Technology,* vol. 200, pp. 1566-1571, 2005.

[33] "House of Japan," 25 July 2012. [Online]. Available: http://www.houseofjapan.com/electronics/fujifilm-expects-to-debut-new-pzt-thin-film-in-2012. [Accessed 7 August 2013].

[34] X. Zhong, X. Wu, Y. Jia and Y. Liu, "Self-repairing vanadium–zirconium composite conversion coating for aluminium alloys," *Applied Surface Science,* vol. 280, pp. 489-493, 2013.

[35] G. K. Chuah, S. H. Liu, S. Jaenicke and J. Li, "High surface area zirconia by digestion of zirconium propoxide at different pH," *Microporous and Mesoporous Materials,* vol. 39, pp. 381-392, 2000.

[36] "EC21 Global B2B Marketplace," Changsha Rock Metal Company Limited, [Online]. Available: http://image.ec21.com/image/rockmetal1/OF0018469556_1/Sell_ZIRCONIUM_INGOT.jpg. [Accessed 25 April 2013].

[37] J. A. McCleverty, T. J. Meyer and A. G. Wedd, Comprehensive Coordination Chemistry II, vol. 4, 2004, pp. 105-175.

[38] F. A. Cotton and G. Wilkinson, Advanced Inorganic Chemistry, Fifth ed., 1988, pp. 776-787.

[39] G. Wilkinson, R. D. Gillard and J. A. McCleverty, Comprehensive Coordination Chemistry, vol. 3, 1987, pp. 364-440.

[40] P. J. Chirik and C. A. Bradley, "Complexes of Zirconium and Hafnium in Oxidation States 0 to II," in *Comprehensive Organometallic Chemistry III:*

From Fundamentals to Applications, vol. 4: Compounds of Groups 3 to 4 and the f elements, 2007, pp. 697-739.

[41] M. M. Opeka, I. G. Talmy, E. J. Wuchina, J. A. Zaykoski and S. J. Causey, "Mechanical, Thermal, and Oxidation Properties of Refractory Hafnium and Zirconium Compounds," *Journal of the European Ceramic Society,* vol. 19, pp. 2405-2414, 1999.

[42] W. G. Fahrenholtz and G. E. Hilmas, "Azom.com The A to Z of Materials," 11 June 2013. [Online]. Available: http://www.azom.com/article.aspx?ArticleID=5127. [Accessed 20 August 2013].

[43] D. A. Skoog, D. M. West, F. J. Holler and S. R. Crouch, Fundamentals of Analytical Chemistry, 8th ed., Brooks/Cole, 2004.

[44] G. Norwitz, "Determination of zirconium in zirconium metal and zirconium powder by use of mandelic acid," *Analytica Chimica Acta,* vol. 35, pp. 491-498, 1966.

[45] H. Gordon and G. Norwitz, "Spectrophotometric determination of calcium in zirconium powder by use of murexide," *Talanta,* vol. 19, no. 1, pp. 1-6, January 1972.

[46] "About.com," [Online]. Available: http://chemistry.about.com/od/factsstructures/ig/Chemical-Structures---M/Murexide.htm. [Accessed 11 August 2013].

[47] G. W. C. Milner and J. W. Edwards, "The determination of zirconium in its binary alloys with niobium and tantalum," *Analytica Chimica Acta,* vol. 13, pp. 230-234, 1955.

[48] S. M. Dhavile, R. Shekhar, S. Thangavel, S. C. Chaurasia and J. Arunachalam, "Determination of trace phosphorus in zirconium–niobium alloy and Zircaloy by UV–vis spectrophotometry," *Talanta,* vol. 76, pp. 134-137, 2008.

[49] N. L. Elliot, M. A. Campbell and L. W. Green, "Determination of trace iron in zirconium by isotope dilution-thermal ionization mass spectrometry,"

International Journal of Mass Spectrometry and Ion Processes, vol. 146/147, pp. 99-108, 1995.

[50] W. Diegor, H. Longerich, T. Abrajano and I. Horn, “Applicability of a high pressure digestion technique to the analysis of sediment and soil samples by inductively coupled plasma-mass spectrometry,” *Analytica Chimica Acta,* vol. 431, pp. 195-207, 2001.

[51] M. Hoshino, Y. Watanabe, K. Sanematsu, Y. Kon and M. Shimizu, “Characteristics of zircon suitable for REE extraction,” *International Journal of Mineral Processing,* Vols. 102-103, pp. 130-135, 25 January 2012.

[52] Z.-m. Yang, “Simultaneous quantification measurement of Si, Fe, Ti, Ca, Mg, Zr in corundum by inductively coupled plasma-atomic emission spectrometry with secondary-melting method,” *Yankuang Ceshi,* vol. 31, no. 4, pp. 617-620, 2012.

[53] D. A. Stephenson, “An Improved Flux-Fusion Technique for X-Ray Emission Analysis,” *Analytical Chemistry,* vol. 41, no. 7, pp. 966-967, June 1969.

[54] Z. Hu, W. Zhang, Y. Liu, H. Chen, R. M. Gaschnig, K. Zong, M. Li, S. Gao and S. Hu, “Rapid bulk rock decomposition by ammonium fluoride (NH4F) in open-vessels at an elevated digestion temperature,” *Chemical Geology,* 2013.

[55] W. Zhang, Z. Hu, Y. Liu, H. Chen, S. Gao and R. M. Gaschnig, “Total rock dissolution using ammonium bifluoride in screw-top teflon vials: A new development in open vessel digestion,” *Analytical Chemistry,* vol. 84, pp. 10686-10693, 2012.

[56] M. B. Arain, T. G. Kazi, M. K. Jamali, N. Jalbani, H. I. Afridi and J. A. Baig, “Speciation of heavy metals in sediment by conventional, ultrasound and microwave assisted single extraction methods: A comparison with modified sequential extraction procedure,” *Journal of Hazardous Materials,* vol. 154, pp. 998-1006, 2008.

[57] Perkin Elmer, “PerkinElmer.com,” [Online]. Available: http://www.perkinelmer.com/Catalog/Product/ID/N3141000. [Accessed 13 August 2013].

[58] A. F. Albores, B. P. Cid, E. F. Gomez and E. F. Lopez, “Comparison between sequential extraction procedures and single extractions for metal partitioning in sewage sludge samples,” *Analyst,* vol. 125, pp. 1353-1357, 2000.

[59] M. Dondi, B. Fabbri and C. Mingazzini, “Use of zirconium oxychloride to neutralize HF in the microwave-assisted acid dissolution of ceramic glazes for their chemical analysis by ICP-OES,” *Talanta,* vol. 45, pp. 1201-1210, 1998.

[60] D.-M. Li, L.-X. Zhang, X.-H. Wang and L.-B. Liu, “Ashing and microwave digestion of aerosol samples with a polypropylene fibrous filter matrix,” *Analytica Chimica Acta,* vol. 482, pp. 129-135, 2003.

[61] G. R. Krishna, H. R. Ravindra, B. Gopolan and S. Syamsunder, “Determination of iron in nuclear grade zirconium oxide by x-ray fluorescence spectrometry using an internal intensity reference,” *Analytica Chimica Acta,* vol. 309, pp. 333-338, 1995.

[62] M. Betti, “Use of a Direct Current Glow Discharge Mass Spectrometer for the Chemical Characterization of Samples of Nuclear Concern,” *Journal of Analytical Atomic Spectrometry,* vol. 11, pp. 855-860, 1996.

[63] S. Oszwaldowski, R. Lipka and M. Jarosz, “Simultaneous determination of zirconium and hafnium as ternary complexes with 2-(5-bromo-2-pyridylazo)-5-diethylaminophenol and fluoride by reversed-phase liquid chromatography,” *Analytica Chimica Acta,* vol. 361, pp. 177-187, 1998.

[64] Q.-Z. Zhai, “Determination of trace amount of oxalic acid with zirconium(IV)–(DBS-arsenazo) by spectrophotometry,” *Spectrochimica Acta Part A,* vol. 71, pp. 332-335, 2008.

[65] A. S. Al-Kady, “Selective and sensitive spectrophotometric method for the determination of trace amounts of zirconium in environmental and biological samples using 4-chloro-N-(2,6-dimethylphenyl)-2-hydroxy-5-

sulfamoylbenzamide," *Spectrochimica Acta Part A: Molecular and Biomolecular Spectroscopy,* vol. 97, pp. 284-289, 2012.

[66] G. V. Rathaiah and M. C. Eshwar, "Rapid spectrophotometric determination of zirconium with 2-(5-bromo-2-pyridylazo)-5-dietheylaminophenol," *Talanta,* vol. 35, no. 6, pp. 502-504, 1988.

[67] A. Abbaspour and L. Baramakeh, "Application of principle component analysis–artificial neural network for simultaneous determination of zirconium and hafnium in real samples," *Spectrochimica Acta Part A,* vol. 64, pp. 477-482, 2006.

[68] R. Purohit and S. Devi, "Determination of nanogram levels of zirconium by chelating ion exchange and on-line preconcentration in flow injection UV-visible spectrophotometry," *Talanta,* vol. 44, pp. 319-326, 1997.

[69] A. Varghese and L. George, "Simultaneous first order derivative spectrophotometric determination of vanadium and zirconium in alloy steels and minerals," *Spectrochimica Acta Part A: Molecular and Biomolecular Spectroscopy,* vol. 95, pp. 46-52, 2012.

[70] J. B. Ghasemi and E. Zolfonoun, "Simultaneous spectrophotometric determination of trace amounts of uranium, thorium, and zirconium using the partial least squares method after their preconcentration by α-benzoin oxime modified Amberlite XAD-2000 resin," *Talanta,* vol. 80, pp. 1191-1197, 2010.

[71] H. M. Dong and V. Krivan, "Direct solid-sampling electrothermal atomic absorption spectrometry methods for the determination of silicon in oxides of niobium, titanium and zirconium," *Spectrochimica Acta Part B,* vol. 56, pp. 1645-1656, 2001.

[72] Y. K. Agrawal, M. Sanyal, P. Shrivastav and S. K. Menon, "Sequential liquid–liquid extraction graphite furnace atomic absorption spectrometric (GFAAS) and spectrophotometric determination of zirconium(IV) with calixarene hydroxamic acid," *Talanta,* vol. 46, pp. 1041-1049, 1998.

[73] S. Shariati and Y. Yamini, “Cloud point extraction and simultaneous determination of zirconium and hafnium using ICP-OES,” *Journal of Colloid and Interface Science,* vol. 298, pp. 419-425, 2006.

[74] A. Hulanicki, J. Surgiewicz and I. Jaron, “Determination of hafnium in air dust filters by inductively coupled plasma atomic emission spectrometry,” *Talanta,* vol. 44, pp. 1159-1162, 1997.

[75] P. Goodall, S. G. Johnson and E. Wood, “Laser ablation inductively coupled plasma atomic emission spectrometry of a uranium-zirconium alloy: ablation properties and analytical behavior,” *Spectrochimica Acta Part B,* vol. 50, pp. 1823-1835, 1995.

[76] S. Chen, D. Lu, Z. Hu and B. Wu, “In-situ vaporization and matrix removal for the determination of rare earth impurities in zirconium dioxide by electrothermal vaporization inductively coupled plasma atomic emission spectrometry,” *Spectrochimica Acta Part B,* vol. 60, pp. 537-541, 2005.

[77] B. A. McKelvey and K. J. Orians, “The determination of dissolved zirconium and hafnium from seawater using isotope dilution inductively coupled plasma mass spectrometry,” *Marine Chemistry,* vol. 60, pp. 245-255, 1998.

[78] L. V. Godfrey, W. M. White and V. J. M. Salters, “Dissolved zirconium and hafnium distributions across a shelf break in the northeastern Atlantic Ocean.,” *Geochimica et Cosmochimica Acta,* vol. 60, pp. 3995-4006, 1996.

[79] X. J. Yang and C. Pin, “Determination of niobium, tantalum, zirconium and hafnium in geological materials by extraction chromatography and inductively coupled plasma mass spectrometry,” *Analytica Chimica Acta,* vol. 458, pp. 375-386, 2002.

[80] P. Peralta-Zamora, L. Cornejo-Ponce, M. I. Bueno and J. W. Martins, “Zirconium and hafnium determination by energy dispersive X-ray fluorescence with solid phase preconcentration,” *Talanta,* vol. 44, pp. 811-816, 1997.

[81] R. M. Winchester and R. Payling, “Radio-frequency glow discharge spectrometry: A critical review,” *Spectrochimica Acta Part B,* vol. 59, pp. 607-666, 2004.

[82] M. Inoue and T. Saka, “Elemental analysis of powders by glow discharge mass spectrometry,” *Analytica Chimica Acta,* vol. 395, pp. 165-171, 1999.

[83] M. Wilke, G. Teichert, R. Gemma, A. Pundt, R. Kirchheim, H. Romanus and P. Schaaf, “Glow discharge optical emission spectroscopy for accurate and well resolved analysis of coatings and thin films,” *Thin Solid Films,* vol. 520, pp. 1660-1667, 2011.

[84] K. Shimizu, H. Habazaki, P. Skeldon and G. E. Thompson, “Impact of RF-GD-OES in practical surface analysis,” *Spectrochimica Acta Part B,* vol. 58, pp. 1573-1583, 2003.

[85] J. Malherbe, H. Martinez, B. Fernandez, C. Pecheyran and O. Donard, “The effect of glow discharge sputtering on the analysis of metal oxide films,” *Spectrochimica Acta Part B,* vol. 64, pp. 155-166, 2009.

[86] R. Shekhar, J. Arunachalam, G. R. Krishna, H. R. Ravindra and B. Gopalan, “Determination of boron in Zr–Nb alloys by glow discharge quadrupole mass spectrometry,” *Journal of Nuclear Materials,* vol. 340, pp. 284-290, 2005.

[87] United States Environmental Protection Agency, Multi-Agency Radiological Laboratory Analytical Protocols Manual, vol. II, 2004, pp. 13-1 - 13-26.

[88] G. A. El-Mahdy, S. S. Mahmoud and H. A. El-Dahan, “Effect of halide ions on the formation and dissolution behaviour of zirconium oxide,” *Effect of halide ions on the formation and dissolution behaviour of,* vol. 286, pp. 289-294, 1996.

[89] T. R. Dulski, A Manual for the Chemical Analysis of Metals, American Society for Testing and Materials, 1996.

[90] M. W. Dünser and J. Rieder, “Hydrofluoric Acid Burn,” 8 February 2007. [Online]. Available: http://www.nejm.org/doi/full/10.1056/NEJMicm055763. [Accessed 26 August 2013].

[91] USD Environmental, Health and Safety Department, “Nitric Acid,” University of South Dakota, [Online]. Available: http://www.usd.edu/research/research-and-sponsored-programs/upload/Nitric-Acid.pdf. [Accessed 6 September 2013].

[92] J. Basset, R. C. Denney, G. H. Jeffery and J. Mendham, Vogel's Textbook of Quantitative Inorganic Analysis, 4th ed., London: Longman Group Limited, 1978.

[93] P. Gaines, “Sample Preparation by Fusion - Trace Analysis Guide: Part 13,” Inorganic Ventures Inc., [Online]. Available: http://www.inorganicventures.com/sample-preparation-fusion. [Accessed 19 August 2013].

[94] F. E. Smith and E. A. Arsenault, “Microwave-assisted sample preparation in analytical chemistry,” *Talanta,* vol. 43, pp. 1207-1268, 43.

[95] K. E. Haque, “Microwave energy for mineral treatment processes - a brief review,” *International Journal of Mineral Processing,* vol. 57, pp. 1-24, 1999.

[96] G. Schwedt, The Essential Guide to Analytical Chemistry, John Wiley & Sons Ltd., 2005.

[97] D. A. Skoog, F. J. Holler and S. R. Crouch, Principles of Instrumental Analysis, 6th ed., Thomson Brooks/Cole, 2007.

[98] F. Rouessac and A. Rouessac, Chemical Analysis: Modern Instrumentation Methods and Techniques, 2nd ed., John Wiley & Sons Ltd., 2007.

[99] M. Resano, M. R. Florez and E. Garcia-Ruiz, “High-resolution continuum source atomic absorption spectrometry for the simultaneous or sequential monitoring of multiple lines. A critical review of current possibilities,” *Spectrochimica Acta Part B,* 2013.

[100] C. B. Boss and K. J. Fredeen, Concepts, instrumentation and techniques in inductively coupled plasma optical emission spectrometry, 2004.

[101] M. B. Knowles, “The latest advances in axially viewed simultaneous ICP-OES for elemental analysis,” 1 November 2010. [Online]. Available: http://www.chem.agilent.com/Library/applications/ICPES-01.pdf. [Accessed 12 August 2013].

[102] J. R. Dean, Practical Inductively Coupled Plasma Spectroscopy, John Wiley and Sons Ltd., 2005.

[103] “PrecisionGlassBlowing.com,” [Online]. Available: http://www.precisionglassblowing.com/catalog/spectro-spray-chamber-scott-large-p-567.html. [Accessed 19 August 2013].

[104] “Present trends and future of zircon in Geochemistry,” GeoScienceWorld.org, [Online]. Available: http://rimg.geoscienceworld.org/content/53/1/243/F3.large.jpg. [Accessed 6 September 2013].

[105] P. Gates, “Gas Chromatography Mass Spectrometry (GC/MS),” University of Bristol, 14 January 2008. [Online]. Available: http://www.bris.ac.uk/nerclsmsf/techniques/gcms.html. [Accessed 19 August 2013].

[106] M. Humayun, “Magnet Lab National High Magnetic Field Laboratory,” [Online]. Available: http://www.magnet.fsu.edu/education/tutorials/magnetminute/spectrometer-transcript.html. [Accessed 19 August 2013].

[107] “How Electron Multipliers work,” SGE Analytical Science Pty Ltd, [Online]. Available: http://www.sge.com/products/electron-multipliers/how-electron-multipliers-work. [Accessed 19 August 2013].

[108] E. Koojiman, K. Mezger and J. Berndt, “Constraints on the U–Pb systematics of metamorphic rutile from in situ LA-ICP-MS analysis,” *Earth and Planetary Science Letters,* vol. 293, no. 3-4, pp. 321-330, 1 May 2010.

[109] Perkin Elmer, “The 30-Minute Guide to ICP-MS,” Perkin Elmer Incorporated, [Online]. Available: http://www.perkinelmer.com/PDFs/Downloads/tch_icpmsthirtyminuteguide.pdf. [Accessed 06 September 2013].

[110] T. W. May and R. H. Wiedmeyer, “A Table of Polyatomic Interferences in ICP-MS,” *Atomic Spectroscopy,* vol. 19, pp. 150-155, September 1998.

[111] “X-ray Fluorescence Spectroscopy,” Amptek Inc., 17 April 2013. [Online]. Available: http://www.amptek.com/xrf.html. [Accessed 6 September 2013].

[112] J. H. Wittke, “X-ray Fluorescence Analysis,” [Online]. Available: http://www4.nau.edu/microanalysis/Microprobe/ProbeIntro-XRF.html. [Accessed 19 August 2013].

[113] “Azom.com The A to Z of Materials,” 2 April 2004. [Online]. Available: http://www.azom.com/article.aspx?ArticleID=2449. [Accessed 9 July 2013].

[114] A. Bogaerts and R. Gijbels, “Fundamental aspects and applications of glow discharge spectrometric techniques,” *Spectrochimica Acta Part B,* vol. 53, pp. 1-42, 1998.

[115] M. Betti and L. A. de las Heras, “Glow discharge spectrometry for the characterization of nuclear and radioactively contaminated environmental samples,” *Spectrochimica Acta Part B,* vol. 59, pp. 1359-1376, 2004.

[116] “Shimadzu.com,” The Shimadzu Corporation, 2013. [Online]. Available: http://www.shimadzu.com/an/elemental/icp/icps7510/icps.html. [Accessed 4 September 2013].

[117] R. Gledhill, “Confessions of a Chemical Feed pump Manufacturer,” Blue-White Industries, Ltd., [Online]. Available: http://www.bluwhite.com/artchemfeedpump.htm. [Accessed 2 September 2013].

[118] “ICPM-8500: The Shimadzu Corporation,” The Shimadzu Corporation, 2013. [Online]. Available: http://www.an.shimadzu.co.jp/icp/icp-ms/index.htm. [Accessed 4 September 2013].

[119] “Leco.com,” Leco Corporation, 2007. [Online]. Available: http://www.leco.com/component/edocman/?task=document.viewdoc&id=49&Itemid=0. [Accessed 4 September 2013].

[120] T. Alavosus and D. Hilligoss, “Effects of Easily Ionisable Elements,” 26 February 2007. [Online]. Available: http://www.vhglabs.com/uploadcache//Presentation_Effects_of_Easily_Ionizable_Elements_EIE.pdf. [Accessed 6 September 2013].

[121] “ICP-OES, ICP-MS & ICP-OES (SAGES),” School of GeoSciences, 5 June 2011. [Online]. Available: http://www.geos.ed.ac.uk/facilities/ICP/. [Accessed 9 September 2013].

[122] UCLA Chemistry and Biochemistry, [Online]. Available: http://www.chem.ucla.edu/harding/lecsups/xray30.pdf. [Accessed 06 January 2014].

[123] Bruker, “SAINT-Plus, Version 7.12 (including XPREP),” Bruker AXS Inc., Madison, 2004.

[124] Bruker, “SADABS Version 2004/1,” Bruker AXS Inc., Madison, 1998.

[125] A. Altomare, M. C. Burla, M. Camalli, G. L. Cascarano, C. Giacovazzo, A. Guagliardi, A. G. G. Moliterni, G. Polidori and R. Spagna, “SIR97,” *Journal of Applied Crystallography,* vol. 32, pp. 115-119, 1999.

[126] G. M. Sheldrick, “SHELXL97, Program for the refinement of crystal structures,” 1997.

[127] L. J. Farrugia, “WINGX,” *Journal of Applied Crystallography,* vol. 21, pp. 837-838, 1999.

[128] K. Brandenburg and H. Putz, “DIAMOND Release 3.0e,” Crystal Impact GbR, Bonn, 2006.

[129] G. C. Hampson and L. Pauling, “The Structure of Ammonium Heptafluozirconate and Potassium Heptafluozirconate and the Configuration

of the Heptafluozirconate Group," *Journal of the American Chemical Society,* vol. 60, pp. 2702-2707, 1938.

[130] A. V. Gerasimenko, I. A. Tkachenko, V. Y. Kavun, N. A. Didenko and V. I. Sergienko, "Synthesis and Complex Investigation of Potassium Ammonium Hexafluorozirconates: I. Synthesis and X-ray Diffraction Study of K2-x(NH4)xZrF6 (0<x<2) Crystals," *Russian Journal of Inorganic Chemistry,* vol. 51, no. 1, pp. 9-22, 2006.

[131] A. V. Gerasimenko, N. A. Didenko and V. Y. Kavun, "Dipotassium hexafluoridozirconate(IV) hydrogen fluoride," *Acta Crystallographica Section E,* vol. 63, no. 8, p. 171, 2007.

[132] J.-P. Laval, "Crystal chemistry of anion-excess ReO3-related phases," *Acta Crystallographica. Section C,* vol. 70, no. 8, pp. 742-748, 2014 .

[133] A. V. Gerasimenko, N. A. Didenko and V. Y. Kavun, "Rubidium Potassium hexafluorido-zirconate(IV) bis(hydrogen fluoride)," *Acta Crystallographica Section E,* vol. E63, p. i198, 2007.

[134] L. Meddar, M. El-Ghozzi and D. Avignant, "New Heptafluorozirconates and -hafnates AIBIIZr(Hf)F7 (AI = Rb, Tl; BII = Ca, Cd) – Synthesis, Structures, and Structural Relationships," *Zeitschrift für anorganische Chemie,* vol. 634, pp. 565-570, 2008.

[135] A. Rahten, I. Leban, S. Milicev and B. Zemva, "Crystal structure and vibrational spectra of hydrazinium (2+) tri-g-fluoro bis[pentafluorozirconate (IV)] fluoride and vibrational spectra of its hafnium analogue," *Journal of Crystallographic and Spectroscopic Research,* vol. 20, no. 1, pp. 9-15, 1990.

[136] Evans Analytical Group, "ICP-OES and ICP-MS Detection Limit Guidance," May 2014. [Online]. Available: http://www.eag.com/documents/icp-oes-ms-detection-limit-guidance-BR023.pdf. [Accessed 19 September 2014].

[137] I. J. Bear and W. G. Mumme, "The Crystal Chemistry of Zirconium Sulphates. V. The Structure of ot-Zr(SO4)2.H20," *Acta Crystallographica,* vol. B26, pp. 1131-1140, 1970.

[138] “American Elements,” [Online]. Available: http://www.americanelements.com/zrs.html. [Accessed 10 September 2014].

[139] C. E. Housecroft and A. G. Sharpe, “Chapter 15: The group 15 elements,” in *Inorganic Chemistry*, 3rd ed., 2008.

[140] R. K. Winge, V. A. Fassel, V. J. Peterson and M. A. Floyd, Inductively Coupled Plasma-Atomic Emission Spectroscopy - An Atlas of Spectral Information, 6th ed., 1993.

[141] M. K. Sharma and B. K. Saikia, “Discharge conditions and emission spectroscopy of N2 and N2+ active species in a variable power DC pulsed plasma used for steel nitriding,” *Indian Journal of Pure and Applied Physics,* vol. 46, pp. 463-470, 2008.

[142] C. L. Whitmarsh, “Review of Zircaloy-2 and Zircaloy-4 properties relevant to N.S. Savannah Reactor Design,” 1982.

[143] T. Ishizuka, Y. Uwamino, H. Morikawa, Y. Iida and A. Tsuge, “Determination of Impurities in Zirconium Carbide and Nitride by Inductively Coupled Plasma Atomic Emission Spectrometry,” *Analytical Sciences,* vol. 6, pp. 315-317, April 1990.

[144] M. Ishikuro and K. Wagatsuma, “Separation and Determination of Zirconium Carbide in Zr50Al10Ni5Cu30 Bulk Metallic Glass Matrix Composites Containing ZrC Particles,” *Materials Transactions,* vol. 51, no. 2, pp. 366-370, 2010.

[145] J. T. Nel, J. L. Havenga, M. M. Makhofane and A. A. Jansen, “The plasma-assisted manufacture of zirconium metal powder from zirconium tetrachloride,” *The Journal of The Southern African Institute of Mining and Metallurgy,* vol. 112, pp. 63-68, January 2012.

[146] “Ammonium fluorosilicate Material Safety Data Sheet,” Fluoride Action Network, [Online]. Available: http://www.fluoridealert.org/wp-content/pesticides/ammonium.fluosilicate.msds.htm. [Accessed 25 September 2014].

[147] R. T. Jones, N. A. Barcza and T. R. Curr, “Plasma Developments in Africa,” Mintek, 19 June 2001. [Online]. Available: http://www.mintek.co.za/Pyromet/Plasma/Plasma.htm. [Accessed 23 09 2014].

[148] J. C. Riviere and S. Myhra, Handbook of Surface and Interface Analysis, 2nd ed., Boca Raton: Taylor & Francis Group, LLC, 2009.

[149] L. Fuhe, “Using GD-OES to Characterize Challenging Thin-Films and Advanced Materials,” 2008. [Online]. Available: http://www.balazs.com/file/otherelement/pj/balazs%20nl%20spring%2037776.pdf. [Accessed 16 September 2014].

[150] R. Payling, D. Jones and A. Bengtson, Glow Discharge Optical Emission Spectrometry, John Wiley & Sons Ltd., 1997.

[151] C. J. Pretorius, W. du Plessis, J. T. Nel and P. L. Crouse, “Kinetics and thermodynamic parameters for the manufacturing of anhydrous zirconium tetrafluoride with ammonium acid fluoride as fluorinating agent,” *The Journal of The Southern African Institute of Mining and Metallurgy,* vol. 7A, pp. 601-604, July 2012.